

---

Doctoral Dissertations

Student Theses and Dissertations

---

Fall 2012

## Saturation effects on mechanical excavatability of Roubidoux sandstone under selected rock cutting tools

Muhammad Zubair Abu Bakar

Follow this and additional works at: [https://scholarsmine.mst.edu/doctoral\\_dissertations](https://scholarsmine.mst.edu/doctoral_dissertations)



Part of the [Geological Engineering Commons](#)

Department: Geosciences and Geological and Petroleum Engineering

---

### Recommended Citation

Abu Bakar, Muhammad Zubair, "Saturation effects on mechanical excavatability of Roubidoux sandstone under selected rock cutting tools" (2012). *Doctoral Dissertations*. 1970.

[https://scholarsmine.mst.edu/doctoral\\_dissertations/1970](https://scholarsmine.mst.edu/doctoral_dissertations/1970)

This thesis is brought to you by Scholars' Mine, a service of the Missouri S&T Library and Learning Resources. This work is protected by U. S. Copyright Law. Unauthorized use including reproduction for redistribution requires the permission of the copyright holder. For more information, please contact [scholarsmine@mst.edu](mailto:scholarsmine@mst.edu).



SATURATION EFFECTS ON MECHANICAL EXCAVATABILITY OF  
ROUBIDOUX SANDSTONE UNDER SELECTED ROCK CUTTING TOOLS

by

MUHAMMAD ZUBAIR ABU BAKAR

A DISSERTATION

Presented to the Faculty of the Graduate School of the  
MISSOURI UNIVERSITY OF SCIENCE AND TECHNOLOGY

In Partial Fulfillment of the Requirements for the Degree

DOCTOR OF PHILOSOPHY

in

GEOLOGICAL ENGINEERING

2012

Approved by

Leslie S. Gertsch, Advisor  
Norbert H. Maerz  
J. David Rogers  
David A. Summers  
Richard L. Bullock

© 2012

MUHAMMAD ZUBAIR ABU BAKAR

All Rights Reserved



## ABSTRACT

This study investigated the differences in the cutting performance of two rock cutting tools in dry and saturated rock. For this purpose, a permeable quartzose sandstone was subjected to a series of full scale linear rock cutting tests, in both dry and saturated conditions, using a constant cross-section (CCS) disc cutter and a radial drag pick at a constant cutting speed.

In this rock, saturation with water reduced the forces acting on the disc cutter by 27-48% (significant at 90% confidence), but also reduced the chip yield by nearly as much. Even though the specific energy of fragmentation went down 8-10%, the difference was not statistically significant.

Contrary to the behavior under the disc cutter, water saturation increased the drag pick cutting forces by 9-10%, which is suggestive but not enough to be statistically significant. It did not increase the chip yield by a concomitant amount, however, so the specific energy went up by 28% (significant at 90% confidence).

The unexpected differences in the effect of water saturation on the rock fragmentation response to these cutters might be explained by the effects due to their different fragmentation mechanisms, such as the relative size of the crushed zone that forms beneath the cutters. The relationship between cutting speed and rock permeability was expected to be a major factor influencing the effective pressure beneath a cutter in saturated rock. However, load-indentation tests with pore pressure measurement at the same speed showed that the pore pressure within the tested sandstone remained too low to affect the rock fracture process. Other possible mechanisms are discussed.

## ACKNOWLEDGMENTS

I would like to express my sincere gratitude to my research advisor, Dr. Leslie S. Gertsch, who provided me an opportunity to work in the area of Mechanical Excavation of Rocks. Without her support and intellectual insight, this work would not have been a possibility. I would also like to thank my committee members, Dr. Norbert H. Maerz, Dr. J. David Rogers, Dr. David A. Summers, and Dr. Richard L. Bullock for their kind suggestions and advice. Special thanks are due to Dr. Richard L. Bullock for his keen interest in my work and his valuable ideas to improve my work.

I am extremely thankful to Dr. Jamal Rostami, Assistant Professor, Pennsylvania State University, USA for co-authoring one of my journal papers from this research work. It was instrumental to have benefited from his technical expertise in field of Mechanical Excavation.

I must appreciate the technical support provided by the staff of Rock Mechanics and Explosives Research Center, especially, Mr. John Tyler, Sr. Research Engineer, and Mr. Mike Bassett, Sr. Research Technician. Their help was crucial for laboratory setups of my experimental work.

I owe my deepest gratitude to my parents for their continuous support and prayers, my wife Shagufta for her encouragement and cooperation, and affection of my daughters Zainab and Menaal.

I would like to acknowledge the financial support provided by the University of Engineering and Technology, Lahore, Pakistan for my studies. I am also indebted to my advisor, Dr. Leslie S. Gertsch for supplementing my living expenses and also for providing necessary funds to attend different conferences to present my research work across the USA.

## TABLE OF CONTENTS

	Page
ABSTRACT.....	iii
ACKNOWLEDGMENTS .....	iv
LIST OF ILLUSTRATIONS.....	ix
LIST OF TABLES.....	xiv
NOMENCLATURE .....	xv
 SECTION	
1. INTRODUCTION.....	1
1.1. BACKGROUND .....	1
1.2. OBJECTIVE .....	3
1.3. APPROACH .....	3
2. LITERATURE REVIEW.....	5
2.1. ROCK CUTTING LITERATURE .....	5
2.1.1. Rock Cutting Tools .....	5
2.1.1.1 Drag tools.....	6
2.1.1.2 Roller cutters.....	8
2.1.2. Mechanical Rock Fragmentation.....	11
2.1.2.1 Rock indentation studies .....	12
2.1.2.2 Theoretical studies on drag pick cutting.....	16
2.1.2.3 Theoretical studies on disc cutting.....	22
2.1.2.4 Field performance estimation of mechanical excavators.....	33
2.1.3. Saturated Rocks Studies .....	37
2.1.3.1 Saturation effects on strength of rocks.....	37
2.1.3.2 Saturation effects on mechanical excavation of rocks .....	40
3. DETAILS AND DESCRIPTION OF TEST EQUIPMENT.....	49
3.1. LINEAR ROCK CUTTING EXPERIMENTS.....	49
3.1.1. Linear Rock Cutting Machine .....	49
3.1.1.1 Load cell.....	49
3.1.1.2 Cutting tool .....	51

3.1.1.3 Motion control .....	55
3.1.1.4 Data acquisition system .....	57
3.1.2. LRCM Testing Procedure .....	57
3.1.3. Sample Preparation and Saturation .....	62
3.1.3.1 Dry samples preparation .....	62
3.1.3.2 Saturated samples preparation .....	64
3.1.4. Load Cell Calibration Constants .....	66
3.1.5. Load Cell Calibration Procedure .....	69
3.1.6. String Potentiometer Calibration.....	72
3.2. LOAD INDENTATION TESTS .....	72
3.2.1. Load Indentation Test Setup.....	72
3.2.2. Load Indentation Test Procedure .....	77
3.3. ROCK SAMPLE.....	78
3.4. ROCK PROPERTY TESTS .....	78
4. EXPERIMENTAL RESULTS .....	82
4.1. DISC CUTTING TESTS .....	82
4.1.1. Force Measures.....	82
4.1.2. Chip Measures .....	82
4.2. RADIAL DRAG PICK CUTTING TESTS.....	90
4.2.1. Force Measures.....	90
4.2.2. Chip Measures .....	94
4.3. LOAD INDENTATION TESTS .....	95
5. DISCUSSION: SATURATION EFFECTS ON DISC CUTTING.....	99
5.1. EFFECT OF CUT SPACING ON CUTTING FORCES .....	100
5.2. EFFECT OF CUTTER PENETRATION ON CUTTING FORCES .....	102
5.3. EFFECT OF CUT SPACING ON SPECIFIC ENERGY.....	103
5.4. EFFECT OF CUTTER PENETRATION ON SPECIFIC ENERGY .....	105
5.5. EFFECT OF s/p RATIO ON SPECIFIC ENERGY .....	107
5.6. EFFECT OF CUTTER PENETRATION ON CUTTING COEFFICIENT ...	110
5.7. EFFECT OF CUT SPACING ON CUTTING COEFFICIENT .....	112
6. DISCUSSION: SATURATION EFFECTS ON DRAG PICK CUTTING .....	115

6.1. OVERALL EFFECTS OF SATURATION.....	115
6.2. EFFECT OF CUT SPACING ON CUTTING FORCES .....	117
6.3. EFFECT OF DEPTH OF CUT ON SPECIFIC ENERGY .....	117
6.4. EFFECT OF CUT SPACING ON SPECIFIC ENERGY.....	123
6.5. EFFECTS OF s/d RATIO ON SPECIFIC ENERGY .....	126
7. DISCUSSION: EVALUATION OF CUTTINGS .....	132
7.1. BACKGROUND .....	132
7.2. DISC CUTTER CUTTINGS ANALYSES .....	135
7.2.1. Nominal and Actual Production Rate.....	135
7.2.2. Relationship between Coarseness Index and Absolute Size Constant .	138
7.2.3. Effect of Large Sized Muck on Absolute Size Constant and Coarseness Index .....	139
7.2.4. Relationship of Absolute Size Constant and Coarseness Index with Production Rate.....	141
7.2.5. Absolute Size Constant and Coarseness Index Variation with Cut Spacing.....	143
7.2.6. Relationship of Coarseness Index and Absolute Size Constant with Specific Energy.....	145
7.2.7. Effect of s/p Ratio on Specific Energy and Coarseness Index .....	147
7.2.8. Effect of Cutter Penetration on Specific Energy and Production Rate	149
7.3. RADIAL DRAG PICK CUTTINGS ANALYSES .....	151
7.3.1. Relationship of Absolute Size Constant with Coarseness Index and Large Sized Muck.....	151
7.3.2. Relationship of Absolute Size Constant and Specific Energy .....	151
7.3.3. Relationship of Coarseness Index and Specific Energy .....	153
7.3.4. Statistical Model for Drag Pick Specific Energy .....	154
8. DISCUSSION: LOAD-INDENTATION TESTS.....	157
8.1. INTRODUCTION .....	157
8.1.1. Load-Indentation Curves and Porewater Pressure Behavior.....	157
8.1.2. Specific Penetration and Specific Energy .....	163
8.2. CUTTING FORCES AND WEAR RESPONSE TO SATURATION .....	167
8.2.1. Radial Drag Pick Cutting Tests .....	167
8.2.2. Disc Cutting Tests .....	169

9. CONCLUSIONS AND RECOMMENDED FUTURE WORK .....	173
9.1. CONCLUSIONS.....	173
9.1.1. Saturation Effects on Cutting Forces.....	173
9.1.2. Saturation Effects on Specific Energy.....	176
9.1.3. Relationships between Specific Energy, Production Rate and Chip Size Indices .....	177
9.2. RECOMMENDED FUTURE WORK .....	179
APPENDICES	
A. 3-D LOAD CELL CALIBRATIONS FOR DISC CUTTER AND DRAG PICK TESTS .....	181
B. DISC CUTTING FORCES AND SIEVE ANALYSIS DATA.....	196
C. DRAG PICK CUTTING FORCES AND SIEVE ANALYSIS DATA .....	206
D. SAS OUTPUTS FOR STEPWISE AND MINIMUM $R^2$ IMPROVEMENT VARIABLE SELECTION METHODS.....	220
BIBLIOGRAPHY .....	229
VITA .....	245

## LIST OF ILLUSTRATIONS

Figure	Page
2.1. Tensile cracking leading to rock failure caused by drag bits and indenters .....	6
2.2. Three main drag pick types.....	7
2.3. V-Profile and constant cross-section disc cutter profiles.....	9
2.4. Single disc cutters .....	9
2.5. Herrenknecht 17 inch single disc cutter cross-section .....	10
2.6. Strawberry cutters .....	11
2.7. Parameters of the median crack configuration.....	14
2.8. Fracture zones in rock under the load of an indenter.....	16
2.9. Assumptions of tensile breaking theory.....	18
2.10. Interplay between pick width and spacing.....	20
2.11. Side chipping caused by tensile stresses .....	24
2.12. Schematic representation of wedge penetration and chip forming process .....	26
2.13. Longitudinal cross-section of cutter-rock contact area for CCS disc cutters.....	27
2.14. Chip formation in different situations.....	30
2.15. General effect of changing s/p ratio on cutter specific energy .....	31
2.16. Drained to undrained condition .....	46
2.17. Failure mechanisms in cone indentation test .....	47
3.1. Schematic view of linear rock cutting machine with disc cutter mounted .....	50
3.2. Schematic view of linear rock cutting machine with drag pick mounted.....	51
3.3. LRCM with long bladed disc cutter .....	52
3.4. Long bladed disc cutter assembly and 3-D load cell .....	52
3.5. LRCM with drag pick .....	53
3.6. Drag pick assembly and 3-D load cell .....	53
3.7. Forces acting on a disc cutter while cutting.....	54
3.8. Forces acting on a drag pick while cutting .....	54
3.9. Drag pick .....	55
3.10. Schematic drawing of data acquisition and control systems for linear rock cutting machine .....	58

3.11. Data window showing 5 data cuts at 76.2 mm spacing .....	60
3.12. LRCM test nomenclature .....	60
3.13. Particle size distribution from a disc cutter data pass at $s = 114.3$ mm, $p = 12.7$ mm .....	61
3.14. Rock sample placed in the center of the upside-down rock box lined with thick plastic sheet .....	62
3.15. Casting a rock sample for LRCM testing .....	63
3.16. Wet surface reached at the top of the block after three days due to capillarity .....	65
3.17. A sandstone block totally submerged after wet surface reached the top .....	65
3.18. Perspective view of force directions .....	66
3.19. Moment arms for disc cutter .....	69
3.20. Moment arms for drag pick .....	69
3.21. Calibration of load transducer 2 for disc cutting tests .....	70
3.22. Calibration of load transducer 1 for radial pick tests .....	71
3.23. Directional arrangement of load transducers of 3-D load cell .....	71
3.24. Load-indentation test setup at Missouri S&T .....	73
3.25. Conical indenter used for load-indentation tests .....	74
3.26. Conical indenter geometry .....	74
3.27. Load-indentation sample cast in hydrostone .....	75
3.28. Bottom platen with pore pressure drainage channels, attached to pressure transducer .....	76
3.29. Load-indentation test schematic .....	77
3.30. Forney 181 ton testing machine .....	80
4.1. A trace of the forces recorded during one of the disc cutting tests .....	85
4.2. Grain size distribution curves for saturated rock cuts at $s = 152.4$ mm using long bladed CCS disc cutter .....	87
4.3. Determination of absolute size constant $x'$ and distribution parameter $b$ using Rosin-Rammler plot for a dry rock cut at $s = 114.3$ mm and $p = 12.7$ mm using long bladed CCS disc cutter .....	88
4.4. A trace of the forces recorded during one of the radial drag pick cutting tests .....	93
4.5. Example of tungsten carbide tips broken off during dry rock cutting .....	93
5.1. Force magnitude variation with cut spacing for dry rock .....	101
5.2. Force magnitude variation with cut spacing for saturated rock .....	101



5.3. Force magnitude variation with cutter penetration for dry rock .....	102
5.4. Force magnitude variation with cutter penetration for saturated rock .....	103
5.5. Specific energy variation with cut spacing for dry rock .....	104
5.6. Specific energy variation with cut spacing for saturated rock .....	105
5.7. Specific energy variation with cutter penetration for dry rock .....	106
5.8. Specific energy variation with cutter penetration for saturated rock .....	106
5.9. Specific energy variation with s/p ratio for dry rock tests .....	108
5.10. Specific energy variation with s/p ratio for saturated rock tests .....	108
5.11. 3-D surface plot of nominal SE vs cut spacing and cutter penetration for dry rock cuts with disc cutter.....	109
5.12. 3-D surface plot of actual SE vs cut spacing and cutter penetration for dry rock cuts with disc cutter.....	109
5.13. 3-D surface plot of nominal SE vs cut spacing and cutter penetration for saturated rock cuts with disc cutter .....	110
5.14. 3-D surface plot of actual SE vs cut spacing and cutter penetration for saturated rock cuts with disc cutter .....	110
5.15. Cutting coefficient variation with cutter penetration for dry rock .....	111
5.16. Cutting coefficient variation with cutter penetration for saturated rock .....	112
5.17. Cutting coefficient variation with cut spacing for dry rock .....	113
5.18. Cutting coefficient variation with cut spacing for saturated rock .....	114
6.1. Effect of depth of cut on cutting forces .....	118
6.2. Effect of depth of cut on normal forces .....	118
6.3. Conditioned rock surface for data pass at s=88.9 mm, d=6.4 mm before cutting ...	119
6.4. Rock surface after cutting .....	119
6.5. Force magnitude variation with cut spacing for dry rock cuts.....	120
6.6. Force magnitude variation with cut spacing for saturated rock cuts .....	120
6.7. Actual specific energy variation with depth of cut for dry and saturated rock .....	121
6.8. Variation in actual and nominal SE with depth of cut for dry rock cuts .....	122
6.9. Variation in actual and nominal SE with depth of cut for saturated rock cuts .....	122
6.10. Specific energy variation with cut spacing for dry rock cuts.....	124
6.11. Specific energy variation with cut spacing for saturated rock cuts .....	124
6.12. A typical dry rock data pass at wide cut spacing and shallow depth of cut before chip collection .....	125

6.13. A typical saturated rock data pass at wide cut spacing and shallow depth of cut before chip collection .....	125
6.14. Variation in actual and nominal SE with s/d ratio for dry rock cuts.....	127
6.15. Variation in actual and nominal SE with s/d ratio for saturated rock cuts .....	127
6.16. Relationship between actual specific energy and production rate .....	128
6.17. 3-D surface plot of nominal SE vs cut spacing and depth of cut for dry rock cuts with drag pick .....	130
6.18. 3-D surface plot of actual SE vs cut spacing and depth of cut for dry rock cuts with drag pick.....	130
6.19. 3-D surface plot of nominal SE vs cut spacing and depth of cut for saturated rock cuts with drag pick .....	131
6.20. 3-D surface plot of actual SE vs cut spacing and depth of cut for saturated rock cuts with drag pick .....	131
7.1. Nominal and actual production rate for saturated rock tests.....	136
7.2. Nominal and actual production rate for dry rock tests.....	136
7.3. Breakage pattern in saturated sandstone for a data pass before chip collection .....	137
7.4. Rock surface condition after chip collection .....	138
7.5. Variation of absolute size constant with coarseness index .....	140
7.6. Relationship between percentage of large chips (> 51 mm or 2 inches) and $x'$ .....	140
7.7. Relationship between percentage of large chips (> 51 mm or 2 inches) and CI .....	141
7.8. Production rate variation with absolute size constant.....	142
7.9. Production rate variation with coarseness index.....	143
7.10. Variation of absolute size constant with cut spacing .....	144
7.11. Coarseness index variation with cut spacing .....	144
7.12. A typical saturated rock cut at wide cut spacing and shallow penetration (s=152.4 mm, p=6.4 mm), before chip collection.....	145
7.13. Relationship between CI and SE for dry and saturated cutting tests .....	146
7.14. Relationship between $x'$ and SE for dry and saturated cutting tests .....	147
7.15. Effect of s/p ratio on SE and CI for saturated sandstone .....	148
7.16. Effect of s/p ratio on SE and CI for dry sandstone .....	149
7.17. SE and production rate variation with cutter penetration for dry cuts.....	150
7.18. SE and production rate variation with cutter penetration for saturated cuts.....	150
7.19. Variation of absolute size constant with coarseness index .....	152

7.20. Relationship between percentage of large chips (> 51 mm or 2 inches) and absolute size constant .....	152
7.21. Actual SE variation with absolute size constant .....	153
7.22. Variation in actual SE with coarseness index .....	154
8.1. Rock failure signatures, representing (L to R) soft, plastic rock; medium hard, elastic rock; and very hard, brittle rock .....	158
8.2. Formation of crushed zone under the indenter in a saturated sandstone sample .....	160
8.3. Load and indentation pressure versus displacement for a typical dry sandstone sample .....	160
8.4. Load and porewater pressure versus displacement for a typical saturated sandstone sample .....	162
8.5. Total load, effective load and indentation pressure versus displacement calculated for the same saturated sandstone sample .....	162
8.6. Box plot of SP values for dry and saturated samples showing mean, median, highest, lowest, 1 <sup>st</sup> quartile, and 3 <sup>rd</sup> quartile values .....	166
8.7. Box plot of SE values for dry and saturated samples showing mean, median, highest, lowest, 1 <sup>st</sup> quartile, and 3 <sup>rd</sup> quartile values .....	166
8.8. Point of impact necessary for water jet to exploit rock damage caused by drag bit .....	167
8.9. Contact shapes of the disc cutter and the drag pick used .....	171
8.10. Comparison of % fines produced for data passes at $s = 76.2$ mm for disc cutter and drag pick at matching penetration levels (6.4 mm, 9.5 mm and 12.7 mm) for dry and saturated cutting tests .....	171

## LIST OF TABLES

Table	Page
3.1. Disc cutting experimental matrix for saturated blocks .....	56
3.2. Disc cutting experimental matrix for dry blocks .....	56
3.3. Test matrix for dry and saturated experiments with radial drag pick .....	57
3.4. Physical properties of the rock samples used .....	81
4.1. Test results for long bladed CCS disc cutter in dry sandstone .....	83
4.2. Test results for long bladed CCS disc cutter in saturated sandstone .....	84
4.3. Example to indicate calculation of coarseness index (CI) for saturated rock at s=152.4 mm and p=16 mm for long bladed CCS disc cutter .....	87
4.4. Computed cutting parameters for CCS disc cutter in dry sandstone .....	89
4.5. Computed cutting parameters for CCS disc cutter in saturated sandstone .....	90
4.6. Cutting test results for radial drag pick in dry sandstone.....	91
4.7. Cutting test results for radial drag pick in saturated sandstone .....	92
4.8. Computed cutting parameters for radial drag pick in dry sandstone .....	94
4.9. Computed cutting parameters for radial drag pick in saturated sandstone .....	95
4.10. Summary of load-indentation tests on saturated sandstone .....	98
4.11. Summary of load-indentation tests on dry sandstone .....	98
5.1. Comparative average forces and specific energy for dry and saturated sandstone using long bladed single disc cutter .....	100
6.1. Comparative average forces and specific energies with related statistical parameters .....	115
6.2. The p-values of means comparison for each spacing and depth of cut combination tested in both dry and saturated cutting.....	116
7.1. Parameter estimates from minimum $R^2$ improvement method for dry tests.....	156
7.2. Parameter estimates from minimum $R^2$ improvement method for saturated tests.....	156
8.1. Contact area differences between disc cutter and drag pick at same penetration or depth of cut .....	170

## NOMENCLATURE

Symbol	Description
<i>TBM</i>	Tunnel Boring Machine
<i>RBM</i>	Raise Boring Machine
<i>CCS</i>	Constant Cross-Section
<i>LRCM</i>	Linear Rock Cutting Machine
<i>RRCM</i>	Rotary Rock Cutting Machine
<i>CI</i>	Coarseness Index
<i>PR</i>	Production Rate
$x'$	Rosin-Rammler Absolute Size Constant
$s$	Cut Spacing
$p$	Cutter Penetration
$d$	Depth of Cut
$s/d$	Spacing to Depth of Cut Ratio
$s/p$	Spacing to Penetration Ratio
<i>LVDT</i>	Linear Variable Differential Transducer
$\sigma_c$	Uniaxial Compressive Strength of Rock
$\sigma_t$	Brazilian Tensile Strength of Rock
<i>UCS</i>	Uniaxial Compressive Strength
<i>BTS</i>	Brazilian Tensile Strength
$V_v$	Volume of Voids
$V$	Volume of Solids
$n$	Rock Porosity
$M_{sat}$	Saturated Mass
$M$	Grain Mass
$\rho_w$	Density of Water
$\rho$	Rock Density
$\rho_d$	Dry Mass Density
$F_N$	Normal Force (Disc Cutter)
$F_R$	Rolling Force (Disc Cutter)

$F_S$	Side Force (Disc Cutter)
$F_d$	Drag or Cutting Force (Drag Pick)
$F_n$	Normal Force (Drag Pick)
$F_s$	Side Force (Drag Pick)
$CC$	Cutting Coefficient
$SE$	Specific Energy
$SE_A$	Actual Specific Energy
$SE_N$	Nominal Specific Energy
$L$	Length of Cut
$\bar{R}$	Average Rolling Force
$m$	Mass of Chips
$PR_N$	Nominal Production Rate
$PR_A$	Actual Production Rate
$PR_L$	Chips > 51 mm or 2 inches
$v$	Cut Speed
$R$	Cumulative Mass (Volume) % Retained on Sieve of Size x
$b$	Distribution Parameter
$F_{pw}$	Porewater Force
$P_{pw}$	Porewater Pressure
$A_{dr}$	Area of Porewater Drainage Tube
$L_{eff}$	Effective Load under the Indenter
$L_{total}$	Total Load under the Indenter
$P_{indenter}$	Indenter Pressure
$S$	Indenter Footprint Surface Area
$SP$	Specific Penetration
$L_p$	Peak Load
$P_p$	Indenter Penetration at Peak Load
$ICR$	Instantaneous Cutting Rate
$HP$	Cutterhead Power
$SE_{opt}$	Optimum Specific Energy
$RPM$	Revolution per Minute

<i>RMR</i>	Rock Mass Rating
<i>RQD</i>	Rock Quality Designation
<i>RMCI</i>	Rock Mass Cutting Index
<i>ROP</i>	Rate of Penetration
<i>A</i>	Tunnel Area

# **1. INTRODUCTION**

## **1.1. BACKGROUND**

As this planet's population continues to grow, the infrastructure that supports it, must be created and maintained in less easily managed environments, including those below the water table and or beneath bodies of water. Not just harbor work, but also tunnels, shafts and foundations are increasingly being constructed under conditions where dewatering is not feasible.

For example, the growing sizes of the ships involved in international commerce, both in the United States and around the world, demand much deeper ports for the new and planned ultra-large container vessels. For many of these projects, dredging of unconsolidated sediments has reached the limits of what it can do. The port of New York/New Jersey was recently deepened to 16 m (50 ft.) (Ashar, 2004), but explosives had to be used because much of its bottoms in bedrock. The blasting was designed to fragment the rock just enough to allow cutter suction dredgers to excavate it, but the process was discontinuous, requiring two steps, and often generated complaints from shore. Underwater blasting is difficult, dangerous, and expensive. Yet as deepwater port facilities are forced to expand, more dredging will be required in the bedrock. One cost-effective answer is to improve the range of rocks that can be mechanically excavated by dredging. This would be a single-step continuous process, reducing the environmental impact of dredging in rock.

Underwater mechanical excavation is not a novel concept. Cutter suction dredgers are often used in shallow-water mining and infrastructure maintenance; however, their application is limited to loose unconsolidated materials and relatively weak rocks (Miedema, 2010). This application could be expanded significantly with the better understanding of saturated rock fragmentation mechanisms.

Moreover, the growing U.S. and the world population necessitate the expansion of subsurface infrastructure in the urban areas. Roughly 33% of the Earth's population lived in cities in 1950; by 2000, that portion was 50% and world population had risen to 6 billion (Parker, 2004). By 2030, this portion is expected to be 61% of a world population of 8.1 billion (Godard, 2004). Additionally, the number of cities with population over 10



million will increase from 19 in 2001 (including New York and Los Angeles) to 60 in 2015. Robust, reliable infrastructure is especially important for these megacities, while their high human densities simultaneously force that infrastructure increasingly underground. In the U.S. alone, projected expenditures for tunneling increased from \$19 billion to \$32 billion between 2001 and 2005 (Monsees, 2006). Approximately 72 miles of tunnels have been constructed for U.S. roadways (Abramson, 2006). Rail and water conveyance tunnels add to this total.

In mining applications, little information is available regarding the actual development of mine drifts. However, one can conservatively assume that each year about 50 miles of tunnels are driven by mining sector in hard rock in North America. This is about the same as the total annual civil tunnels (Rostami, 1997).

This rapid growth in the underground infrastructure development works and progressively increasing mining activity has increased the use of tunnel boring machines (TBM) as well as other mechanical excavators for the construction of tunnels, shafts, raises, and other mining related excavations. The traditional drilling and blasting technique is largely being replaced by these excavators. These excavators usually employ disc and drag cutters, which are exposed to a variety of ground conditions during their operation. While in some cases they cut dry rock, in reality, they are often used in wet conditions and in many instances in saturated rocks.

The cutting forces acting on disc and drag cutters have been extensively studied in different rock types from numerical, analytical and experimental perspectives (Roxborough and Rispin, 1973; Bilgin, 1977; Ozdemir et al., 1978; Sanio, 1985; Rostami and Ozdemir, 1993; Sato et al., 1991; Rostami, 1997; Yagiz, 2002; Gertsch et al., 2007 among many) but in most, if not all cases, the testing has been performed in dry rock. Meanwhile, it is well established that rock behavior changes at the presence of water and thus the cutting behavior of rock at various moisture contents and perhaps under saturated conditions, could impact the excavation rate of any given machine.

Improved quantification of the differences between cutting dry and saturated rock would help to improve:

- Mechanical excavation of tunnels, foundations, and other engineered cavities in saturated rocks.

- Mining of orebodies located in saturated rock formations, leading eventually to fully autonomous mining of formerly inaccessible mineral deposits.
- Dredging of hard-bottomed channels, ports, and harbors for deeper-draught ships and more frequent ship traffic.
- Exploration and extraction of reservoirs of oil, natural gas, and potable groundwater.

The aforementioned industries traditionally base production estimates on procedures derived from studies of dry rock. Such endeavors involve economic and environmental risks, which would be lessened with improved understanding of saturated rock excavation.

## **1.2. OBJECTIVE**

The main objective of this study is to add to the body of knowledge on the excavation of rock for engineering purposes, specifically the effects of water saturation. This study, through a comprehensive set of full scale fragmentation experiments, finds the differences between cutting dry and saturated rock.

## **1.3. APPROACH**

To achieve the targets of the study, two major types of rock cutting tools, disc and drag type cutters, were chosen. These types of cutting tools are representative of the industry practice and are widely employed on the rock excavation machines like, TBMs, raise and shaft borers, roadheaders, drum shearers, continuous miners, cutter suction dredgers and several other excavators. The chosen disc cutter was a constant cross-section (CCS) long bladed single disc cutter, whereas, one type of radial drag pick was selected as a drag cutter. Full scale linear rock cutting machine (LRCM) which is a basic research device used for parameters estimate of the mechanical excavators, was used for all full scale rock cutting experiments. The cutting experiments were conducted on dry and saturated blocks of one rock type (Roubidoux Sandstone).

Dry and saturated rock core samples were subjected to necessary rock physical property measurement tests. Rock cutting forces (normal, rolling or drag, side) measured

from full scale LRCM tests, were analyzed in detail for both dry and saturated cutting conditions. Differences in cutting forces for both the conditions were evaluated. The measured cutting forces were used for calculation of cutting specific energy values. The chips/fragments produced from all cutting tests were subjected to sieve analysis, which was further used for computation of different performance indices like coarseness index ( $CI$ ), production rate ( $PR$ ) and Rosin-Rammler absolute size constant ( $x'$ ). The relationships of these indices with the specific energy of cutting were evaluated for both the dry and saturated cutting conditions. Statistical analyses of the cutting forces, specific energy and other performance related parameters were performed to validate the differences between dry and saturated cutting conditions.

Load-indentation tests with porewater pressure measurement facility were designed to measure excess porewater pressure buildup under an indenter. These tests were conducted to evaluate the possible role of porewater pressure buildup in the rock fracture process under an indenter like a disc cutter.

## 2. LITERATURE REVIEW

The literature presented in this section is divided into three main parts; rock cutting literature, saturation effects on physical properties of rocks and saturated rock excavation. A limited number of research studies have been done on rock saturation effects on mechanical excavatability.

### 2.1. ROCK CUTTING LITERATURE

**2.1.1. Rock Cutting Tools.** Mechanical excavators like tunnel boring machines (TBM), raise boring machines (RBM), roadheaders, mobile miners, continuous miners and other excavation machines are employed in the mining and tunneling industry to achieve rock breakage. All these machines transfer energy to the rock surface through an array of cutting tools which in effect impart rock breakage. Different types of cutting tools are employed on these excavation machines depending upon the needs and conditions of the job. Two commonly employed types of cutting tools on these machines are drag tools and the roller cutters.

All types of roller cutters, disc cutters, rolling cone bits, etc. break the rock in an indentation process. Similarly, all types of percussive tools, including percussion drill bits, down-hole drill bits and high-energy impact bits induce rock fracture by indentation. Only rotary drill bits and drag picks such as those employed on coal excavation machines break the rock by applying the main force in a direction parallel to the rock surface. (Hood and Roxborough, 1992).

The breakage mechanism of drag tools and indenters is different. A drag tool breaks rock as it moves in a direction parallel to the rock surface, whereas rolling tools indent the rock under a normal force to achieve fragmentation. The wedging action of sharp drag picks produces tensile stresses in the rock in a fairly direct manner. An indenter applies a compressive load to the rock, forming a zone of crushed and confined rock beneath the tool. Continued application of this load causes tensile stresses to be induced in the rock surrounding this crushed zone (Hood and Alehossein, 2000) (Figure 2.1). Each tool has relative merits and limitations which will be discussed in this section.

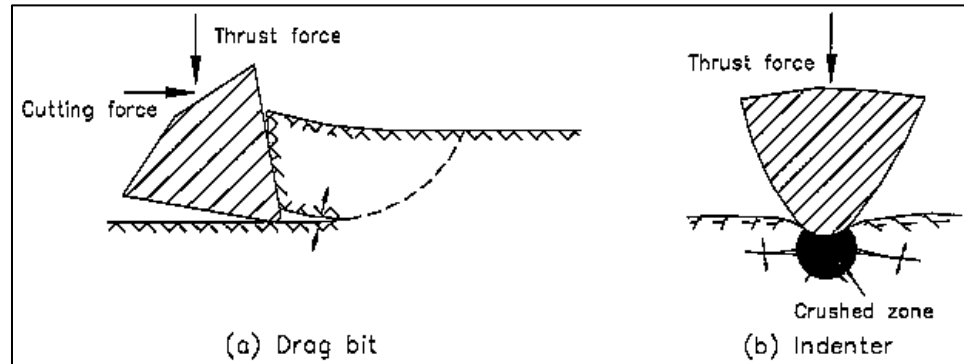


Figure 2.1. Tensile cracking leading to rock failure caused by drag bits and indenters (after Hood and Alehossein, 2000)

**2.1.1.1 Drag tools.** Drag tools/picks are limited to rock cutting applications in weak to moderate strength rocks of low abrasivity. This type of tool is usually employed on several types of underground and surface excavators including roadheaders, continuous miners, drum shearers, surface miners, chain cutters, road planers and trenchers. These tools comprise an alloy steel body with a tungsten carbide insert cutting tip, though alloy steel tips are used in weak, non-abrasive applications (Fowell, 1993). Drag picks are unsuitable for excavation in rock where the unconfined compressive strength (UCS) exceeds 80 MPa (11,600 psi); feasible UCS may be no more than 40-50 MPa (5800-7250 psi) when the rock is abrasive or massive (Roxborough and Sen, 1986). However, use of high pressure waterjet has been reported to have increased a roadheader's cutting capability to 150 MPa (22,000 psi) compressive strength (Summers, 1995).

Drag picks can be categorized into three main types, namely; radial picks, pointed picks or point attack picks, and forward attack picks (Figure 2.2).

Radial picks or simple wedge (chisel) is the most efficient shape of pick. When operating at the same cutting depth, a wedge shaped pick always requires a lower specific energy than any alternative shape. The wedge, however, requires higher cutting and normal forces than other shapes to achieve and maintain that depth of cut. The apparent incongruity of the wedge's higher cutting force, resulting in a lower specific energy, is accounted for by the fact that for a given cutting depth it produces a much higher yield

than other shapes. The reason that more complex shapes (like point attack picks) are often preferred in practice lies in the fact that their better penetrating capabilities enable them to cut deeper than the wedge for a given availability of normal force (Roxborough and Sen, 1986). Radial picks are the most efficient tools only when they are new. The slightest visible wear on the tip of a radial pick can increase normal force requirements by two to three times (Cigla and Ozdemir, 2000). Although the geometry of simple chisel tools is very efficient, in rock cutting practice radial drag tools of complex geometries (with varying base and side rake angles along with front rake and back clearance angles) are preferred because of their improved durability (Altinoluk, 1981; Fowell et al., 1987).

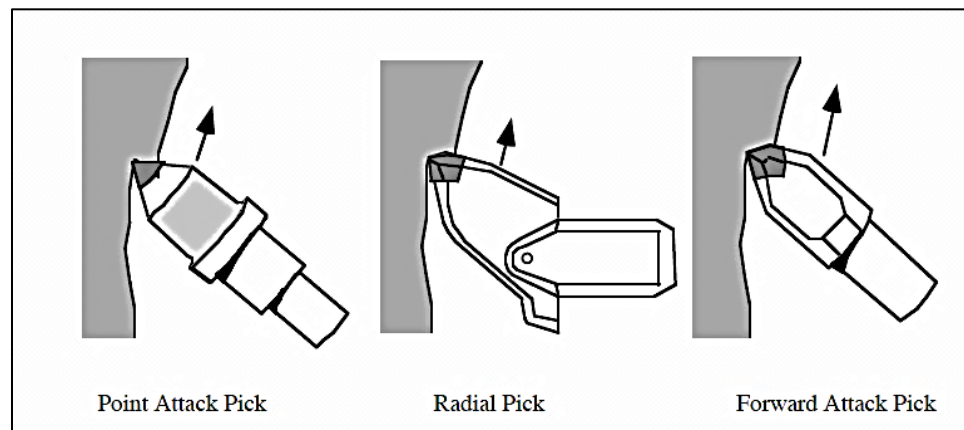


Figure 2.2. Three main drag pick types (after Summers, 1995).

Point attack picks are considered to be probably stronger than radial picks in respect of high rates of heavy impact loading, especially when applied axially (Morris, 1985). Point attack picks are very popular on excavation machines, having the advantage that the cutting tool rotates in the pick holder, forming a stabilized geometry as the rock being excavated wears away the carbide and parent steel (Fowell, 1993). However, the ability of point attack picks to rotate freely is often lost in practice due to uneven wear and other operational and design reasons (Fowell et al., 1987; Yilmaz et al., 2007). Roxborough (1985) measured the effect of such wear and found two to three times

increase in cutting forces and specific energy and three to five times increase in normal force.

Forward attack picks are designed in such a way that they can be set at any attack angle, but they have decreased in popularity (Hurt, 1988). Forward attack picks are designed to allow greater axial thrust to be transmitted during the cutting mode. The pick box is more favorably aligned to accept large cutting forces. The pick shank is less vulnerable to radial damage in the forward attack cutting mode (Whittaker and Frith, 1990).

**2.1.1.2 Roller cutters.** For hard and abrasive rock conditions roller cutters are the choice. Roller cutters roll about their axes over the rock surface to impart breakage. Roller cutters are employed on full face excavation machines like tunnel boring machines, shaft and raise borers and blind-hole drills. These cutters require high level of thrust forces to maintain a certain level of penetration, required to break the rock. Different types of roller cutters are employed on excavators depending upon the job needs. Two very common types: disc cutters and strawberry cutters are discussed here.

Use of disc cutters on full face tunnel boring machines started in 1956 by an engineer James Robbins (Friant, 1997). Early disc cutters had a V-profile which were very efficient in cutting rock when relatively new and suffered rapid drop in efficiency as the tip wear started. Drop in efficiency was attributed to the increase in disc area of contact with rock requiring more thrust forces to maintain same level of penetration. V-profile disc cutters were replaced by constant cross-section (CCS) disc cutters in late 1970s, which maintain the same cutting efficiency as the tip wears out (Figure 2.3).

Single disc cutters (Figure 2.4 and Figure 2.5) are the most commonly used roller cutters on hard rock tunnel boring machines. These cutters have replaceable disc rings of special hardened steels, selected to achieve a desired balance between hardness, toughness and abrasion resistance. In softer rock, where cutter loading is lower and less variable, disc material with reduced fatigue life but with increased material hardness may be chosen. In stronger rock, high thrust and impact loads are expected, and so fatigue, toughness and abrasion properties must be balanced. In extremely abrasive rock, tungsten carbide discs may be used. Typical CCS cutter tip widths are 12-19 mm (0.47-0.75 in),

and allowable cutter loading has increased from 220 kN up to about 270 kN (Nelson, 1993).

Single disc cutters provide true rolling action and are the most efficient type of the cutters since the entire load on a single disc cutter is concentrated on one edge which develops high stresses and allows for deep penetration. Multi-row disc cutters in one bearing are not very efficient since they suffer from low edge loading (Ozdemir, 1995).

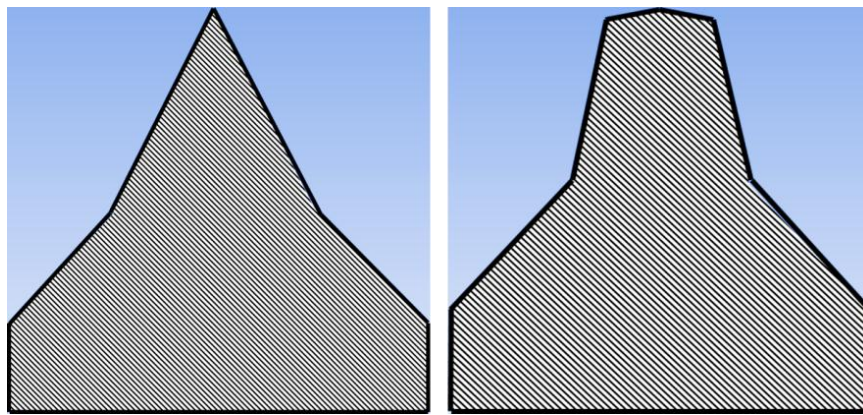


Figure 2.3. V-profile and constant cross-section disc cutter profiles.



Figure 2.4. Single disc cutters (Herrenknecht cutter tools, 2012).



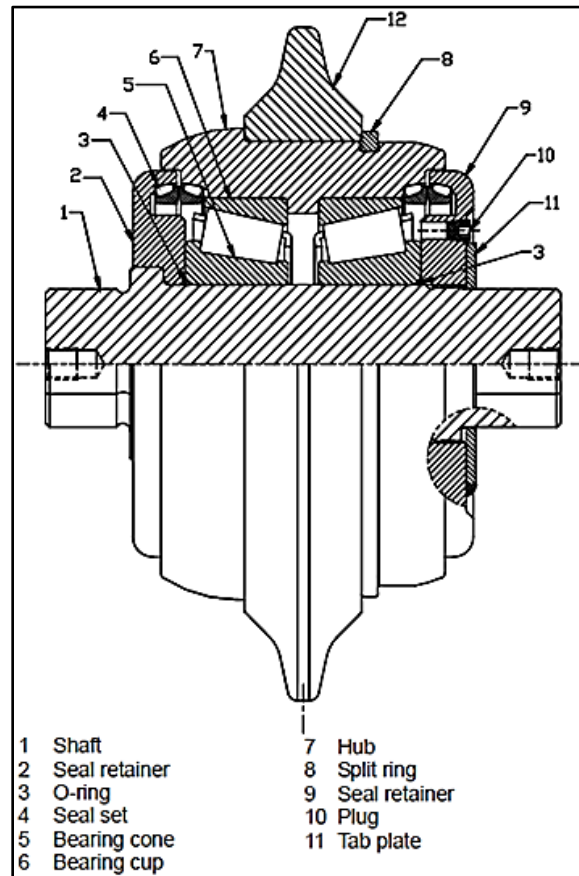


Figure 2.5. Herrenknecht 17 inch single disc cutter cross-section (Frenzel, 2011).

The second type of roller cutters is the button or strawberry cutters (Figure 2.6). This type of cutter is highly inefficient in terms of specific energy, since the rock excavation process is by virtue of grinding and pulverizing action rather than by creating fragmented chips of rock. Although the penetration rate is likely to be slow with the production of large amount of fines, this type of cutter is the most successful type for the highest strength of rocks likely to be encountered in machine tunneling (Thon, 1983). This type of cutter is true rolling at only one radius on the machine; at other locations, cutter skidding occurs, causing accelerated wear of the carbides, increased rolling friction and consequently higher machine torque requirements (Ozdemir, 1995). Button cutters are used on raise boring and shaft drilling applications. These are advantageous in that they last longer in terms of footage bored, requiring less often cutter change operations.

This feature is highly beneficial for raise and shaft boring to minimize the cutter changes since the face is inaccessible (Cigla and Ozdemir, 2000).



Figure 2.6. Strawberry cutters (Sandvik raise boring users manual, 2012).

**2.1.2. Mechanical Rock Fragmentation.** Research studies on mechanical rock fragmentation process can be divided into the following categories (Rostami, 1997).

- Study of the indentation process in small scale laboratory tests,
- Investigations of the rock cutting process by using full scale tests under controlled conditions in the laboratory,
- Evaluation of the machine performance and geological parameters in the field.

**2.1.2.1 Rock indentation studies.** Most rock drilling and rock cutting methods are characterized by the indentation of a tool into a rock surface. The type of stresses generated due to indentation may vary, according to tool shape, tool geometry, direction of load or loading rate, but principally a static or quasi-static indentation process causes rock fragments to be removed from the rock surface.

A number of investigators have studied the rock fracture mechanism under an indenter from analytical, numerical and experimental perspectives. A main requirement for a sound treatment of an indentation problem is a good knowledge of the stress field imposed by the indenter. Boussinesq (1885) presented the first analytical solution to the stress field generated under a point-load in an elastic half-space, called the Boussinesq field, which was later calculated and analyzed by Lawn and Swain (1975). Numerous investigators have proposed failure models explaining the force-indentation behavior of rocks based on these solutions.

Tandanand and Hartman (1961) showed that the stresses beneath a wedge were similar to those produced by a line load on a semi-infinite plate and the geometry of the chips produced was dependent upon the cutter's wedge angle and the amount of applied load.

Reichmuth (1963) developed a model based on elastic analysis (Equation 2.1). The model provides a relationship between the semi-included bit tooth angle  $\beta$  and the coefficient of sliding friction  $\mu$  at the rock-bit interface:

$$\beta = \tan^{-1}\left(\frac{\pi-2\mu}{2+\pi\mu}\right) \quad (2.1)$$

If  $\beta$  is numerically greater than the expression on the right-hand side of the equation, the stress distribution is effectively localized in a region below the penetrating tooth, thereby causing considerable crushing and compaction of rock and inhibiting the formation of chips. Conversely if  $\beta$  is numerically less, fractures develop close to the rock's surface, resulting in the formation of chips with comparably little crushing and compaction (Cheatham and Gnirk, 1966).

Paul and Sikarskie (1965) developed a model to explain the mechanics of rock breakage process due to static indentation of a rigid wedge. It was concluded in the model

that the failure of rock along the fracture plane occurs when the Coulomb-Mohr failure criterion is satisfied. Moreover, it was concluded that the chipping ceases if the sum of the half angle of the penetrating wedge and the angle of internal friction exceeds  $90^\circ$ . If the sum was exceeded the entire wedge penetration process was due to crushing.

Benjumea and Sikarskie (1969) extended the work of Paul and Sikarskie to explain the effects of bedding planes on the existing wedge penetration theory for isotropic brittle materials. To extend the earlier theory to the anisotropic materials, they utilized Jaeger's modification of the Coulomb-Mohr failure criterion. Their experiments concluded that a wedge angle greater than  $120^\circ$  caused rock powder under the indenter instead of chipping.

Lindqvist (1982) introduced fracture mechanics principles in indentation studies and tested a model developed by Lawn and Swain (1975) to compare the median crack length developed in load-indentation tests. This model (Equation 2.2) was developed to calculate "median crack" length ( $C$ ), which is a crack parallel or at an acute angle to the loading direction (Figure 2.7).

$$C = F \left( \frac{\psi(\nu)}{2\Gamma} \right) \left( \frac{\alpha}{\beta^2} \right) \left( \frac{H}{E} \right) \quad (2.2)$$

Where

$F$ = Applied load (kN)

$\psi(\nu) = (1 - \nu^2)(1 - \nu)^2 / 2\pi^4$

$\Gamma$ = Crack surface energy ( $\text{J/m}^2$ )

$H$ = Hardness  $\approx p_0$ = constant, if the contact complies with the principle of geometric similarity, e.g. as with Vickers pyramidal indenter.

$E$ = Young's modulus

$\alpha$ = Rock constant

$\beta = (z_0/a)$  reflects the depth of inelastic zone, where  $z_0$  is the depth of indenter.

$a$ = Radius of indenter (mm)

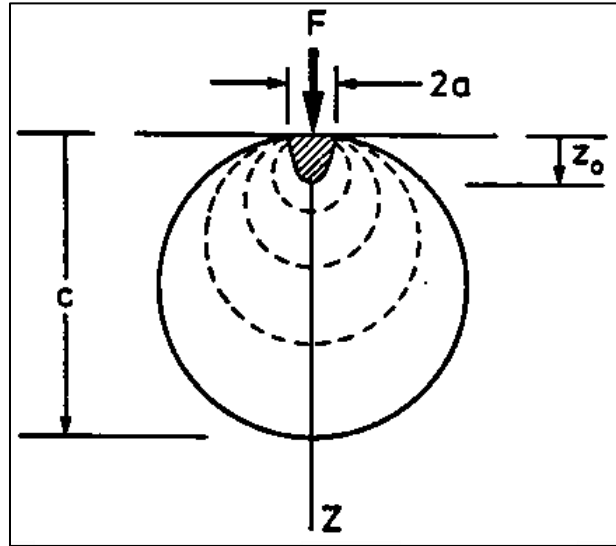


Figure 2.7. Parameters of the median crack configuration. Broken lines represent stress contours, heavy line shows crack profile, and shading indicate inelastic deformation zone (after Lawn and Swain, 1975; Lindqvist, 1982).

Cook et al. (1984) performed a series of tests to study the rock fragmentation process induced by circular flat-bottomed punches from 5 to 20 mm diameter loading flat surface of cylindrical samples of Sierra granite. They found that the rock deforms elastically until the applied load exceeds 45% of the maximum load that the rock could sustain. At loads greater than 45% of the maximum, a crack is initiated around the perimeter of the punch and this crack propagates in the well-known conical Hertzian manner. They proposed an equation for estimating the stress required by an indenter to penetrate a certain distance into the rock as follows:

$$\sigma_n = \frac{E.p}{0.54(1-\nu^2)a} \quad (2.3)$$

Where

$\sigma_n$  = Normal stress under the indenter

$E$  = Elastic modulus of rock

$p$  = Average displacement of the punch

$\nu$  = Poisson's ratio

$a$  = Area of indenter

Peng et al. (1989) proposed a model for simulating the force-indentation behavior considering conical and wedge shaped indenters. The model was mainly dependent on the geometry of the indenter tip-rock contact area. The force required for a wedge shaped indenter was calculated as:

$$F_s = \sigma_0 (\sin \theta + \mu \cos \theta) \left( \frac{2wx}{\cos \theta} \right) \quad (2.4)$$

For conical shape indenters:

$$F_s = \left[ \sigma_0 (\sin \theta + \mu \cos \theta) \left( \frac{\pi \tan \theta}{\cos \theta} \right) \right] x^2 \quad (2.5)$$

Where

$F_s$  = Normal force

$\sigma_0$  = Constant stress in crushed zone

$\theta$  = Half-cone angle

$w$  = Width of indenter

$x$  = Depth of indentation

Peng et al. also reported that the models based on Coulomb-Mohr failure criterion overpredict the force necessary for chipping. In their model, the failure strength of brittle rock was modified by a Weibull parameter to account for a size effect and tip shape factor.

All the theoretical models developed to study the load indentation process have consensus in one way or other about the chip forming process under an indenter. Figure 2.8 shows the indentation process of rock under an indenter. When an indenter is loaded on a rock surface, stresses are built up underneath the area of contact. The stresses increase with increasing load and the material is deformed elastically. At the contact surface irregularities deform and beneath the indenter a zone of crushed rock is developed. This crushed zone behaves as a plastic zone. The plastic zone distributes the applied load as stresses to the surrounding rock, in all directions as the indenter continues to penetrate the rock. Radial cracks are propagated around the crushed zone as the applied load and stresses in the plastic zone increase. When the load reaches a sufficient level, a chip is formed and the stresses are released. The stored energy in the chip is

released as the chip moves out of the way. Each time a chip is formed the load drops temporarily and must be built up to a new, higher level to achieve chipping. The crushing and chipping creates a crater.

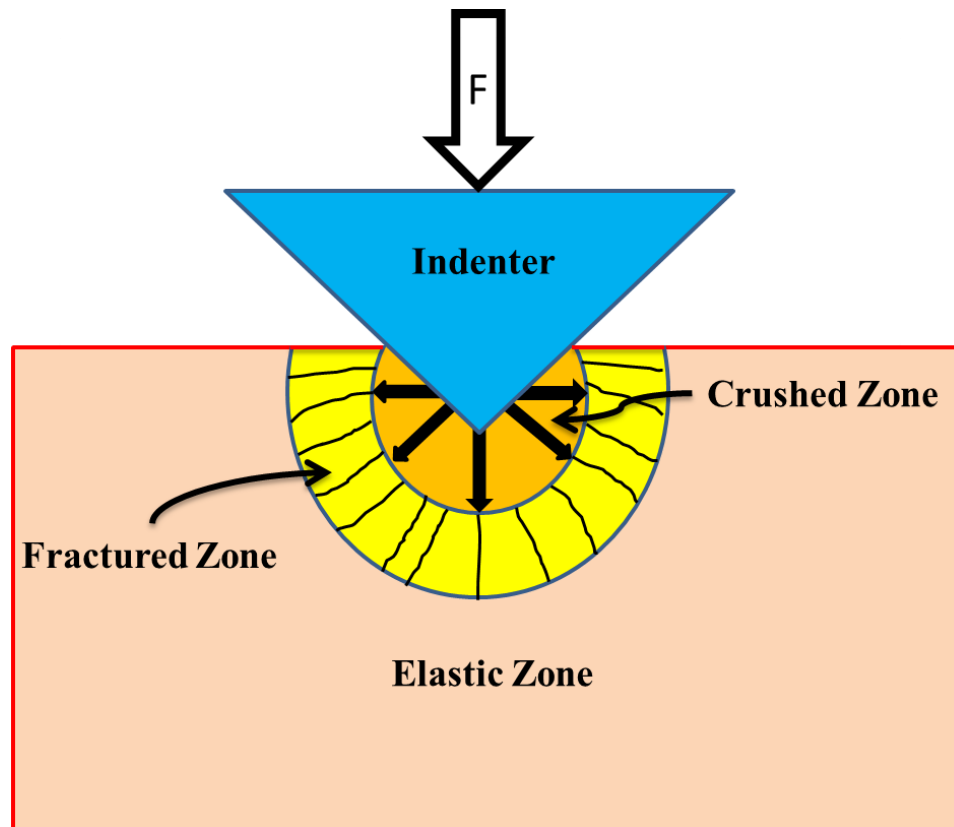


Figure 2.8. Fracture zones in rock under the load of an indenter.

**2.1.2.2 Theoretical studies on drag pick cutting.** Potts and Shuttleworth (1958) adopted and modified the Merchant (1954) theory, initially developed for metal cutting, to study the coal cutting process. This was one of the earliest attempts to model the rock cutting forces with drag tools. They assumed that coal cutting by a plane cutting blade and wedge was a discontinuous process of shear failure instead of continuous cutting as in metals. The cutting force  $F_c$  required to form a major chip was given by the following equation (Whittaker et al., 1992).

$$F_c = \frac{\tau_c \cdot d \cdot W \cdot \cos(\phi' - \alpha)}{\sin \phi \cdot \cos(\phi' + \phi - \alpha)} \quad (2.6)$$

Where

$F_c$  = Cutting force

$\tau_c$  = Shear strength of rock

$d$  = Depth of cut

$W$  = Width of wedge

$\alpha$  = Rake angle

$\phi$  = Angle of shear

$\phi'$  = Angle of friction between the wedge and rock

A good qualitative and limited quantitative value was ascribed to this model in that it:

- Indicated a linear increase in drag bit forces with depth of cut.
- Described the monotonic decrease in forces with increasing rake angle.
- Showed drag bit forces to increase linearly with rock strength, in this case specifically shear strength.

This model is limited, however, in the sense that it is two-dimensional, whereas rock cutting is a three-dimensional process. Moreover, the observed chip failure pattern caused by wedge penetration into coal was argued to be essentially tensile, rather than shear, in character (Hood and Roxborough, 1992).

The pioneering work explaining the rock failure mechanism ahead of the drag picks studying coal cutting was conducted by Evans (1962, 1965). The theory was largely based on observations of experiments. Evans considered that the breakage of coal is essentially tensile and occurs along a failure surface, which approximates a circular arc  $cd$ . Evans developed his model by studying the penetration of a wedge normal to a rock surface as shown in Figure 2.9. For a symmetric wedge the following equation was developed to calculate the tool cutting force:

$$F_c = \frac{2\sigma_t d \sin \theta}{1 - \sin \theta} \quad (2.7)$$

Since many cutting tools have the shape of a half-wedge, for this case the following relationship for the cutting force  $F_c$  was derived:



$$F_c = \frac{2\sigma_t dW \sin \frac{1}{2}(90-\alpha)}{1 - \sin \frac{1}{2}(90-\alpha)} (N) \quad (2.8)$$

Where

$\sigma_t$ = Tensile strength of rock (MPa)

$d$ = depth of cut (mm)

$W$ = width of the chisel shaped tool (mm)

$\alpha$ = Rake angle of the wedge ( $^\circ$ )

Evans showed that the friction between tool wedge and the rock can be taken into consideration by including the angle of sliding friction of rock against tool material  $\phi^{r,t}$ :

$$F_c = \frac{2\sigma_t dW \sin \{\frac{1}{2}(90-\alpha) + \phi^{r,t}\}}{1 - \sin \{\frac{1}{2}(90-\alpha) + \phi^{r,t}\}} (N) \quad (2.9)$$

Evans found the normal force component  $F_n$  in the case of a clearance angle of zero and taking rock-tool friction into consideration as:

$$F_n = \frac{F_c}{2 \tan(90-\alpha + \phi^{r,t})} (N) \quad (2.10)$$

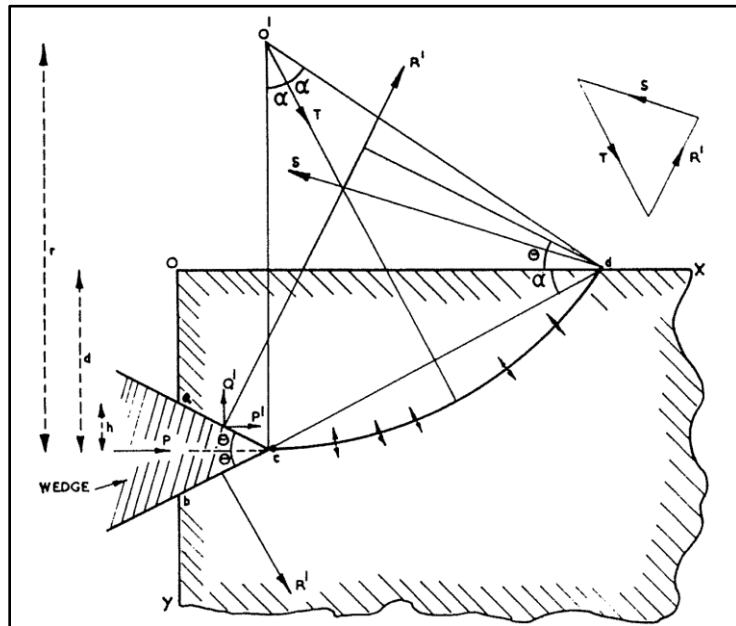


Figure 2.9. Assumptions of tensile breaking theory (after Evans, 1962).

Evans model matches observed trends almost exactly and so long as rock failure is occurring in tension, it gives force values that are in tolerable agreement with the measured data (Roxborough and Sen, 1986).

Evans (1984) also proposed a cutting model for point attack picks and derived the following equation:

$$F_c = \frac{16\pi\sigma_t d^2}{\sigma_c \cos^2 \theta} (N) \quad (2.11)$$

Where

$\sigma_t$  = Tensile strength of rock (MPa)

$\sigma_c$  = Compressive strength of rock (MPa)

$d$  = Depth of cut (mm)

$\theta$  = Cone angle of the pick point

It is observed in practice, however, that as the pick rake angle reduces, tensile failure eventually gives way to a process of shear failure (Roxborough and Sen, 1986). Nishimatsu (1972) developed a model for this situation by invoking Mohr-Coulomb failure criterion along a plane which predicts the cutting force required to cause failure by shearing. The formula of resultant cutting force per unit width of tool edge is given by:

$$F = \frac{2\tau_u d \cos \phi}{(n+1)[1 - \sin(\phi^{r,t} + \phi - \alpha)]} (N) \quad (2.12)$$

Where

$n$  = Stress distribution factor; a constant concerned with the state of stress in the rock-cutting process

$\tau_u$  = Unconfined shear strength of specimen rock (MPa)

$d$  = Depth of cut (mm)

$\phi^{r,t}$  = Angle of sliding friction between rock and tool ( $^\circ$ )

$\alpha$  = Rake angle of the cutting tool ( $^\circ$ )

$\phi$  = Angle of internal friction of the intact rock material ( $^\circ$ )

The cutting force  $F_c$  and the normal force  $F_n$  components of the resultant force  $F$  are:

$$F_c = F \cos(\phi^{r,t} - \alpha); F_n = F \sin(\phi^{r,t} - \alpha) \quad (2.13)$$

Nishimatsu determined  $\tau_u$  and  $\phi$  from Mohr-Coulomb failure criterion:

$$\tau_u = \frac{\sigma_c \sigma_t}{2 \sqrt{\sigma_t(\sigma_c - 3\sigma_t)}} (MPa); \quad \tan \phi = \frac{\sigma_c^2 - 4\tau_u^2}{4\sigma_c \tau_u} \quad (2.14)$$

Pomeroy and Brown (1968) observed in coal cutting that the volume excavated by a pick exceeds the volume swept by the pick. Roxborough (1973) extended the Evans cutting theory by considering the work done during rock cutting. When a pick cuts its way through the rock, rock breaks away at each side of the tool. This is termed as “sidesplay” or “breakout”. Amount of sidesplay increases with depth of cut. Although the resulting sides of the cut groove are irregular, it is possible to calculate an average breakout angle from measurement of the volume of the cut rock. Within reasonable limits in stronger rocks, this angle appears constant for different depths of cut. Roxborough recognized the fact that measurement of pick forces only was of little value unless some reference to the amount of rock excavated by the pick was made. Therefore, the parameter of specific energy was introduced, which was a measure of energy consumed in producing a fixed quantity of rock.

Roxborough (1973) calculated from the geometry of the cut (Figure 2.10), the area  $A$  of the excavated groove from:  $A = W \cdot d + d^2 \cdot \tan \theta$ ; and the volume:  $V = L \cdot (W \cdot d + d^2 \cdot \tan \theta)$ .

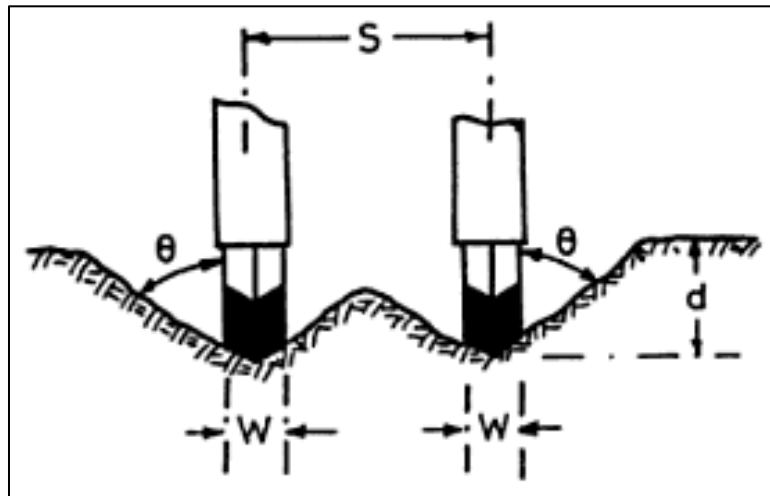


Figure 2.10. Interplay between pick width and spacing (Roxborough, 1973).

The work done in excavating the groove was given by:  $E = F'_c \cdot L$ . The specific energy,  $SE$  was given by:

$$SE = \frac{F'_c \cdot L}{A \cdot L} = \frac{F'_c}{W \cdot d + d^2 \cdot \tan \theta} \quad (2.15)$$

Where

$F'_c$  = Mean cutting force

$L$  = Length of cut

$d$  = Depth of cut

$S$  = Spacing between the adjacent cuts

$\theta$  = Breakout angle

To have an optimal array of cutting tools (giving minimum specific energy) on the cutting drum of the excavators, for chisel shaped tools, Evans (1972) estimated the optimum spacing using the width of the chisel ( $w$ ) and cutting depth ( $k$ ) by:

$$\frac{s}{w} = \frac{1}{2} \left\{ 1 + \sqrt{\left(1 + \frac{20}{k^2}\right)} \right\} \quad (2.16)$$

Roxborough (1973) introduced a relationship for finding an optimum spacing-to-depth of cut ratio ( $s/d$  ratio) where interaction between adjacent tools was maximized. Interaction between adjacent tools is likely to occur when the sidesplay produced by each tool meets or overlaps. If the breakout angle is constant, then the spacing between tools at which interaction begins, increases with depth of cut. The interaction between adjacent cuts begins when:

$$\frac{s}{d} < 2 \tan \theta \quad (2.17)$$

For pointed picks, Evans (1984) presented a solution for spacing between the adjacent picks using depth of cut ( $d$ ):

$$s = 2d\sqrt{3} \quad (2.18)$$

Where

$d$  = Depth of cut

$\tan^{-1} \sqrt{3} = 60^\circ$ ; the breakout angle caused by single point attack pick was found to be a constant of  $60^\circ$ .

Goktan (1997) proposed a modification in Evans' (1984) cutting theory for point attack picks. He proposed the following equation which fit the previously published experimental data.

$$F_c = \frac{4\pi\sigma_t d^2 \sin^2(\frac{\phi}{2} + \psi)}{\cos(\frac{\phi}{2} + \psi)} \quad (2.19)$$

Where

$\psi$ = Friction coefficient between cutting tool and rock

$\phi$ = Tip angle

$\sigma_t$ = Tensile strength of rock

$d$ = Depth of cut

**2.1.2.3 Theoretical studies on disc cutting.** It was postulated by Evans (1974) that the breakage caused by a disc cutter is in shear mode rather than a tensile mode. He assumed that the cross-section of a disc cutter is a wedge and the pressure exerted by the surfaces of the wedge cause failure of the rock along shear planes rising from the apex of the wedge to the surface of the material. He developed a model to calculate the disc cutting forces based on the principle of passive earth pressure on a retaining wall as used in Soil Mechanics:

$$F_c = 2 \left[ \frac{c.d.\cos\phi.\sin(\theta+\psi)}{\sin^2(\frac{\pi}{4} - \frac{1}{2}(\theta+\psi+\phi))} \right] \quad (2.20)$$

Where

$F_c$ = Thrust force on the disk necessary to form a rock chip

$d$ = depth of penetration of wedge

$\phi$ = Angle of internal friction of rock

$\psi$ = Friction angle between wedge and rock

$\theta$ = Half angle of wedge

$c$ = Cohesive strength of rock

Roxborough and Phillips (1975) developed a predictive model for disc cutting forces based on the basic principles and cutting geometry for calculation of theoretical

normal and rolling forces on a single V-profile disc cutter. They calculated the normal and rolling forces on the disc cutter from:

$$F_T = 4 \cdot p \cdot \sigma \cdot \tan \frac{\phi}{2} \cdot \sqrt{Dp - p^2} \quad (2.21)$$

$$F_R = 4 \cdot \sigma \cdot p^2 \cdot \tan \frac{\phi}{2} \quad (2.22)$$

Where

$\sigma$ = Uniaxial compressive strength of rock

$p$ = Cutter penetration

$D$ = Disc diameter

$\frac{\phi}{2}$ = Half angle of the disc

Ozdemir et al. (1976) developed a model for disc cutting forces incorporating spacing between adjacent discs, which was not taken into consideration in the earlier models. In developing this model, it was maintained that the magnitude of the thrust force depends in part on the compressive strength of the rock and in part on the shear component of this force that causes chips to form between adjacent cuts. The following model was developed for thrust ( $F_T$ ) and rolling ( $F_R$ ) force:

$$F_T = \tan \theta \sqrt{Dd^3} \left[ \frac{4C_0}{3} + 2S_0 \left( \frac{s}{d} - 2 \tan \theta \right) \right] \quad (2.23)$$

$$F_R = \frac{\tan \theta [d^2 C_0 + 4S_0 \Phi (s - 2d \tan \theta)]}{D(\Phi - \sin \Phi \cos \Phi)} \quad (2.24)$$

Where

$$\Phi = \cos^{-1} \left( \frac{D-2d}{D} \right)$$

$C_0$ = Compressive strength of rock

$S_0$ = Shear strength of rock

$D$ = Disc diameter

$d$ = Depth of cutter penetration

$s$ = Spacing between adjacent cuts

In contrast to the predictor equations of Roxborough and Phillips (1975) and Ozdemir et al. (1976), Lindqvist and Ranman (1980) developed a model based on the assumption that chipping is principally caused by tensile stresses. This model also assumes that the vertical thrust is mainly directed into the rock. The presumptive chip is only exposed to small horizontal (side) forces, in the case of multiple discs, two forces with opposite directions. The rock directly under the disc will be pressed down elastically. The potential chip is not in contact with them at all. The chip will be bent down near the discs by the elastic depression of a large rock volume. The stiffness of the chip will cause tensile stresses along a line between the disc edges. When the stiffness is high enough, a tensile crack will propagate from the extremely fissured rock near the edge (Figure 2.11).

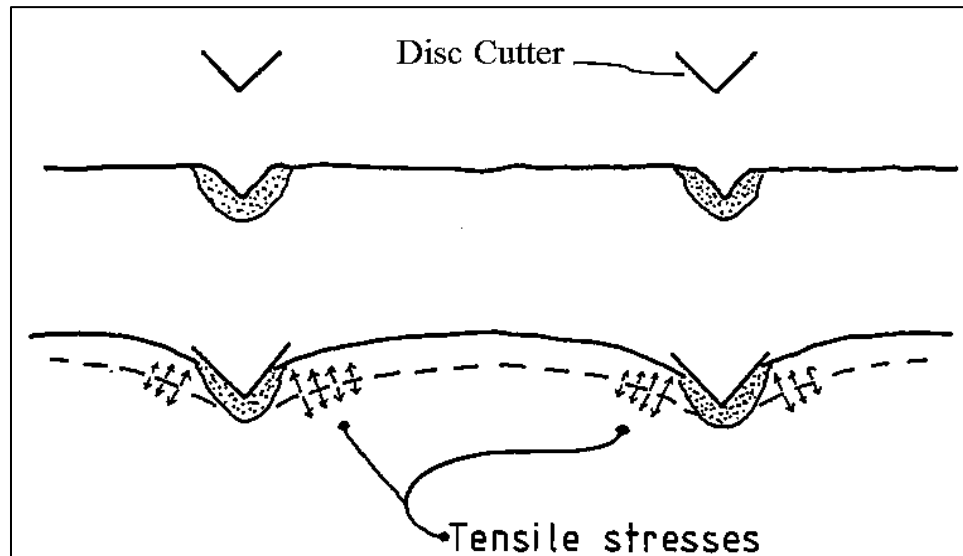


Figure 2.11. Side chipping caused by tensile stresses (after Lindqvist, 1982).

They came up with the following equation for the disc cutters relating chip geometry with disc forces and rock properties (Lindqvist, 1982):

$$t = \left( \frac{2.09\sigma_t p l^4}{F_s(1-\nu^2)} \right)^{1/3} \quad (2.25)$$

Where

$\sigma_t$ = Rock tensile strength

$t$ = Chip thickness

$p$ = Penetration of the disc

$l$ = Length of console (= half of the spacing)

$F_s$ = Force on sphere

Sanio (1985) developed a model based on the assumption that tensile rather than shear failure is the dominant chip forming mechanism of disc cutters. The model incorporates the role of the crushed zone under the disc (Figure 2.12). The model hypothesizes that: as a result of high stress concentration, the rock is first crushed in a zone just below the tool. An approximate hydrostatic state of stress exists within this crushed zone causing tangential stresses to be generated in the surrounding undamaged rock. When these reach the tensile strength, tensile cracks develop which extend radially from the cutting edge. Once such a crack reaches a free surface of the rock, a chip is formed which removes the rock between the neighboring cuts. The following equations of the model were developed for calculating normal and rolling forces:

$$F_N = Sk \cdot \sqrt{d \cdot s \cdot p} \tan\left(\frac{\varepsilon}{2}\right) \quad (2.26)$$

$$F_R = \frac{4}{5} \sqrt{\frac{p}{d}} \cdot F_N \quad (2.27)$$

Where

$Sk$ = Rock constant dependent on the degree and orientation of strength anisotropy ranging from 0.17 to 0.47

$\varepsilon$ = Wedge angle

$d$ = Disc diameter

$p$ = Penetration of disc

$s$ = Crack length equal to spacing



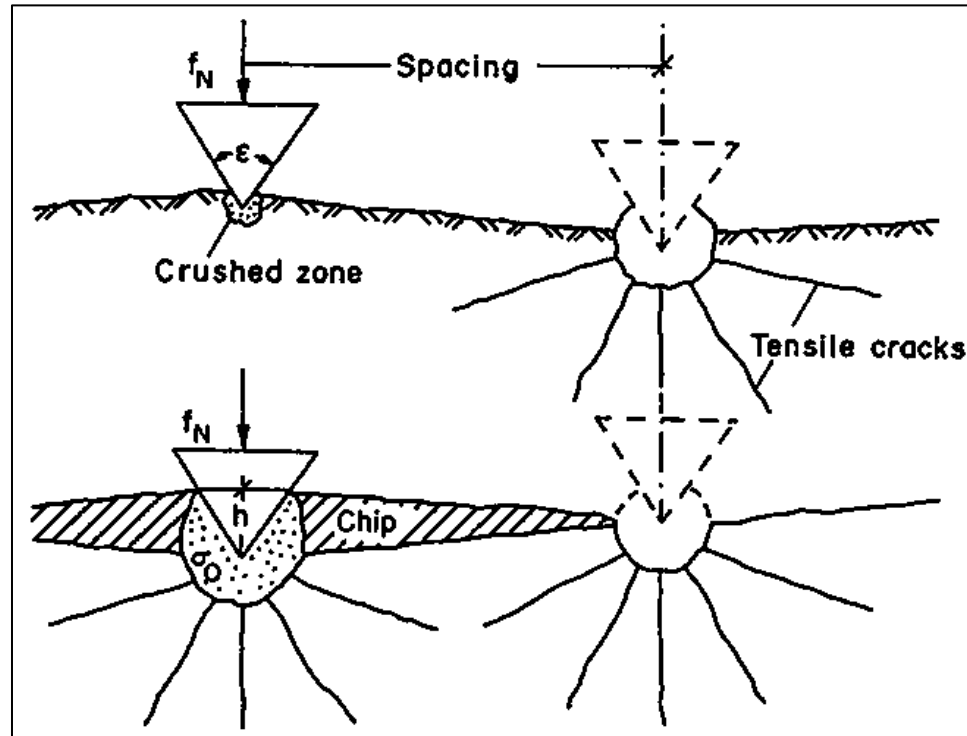


Figure 2.12. Schematic representation of wedge penetration and chip forming process (after Sanio, 1985).

Sato et al. (1991, 1993) used an empirical approach to compute expressions for normal and rolling force for V-profile disc cutters. The approach followed by this group of researchers was similar to the one adopted by Sanio (1985):

$$F = kP^a S^b \quad (2.28)$$

Where

$F$ = Force

$k$ = Coefficient of cutting

$P$ = Penetration

$S$ = Spacing

$a$ = Penetration coefficient,  $\sim 0.5$  for normal force,  $\sim 1$  for rolling force

$b$ = Spacing coefficient,  $\sim 0.5$  (0.43) for both forces

All the disc cutter models cited up to this point were based on V-profile disc cutters. V-profile disc cutters were replaced by constant cross-section (CCS) disc cutters in late 1970s. Rostami and Ozdemir (1993) and Rostami (1997) developed a model for cutting force estimation of CCS disc cutters based on tensile failure mode for chip formation. CCS cutters cause no wedging effect; therefore, the shear forces induced within the rock are minimal. Rostami's suggested model was based on the observation of radial cracks propagating from the crushed zone developed under tip of the cutter (Figure 2.13).

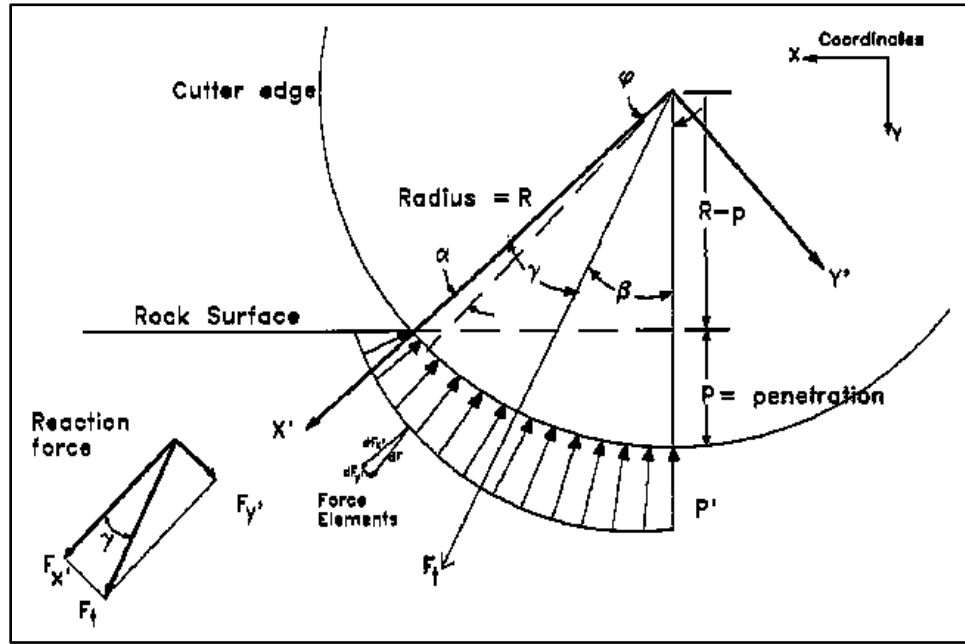


Figure 2.13. Longitudinal cross-section of cutter-rock contact area for CCS disc cutters (Rostami and Ozdemir, 1993; Rostami, 1997)

The total estimated resultant cutting force was derived as under:

$$F_t = \int_0^\phi TPR d\theta = \int_0^\phi TRP' \left(\frac{\theta}{\phi}\right)^\psi d\theta = \frac{TRP'\phi}{1+\psi} \quad (2.29)$$

Where

$F_t$ = Total thrust force

$T$ = Cutter tip width

$R$ = Cutter radius

$\theta$ = Angle from normal

$\phi$ = Angle of contact area between rock and cutter,

$$\phi = \cos^{-1} \left[ \frac{(R-p)}{R} \right] \quad (2.30)$$

$P$ = Pressure of crushed zone, defined by a power function as,

$$P = P' \left( \frac{\theta}{\phi} \right)^\psi \quad (2.31)$$

$\psi$ = Power of pressure function; varies between 1.0 for V-shape and very sharp cutters to -0.25 for wide tip cutters

$P'$ = Base pressure in the crushed zone at the point directly underneath cutter

In this prediction model,  $T$  and  $R$  are cutter geometry parameters which are known. Using the equations derived from multiple regression analysis of measured forces, base pressure  $P'$  can be estimated as a function of following parameters:

$$P' = f(S, \sigma_c, \sigma_t, R, T, p) \quad (2.32)$$

Where

$S$ = Spacing between the cuts

$p$ = Penetration

$\sigma_c$ = Uniaxial compressive strength of rock

$\sigma_t$ = Tensile strength of rock

The normal and rolling forces can be estimated from total force by using the angle of resultant force  $\beta$ , as follows:

$$F_n = F_t \cos \beta ; F_r = F_t \sin \beta ; \tan \beta = \frac{F_r}{F_n} \quad (2.33)$$

Rostami's model can be used for estimation of cutting forces for V-shape disc cutters or worn cutters by using an approximate value for tip width  $T'$  as follows:

$$T' = T + w \tan \left( \frac{\alpha}{2} \right) \quad (2.34)$$

Where

$T'$  = Tip width for V-shape or worn cutter

$T$  = Tip width of sharp cutter or 0 for V-shape

$w$  = Tip lost (worn out from radius)

$\alpha$  = Tip angle; 5-10 for CCS and 90-120 for V-shape cutters

The discussion about disc cutters would remain incomplete without mentioning the role of spacing and penetration on excavation performance. The effects of cutter spacing and penetration have been studied extensively by Ozdemir et al. (1978). They established that the magnitude of cutting forces increases as the spacing between the adjacent cuts increases. Depth of penetration also had the same effect on cutting forces. Both the normal and rolling forces increase in a relatively linear fashion with increase in spacing and penetration. The observed behavior of disc cutting forces with varying spacing can be divided into three zones (Figure 2.14).

For a given cutter penetration, there exists a spacing value where maximum interaction occurs between adjacent cuts. The spacing at which the cut interaction is maximized is called the optimum spacing. If the spacing is small, overcrushing of rock occurs, creating small particle sizes and hence higher specific energy requirements. On the other hand, if the cuts are spaced too far apart, then interaction between cuts ceases to occur for every passage of the cutter. This means chip formation requires more than one pass of the cutter in order to deepen the grooves to a depth sufficient to cause rock failure. This also causes additional crushing of rock and hence reduced boring performance. In extreme case, if the cut spacing is made very large, the boring process may come to a halt as the cutter hubs come in contact with the rock ridges between the adjacent cuts (Ozdemir, 1995).

In order to account for its dependence on cutter penetration, the optimum spacing is expressed as a dimensionless ratio of spacing to penetration ( $s/p$  ratio). As shown in Figure 2.15, the specific energy of cutting decreases with increasing  $s/p$  ratio until the optimum ratio is reached, beyond this ratio, the specific energy requirements begin to increase as the large cut spacing does not allow effective chip formation. Extensive laboratory research and field data analysis of TBM performance have shown optimum  $s/p$

ratio of 10-20. For relatively soft and less brittle rocks this ratio is close to 10 (Ozdemir, 1995).

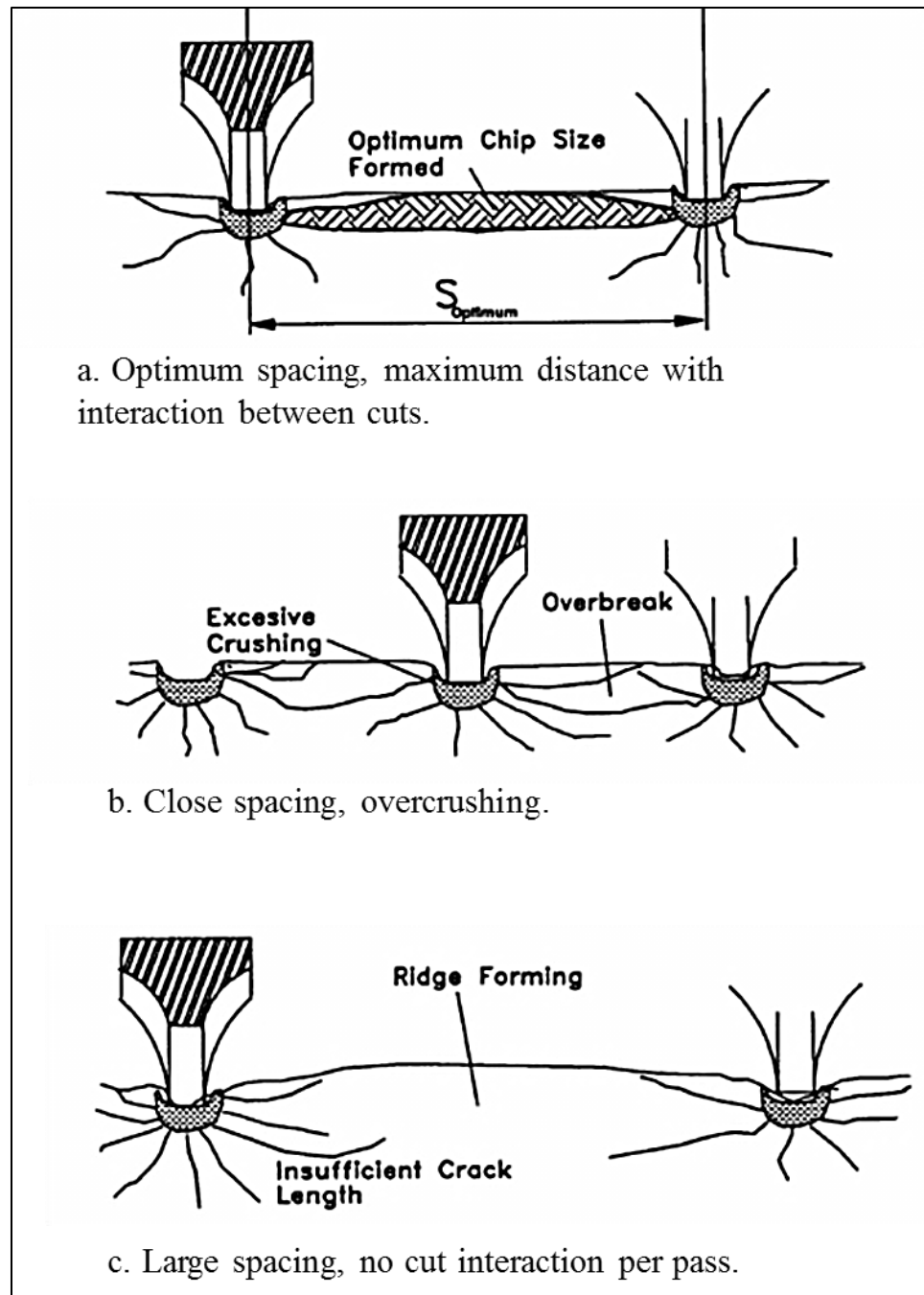


Figure 2.14. Chip formation in different situations (Ozdemir, 1995).

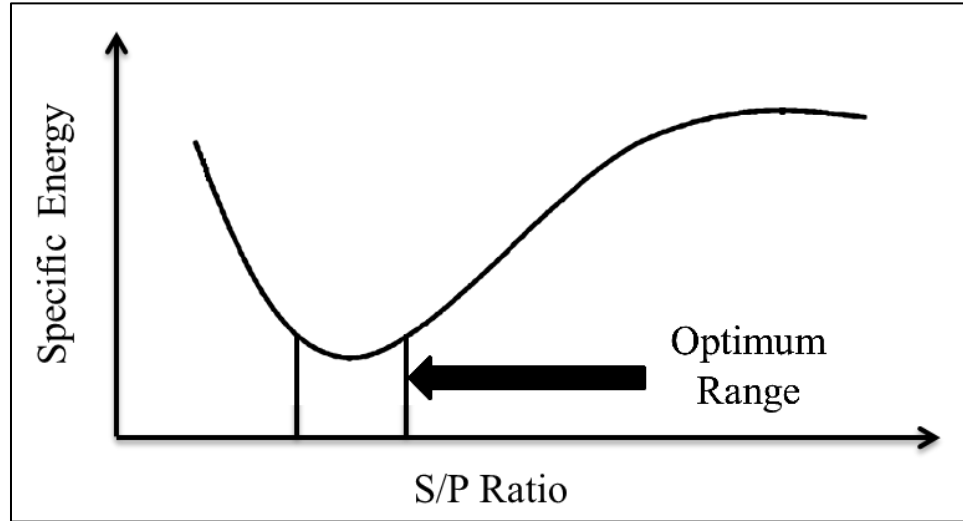


Figure 2.15. General effect of changing  $s/p$  ratio on cutter specific energy (Ozdemir, 1995, Bilgin et al., 2006).

A number of researchers have made attempts to explain rock cutting phenomenon using fracture mechanics principles coupled with numerical approaches of finite and boundary element methods (Hardy, 1973; Saouma and Kleinosky, 1984; Ingraffea, 1987) and the displacement discontinuity method (Hua Guo, 1990; Sun et al., 1992). In most of the studies, it is assumed that linear elastic fracture mechanics (LEFM) always prevails in all situations.

Deliac (1986, 1993) analyzed the forms of major chip formation due to drag picks. He proposed two fundamental chipping modes referred to as mode A and mode B. Mode A is a typical shear and compressive fracture of rock and chip formation can be approximately modeled by the Coulomb's criterion. Mode A (Equation 2.35) chip formation occurs when the pick is wide, rock is relatively soft, and the depth of cut is high. Mode B (Equation 2.36) chip formation is dominant when the pick is sharp and rigid, and the rock is brittle and the depth of cut is small. Deliac derived the following expressions to calculate the cutting force involved using a single isolated pick:

$$F_c = C \cdot \sigma_c \cdot d \cdot (d + W) \quad (2.35)$$

$$F_c = C' K_{1c} d^{3/2} \quad (2.36)$$

Where

$\sigma_c$ = Uniaxial compressive strength

$C$ = Coefficient  $\sim 1$

$d$ = Depth of cut

$W$ = Pick width

$K_{1C}$ = Mode I fracture toughness

$C'$ = Coefficient dependent on rock type and tool sharpness

Ingraffea (1987) describes the use of a finite element program to simulate the rock cutting process using drag picks. This program simulates a plane strain analysis of chip formation under a cutter. The cutter has the material properties of steel, and is not allowed to crush into or slip relative to the rock face against which it will be forced. The problem is solved twice. In case I, the cutter load has only a horizontal component. In case II, the cutter load has a vertical (upward) component equal to one-quarter of the horizontal component.

Van Kesteren (1995) used the formulae developed by Broek (1982) and Kemeny (1986) from linear elastic fracture mechanics for a rough approximation of the stress intensity factors at the tip of the shear crack in his crack bifurcation theory. The formulae used were:

$$K_{Ic} = K_I \cos^3 \left( \frac{\psi}{2} \right) - 3K_{II} \cos^2 \left( \frac{\psi}{2} \right) \sin \left( \frac{\psi}{2} \right) \quad (2.37)$$

$$K_i = S_{bd} \sqrt{h_{in}} g_i \left( \alpha, \beta, \delta, \phi, \frac{h}{h_{in}} \right); i = I, II \quad (2.38)$$

$$4 \tan \left( \frac{\psi}{2} \right) = \frac{K_I}{K_{II}} \mp \sqrt{\left( \frac{K_I}{K_{II}} \right)^2 + 8} \quad (2.39)$$

Where

$K_{1C}$ = Mode I fracture toughness

$\alpha$ = Cutting angle

$\beta$ = Shear plane angle

$\delta$ = Friction angle chisel-rock

$\phi$ = Residual internal friction angle

$\psi$ = Angle between tensile crack and shear plane

$h$ = Vertical position of tip shear plane

$h_{in}$ = Indentation depth

For simplicity the principle stress criterion is used for the mixed mode loading. The maximum intensity factor outside the crushed zone determines the location where bifurcation to a tensile crack may occur. When the stress intensity distribution is compared with the boundary of the crushed zone, it may be concluded that bifurcation occurs when:

$$\frac{K_{Ic}}{S_{bd}\sqrt{h_{in}}} = 0.6 \quad (2.40)$$

**2.1.2.4 . Field performance estimation of mechanical excavators.** Theoretical prediction models have certain weaknesses that limit their usefulness for solving field problems in machine design and performance. These weaknesses relate to a poor understanding of both the state of stress developed in the rock as a result of the applied forces and the mechanics of crack initiation and propagation. In addition, materials are generally considered to be homogenous, and the important influence of pre-existing fractures and discontinuities is ignored. In the case of roadheaders, the limitations of these models are compounded by the relatively large number of pick geometries available, the mode of roadheader operation and a generally less controlled cutting environment. In the case of TBMs theoretical modeling problems are less acute. Here, variations in cutter geometries are limited to disc diameter and blade width. In addition, the cutting process is more controlled, involving relatively constant penetration rate and depth of cut, and only a single cutting mode (Breeds and Conway, 1992).

It is clear that neither geology alone, laboratory and field testing alone, experience alone nor equipment design and operation expertise alone can get an engineer to the point where underground excavation is a clearly defined engineered process. Integration of all these knowledge bases is required to raise the level of engineering contribution to underground construction (Nelson, 1993).



One of the earliest models developed from field performance analysis is the NTH-method developed at University of Trondheim, Norway in 1960,s for evaluating the drillability of rocks by percussive drilling. The NTH hard rock TBM prognosis model is based primarily on empirical correlations between geological/rock mechanical parameters and actual tunneling performance. Along with detailed joint mapping, representative, 10-15 kg samples of the different rock types along the tunnel are taken to the laboratory and the following standard tests are performed for calculating TBM performance related parameters (Nilsen and Ozdemir, 1993).

- Brittleness test
- Siever's J-test
- Abrasion test

Handewith (1970) presented a disc cutter performance predictive method based on a punch test. The method was based on drawing a best fit straight line on the force-penetration graph through the origin and force-penetration data and then directly estimating from this line the expected cutter loads and penetrations during excavation using the slope of the line measured in lb/in, called the penetration index.

Early applications of this method to predicting raise and tunnel boring machines performance, in fact, resulted in reasonably good estimates of penetration rates for both low strength rocks and lower cutter path loads. In higher strength rock conditions, however, where higher cutter path loads were required, the penetration index method was observed to be less successful and tended to under estimate the actual penetration rates (Dollinger et al, 1998).

Tarkoy (1979) used rock hardness index properties for prediction of TBM penetration rates. He used rebound hardness and rock abrasive properties for development of his empirical relationship between total hardness and TBM penetration rate. The rebound hardness values were determined from Shore Scleroscope and Schmidt rebound hammer. Taber abraser was modified to measure rock abrasiveness and abraadeability.

Nelson et al. (1983) studied the penetration rates of different TBM projects in sedimentary rocks. It was found that there is no statistically significant correlation between the penetration rate and the rock compressive or tensile strength, point load

index and fracture toughness. Their study found good correlations between penetration rate  $P_r$  (mm/rev) and abrasion hardness and field penetration index  $R_f$  (kN/mm) and total hardness as expressed by following equations:

$$P_r = 10.45 - 1.19H_A \quad (2.41)$$

$$R_f = 5.95 + 0.18H_T \quad (2.42)$$

Where

$H_A$ = Taber abrasion hardness

$H_T$ = Total hardness

McFeat-Smith and Fowell (1977) studied the relationship between rock index properties, laboratory specific energies, in-situ specific energies and instantaneous cutting rate for a variety of British coal measures rocks. The instantaneous cutting rate which is the effective average advance per cutterhead revolution was shown to correlate with the specific energy by the following expression:

$$SE = \frac{HP}{ICR} \quad (2.43)$$

Where

$SE$ = Specific energy

$HP$ = Cutterhead power

$ICR$ = Instantaneous cutting rate

Bilgin et al. (1988) developed a model which uses rock compressive strength, RQD and machine power to estimate an index that is related to the production rate.

$$RMCI = \sigma_c \left( \frac{RQD}{100} \right)^{2/3} \quad (2.44)$$

$$ICR = 0.34 \cdot HP \cdot 0.976^{RMCI} \quad (2.45)$$

Where

$RMCI$ = Rock mass cutting index (kg/cm<sup>2</sup>)

$\sigma_c$ = Uniaxial compressive strength of rock (MPa)

$ICR$ = Instantaneous cutting rate ( $m^3/hr$ )

$HP$ = Machine power (kW)

Rostami et al. (1994) calculated the  $ICR$  by using the following relationship:

$$ICR = P_n \times RPM \times C(D * f)^2 \quad (2.46)$$

Where

$RPM$ = Cutterhead RPM

$C$ = Conversion factor

$D$ = Cutterhead diameter

$P_n$ = Nominal penetration =  $10*f$

$f$ = Factor to estimate depth of sump of cutterhead into rock.

Neil et al. (1994) estimates ' $f$ ' using rock compressive and tensile strengths,  $RQD$ , and machine cutterhead diameter. ' $f$ ' is a ratio reflecting the sumping depth that operators choose intuitively based on perceived ease of cutting.  $f=1$  means that a machine can achieve a sumping depth equal to full cutterhead radius of roadheader.  $f < 1$  indicates less sumping depth is likely:

$$f = 1 - 0.06(R - 7) - 0.5 \left( \frac{RQD - 25}{25} \right)^{B1} - \left( \frac{\sigma_c - 5000}{5000} \right)^{B2} \quad (2.47)$$

Where

$R$ = Ratio of compressive to tensile strength

$B1, B2$ = Constants equal to 0.4 and 2 respectively

$\sigma_c$ = Uniaxial compressive strength

Gehring (1989) and Thuro and Plinninger (1999) have also developed empirical equations for  $ICR$  calculation based on uniaxial compressive strength of rocks and performance data of roadheaders working on different mining and tunneling projects. Models developed to compute  $ICR$  based on laboratory specific energy do not take discontinuities into account. Balci (2009) calculates  $ICR$  to incorporate discontinuities at the tunnel face using the equation:

$$ICR = p \times RPM \times A \quad (2.48)$$

Where

$p$ = Optimum penetration (mm/rev) for cutter spacing

$RPM$ = Revolutions per minute

$A$ = Tunnel area in  $m^2$

Khademi et al. (2010) developed a TBM field penetration index (FPI) based on the data collected from 8.5 km long tunnel using five basic parameters of the rock mass rating (RMR) rock mass classification system. The analysis of relationship between FPI and the five basic RMR input parameters plus tunnel depth and the angle of joints with tunnel axis showed that FPI had a statistically insignificant correlation with tunnel depth and the groundwater condition parameter of RMR classification system. Inter-correlation of UCS and joint spacing led to the exclusion of joint spacing from the analysis. The TBM FPI developed is given as follows:

$$FPI = 4.161 + 0.091UCS + 0.077RQD + 0.117J_c + 1.077 \log(\alpha) \quad (2.49)$$

Where

UCS= Uniaxial compressive strength

RQD= Rock quality designation

$J_c$ = RMR joint condition rating

$\alpha$ = Angle between the tunnel axis and the planes of weakness

A recent study by Farrokh et al. (2012) reviews various TBM penetration rate estimation models. This study also proposes a new model for the estimation of penetration rate. This model is generated on the basis of the analysis of data from more than 300 TBM projects around the world.

**2.1.3. Saturated Rocks Studies.** These studies can be divided into two parts:

- Saturation effects on strength of rocks; and
- Saturation effects on mechanical excavation of rocks.

**2.1.3.1 .Saturation effects on strength of rocks.** The effect of water saturation on the mechanical properties of rocks has been a point of focus of several past investigations. Most of these investigations reported an appreciable reduction in strength (Uniaxial Compression and Brazilian Tensile) of rocks saturated with water. A number of mechanisms for this strength reduction have been proposed.

Rehbinder and Lichtman (1957) studied the effects of surface active media on strains and ruptures in solids. They established that the resistance of solids to strain and rupture is reduced by adsorption from the surrounding medium. This is due to decrease in the surface energy of the interfaces newly formed in the defects (ultra-microcracks) arising in the strained solid. The weakening effect due to adsorption, i.e. molecular interaction with the medium, is generally of a kinetic nature and takes place on the simultaneous fulfillment of two conditions: (1) The state of stress should aid the development of weak spots (ultra-microcracks) in the surface layers of the solid, i.e. sufficiently high tensions (superstresses) should be present, and (2) During the time of the development of defects the surface energy over a sufficiently large portion of the newly formed solid surface should be lowered by penetration of surface active components from the medium in the form of adsorption layers. The greatest adsorption effects were observed on the prolonged action of favorable stresses in the solid surface including creep or fatigue or long-time tensile stresses.

Colback and Wiid (1965) showed that the surface-free energy of a solid submerged in a liquid is a function of the surface tension of the liquid. Since the uniaxial compressive strength is directly related to the uniaxial tensile strength and this in turn to the molecular cohesive strength ( $\sigma_m$ ), then  $\sigma_m$  can be found by:

$$\sigma_m = \sqrt{\frac{2\gamma E}{a}} \quad (2.50)$$

Where

$\gamma$ = Surface free energy of the material

$E$ = Young's modulus

$a$ = Spacing between neighboring atomic planes

Their tests on specimens of quartzitic shale and quartzitic sandstone indicated that the compressive strength under water saturated condition was of the order of 50 percent of that under dry conditions. They postulated that the immersion liquid reduces the surface-free energy of the rock and hence its strength.

Brace and Martin (1968) examined the effect of porewater pressure on the strength of low porosity crystalline rocks. They concluded that the effective stress

concept was valid if the mechanical loading rate was kept low enough so that pore pressure continuity within the sample was maintained. They noted an increase of strength (at some constant pore pressure) with increased strain rate. This effect was attributed to increasing porosity (dilatancy) as failure was approached. Consequently, internal pore pressure lagged behind those measured externally, leading to a strengthening effect (Van Eeckhout, 1976).

Vutukuri (1974) studied the effect of various liquids on the tensile strength of an oolitic limestone. The liquids used were water, glycerine, ethylene glycol, nitrobenzene, ethyl alcohol, benzaldehyde, and n-butyl alcohol. He concluded that increases in dielectric constant and surface tension of the saturating liquid decrease the tensile strength of rock. The tensile strength is directly related to the molecular cohesive strength which is proportional to the surface free energy ( $\gamma$ ) of the material. Since the surface free energy of a solid saturated with a liquid is a function of the fluid properties such as surface tension and dielectric constant, it can be postulated that the influence of the saturated liquid is to alter the surface free energy of the rock and hence its strength. The results indicated that the best liquid was water (of those tested) in reducing the tensile strength of rock, thereby increasing the efficiency of drilling, crushing, grinding, pulverizing, fracturing and machining operations.

Van Eeckhout (1976) attributed reduction of rock strength with moisture to fluid-induced reduction in fracture energy, decrease in capillary tension, increase in pore pressure, reduction of internal friction, and corrosive chemical deterioration. None of these mechanisms can be discounted outright, but some are more likely than others for certain rock types and loading conditions. Examining the data collected for coal mine shales, he attributed the reduction in strength of coal mine shales to two mechanisms: (1) the expansion-contraction characteristics which lengthen internal cracking, and (2) the lessening of fracture energy with increased moisture.

Broch (1979) performed point load tests on a wide variety of rocks like gabbro, gneiss, diorite, amphibolite, and marble in dry as well as in water saturated conditions. He found that the strength reduction with water saturation increases with increasing amounts of mafic silicate minerals (biotite, amphiboles, pyroxenes), and also with

increasing development of schistosity and anisotropy in rocks. Moisture induced strength reduction of 20 to 45% was recorded for the rock types tested.

Dyke and Dobereiner (1991) reported that small variations in moisture content can create significant changes in the mechanical response of sandstones during compression. Increase in moisture content tends to reduce the range of elastic behavior by promoting stress corrosion-aided microcracking at low levels of applied stress. A decrease in moisture content tends to suppress the onset of dilatancy and microcracking, leading to an increase in peak strength. The elastic range of material behavior for sandstone is often below 20% of peak strength. Consequently, they concluded that elastic properties should be measured at low stress levels rather than at 50% of peak strength.

Hawkins and McConnell (1992) found that an increase in moisture content of as little as 1% from dry state can have a marked effect on both strength and deformability of sandstones. They reported a 78% reduction in uniaxial compressive strength of clay rich sandstones upon saturation, whereas siliceous sandstones reduced their strength by 8% upon saturation. Their research also indicated that development of pore pressure during loading is negligible especially in pure sandstones and hence does not play a significant role in moisture related strength reduction. They concluded that the degree of sensitivity to moisture content is controlled primarily by the proportions of quartz and clay minerals present and to a lesser extent by the rock microfabric.

Erguler and Ulusay (2009) report reductions of up to 90%, 93% and 90% with increasing water in UCS, average modulus of elasticity and tensile strength respectively of clay bearing rocks. The tested rocks were collected from different parts of Turkey and included marl, mudstone, siltstone, sandstone and tuff. In their tested rocks, much of the strength reduction occurred between 0% and 2% water content, particularly with stronger rocks.

Yilmaz (2010) also reports considerable loss in the strength of gypsum with a very small (1-2%) increase in the water content.

**2.1.3.2 .Saturation effects on mechanical excavation of rocks.** The saturation of rock by water affects the rock's behavior through two classes of mechanisms: mechanical and chemical. Mechanical refers to the effects of both pore pressure and capillary pressure on effective stress. If the cutting strain rate is high enough and the rock

permeability is low enough to dissipate excess porewater pressure, saturation reduces the effective stress and the rock appears stronger. For rocks the critical strain rate of  $10^5 \text{ s}^{-1}$  has been reported, which is far below the practical strain rates of  $10^3 \text{ s}^{-1}$  experienced in some rock cutting operations like dredging, resulting in drained behavior (Van Kesteren, 1995).

If the cutting strain rate is low enough and the rock permeability is high enough to dissipate the excess porewater pressure buildup due to passage of the cutting tool, no mechanical effect exists. Thus, the rock's fabric, a result of both its formation and its subsequent history, affects the sensitivity of its cuttability to water saturation. In addition, in low-permeability rock, the mechanical effects of capillary pressure (which develop when two immiscible fluids fill the pores) can be significant (Schmitt et al., 1994). In low permeability rocks like shale, motion of the pore fluid is restricted under the movement of the indenter, producing undrained behavior (Thiercelin and Cook, 1988; Cook and Thiercelin, 1989).

The chemical effects of saturation include both molecular adsorption and stress corrosion cracking (Atkinson, 1984). Stress corrosion cracking is known to be a rate-dependent phenomenon. A limiting crack velocity exists beyond which stress corrosion plays no part in fracture propagation. For most brittle materials, including rock, this limiting velocity is of the order  $10^{-4} \text{ m/sec}$  to  $10^{-1} \text{ m/sec}$  (Barton, 1982). Stress corrosion cracking is at least two orders of magnitude slower than the fracture propagation velocity of rock during the rock cutting process (Tutluoglu et al., 1983). Molecular adhesion is much faster than stress corrosion. It is slower, however than the fracturing velocity (Borodich, 1996). Accordingly, neither is expected to immediately influence cracks generated during a specific cut. Their effects could be induced, however before the next passage of the cutting tool (Li et al., 2001; Saperstein et al., 2007). In the adsorption process, water interacts with the exposed molecules of the solid, lowering the surface energy. The breaking of silicon-oxygen bonds is not a fast process. It is fast enough, however to weaken rocks soaked for a period of time (Lockner, 1995).

A great deal of analytical, numerical and empirical research has been conducted in connection with the performance prediction and design of mining, drilling and tunneling machines, mostly based, however, on study of dry rocks. The design and



performance estimates based on procedures derived from studies of dry rock involve economic and environmental risks. Saturated rock behavior under a cutting tool, particularly, the mechanical excavatability of saturated rocks has been examined by only a few researchers. All of these studies had differing findings depending upon the test procedure, rock type and tool used.

Robinson and Holland (1969) studied the effect of pore fluid on rock failure in connection with deep oil well drilling. They reported that as the tooth of the drilling bit loads the rock, the region under the tooth tends to form a crushed zone and wing shaped fractures. If a small differential pressure exists between the mud pressure and the pore pressure, the pore volume in the disturbed region begins to increase as failure starts. If a fluid is supplied to this disturbed region, the effective differential pressure remains the same and the rock remains relatively brittle. If, however, fluid cannot be supplied as rapidly as the pore volume increases, the pore pressure in the region of failure decreases. The decreased pore pressure increases the effective confining pressure. This tends to make the rock more plastic and stronger, requiring greater force to form chips and drill.

Kaitkay and Lei (2005) found increases in the cutting forces and the length of the rock chips produced by a polycrystalline diamond compact (PDC) bit with increase in external hydrostatic pressure. The external hydrostatic pressure can transform the cutting process from a dominantly brittle fracture to an intermediate ductile-brittle mode in case of rocks. The chip length increase is attributed to the formation of small cracks and pressure-induced plastic deformation ahead of the cutting tool. When an external pressure is applied, failure in shear increases, resulting in more shear flow during chip formation. The longer chips may be assumed to be made up of small rock particles with internal fractures suppressed by the external pressure.

Some instrumented cutting studies report significant reduction in cutting forces, specific energy and pick wear rate with water saturation, whereas some researchers find no appreciable differences in dry and saturated rock cutting modes. Findings of the few studies performed on different rock types are presented here.

Roxborough and Rispin (1973) performed rock cutting experiments on dry and wet chalk (Lower Chalk of Upper Cretaceous of Southern England) using drag, disc, roller and button cutters installed on an instrumented linear cutting rig. For drag picks

particularly, the cutting force values were found to be the same for both dry and wet chalk. The normal forces generated in the wet chalk were generally lower than for dry chalk. Since the uniaxial compressive strength of the dry chalk was five times greater than the wet chalk, it was believed initially by the authors that higher specific energy would be required in the dry chalk. Exactly reverse was found to be the case. The wet chalk specific energy values were 50% higher than the dry chalk drag pick cutting. The increase in wet chalk specific energy was attributed to the lower values of coarseness index (*CI*) for wet chalk cutting experiments. For disc and roller cutters, thrust and rolling forces were higher in dry chalk than in wet chalk.

O'Reilly et al. (1979) also conducted tests on chalk (Lower Chalk of Southern England) to provide numerical data on the performance of tunneling machines and to examine the relations between the full scale situation and the results of single and multiple tool rock cutting experiments in the laboratory. They performed a series of instrumented cutting tests on both dry and saturated chalk using drag and disc cutters. Their study found that the specific energy requirements for excavating wet and dry chalk were similar, although average compressive strength differed over fivefold for these conditions. The optimum spacing/depth and spacing/penetration ratios were higher in dry chalk. To establish a linkage between the laboratory studies using a single tool and the full scale situation, a 1 m diameter pilot scale boring rig was also developed in the study. The pilot-scale tests were undertaken on 8 m<sup>3</sup> blocks of reconstituted chalk with UCS of 2-10 MPa. Trials using pilot scale rig revealed problems of tool arrangement that were not apparent on single tools in the laboratory in that with drag picks mounted side by side the debris produced during cutting rapidly clogged up the head. This difficulty was overcome by arranging the tools around the head to form spiral which increased up to sevenfold the radial spacing of tools.

Phillips and Roxborough (1981) performed experiments on chalk and Bunter Sandstone (UCS = 50MPa; massive formation found in midlands and north of England) using drag tools, in order to assess the influence of the intimacy of water at the tool rock interface. Cutting wet rock produced less wear than in the dry condition. The role of this water in the dissipation of heat was very evident from the large volumes of steam generated during the wear tests. The authors maintained that, if a rock remains competent

after saturation, the forces required to cut it can be higher than for dry rock. The reason is not fully understood but they attributed it to porewater dissipation of the high local stress concentrations associated with crack development.

Ford and Friedman (1983) found 50% reduction in the cutting forces while performing their drag tool cutting experiments on limestone and sandstone rocks. The sandstone used had porosity between 5 and 8 percent; whereas both the limestone and sandstone were free from significant weakness planes. They attributed the force reduction to two factors: (1) lubrication of tool/rock interface thus lowering frictional forces, and (2) strength degradation of rock due to saturation. Based on friction coefficients differences between dry and saturated conditions, they pointed out that lubrication alone could not have been responsible for the cutting force reductions.

Tiryaki and Dikmen (2006) performed linear cutting tests on different types of sandstones collected from Ankara, Turkey using chisel type picks. The sandstones were cut in air dry condition. They noted a decrease in specific energy of drag pick cutting with increases in effective porosity and pore volume, both parameters being directly related to bulk rock strength along with the strength of the intact rock.

Mammen et al. (2009) conducted a study on the effect of moisture content on rock cutting performance using 57 mm (2.25 in) sandstone core test samples (Triassic Argillaceous quartz sandstone; Dry UCS = 57 MPa, Wet UCS = 22 MPa). They found reductions of up to 40% and 49% in cutting and normal forces, 38% for specific energy, 80% for impact wear of the drag cutting tool and 68% in compressive strength. Significantly in most cases the magnitude of the reduction in performance parameters was greatest with only the slightest addition of water to the rock.

Uchibayashi (1970) working on different dredging projects, noted the role of discontinuities in dredging operations. He found that hard brittle rocks containing fissures were not difficult to excavate with a cutter suction dredger, as more cracks could be easily propagated, but when the rocks were tough and contained few cracks or fissures, dredging was very difficult. Dredging was still possible in layered hard rocks without fissures if the bottom layers were weaker than the top layers.

Hignett and Banks (1984) explored the possibilities of using partial face tunneling machines' cutterheads (roadheader cutterheads) for medium strength rocks in dredging

operations. The operation of a partial face tunneling machine and a dredging head is similar, with the exception that a dredging head has to remove the cut debris and therefore requires an open head design to include suction parts for hydraulic removal of material. The authors designed a cutting head for limestone with a compressive strength of 80 MPa. Peak cutting force data were obtained for the cutting tools being employed and used to calculate the stress distribution and deflections that could arise on the helical cutter tool mounting arms. It was established that the arms were acting as fairly soft springs relative to the forces being applied, and were unsuitable for the mounting of the rock cutting tools. Designs were considered that provided stiffening braces to the mounting arms, but were found to be incompatible with the other prime aim of suction dredging head. Finally, it was decided to use a cutterhead with point attack picks and stiff open shell monocoque construction with scoops and space for hydraulic dredging.

Van Kesteren (1995) reports extensive tests conducted on saturated rocks at Delft Hydraulics to get an insight of the cutting process ahead of a rock cutting tool in a saturated environment especially in rock dredging operations. He examined the effect of porewater pressures in rocks by differentiating drained and undrained conditions. In the drained condition, porewater flow due to porewater pressure gradients is possible without affecting the behavior of the porous system itself. In the undrained condition, porewater is not allowed to flow through the pores and porewater pressures affect the stress state in the rock fabric. He calculated the porewater pressures caused by an external isotropic stress  $S$  as a function of the Peclet number ( $\xi_{Pe}$ ) for porewater pressure dissipation (Figure 2.16). This number is defined as:

$$\xi_{Pe} = \frac{V \cdot h_s}{D} \quad (2.51)$$

Where

$V$ = Cutting velocity (m/sec)

$h_s$ = Cutting depth (m)

$D$ = Diffusion coefficient of porewater pressure (m<sup>2</sup>/sec)

$D$  is given by the following equation:

$$D = \frac{k/\gamma_w}{c_f - \alpha c_s + n(c_w - c_s)} \quad (2.52)$$

Where

$k$ = Permeability (m/sec)

$\gamma_w$ = Unit weight of water (N/m<sup>3</sup>)

$C_w$ = Compressibility of porewater (m<sup>2</sup>/N)

$C_s$ = Compressibility of solids (m<sup>2</sup>/N)

$C_f$ = Compressibility of rock fabric (m<sup>2</sup>/N)

$n$ = Rock porosity

$\alpha$ = Coefficient for solid compression

From Figure 2.16, it follows that the drained condition is valid when  $\xi_{pe} < 1$  and that undrained behavior will occur when  $\xi_{pe} > 10$ . The limit porewater pressure, which will be generated in the perfectly drained case, follows from:

$$\frac{S}{u_{undr}} = 1 + n \cdot \frac{C_w - C_s}{C_f - \alpha C_s} \quad (2.53)$$

Where

$S$ = Total isotropic stress (MPa)

$u_{undr}$ = Undrained porewater pressure (MPa)

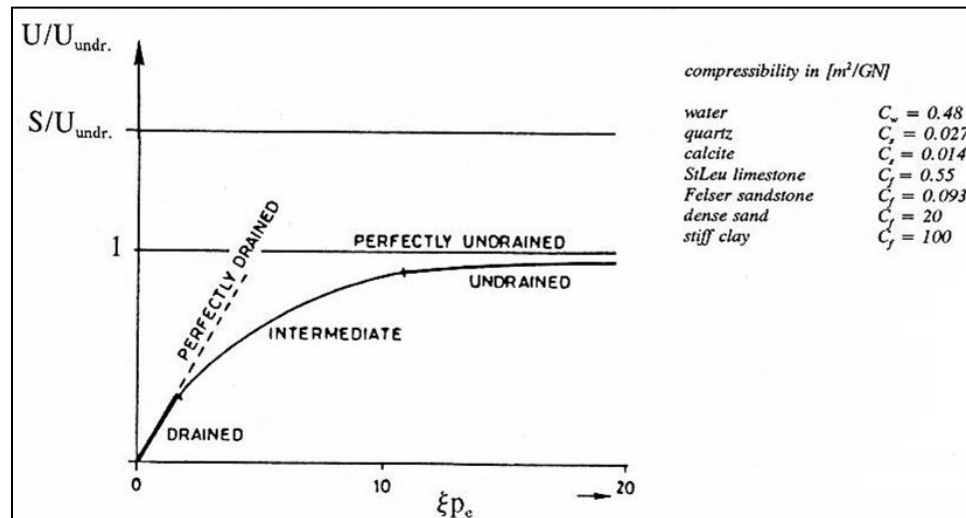


Figure 2.16. Drained to undrained condition (after Van Kesteren, 1995).

He also performed cone indentation tests on limestone to study the effect of indentation velocity on porewater pressure. At low velocity (25 mm/sec) porewater is able to flow out of the porous system fast enough to result in a zone around the cone in which pore compaction balances the indented volume. At an intermediate velocity (100 mm/sec) the size of the crushed zone is reduced due to the resistance of the porewater pressure. The cone volume cannot be balanced anymore by pore compaction and shearing occurs towards the free surface where eventually chips are formed. At a velocity of 1000 mm/sec the undrained condition around the cone occurs. Due to the high porewater pressures liquefied crushed rock is squeezed out along the cone face (Figure 2.17).

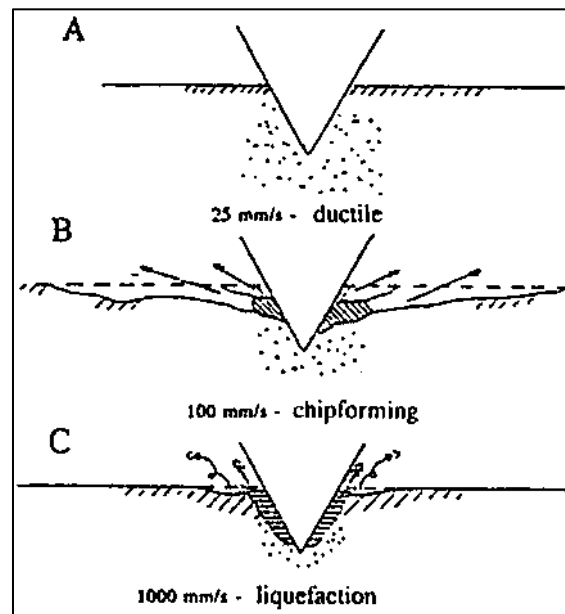


Figure 2.17. Failure mechanisms in cone indentation test (Van Kesteren, 1995).

Jackson et al. (2007) give the differences between terrestrial and deepwater rock cutting while evaluating the performance of a subsea mechanical trenching wheel. Those differences are: (1) hydrostatic pressure transforms the cutting process from a dominantly brittle fracture to a more ductile fracture mode, (2) presence of water and marine growth acts as lubricant between the cutters and the host rock and reduces frictional wear. The

picks transfer more heat to surrounding fluid through convection, as water has higher heat capacity than air, (3) as a rock chip is broken out, a cavity is created, and hence a pore suction. This needs to be balanced by water flow either via the crack or through the rock itself. The viscosity of water reduces the speed at which the chip can leave the host rock compared to the same situation in air. This delay increases the remaining chips in the trench and can result in a negative re-grinding effect, and (4) the drag force on the cutter increases due to surrounding water and to the leftover chips in the trench.

### 3. DETAILS AND DESCRIPTION OF TEST EQUIPMENT

This section contains the description of the test equipment used in this research study, the selection criteria, setup, testing procedures, the data acquisition and analysis.

#### 3.1. LINEAR ROCK CUTTING EXPERIMENTS

**3.1.1. Linear Rock Cutting Machine.** The linear rock cutting machine (LRCM) is one of two main test machines used in this study. This is a basic research device for rock excavation studies used for performance estimation of mechanical excavators like tunnel boring machines (TBMs), roadheaders, raise borers, shaft borers, continuous miners and mobile miners. This machine holds a cutting tool firmly in a stiff frame and forces a sample of the material to be excavated past the tool. The main advantage of using the LRCM is to simulate the rock cutting conditions at full scale. It reduces (though not eliminates) the effects of boundary and end conditions. The LRCM used in this study is one of only two built in the United States that are still in use. Similar machines are located in Germany, Turkey, Japan and South Korea.

The LRCM used at the Rock Mechanics and Explosives Research Center (RMERC) of Missouri S&T permits full scale cutting tests at normal loads up to 27 tons (60,000 lbs.). The basic design of the machine is a load bearing frame beneath which the cutting tool is mounted, perpendicular to and above a table on which a sample of the target material is fixed and can be moved beneath the cutter (Figure 3.1 through Figure 3.6).

**3.1.1.1 Load cell.** A 3-D load cell assembly is mounted between the cutter assembly and the stiff reaction frame, separated by cutter penetration spacer plates. The 3-D load cell consists of four load transducers arranged in a square diamond pattern, centered over the cutter. The load cell transmits the load from the loading beam of the frame down to the cutter. By using four gages it is possible to get a measure of the normal (vertical or thrust) load, the rolling (in-line) and the side (out-of-alignment) load on the cutter acting in three mutually perpendicular directions.

The normal force component is perpendicular to the rock surface and is required to maintain a constant penetration. The rolling force acts in the direction of cutter



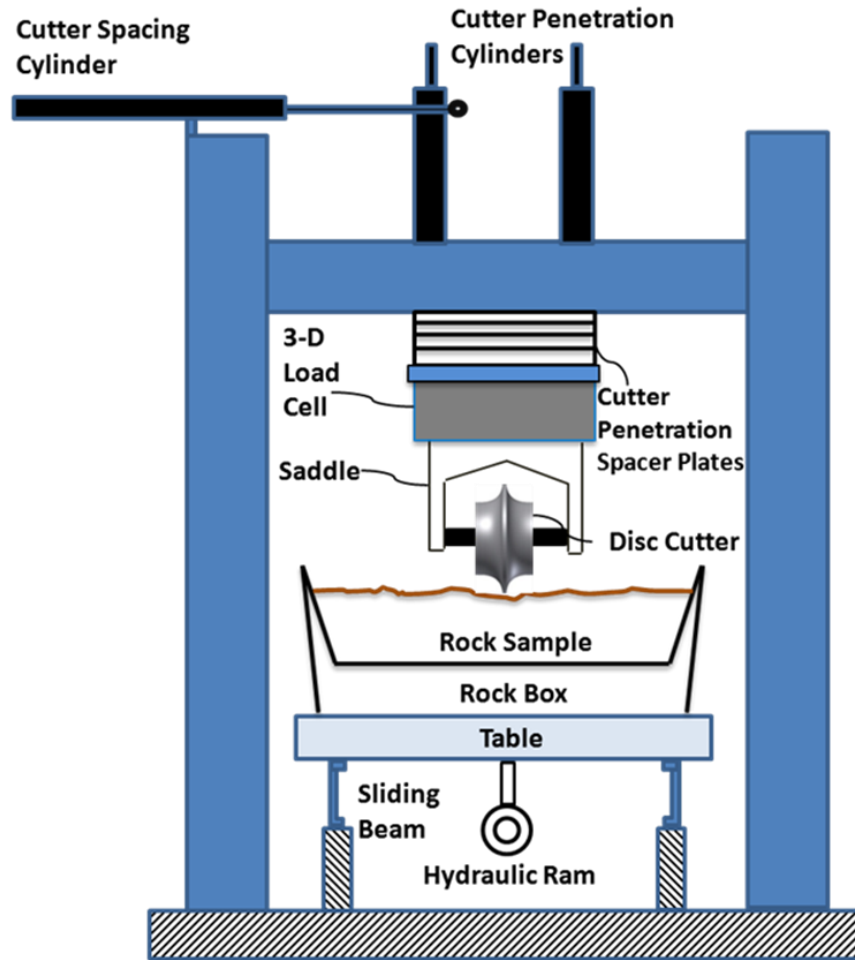


Figure 3.1. Schematic view of linear rock cutting machine with disc cutter mounted.

traverse, parallel to the cutting surface. This force component controls the machine torque requirements. The side force acts perpendicular to the direction of the traverse in the plane of the surface being cut. Its primary use comes in determining the overturning moments imposed on the cutter during excavation. The three force components acting on disc cutter and drag pick while cutting is in progress are shown in Figures 3.7 and 3.8. This load cell design is more sensitive to the rolling and side forces while maintaining sensitivity to the much higher normal forces (Gertsch and Summers, 2006).

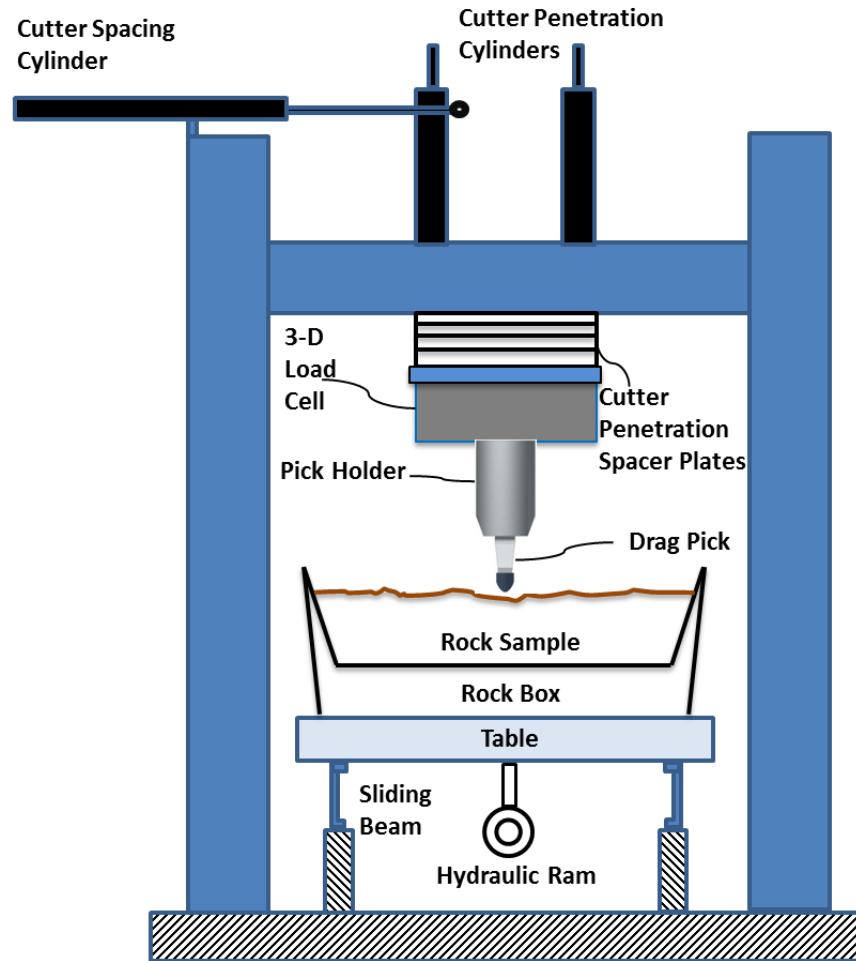


Figure 3.2. Schematic view of linear rock cutting machine with drag pick mounted.

#### 3.1.1.2 Cutting tool. Two types of rock cutting tools were used in this research.

- Disc cutter.** A 292 mm (11.5 in) diameter constant cross-section (CCS) long bladed disc cutter manufactured by Robbins Company was used for all disc cutting experiments. The blade of the cutter has a width of 11 mm (0.43 in) (Figure 3.4). The matrix of spacing and penetration combinations used for disc cutting tests is shown in Tables 3.1 and 3.2 for dry and saturated blocks.
- Radial drag pick.** One type of radial drag pick (model AM 239 MB) manufactured by Kennametal Inc. was used for all drag pick cutting experiments. The pick geometry is: rake angle  $5^\circ$ , back clearance angle



Figure 3.3. LRCM with long bladed disc cutter. Penetration spacer plates are hidden behind the locking beam above the load cell.



Figure 3.4. Long bladed disc cutter assembly and 3-D load cell.

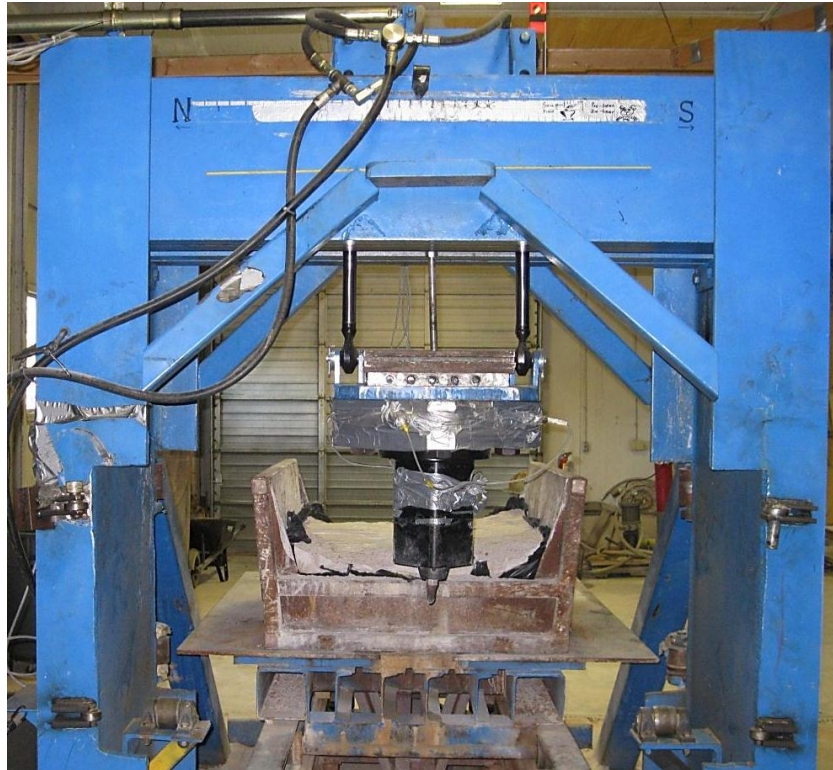


Figure 3.5. LRCM with drag pick. The cutter mount assembly and the load cell are at their fullest extension depth, though the penetration spacer plates are not yet loaded above the load cell.

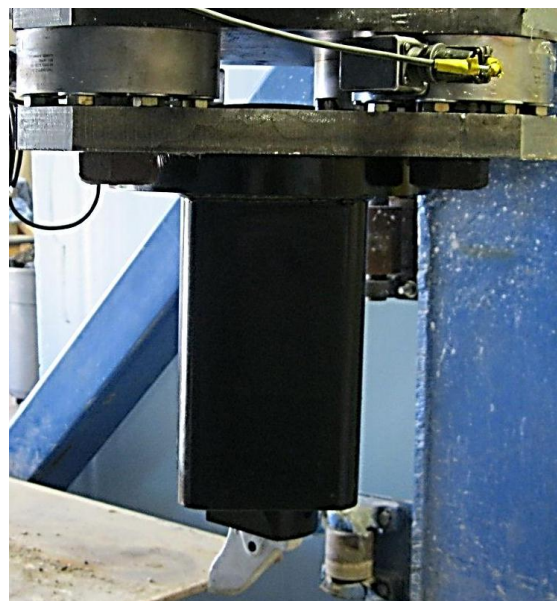


Figure 3.6. Drag pick assembly and 3-D load cell. The vertical mount locates the tip of the pick at the same depth as the bottom of the disc cutter.



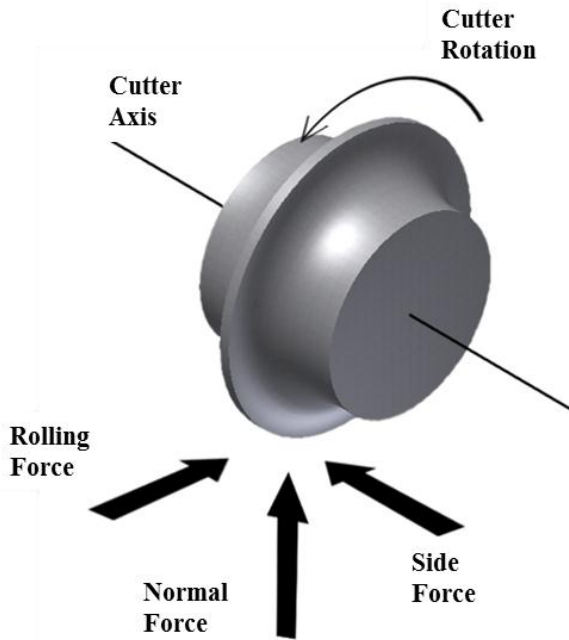


Figure 3.7. Forces acting on a disc cutter while cutting.

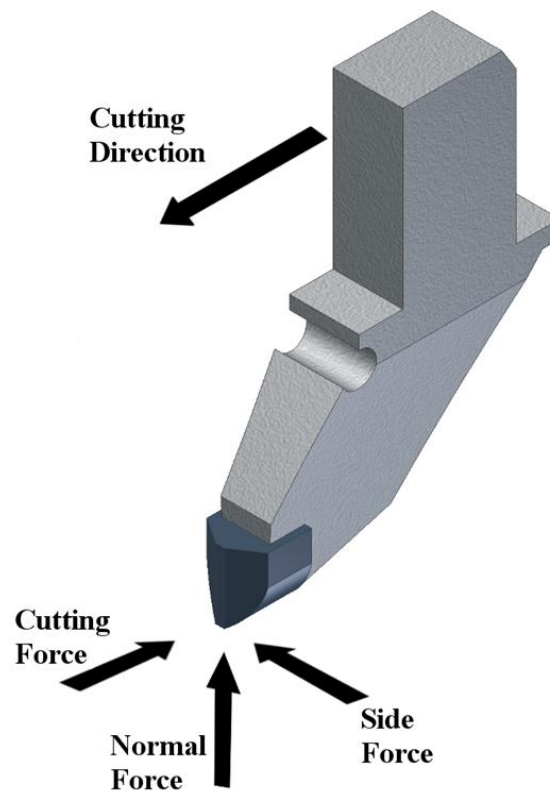


Figure 3.8. Forces acting on a drag pick while cutting.

10°, pick width 19.32 mm (0.76 in), pick gage 80 mm (3.15 in), shank width 41 mm (1.6 in), shank height 63 mm (2.5 in) (Figure 3.9). Table 3.3 gives the matrix of spacing and depth of cut combinations used for drag pick cutting experiments.

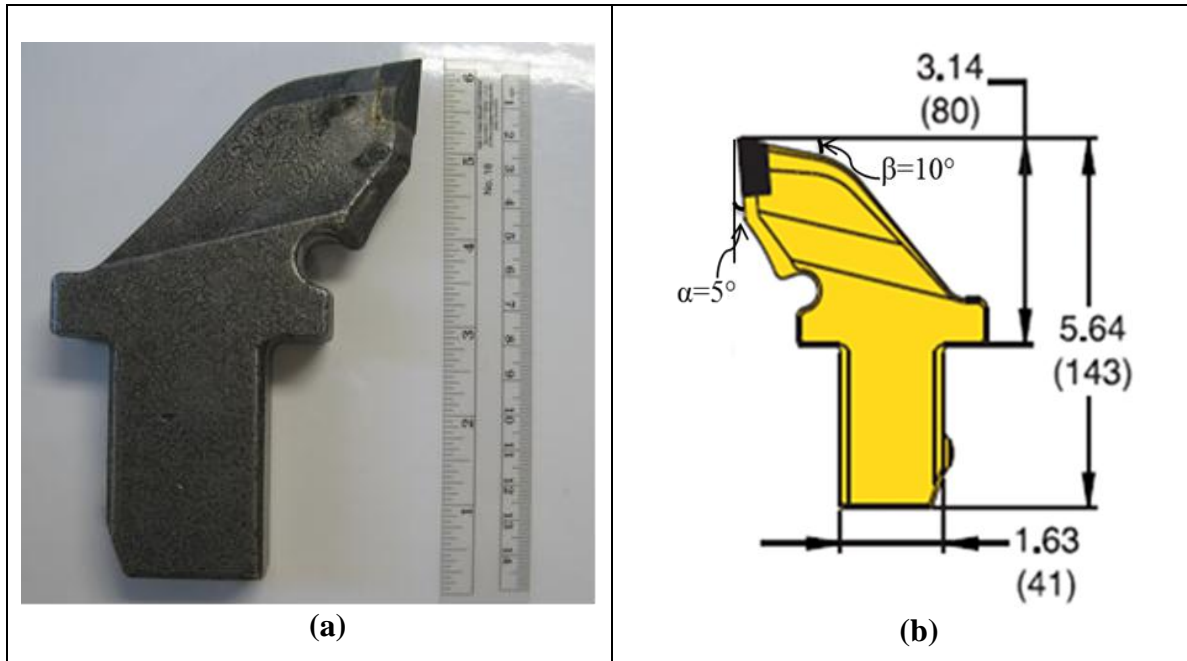


Figure 3.9. Drag pick (a) radial drag pick (b) radial pick dimensions ( $\alpha$ = rake angle,  $\beta$ = back clearance angle) (Kennametal Catalog, 2012).

**3.1.1.3 Motion control.** There are three motion control systems on the LRCM. The first one is the “spacing control”. The cutterhead is moved sideways by using the cutter spacing cylinder attached at the top of the frame of LRCM. This movement control manages the spacing parameter of the cutting and is activated only when cutting is not occurring.

The second one is “penetration control”. Penetration spacer plates or shims are held in place between the load cell and the frame of the machine by a pair of hydraulic rams. These hydraulic rams move up to clamp the shims.

The third control is the “linear actuator” used to move the rock table linearly forward (during cutting) and backward (after a cut) by a hydraulic ram at a controlled speed. This allows the rock box on the table to pass under the cutter at a depth of cut set by the penetration plates and positioned by the spacing control.

Table 3.1. Disc cutting experimental matrix for saturated blocks (cell values are the spacing/penetration ratios).

Spacing(in)		Penetration(in)				Spacing(mm)	
		0.25	0.375	0.5	0.625		
3	12	8	6			76	
4.5	18	12	9			114	
5	20	13.33	10			127	
6	24	16	12	9.6		152	
9	36			14.4		228	
		6.4	9.5	12.7	15.9		
		Penetration(mm)					

Table 3.2. Disc cutting experimental matrix for dry blocks (cell values are the spacing/penetration ratios).

		Penetration(in)						Spacing(mm)	
		0.25	0.375	0.5	0.625	0.75	0.875	1	
3	12	8	6						76
4.5	18	12	9						114
5	20	13.33	10						127
6	24	16	12	9.6					152
9				14.4	12	10.3			228
10					13.33		10		254
12					16	13.7	12		304
		6.4	9.5	12.7	15.9	19	22.2	25.4	
		Penetration(mm)							

Table 3.3. Test matrix for dry and saturated experiments with the radial drag pick (cell values are the spacing/depth of cut ratios).

Spacing (in)	Depth of Cut (in)				Spacing (mm)
	0.125	0.25	0.375	0.5	
1	8	4	2.7	2	25.4
2	16	8	5.3	4	50.8
2.5	20	10	6.7	5	63.5
3	24	12	8	6	76.2
3.5	28	14	9.3	7	88.9
	3.2	6.4	9.5	12.7	
	Depth of Cut (mm)				

**3.1.1.4 Data acquisition system.** A computer based data acquisition system is used to record the outputs from the 3-D load cell and the linear variable differential transducer (LVDT) attached for rock position measurement. The data logging software (National Instruments Labview 8.5) is programmed to scan each force and displacement channel at 5000 samples per second, providing several thousand readings for each cut made across the rock sample. The data acquired from the software is processed using calibration constants derived to obtain average, maximum and minimum cutting forces, ratio of forces, cutting coefficients, specific energy of cutting and other relevant data (Section 3.1.4). Figure 3.10 shows the schematic drawing of the LRCM control and data acquisition system.

**3.1.2. LRCM Testing Procedure.** As shown in Figure 3.3 and 3.5, the rock sample for LRCM testing is held firmly within a structural steel box having a tapered section to provide sample confinement and to avoid splitting of the sample while it is being cut. The tapered section also provides ease of the sample removal from the rock box after the intended tests are completed.



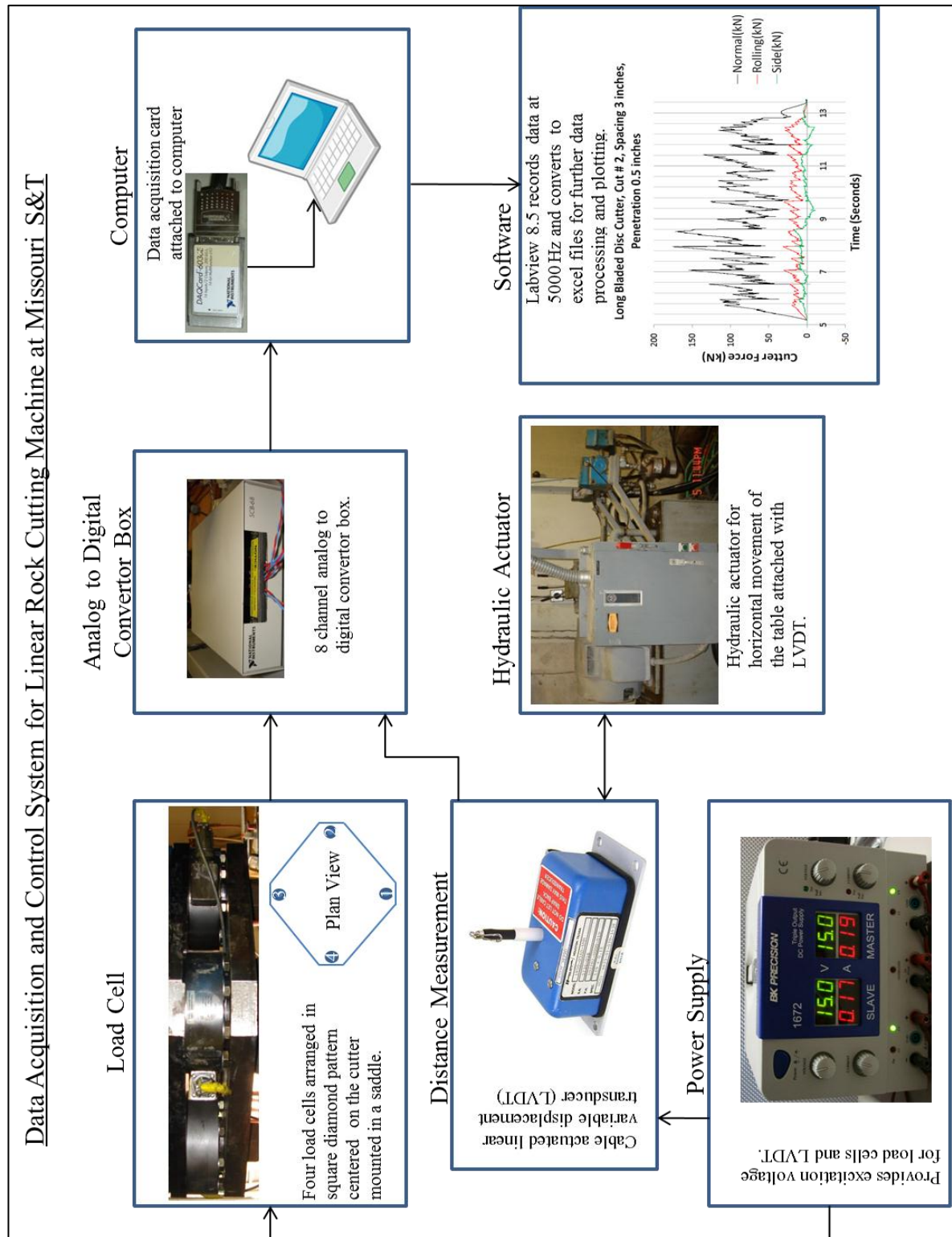


Figure 3.10. Schematic drawing of data acquisition and control systems for linear rock cutting machine.

The particular sequence for cutting rock on a LRCM is as follows:

1. The rock sample cast in concrete is placed on the table of LRCM and the steel rock box welded to it to hold rock sample firmly while cutting is in progress.
2. The distance between the cutting tool and the top of the material sample is first adjusted precisely to ensure that a consistent penetration of the cutter into the sample will occur. This is achieved by placing a series of cutter penetration spacer plates of several thicknesses between the cutter support and the frame of the machine and then held in place by a pair of locking beams (one in front and one in back, not shown in the schematic).
3. A series of conditioning passes are made at the desired spacing and penetration. Conditioning passes are required to create the damaged rock surface similar to field conditions where the cutters are always cutting in the damaged rock from the previous passes of the cutters on the excavator. Conditioning also levels the rock surface.
4. Once the conditioning passes are made and the surface of the rock sample is ready for actual testing, a data window is marked on the rock sample (Figure 3.11). The number of cuts in the data window varies for each pass, dependent upon the selected spacing and the rock surface condition (Figure 3.12).
5. Data pass is made and the signal outputs from the load cell and the LVDT attached to the table are recorded. To minimize end effects, the data cuts within the data window are marked 3-4 inches from both the ends of the rock sample. The side cuts (adjacent to the casting concrete) are also not included in the data analysis to minimize side boundary effects.
6. The broken chips within the data window are collected carefully so as to avoid any further breakage during handling. Collected chips are sieved for particle size analysis and mass of each particle size is recorded for further analysis. The saturated fragments from saturated rock blocks are oven dried for 24 hours at 105 C° to dry them fully prior to sieving. Figure 3.13 shows the particle size distribution of the chips collected from a typical test.
7. Once all the cuts at a particular spacing and penetration are completed, steps 1-6 are repeated at different spacing and penetration values.

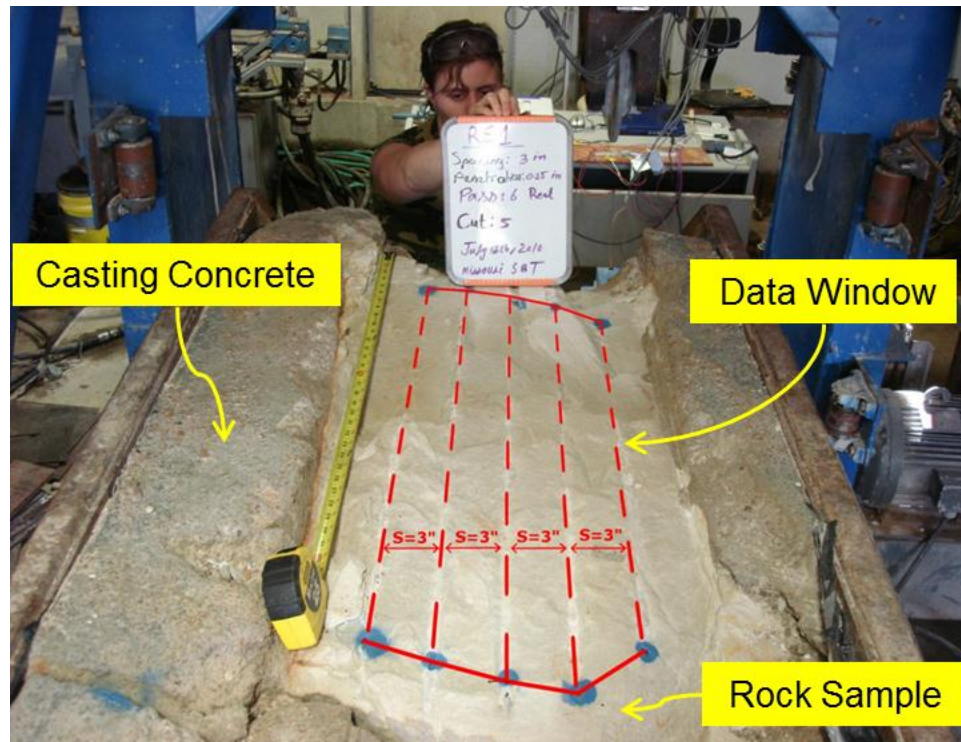


Figure 3.11. Data window showing 5 data cuts at 76.2 mm (3 in) spacing.

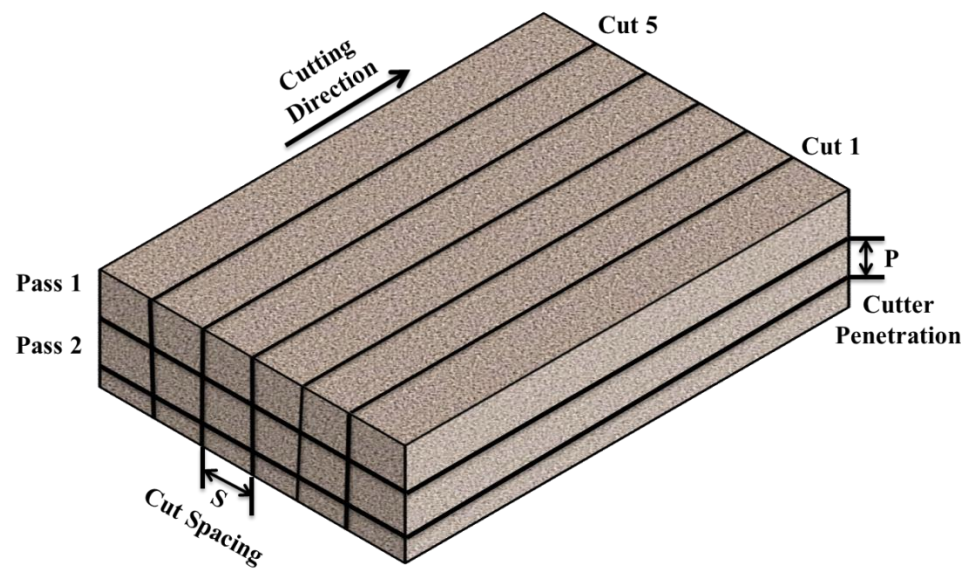


Figure 3.12. LRCM test nomenclature.





Figure 3.13. Particle size distribution from a disc cutter data pass at  $s = 114.3$  mm (4.5 in),  $p = 12.7$  mm (0.5 in).

**3.1.3. Sample Preparation and Saturation.** The rock samples for the test program were obtained from a commercial quarry located 15 miles from the campus of Missouri S&T. They were split at the quarry into blocks of appropriate dimensions for the size of the testbed. Once delivered, the blocks were cored to obtain samples with which to determine the standard suite of rock strengths, then divided randomly into those to be used for the air-dry cutting tests and those to be used for the saturated cutting tests.

**3.1.3.1 Dry samples preparation.** The rock samples to be tested are cast in concrete in the steel rock boxes and allowed to cure for about a week prior to testing. The rock box is turned upside-down to leave the concreted side at the bottom and the rock exposed at the top. Plywood or steel “dams” are clamped to close the cutouts at the ends of the rock box. The rock sample is centered in the steel box, which is lined with a thick plastic sheet. The plastic sheet serves the purpose of preventing the flow of wet concrete out of the rock box and also makes the removal of leftover rock and concrete from the box much easier (Figure 3.14). Different rock box sizes are used depending upon the rock block size. Concrete is prepared in a small electric mixer and placed by hand (Figure 3.15).



Figure 3.14. Rock sample placed in the center of the upside-down rock box lined with thick plastic sheet.

The concrete used for casting is commercial grade concrete with much higher percentage of sand added to it. This is required to make it weaker than the rock being tested and still strong enough to hold the rock in place.



Figure 3.15. Casting a rock sample for LRCM testing.

**3.1.3.2 Saturated samples preparation.** The rock blocks are saturated in accordance with the method suggested by US Army Corp of Engineers for dredging research (1995). Though intended to be used for rock cores, it was successfully applied to the large rock blocks of approximately 46 cm (18 in) thickness and 76 cm by 107 cm (30 by 42 in) in area for the LRCM tests.

This method enlists capillary forces to saturate rock samples progressively without the need for either high fluid pressure or a vacuum. Complete submergence of rock samples in water has been previously reported (Mammen et al. 2009; Roxborough and Rispin, 1973), but complete submergence leaves dry zones inside the rock samples from which the pore air cannot escape.

The rock sample is placed carefully in a large container with water less than 1 cm (0.4 in) deep that covers the entire bottom of the rock. If the rock bottom is smooth, several thin wedges or pebbles are placed beneath it. The water slowly rises upward through the rock pores at a rate dependent on both the rock's permeability as well as its mineralogy. At one-day intervals (more often if the permeability is high); the water level is increased to no more than half the additional vertical distance gained by the wetting front during the preceding time interval. This incremental deepening of the soaking water continues until the wetting front reaches the top of the rock (Figure 3.16), after which the container is filled to cover the sample completely (Figure 3.17). Because of the high permeability of the Roubidoux sandstone, most of the blocks achieved full saturation within one week. Each saturated block was tested after an average 3 and 10 months of continuous submergence for disc cutting tests and drag pick tests respectively.

The saturated rock samples are also cast in concrete in steel rock boxes by using the same method as described for dry rock samples. To prevent likely drying of the rock during preparatory work, all saturated blocks mounted on the LRCM are maintained and cut under slow, continuous water flow. The quantity of dripping water is enough to moisten the rock surface, but not sufficient to flush rock chips.



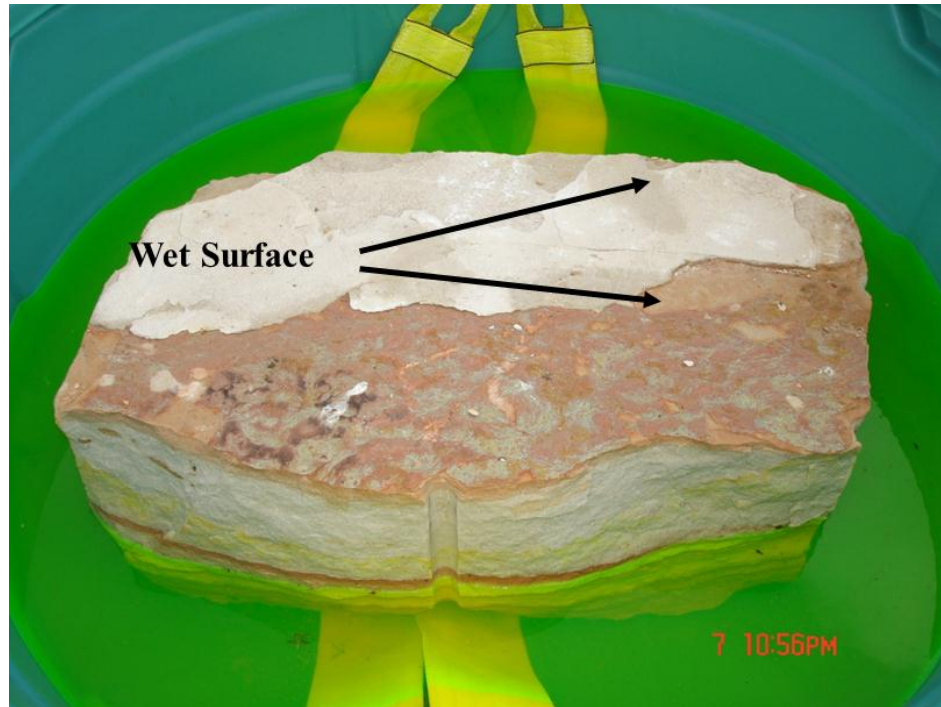


Figure 3.16. Wet surface reached the top of the block after three days due to capillarity.



Figure 3.17. A sandstone block totally submerged after wet surface reached the top. The tub is 1.65 m in diameter and 0.6 m deep.



**3.1.4. Load Cell Calibration Constants.** Load cell calibration constants are calculated according to the rules of statics. In equilibrium condition the sum of all external forces acting on a body is equal to zero and the sum of the moments of the external forces about a point is equal to zero. Figure 3.18 shows the force directions whereas Figure 3.19 and Figure 3.20 show the moments arms for the disc cutter and the drag pick.

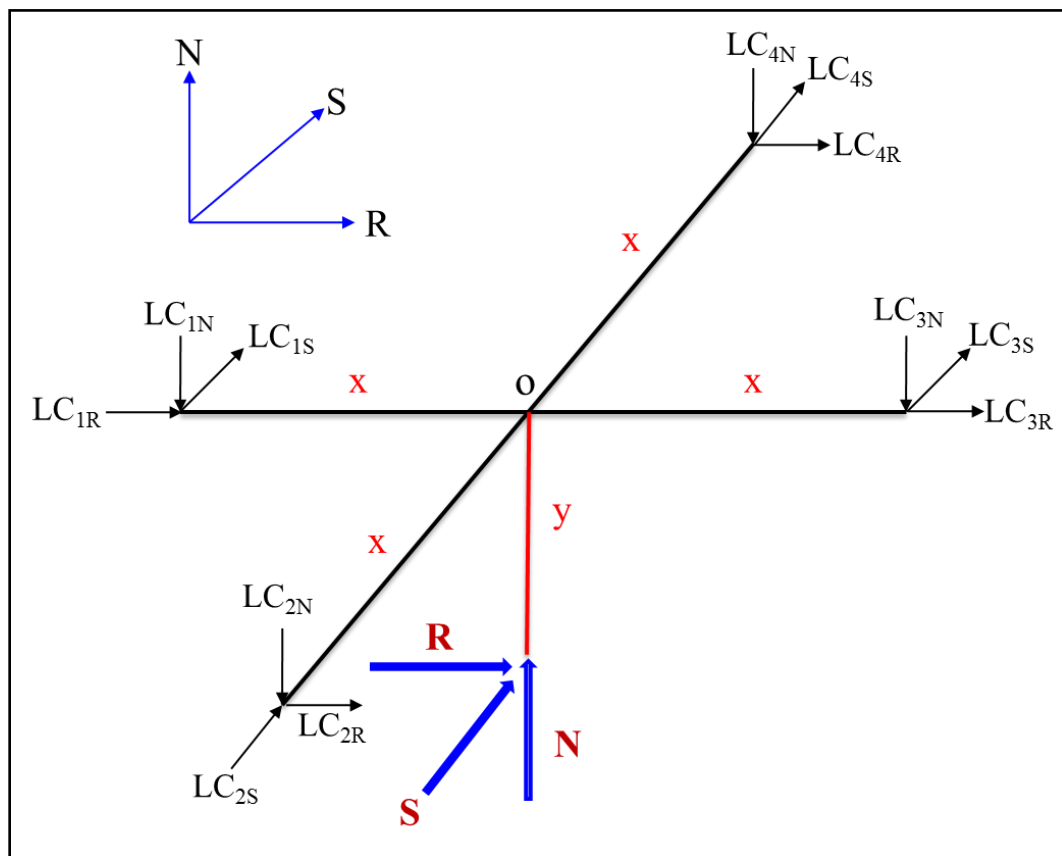


Figure 3.18. Perspective view of force directions.

**For force equilibrium:**

$$\Sigma F_N = 0; \Sigma F_R = 0; \Sigma F_S = 0$$

$$\Sigma F_N = 0$$

$$N - (LC_{1N} + LC_{2N} + LC_{3N} + LC_{4N}) = 0$$

$$N = \Sigma LC_N \quad (3.1)$$

$$\Sigma F_R = 0$$

$$R - (LC_{1R} + LC_{2R} + LC_{3R} + LC_{4R}) = 0$$

$$R - \Sigma LC_R = 0$$

$$R = \Sigma LC_R \quad (3.2)$$

$$\Sigma F_S = 0$$

$$S - (LC_{1S} + LC_{2S} + LC_{3S} + LC_{4S}) = 0$$

$$S - \Sigma LC_S = 0$$

$$S = \Sigma LC_S \quad (3.3)$$

**For moment equilibrium:**

$$\Sigma M_N = 0; \Sigma M_R = 0; \Sigma M_S = 0$$

$$\Sigma M_N = 0$$

$$(LC_{3S} - LC_{1S}).x + (LC_{2R} - LC_{4R}).x = 0 \quad (3.4)$$

$$\Sigma M_R = 0$$

$$(LC_{2N} - LC_{4N}).x + S.y = 0 \quad (3.5)$$

$$\Sigma M_S = 0$$

$$(LC_{3N} - LC_{1N}).x + R.y = 0 \quad (3.6)$$

From equation 3.4:

$$(LC_{3S} - LC_{1S}).x = -(LC_{2R} - LC_{4R}).x$$

or

$$(LC_{1S} - LC_{3S}) = (LC_{2R} - LC_{4R})$$

From equation 3.5 and equation 3.3:

$$(LC_{2N} - LC_{4N}).x = -S.y$$

or

$$S = (LC_{4N} - LC_{2N}).\frac{x}{y} = \Sigma LC_S \quad (3.7)$$

From equation 3.6 and equation 3.2:

$$(LC_{3N} - LC_{1N}).x = -R.y$$

or

$$R = (LC_{1N} - LC_{3N}).\frac{x}{y} = \Sigma LC_R \quad (3.8)$$

Where

N= normal force

R= rolling force in case of disc cutter and drag force in case of drag pick

S= side force

LC<sub>1</sub>= load cell one

LC<sub>2</sub>= load cell two

LC<sub>3</sub>= load cell three

LC<sub>4</sub>= load cell four

y= vertical distance between the load cell and cutter-rock contact (vertical moment arm to the center of the load cell)

- **Moment Arm Ratio for Long Bladed Disc Cutter**

$$x = 10.076''$$

$$y = 14'' \text{ (disc cutter + saddle)} + 1.25'' \text{ (lower plate thickness)} + 0.375'' \text{ (bottom of load cells)} + (1+13/16)/2'' \text{ (half of load cell thickness)}$$

$$\text{Moment Arm Ratio} = x/y = 0.6095$$

- **Moment Arm Ratio for Radial Drag Pick**

$$x = 10.076''$$

$$y = 3.11'' \text{ (pick height)} + (1+10/16)'' \text{ (pick holder)} + (10+6/16)'' \text{ (square cylinder)} + 1.25'' \text{ (new round plate)} + 1.25'' \text{ (lower plate thickness)} + 0.375'' \text{ (bottom of load cells)} + (1+13/16)/2'' \text{ (half of load cell thickness)}$$

$$\text{Moment Arm Ratio} = x/y = 0.5334$$

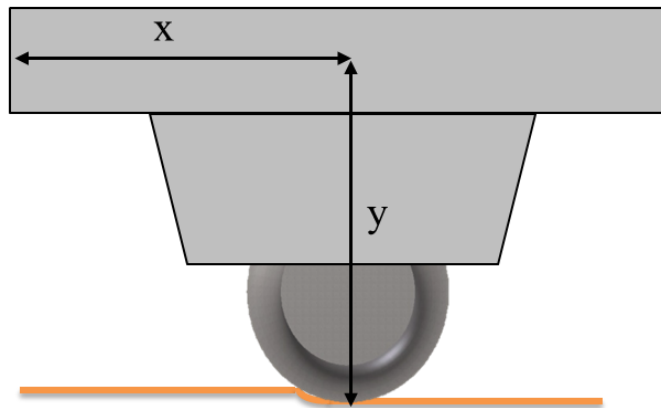


Figure 3.19. Moment arms for disc cutter.

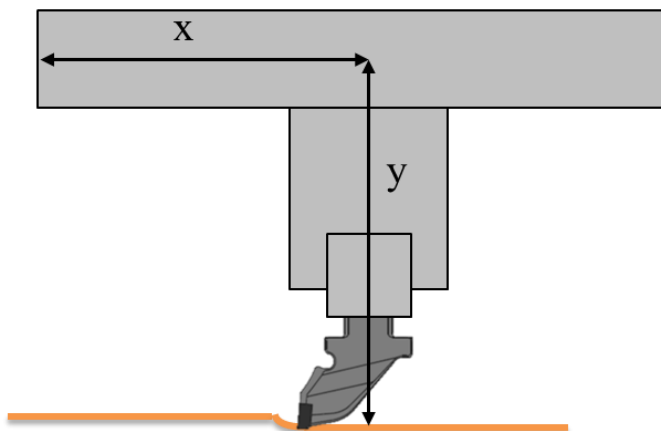


Figure 3.20. Moment arms for drag pick.

**3.1.5. Load Cell Calibration Procedure.** Figure 3.21 and Figure 3.22 show the calibration setup for disc cutter and radial drag pick, whereas Figure 3.23 shows the directional arrangement of load transducers. The 3-D load cell mounted above the cutter assembly is calibrated prior to the actual testing on LRCM and at other times as necessary, for example when the cutter is changed. The calibration is achieved by applying pressure to the cutter using a hydraulic ram (Figure 3.21 and Figure 3.22) and measuring the resulting voltages from the four load transducers. Labview 8.5 data

acquisition software at a sampling rate of 5000 samples/second is used to record the voltage outputs of the load cell, the same as used during testing.

The loading of the cutter is achieved at an angle of  $7.5^\circ$  by placing a metallic wedge under the hydraulic ram. The angled loading of the cutter is done to simulate closely the direction of forces in actual field cutting. The calibration starts by placing the angled ram under one of the load transducers (opposite to the one being calibrated), applying the pressure in the increments of 6.89 MPa (1000 psi) and recording the signal output at each increment. This pressure is increased up to 34.47 MPa (5000 psi) and then decreased in decrements of 6.89 MPa (1000 psi) to zero. At each pressure decrement the voltage output from the load transducers is also recorded.

This whole procedure is repeated for each load transducer, producing 48 data files (12 files for each load transducer) which are processed using Microsoft Excel. The calibration constants are calculated using force and moment equilibrium equations. (Detailed calculations are provided in Appendix A).

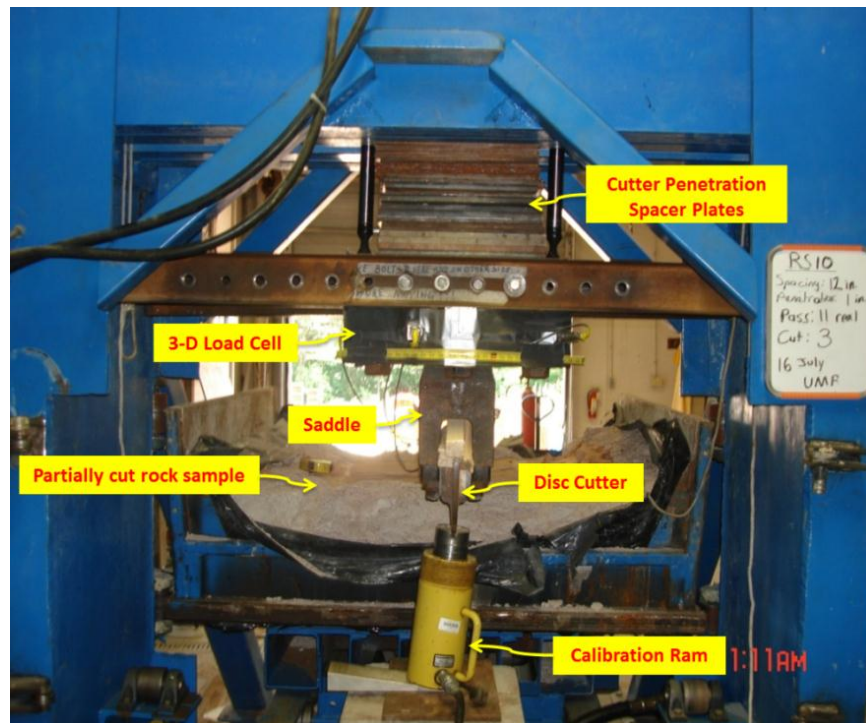


Figure 3.21. Calibration of load transducer 2 for disc cutting tests; note: wedge placed under load transducer 4 (Figure 3.23 shows the arrangement of load transducers).



Figure 3.22. Calibration of load transducer 1 for radial pick tests; note: wedge placed under load transducer 3 (Figure 3.23 shows the arrangement of load transducers).

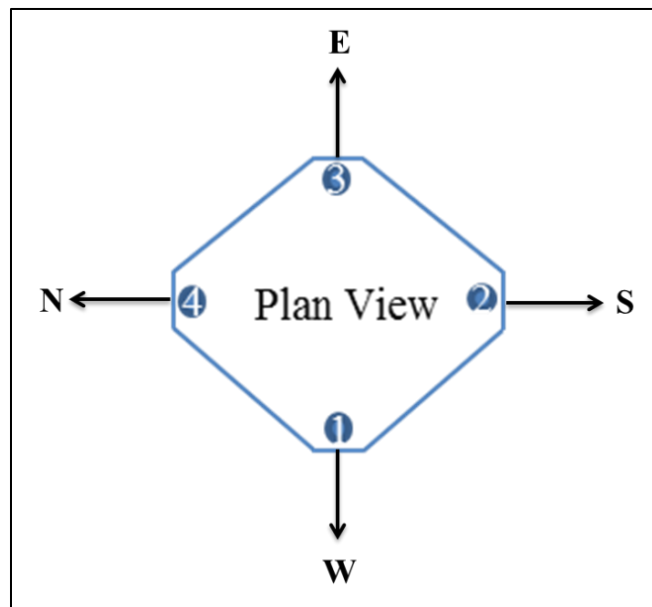


Figure 3.23. Directional arrangement of load transducers of 3-D load cell.

**3.1.6. String Potentiometer Calibration.** A cable actuated potentiometer or linear variable differential transducer (LVDT) attached to the table of the LRCM is also calibrated prior to the start of the testing. The stringpot is removed from the table of the LRCM and clamped to a stable surface. The string of the potentiometer is attached to a precision height gage used by machinists, which is then moved in increments of 2.54 cm (1 in). The resulting voltage outputs are recorded using the Labview 8.5 data acquisition system. 20 readings are recorded to calculate the calibration constant used for calculation of distance traveled by the rock table during the cutting experiments.

### **3.2. LOAD-INDENTATION TESTS**

Load-indentation tests were the second main set of experiments conducted in this research. Load-indentation test, also known as punch penetration test, is an empirical laboratory test that was originally designed to provide a direct method for estimating the normal loads on button and disc cutters during mechanical excavation of rocks. The first punch test apparatus was designed by Handewith (1970). Since this test directly determines the cutter normal loads during TBM and RBM (Raise Boring Machine) excavation, it belongs to the same category of laboratory tests as the linear cutting and rotary cutting tests. The advantage of this test method over the full scale LRCM tests is that it is simpler to perform and much less expensive to own and operate. This is also more practical because it uses much smaller test samples which allows for many tests to be run in a limited budget (Dollinger et al., 1998). However, the smaller sample size cannot take rock discontinuities or fractures into account. Moreover, in a load-indentation test, variation of spacing to incorporate effect of interaction between adjacent cuts is not possible.

**3.2.1. Load-Indentation Test Setup.** Figure 3.24 shows the main test setup for load-indentation tests. In the load-indentation test a hydraulic ram pushes an indenter perpendicularly into a saw-cut rock surface. The indenter used in this research was of conical shape and was made of tungsten carbide. Figure 3.25 shows the indenter itself whereas Figure 3.26 shows geometry of the indenter. The hydraulic ram used to push the indenter into the rock sample is fixed to the load frame and is actuated using a hydraulic pump.



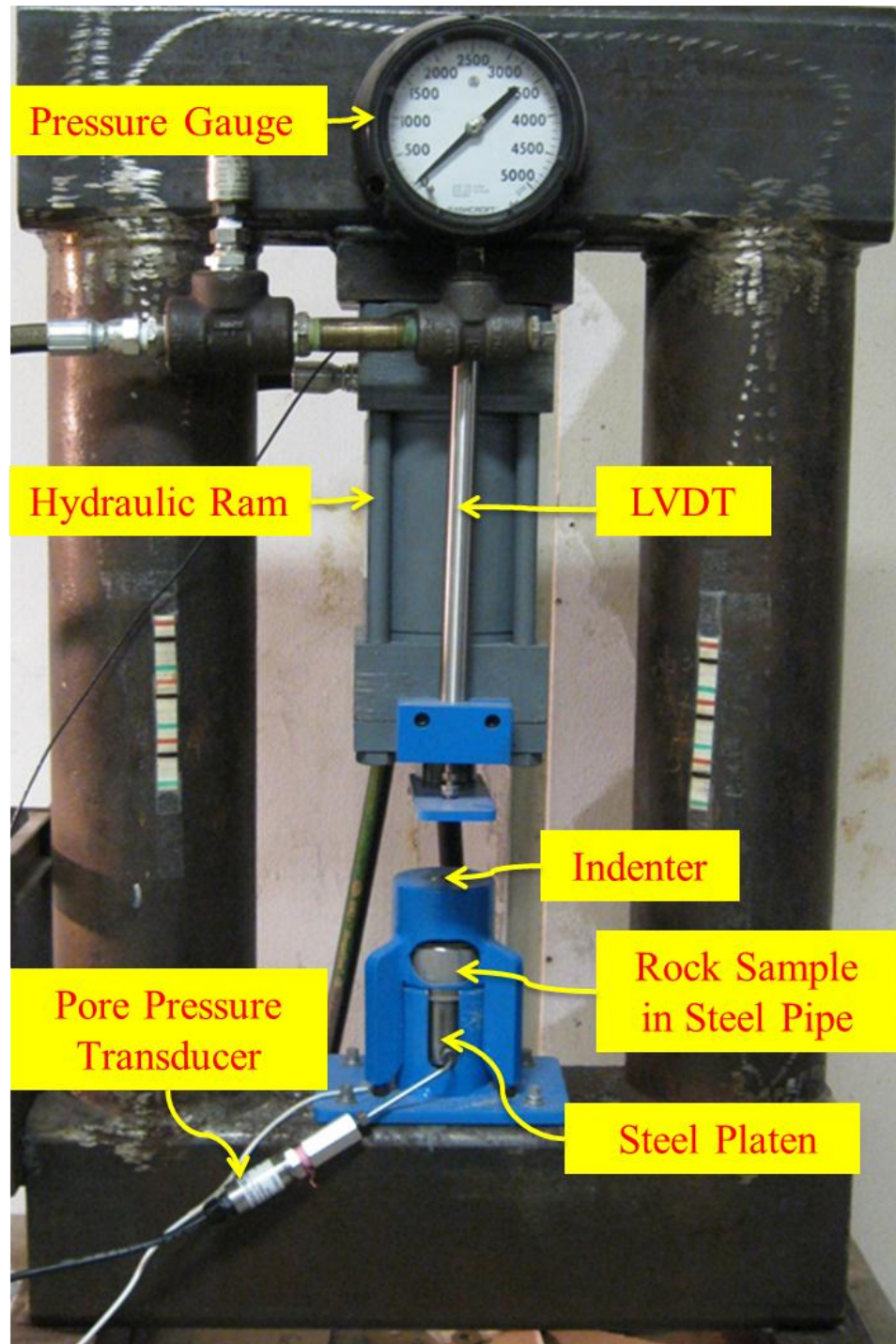


Figure 3.24. Load-indentation test setup at Missouri S&T.





Figure 3.25. Conical indenter used for load-indentation tests.

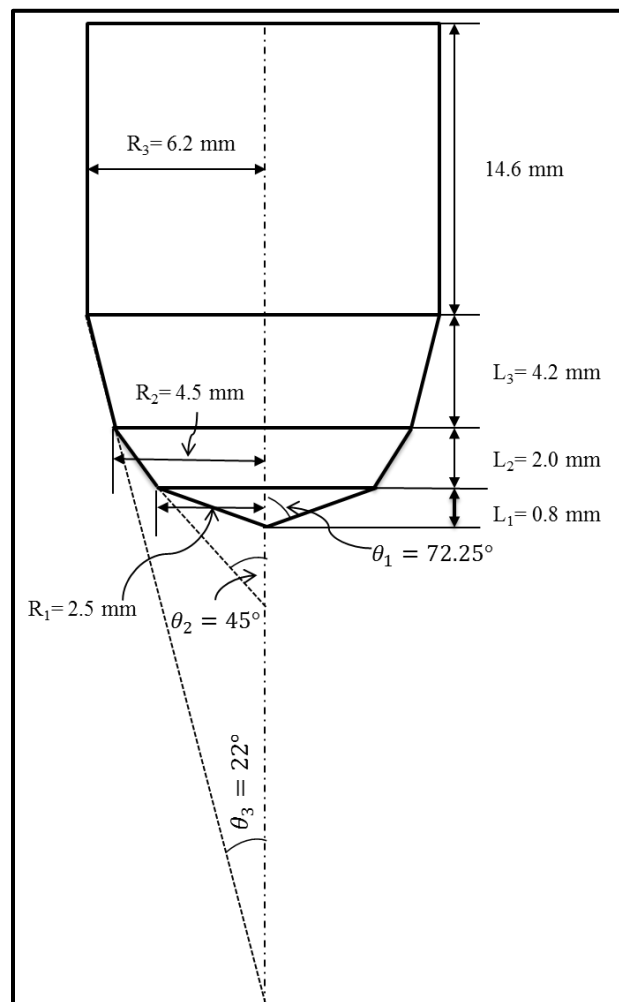


Figure 3.26. Conical indenter geometry (not drawn to scale).

The rock sample was confined by Hydrostone (a high strength plaster of Paris) within steel pipe of 60 mm (2.375 in) diameter. The 25.4 mm (1.0 in) thick rock samples were of 44.70 mm (1.75 in) in diameter (Figure 3.27). Confinement of the samples in the steel pipes with Hydrostone is required to simulate the partially confined rock condition at the tunnel face and to prevent the samples from failing prematurely due to tensile splitting. Hydrostone swells as it sets and provides a small confining pressure on the sample (Dollinger et al., 1998). This material has an expansion factor of 0.002-0.003% and produces a confining pressure of approximately 100 psi on standard NX core size (Dollinger, 1978).



Figure 3.27. Load-indentation sample cast in hydrostone.

It was required to measure the porewater pressure generated during the indentation of saturated rock samples. For this purpose, a hardened steel platen with a set of drainage channels connected to a central drainage hole was attached to the bottom of the steel pipe containing the rock sample (Figure 3.28). The drainage hole had an inner diameter of 2 mm (0.079 in). Rubber O-rings provided the necessary sealing against

leakage of water. The drainage hole of the platen was attached to a 50 psig pressure transducer with appropriate couplings. Measurement of the porewater pressure during indentation was a new addition which is absent in traditional load-indentation test setups.

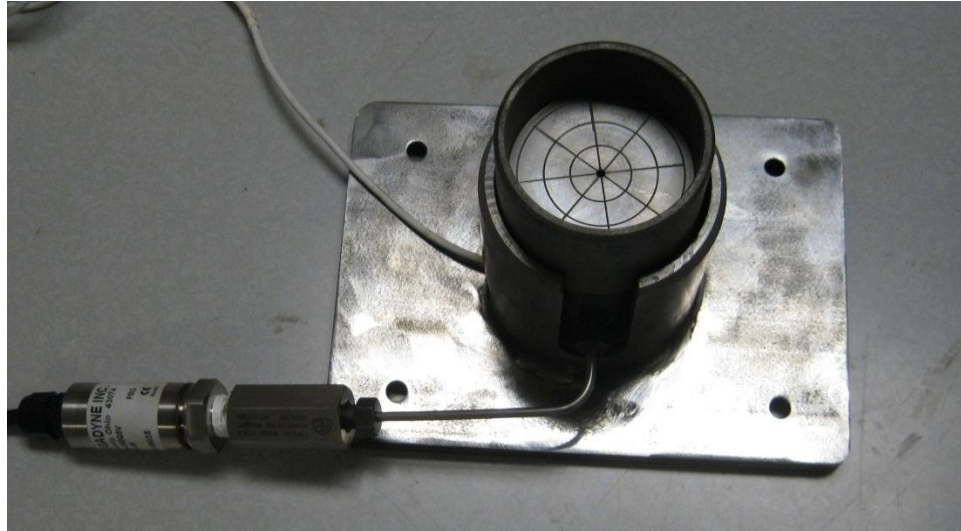


Figure 3.28. Bottom platen with pore pressure drainage channels, attached to pressure transducer.

The displacement of the indenter into the rock sample was monitored by a linear variable differential transducer (LVDT) attached to the hydraulic ram. The load transmitted through the test sample was monitored by a load cell placed under the porewater pressure platen. The output voltages from the LVDT, load cell and porewater pressure transducer were converted from analog to digital form and were recorded using a computer based Labview 8.5 data acquisition system at a sampling rate of 1000 samples/sec. Figure 3.29 shows the schematic of the load-indentation test setup.

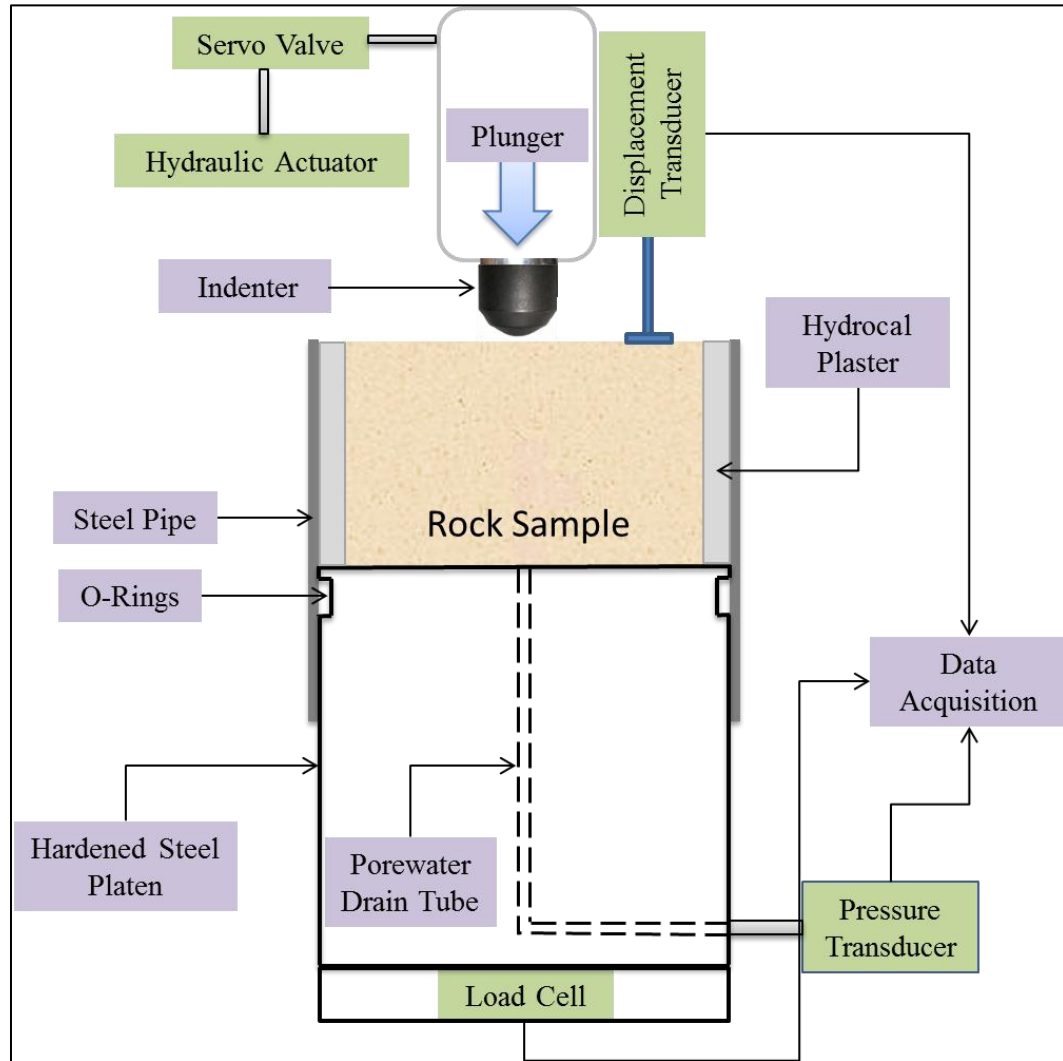


Figure 3.29. Load-indentation test schematic.

**3.2.2. Load-Indentation Test Procedure.** The particular sequence of load-indentation test is as follows:

- The saw cut rock sample is cast in the steel pipe using Hydrostone.
- The test sample is attached to the porewater pressure platen.
- The test sample is positioned under the indenter.
- The hydraulic pump is pressurized.

- The hydraulic ram is pushed into the rock sample and the outputs from the LVDT, load cell and the porewater pressure transducer are recorded using the Labview 8.5 data acquisition system.
- Calibration constants are used to calculate the load, displacement, the pore pressure generated and the indenter pressure.

### 3.3. ROCK SAMPLE

The rock sample used in this research program was Ordovician-age Roubidoux Sandstone, a medium grained, laminated to thinly bedded quartz sandstone that is porous and somewhat friable. It is usually found in white or red varieties depending on iron coloration. According to Dake (1918), the Roubidoux Sandstone has a larger surface outcrop than any other sandstone in Missouri, and the formation is widely variable in its characteristics from point to point. Formations vary from 100 to 150 feet thick with an aggregate of 30 to 60 feet of sandstone (Selimoglu, 2009).

The sand grains are nearly euhedral double-ended quartz prisms that show little wear or abrasion (Gertsch and Summers, 2006). X-ray diffraction of this sandstone shows that it comprises almost 94% quartz and 6% kaolinite. The clay and trace amounts of iron oxides are the sparse cement that holds the grains together.

### 3.4. ROCK PROPERTY TESTS

In this research program, three main rock property tests were conducted. Table 3.4 lists the physical properties of the rock samples used in both the LRCM and the load-indentation tests.

The first tests applied to the rock samples were uniaxial compressive strength (UCS) tests. These tests were performed on both dry and saturated rock samples. The samples were prepared to satisfy the requirements of ASTM D4543. The UCS tests were performed in accordance with the method suggested by ASTM D7012-10. The uniaxial strength ( $\sigma_c$ ) was calculated using the equation:

$$\sigma_c = \frac{F}{A} \quad (3.1)$$

Where

$F$ = maximum load on failure

$A$ = area of the surface under the load ( $A = \pi r^2$ )

The second rock property measured was Brazilian tensile strength (BTS). BTS was measured for both dry and saturated samples. The samples were prepared in accordance with the requirements of ASTM D4543. The BTS tests were performed in conformance with ASTM D3967-08. The indirect tensile strength ( $\sigma_t$ ) was calculated using the equation:

$$\sigma_t = \frac{2P}{\pi DL} \quad (3.2)$$

Where

$P$ = maximum load on failure

$D$ = sample diameter

$L$ = length of sample

The UCS and BTS tests were conducted on the 181 ton (400,000 lbs.) Forney testing machine at RMERC (Figure 3.30).

The third group of rock property tests determined the effective rock porosity and dry density. The tests were performed in accordance with the saturation and caliper method suggested by ISRM (1981) using the following equations:

$$V_v = \frac{M_{sat} - M_s}{\rho_w} \quad (3.3)$$

$$n = \frac{100V_v}{V} \% \quad (3.4)$$

$$\rho_d = \frac{M_s}{V} \quad (3.5)$$

Where

$V_v$  = volume of voids

$V$  = volume of solids

$M_{sat}$  = saturated mass of sample

$M_s$  = grain mass

$n$  = porosity

$\rho_d$  = dry mass density

$\rho_w$  = density of water



Figure 3.30. Forney 181 ton testing machine.

Table 3.4. Physical properties of the rock samples used.

<b>Rock Property</b>	<b>SI Units</b>	<b>English Units</b>
Uniaxial compressive strength (dry)	51 MPa	7400 psi
Uniaxial compressive strength (saturated)	43 MPa	6240 psi
Brazilian tensile strength (dry)	1.10 MPa	160 psi
Brazilian tensile strength (saturated)	1.00 MPa	145 psi
Dry density	2150 kg/m <sup>3</sup>	134 lb/ft <sup>3</sup>
Porosity	18%	18%
Constituents	Quartz 94%, Kaolinite 6%	
Structure	Medium grained, laminated to thinly bedded.	



## 4. EXPERIMENTAL RESULTS

This section encompasses the results of the tests performed in this study (outlined in Section 3). The computed parameters are also described here.

### 4.1. DISC CUTTING TESTS

Disc cutting tests were conducted on dry and saturated blocks of Roubidoux Sandstone using a long bladed constant cross-section (CCS) single disc cutter. Dry tests were performed at much wider cut spacing and cutter penetrations in relation to the saturated tests. Cut spacing ( $s$ ) and the cutter penetration ( $p$ ) are the parameters, which were changed during the tests according to the pre-defined experimental matrix described in Section 3.

**4.1.1. Force Measures.** The experimental results of 36 tests at given spacing and penetration, which were completed in 58 data passes encompassing 600 data cuts, are presented in Table 4.1 and Table 4.2 for dry and saturated cutting tests, respectively. Figure 4.1 shows a typical force trace of a disc cutting test. This trace represents a single cut. Normal, rolling and side forces are shown as separate force traces. Normal force is larger in magnitude than rolling and side forces. It can be observed that normal and rolling forces are very well correlated, and their force traces have similar shapes.

These three traces were plotted for each cut in each data pass. For the individual cuts on each data pass, the average, standard deviation and maximum forces were calculated (Table 4.1). The cut lengths and the cutting speed were also computed for each data cut (Appendix B). Weighted average values of cutting forces and other measured or calculated parameters were calculated from at least three data cuts at larger cut spacings and up to five data cuts at smaller spacings. The cut length of each data pass was taken as the weighting factor for averaging the different cutting related parameters.

**4.1.2. Chip Measures.** From the measured forces and collected chip masses (Appendix B) several parameters required for the performance prediction of excavators were calculated:

The cutting coefficient ( $CC$ ) which is the ratio of the rolling force to the normal force, expressed as a percent is considered as an indicator of the amount of torque needed

for a given amount of thrust. The higher the  $CC$ , the higher the torque needed by the tunnel boring machine. It also relates the rolling force to the normal force (Gertsch et al., 2007).

Table 4.1. Test results for long bladed CCS disc cutter in dry sandstone.

$s$	$p$	$s/p$	Avg. $F_N$	Avg. $F_R$	Avg. $F_S$	Peak $F_N$	Peak $F_R$	Peak $F_S$	$CC$
mm	mm		kN	kN	kN	kN	kN	kN	%
76.2	6.4	12	43.6	5.8	5.7	160.3	23.0	22.6	13.3
76.2	9.5	8	34.0	5.5	5.5	179.1	35.0	25.4	16.2
76.2	12.7	6	47.0	8.5	1.2	167.4	39.1	33.9	18.1
114.3	6.4	18	69.8	9.6	4.7	168.9	38.2	21.4	13.8
114.3	9.5	12	64.7	10.3	3.9	174.4	24.1	25.6	15.9
114.3	12.7	9	58.6	9.1	3.5	164.3	51.7	24.1	15.5
127	6.4	20	42.2	9.1	0.7	175.3	31.6	21.7	21.6
127	9.5	13.3	46.6	11.1	1.4	119.9	26.2	11.4	23.8
127	12.7	10	95.3	23.3	4.1	188.3	36.0	15.7	24.4
152.4	6.4	24	56.7	12.8	0.2	246.1	61.7	16.5	22.6
152.4	9.5	16	88.3	18.6	1.2	161.7	34.2	19.2	21.1
152.4	12.7	12	55.8	14.0	1.8	225.9	50.9	18.6	25.1
152.4	15.9	9.6	57.1	15.5	9.6	153.8	46.4	10.8	27.1
228.6	15.9	14.4	69.2	16.7	4.9	182.8	45.1	26.9	24.1
228.6	19.05	12	68.7	20.7	4.7	170.6	48.7	22.5	30.1
228.6	22.23	10.3	80.2	27.1	9.3	196.2	53.9	18.1	33.8
254	19.05	13.3	169.1	43.6	9.3	190.2	73.4	40.1	25.8
254	25.4	10	109.7	33.7	7.7	300.5	91.4	29.3	30.7
304.8	22.23	13.7	67.9	21.7	6.4	215.4	87.1	40.6	31.9
304.8	19.05	16	69.3	16.6	6.5	162.6	64.9	16.2	23.9
304.8	25.4	12	106.1	24.4	7.4	142.9	45.4	25.0	23.0
$s$ – cut spacing, $p$ – cutter penetration, $s/p$ – spacing to penetration ratio, $F_N$ – normal force, $F_R$ – rolling force, $F_S$ – side force, $CC$ – cutting coefficient.									

The specific energy ( $SE$ ) of rock fragmentation, which is defined as the amount of energy consumed for excavation of unit volume (mass) of the rock was calculated by two methods. The actual  $SE$  ( $SE_A$ ) in kW-hr/m<sup>3</sup> was calculated from measured chip mass as follows:

$$SE_A = 0.278 \frac{\bar{R}L\rho}{m} \quad (4.1)$$

Where

$\bar{R}$  = average rolling force (kN)

$L$  = length of cut (mm)

$\rho$  = rock density (g/cm<sup>3</sup>)

$m$  = mass of chips (g)

Table 4.2. Test results for long bladed CCS disc cutter in saturated sandstone.

$s$	$p$	$s/p$	Avg. $F_N$	Avg. $F_R$	Avg. $F_S$	Peak $F_N$	Peak $F_R$	Peak $F_S$	CC
mm	mm		kN	kN	kN	kN	kN	kN	%
76.2	6.4	12	24.7	3.9	2.8	92.1	22.0	14.2	15.8
76.2	9.5	8	23.2	3.5	2.2	99.0	25.2	12.6	15.1
76.2	12.7	6	44.3	6.6	3.9	126.0	28.2	15.9	14.9
114.3	6.4	18	47.0	7.8	3.7	136.0	26.5	13.9	16.6
114.3	9.5	12	53.1	9.4	3.0	126.4	32.4	12.5	17.7
114.3	12.7	9	58.5	9.1	4.1	155.0	36.3	18.3	15.6
127	6.4	20	32.8	8.3	3.1	102.8	25.3	6.2	25.3
127	9.5	13.3	48.0	9.9	0.8	151.1	30.7	17.2	20.6
127	12.7	10	61.4	9.1	4.1	169.0	34.2	24.9	14.8
152.4	6.4	24	43.8	8.6	0.8	120.9	22.6	12.7	19.6
152.4	9.5	16	80.2	12.2	2.7	217.3	45.4	25.2	15.2
152.4	12.7	12	61.6	9.8	2.3	222.0	39.0	21.5	15.9
152.4	15.9	9.6	69.4	14.6	0.9	193.5	52.8	13.4	21.0
228.6	6.35	36	43.1	7.9	1.2	106.9	21.6	12.1	18.3
228.6	15.9	14.4	74.1	16.5	0.6	204.4	57.7	19.8	22.2
$s$ – cut spacing, $p$ – cutter penetration, $s/p$ – spacing to penetration ratio, $F_N$ – normal force, $F_R$ – rolling force, $F_S$ – side force, CC – cutting coefficient.									

The more common method of calculation of  $SE$  is nominal ( $SE_N$ ), which uses the theoretical cutting volume, was calculated as:

$$SE_N = 0.278 \frac{\bar{R}L}{spL} \quad (4.2)$$

Where

$s$  = cut spacing (mm)

$p$  = cutter penetration (mm)

Nominal production rate ( $PR_N$ ) in kg/min was calculated from the dimensions of the cut and the cutting speed for each test as follows:

$$PR_N = \frac{s}{1000} \times \frac{p}{1000} \times v \times \rho \quad (4.3)$$

Where

$s$  = cut spacing (mm)

$p$  = cutter penetration (mm)

$v$  = cut speed (m/min)

$\rho$  = mass density ( $\text{kg/m}^3$ )

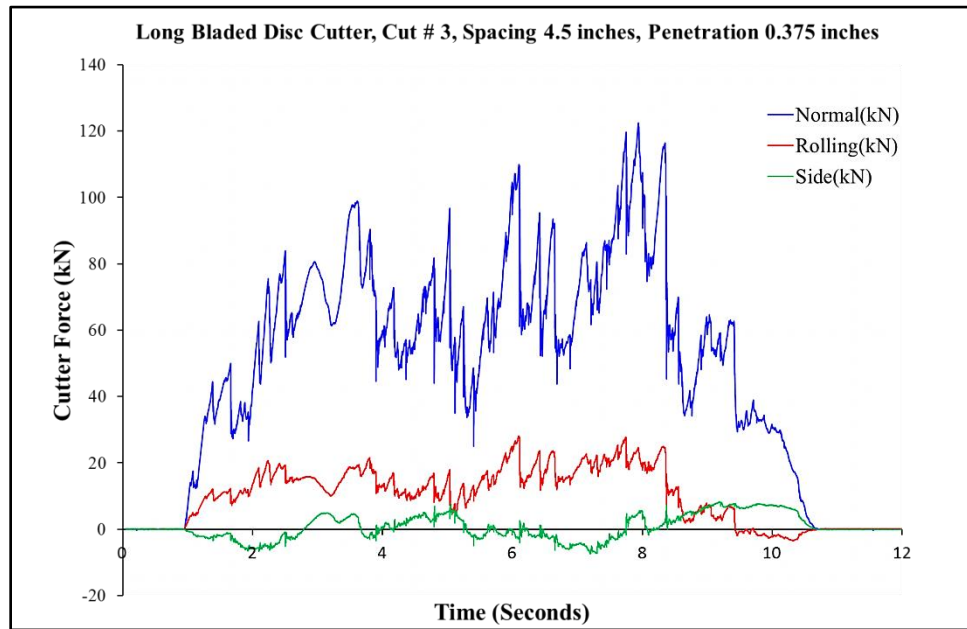


Figure 4.1. A trace of the forces recorded during one of the disc cutting tests.

By comparing nominal production rate with the actual production rate (computed from actual chip mass), it is possible to identify overbreaks and underbreaks (ridge formation). The differential between these two show the efficiency or validity of the cuts and related data.

Coarseness index (*CI*) (Barker, 1964; Roxborough and Rispin, 1973) and actual production rate or yield ( $PR_A$ ) in kg/min ( $m^3/min$ ) for each cutter spacing and penetration combinations were calculated from the results of sieve analysis.

*CI* values were calculated by adding the cumulative mass percentages of the chips retained on each sieve. Table 4.3 shows an example calculation for a particular data pass at  $s = 152.4$  mm and  $p = 16$  mm; Figure 4.2 shows grain size distribution curve for the same sample. Grain size distribution curves for other muck samples at same cut spacing and different cutter penetrations are included to show that the percentage of the coarser fragments decreases as the cutter penetration decreases keeping the spacing as constant. This is anticipated since increased penetration will improve chipping process and amount of chips will increase relative to the fines and dust created under the cutters.

Another set of measures was determined from the Rosin-Rammler approach frequently used to analyze the products of tumbling mills in the mineral processing industry. The Rosin-Rammler distribution describes the mass (volume) distribution function in exponential form as:

$$R = 100 \exp \left[ - \left( \frac{x}{x'} \right)^b \right] \quad (4.4)$$

Where

$R$  = cumulative mass (volume) % retained on sieve of size  $x$

$x'$  = absolute size constant or size parameter, and

$b$  = distribution parameter

Rearranging and taking logarithm twice of both sides of equation 4.4 gives:

$$\log \left[ \log \left( \frac{100}{R} \right) \right] = b \cdot \log x + Constant \quad (4.5)$$

Table 4.3. Example to indicate calculation of coarseness index ( $CI$ ) for saturated rock at  $s = 152.4$  mm and  $p = 16$  mm for long bladed CCS disc cutter.

Size Fraction (mm)	Retained Mass (kg)	Cumulative Mass (%)
+ 50.8	11.471	63.1
- 50.8 + 25.4	2.079	74.5
-25.4 + 9.42	1.444	82.4
-9.42 + 1.65	0.512	85.2
-1.65	2.683	100
<b>Total mass</b>	<b>18.189</b>	<b><math>CI = 405.2</math></b>

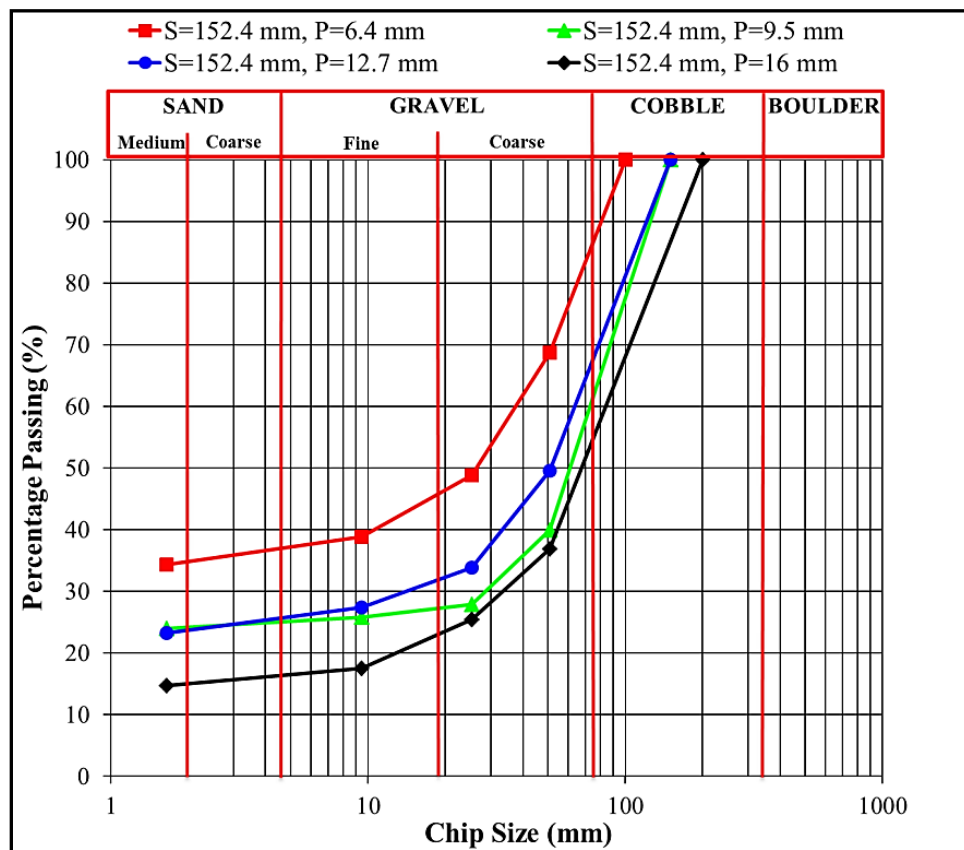


Figure 4.2. Grain size distribution curves for saturated rock cuts at  $s = 152.4$  mm using long bladed CCS disc cutter.

A plot of  $\log [\log (100/R)]$  versus  $\log x$  gives a straight line. The parameters of the Rosin-Rammler distribution,  $b$  and  $x'$  are obtained from the slope of the straight line

and the intercept at the horizontal line at  $R=36.79\%$ , respectively. Together they completely describe the size distribution. To simplify the calculations of the double log, special graph paper, Rosin-Rammler graph paper is used. The value of the  $x'$  is the absolute size constant and distribution parameter,  $b$ , measures distribution of material over the size range, since for small values of  $b$ , the size curve is close to the size-axis, and the material is spread over a wide size range; whereas if  $b$  is large, the curve is steeper and the material is spread over a narrower range of sizes (Gupta and Yan, 2006). Determination of  $x'$  and  $b$  for a dry rock cut at  $s = 114.3$  mm and  $p = 12.7$  mm using long bladed CCS disc cutter is shown in Figure 4.3 as an example.

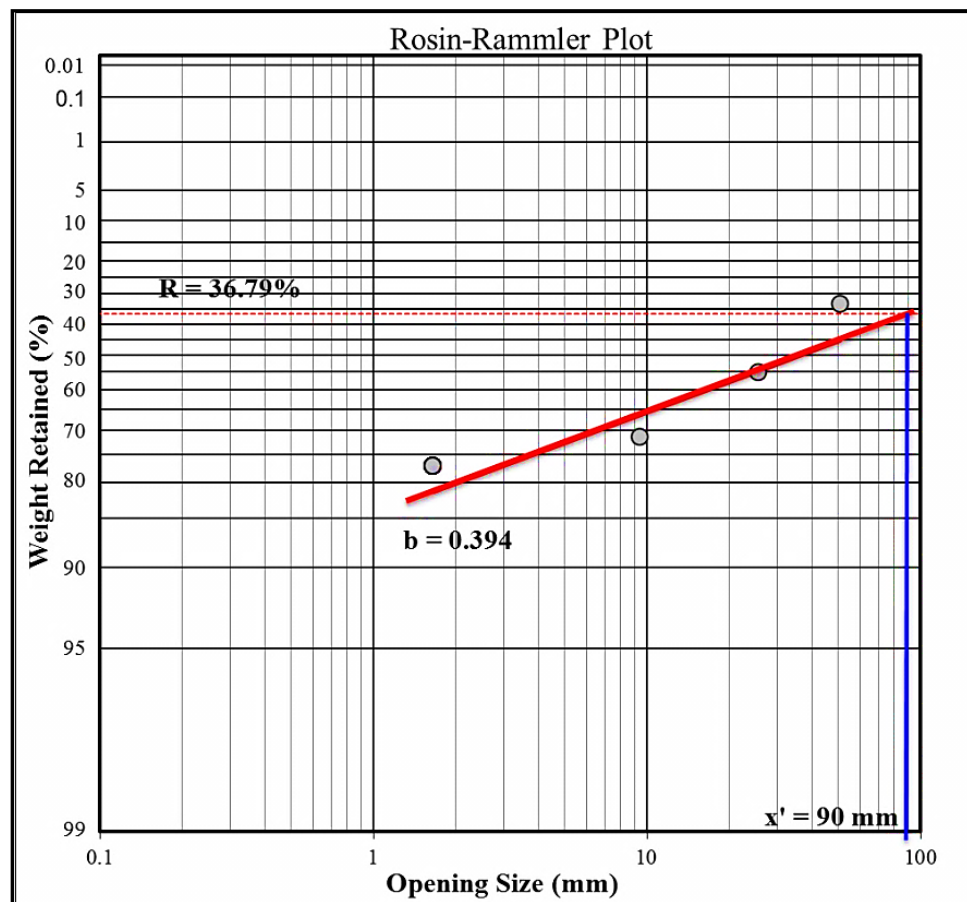


Figure 4.3. Determination of absolute size constant  $x'$  and distribution parameter  $b$  using Rosin-Rammler plot for a dry rock cut at  $s = 114.3$  mm and  $p = 12.7$  mm using long bladed CCS disc cutter.





Table 4.5. Computed cutting parameters for CCS disc cutter in saturated sandstone.

$s$	$p$	$s/p$	$SE_A$	$SE_N$	$PR_A$	$PR_N$	$PR_L$	$x'$	$CI$	Cut. Eff.
mm	mm		kW-hr/m <sup>3</sup>	kW-hr/m <sup>3</sup>	kg/min	kg/min	%	mm		%
76.2	6.4	12	1.93	2.26	5.4	5.5	11.3	13.5	257.6	99
76.2	9.5	8	0.90	1.33	10.3	8.2	28.3	27	292.8	125
76.2	12.7	6	1.48	1.90	14.0	10.9	12.1	8	232.2	128
114.3	6.4	18	1.66	2.89	15.9	8.2	31.2	98.5	327.7	241
114.3	9.5	12	2.63	2.75	11.3	12.2	24.1	46.5	285.5	91
114.3	12.7	9	1.56	1.67	18.4	16.4	30.4	110	322.8	109
127	6.4	20	2.79	2.86	9.3	9.1	26.7	33	306.6	103
127	9.5	13.3	1.95	2.29	15.9	13.6	44.1	100	341.8	118
127	12.7	10	1.25	1.56	22.7	18.2	48.6	160	350.6	125
152.4	6.4	24	2.28	2.17	11.9	10.9	31.3	206.5	361.7	99
152.4	9.5	16	0.99	2.33	38.3	16.2	70.0	390	426.1	236
152.4	12.7	12	1.33	1.41	23.1	21.8	50.4	165	366.0	106
152.4	15.9	9.6	1.04	2.79	44.3	11.0	71.9	360	405.2	118
228.6	6.35	36	4.36	2.00	5.7	16.4	60.0	6.5	226.1	112
228.6	15.9	14.4	1.02	1.68	50.6	27.3	63.1	850	436.8	162
$s$ – cut spacing, $p$ – cutter penetration, $s/p$ – spacing to penetration ratio, $CI$ – coarseness index, $SE_A$ – actual specific energy, $SE_N$ – nominal specific energy, $PR_A$ – actual production rate, $PR_N$ – nominal production rate, $PR_L$ – chips > 51 mm (2 in) $x'$ – absolute size constant, Cut. Eff. – total cutting efficiency.										

## 4.2. RADIAL DRAG PICK CUTTING TESTS

Radial drag pick cutting tests were performed on dry and saturated blocks of Roubidoux Sandstone. Cut spacing ( $s$ ) and the depth of cut ( $d$ ) are the parameters which were changed during the tests according to the pre-defined experimental matrix described in Section 3.

**4.2.1. Force Measures.** The experimental results of 40 tests at given cut spacing and depth of cut which were completed in 50 data passes, encompassing 350 data cuts, are presented in Table 4.6 and Table 4.7 for dry and saturated cutting tests respectively. The values presented herein are weighted average values obtained from 6 to 17 data cuts each (number of cuts varies inversely with the cut spacings). Cut length of each data pass is taken as weighting factor for averaging different cutting related parameters. Figure 4.4 shows a typical force trace of a radial drag pick cutting test. This



Table 4.7. Cutting test results for radial drag pick in saturated sandstone.

$s$	$d$	$s/d$	Avg. $F_d$	Avg. $F_n$	Avg. $F_s$	Peak $F_d$	Peak $F_n$	Peak $F_s$
mm	mm		kN	kN	kN	kN	kN	kN
25.4	3.2	8	5.6	3.9	0.5	34.5	20.9	9.0
25.4	6.4	4	8.2	5.9	1.0	48.1	30.1	9.6
25.4	9.5	2.7	7.1	4.8	1.3	50.8	33.8	13.6
25.4	12.7	2	7.7	5.1	1.6	63.5	51.9	14.8
50.8	3.2	16	7.4	5.1	1.0	39.1	32.9	9.0
50.8	6.4	8	7.4	4.7	0.8	44.4	33.8	6.1
50.8	9.5	5.3	8.0	4.8	1.3	49.1	34.7	8.2
50.8	12.7	4	7.5	4.6	1.5	49.0	31.4	15.3
63.5	3.2	20	7.6	4.5	2.0	30.2	16.7	7.0
63.5	6.4	10	9.2	5.5	0.3	42.8	25.2	7.3
63.5	9.5	6.7	10.7	6.0	0.9	56.1	35.3	13.6
63.5	12.7	5	11.8	6.8	1.4	60.4	41.6	10.8
76.2	3.2	24	6.9	4.5	0.3	25.9	15.2	6.4
76.2	6.4	12	7.5	3.6	2.8	30.7	17.3	14.3
76.2	9.5	8	7.4	4.4	0.9	57.5	32.0	8.6
76.2	12.7	6	7.0	3.6	0.8	37.3	25.0	7.1
88.9	3.2	28	5.5	3.7	0.5	25.9	17.3	6.1
88.9	6.4	14	17.3	10.3	1.4	68.3	45.4	12.6
88.9	9.5	9.3	5.1	3.3	0.3	37.5	23.0	6.3
88.9	12.7	7	12.6	7.0	1.6	53.6	34.4	9.3
$s$ – cut spacing, $d$ – depth of cut, $s/d$ – spacing to depth of cut ratio, $F_d$ – drag or cutting force, $F_n$ – normal force, $F_s$ – side force.								

It is pertinent to mention here that the tungsten carbide tips of the drag picks used in dry rock tests experienced several instances of thermal fatigue failure evident in the form of broken tips (Figure 4.5), which resulted in frequent replacement of the picks. The temperature at the rock-bit interface can exceed 1000 C° (Hood, 1977a). The hardness of the tungsten carbide inserts used at the point of these bits decreases rapidly with increasing temperature. At these high temperatures, the hardness of quartz is similar to that of tungsten carbide, hence rapid wearing of localized hot spots is to be expected (Fowell, 1993). Water cooling of cutting tools is beneficial as evidenced by the pick replacement rate of zero for all saturated rock tests, showing that the dripping water was also playing a role in cooling the pick and hence reducing the thermal fatigue (Section 3).

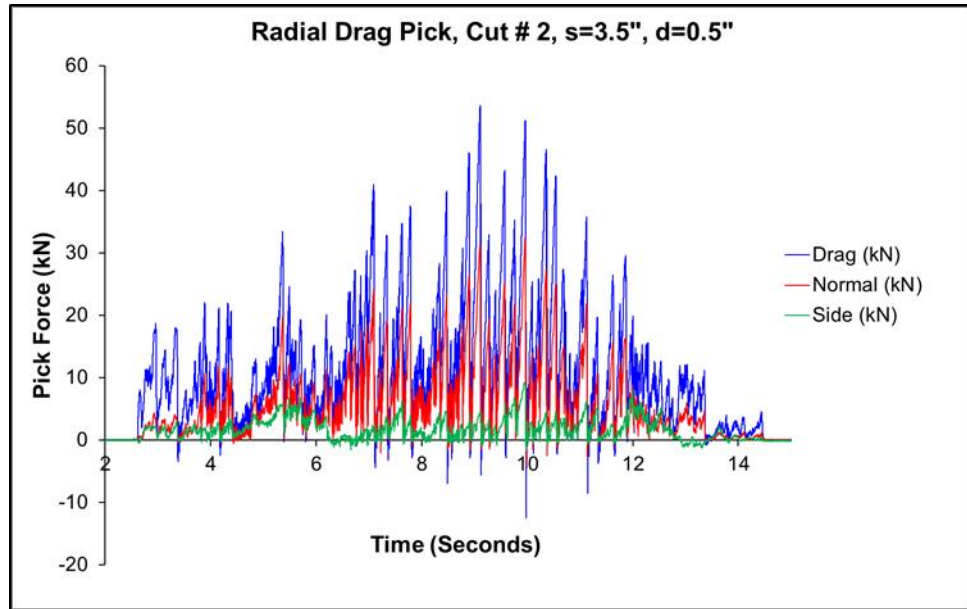


Figure 4.4. A trace of the forces recorded during one of the radial drag pick cutting tests.



Figure 4.5. Example of tungsten carbide tips broken off during dry rock cutting.



Table 4.9. Computed cutting parameters for radial drag pick in saturated sandstone.

$s$	$d$	$s/d$	$SE_A$	$SE_N$	$PR_A$	$PR_N$	$PR_L$	$x'$	$CI$	Cut. Eff.
mm	mm		kW-hr/m <sup>3</sup>	kW-hr/m <sup>3</sup>	kg/min	kg/min	%	mm		%
25.4	3.2	8	24.3	19.3	0.7	0.9	0.0	7	217.0	80
25.4	6.4	4	13.0	14.1	2.0	1.8	0.0	8.9	237.9	108
25.4	9.5	2.7	6.1	8.2	3.7	2.7	8.7	13.5	261.8	134
25.4	12.7	2	4.2	6.6	5.0	3.2	8.7	16	279.2	156
50.8	3.2	16	11.2	12.7	1.8	1.6	6.9	13	274.9	114
50.8	6.4	8	4.9	6.4	4.1	3.2	4.0	12	264.4	129
50.8	9.5	5.3	3.5	4.6	6.2	4.8	15.8	19	299.2	129
50.8	12.7	4	2.7	3.2	7.8	6.4	9.2	16	270.5	121
76.2	3.2	24	12.7	9.6	1.3	2.4	14.0	9	238.8	52
76.2	6.4	12	3.0	5.2	4.9	4.8	27.3	135	369.8	103
76.2	9.5	8	2.8	3.4	11.1	7.1	38.4	18	296.8	155
76.2	12.7	6	1.7	2.4	11.7	9.6	30.6	80	382.0	122
63.5	3.2	20	16.6	8.7	1.5	2.0	4.5	6	221.0	75
63.5	6.4	10	5.1	5.3	6.6	3.8	53.6	29	311.0	173
63.5	9.5	6.7	2.6	4.1	7.4	6.0	11.1	60	340.6	122
63.5	12.7	5	2.8	3.4	11.4	8.0	45.7	40	325.6	143
88.9	3.2	28	8.1	5.4	1.9	2.8	26.2	16	258.5	67
88.9	6.4	14	8.7	8.5	5.4	5.6	26.8	30	307.8	98
88.9	9.5	9.3	1.5	1.7	9.5	8.4	48.9	120	354.2	113
88.9	12.7	7	2.7	3.1	13.0	11.2	23.3	36	296.4	116
$s$ – cut spacing, $d$ – depth of cut, $s/d$ – spacing to depth of cut ratio, $CI$ – coarseness index, $SE_A$ – actual specific energy, $SE_N$ – nominal specific energy, $PR_A$ – actual production rate, $PR_N$ – nominal production rate, $PR_L$ – chips > 51 mm (2 in), $x'$ – absolute size constant, Cut. Eff. – total cutting efficiency.										

#### 4.3. LOAD-INDENTATION TESTS

The quantities measured from the load-indentation tests (described in Section 3) were used to compute several parameters.

The first parameter of interest was the porewater force (kN) induced by the porewater in the pores of the saturated rock samples under the indentation process. It was computed by multiplying the measured porewater pressure values (from the porewater pressure transducer) with the area of the porewater drain tube (described in Figure 3.28). Porewater force was calculated as:

$$F_{pw} = P_{pw} \times A_{dr} \quad (4.6)$$

Where

$F_{pw}$  = porewater force (kN)

$P_{pw}$  = porewater pressure (kPa)

$A_{dr}$  = area of porewater drainage tube (m<sup>2</sup>)

Porewater force was then used to compute the effective load (kN) on the rock sample under the indenter. This was computed according to the Terzaghi's principle of effective stress as:

$$L_{eff} = L_{total} - F_{pw} \quad (4.7)$$

Where

$L_{eff}$  = effective load under the indenter (kN)

$L_{total}$  = total load under the indenter (kN)

The pressure applied by the indenter to the rock surface (indenter pressure) was calculated by dividing the measured load on the indenter by the surface area of the indenter footprint. The indenter footprint is the areal projection of the buried portion of the indenter. Indenter pressure provides a first insight into the failure mechanism, because the magnitude of the pressures involved reflects the energy required to achieve failure (Gertsch, 2000).

Since the used indenter was of truncated tri-cone in section, the footprint surface area varied with the indentation into the rock sample. This was accounted for by calculating the indenter surface area at each incremental indenter penetration into the rock sample. The indenter pressure was calculated as:

$$P_{indenter} = \frac{L_{eff}}{S} \quad (4.8)$$

Where

$P_{indenter}$  = indenter pressure (MPa)

$L_{eff}$  = effective load under the indenter (kN)

$S$  = indenter footprint surface area

The indenter footprint surface area was calculated as:

$$S = 2. \pi. R. h \quad (4.9)$$

Where

$R$ = radius of each conic section of indenter (mm)

$h$ = indenter incremental penetration (mm)

Specific penetration ( $SP$ ), which is the force required to penetrate a unit depth into the material, measured at first failure was also calculated from load-indentation test data. First failure refers to the point at which the first significant drop in indenter load is observed. In plots of load versus indentation, this is the first force peak, or “sawtooth” (Gertsch, 2000). Specific penetration has also been referred to as penetration index or crushing slope at several places (Dollinger, 1977; Dollinger, 1978; Dollinger et al, 1998) and has been reported to get steeper with increase in the strength of the rock and the bluntness of the indenter. It was calculated as:

$$SP = \frac{L}{P} \quad (4.10)$$

Where

$L$ = load on indenter at first failure

$P$ = indenter penetration at first failure

Specific energy (defined earlier) was also calculated. In load-indentation tests, it is the total energy expended (the area under the force-penetration curve) divided by the volume of the fragments produced (Gertsch, et al., 2006). It was calculated from:

$$SE = \frac{L_p \cdot P_p}{V} \quad (4.11)$$

Where

$L_p$ =peak load

$P_p$ = indenter penetration at peak load

$V$ = chip volume

Table 4.10 and Table 4.11 give the summary of load-indentation tests for saturated and dry Roubidoux Sandstone samples.



Table 4.10. Summary of load-indentation tests on saturated sandstone.

Sample No.	$L_p$	Peak $P_{pw}$	Peak $P_{indenter}$	$SP$	$SE$
	(kN)	(kPa)	(MPa)	(kN/mm)	J/cm <sup>3</sup>
1.	67.3	12.4	350.2	5.7	160.5
2.	56.4	6.7	253.5	7.6	150.5
3.	46.5	12.0	244.7	5.1	91.2
4.	39.1	11.1	159.0	3.3	253.5
5.	49.3	7.6	391.2	6.2	138.4
6.	56.5	14.8	230.2	5.2	141.3
7.	46.9	9.4	421.5	6.7	183.7
8.	29.0	16.5	555.9	9.7	29.1
9.	46.4	20.1	324.1	5.5	158.0
10.	29.8	6.3	466.9	6.9	56.1
11.	63.9	23.5	313.8	5.7	164.1
12.	57.2	17.5	681.7	9.9	109.4
13.	33.6	26.1	254.3	4.4	46.5
14.	44.9	10.7	503.3	7.6	171.0
15.	59.1	13.3	387.6	5.7	152.0
<b>Mean</b>	<b>48.4</b>	<b>13.9</b>	<b>369.2</b>	<b>6.3</b>	<b>133.7</b>
<b>St. Dev.</b>	<b>11.9</b>	<b>5.94</b>	<b>140.1</b>	<b>1.8</b>	<b>58.6</b>
$L_p$ – peak load, $P_{pw}$ – peak porewater pressure, $P_{indenter}$ – peak indenter pressure, $SP$ – specific penetration, $SE$ – specific energy, $St. Dev.$ – Standard Deviation.					

Table 4.11. Summary of load-indentation tests on dry sandstone.

Sample No.	$L_p$	Peak $P_{indenter}$	$SP$	$SE$
	(kN)	(MPa)	(kN/mm)	J/cm <sup>3</sup>
1.	35.3	176.2	3.2	245.2
2.	50.2	353.2	5.4	199.1
3.	18.2	256.5	3.8	26.9
4.	26.4	653.4	8.1	73.2
5.	52.1	571.0	8.4	43.5
6.	49.9	417.5	6.1	219.9
7.	44.2	436.1	4.9	38.1
8.	31.9	622.2	9.3	11.0
<b>Mean</b>	<b>38.5</b>	<b>435.8</b>	<b>6.2</b>	<b>107.1</b>
<b>St. Dev.</b>	<b>14.3</b>	<b>162.8</b>	<b>1.9</b>	<b>83.8</b>
$L_p$ – peak load, $P_{indenter}$ – peak indenter pressure, $SP$ – specific penetration, $SE$ – specific energy, $St. Dev.$ – Standard Deviation.				

## 5. DISCUSSION: SATURATION EFFECTS ON DISC CUTTING

This section discusses the full scale linear rock cutting tests conducted on dry and saturated Roubidoux Sandstone using a long bladed single disc cutter (292 mm diameter, 11mm wide constant cross-section blade). The detailed results of the tests conducted are outlined in Section 4.

The discussion of the results in this section is confined to the reaction of normal forces, rolling forces, side forces, specific energy ( $SE$ ), and cutting coefficient ( $CC$ ) to the spacing, penetration and spacing/penetration ( $s/p$ ) ratio. An overall comparison of the cutting forces and specific energy values (Table 5.1) reveals noticeable decreases of 27.5%, 44% and 48.2% in the normal, rolling and side forces respectively when cutting saturated rock as compared to cutting dry rock. Nearly 10% reduction in nominal specific energy ( $SE_N$ ) and 8.4% reduction in actual specific energy ( $SE_A$ ) were also observed when comparing saturated rock cutting to dry rock cutting.

To check the statistical significance of the differences in both the average forces and the energies between dry and saturated cutting tests, hypothesis testing about the means was performed. The  $z$ -statistics values, assuming normal (Gaussian) distribution, were computed for differences in the overall means of normal, rolling and side forces, and actual and nominal specific energy for both dry and saturated cutting tests. The significance level ( $\alpha$ -value) of the  $z$ -test was set at 0.1 (90% Confidence Interval). The  $p$ -value (the probability of obtaining a result at least as extreme as the one that was actually observed), assuming that the null hypothesis is true, was also computed for each means comparison. Each comparison of the means was considered statistically significant (rejected null hypothesis) if the  $p$ -value was found to be less than the  $\alpha$ -value.

Table 5.1 illustrates that the  $p$ -values for normal, rolling and side forces are statistically significant at the chosen level of significance ( $\alpha = 0.1$ ) (highlighted bold faced values). The mean difference between dry and saturated specific energy values (both  $SE_N$  and  $SE_A$ ) is statistically insignificant at  $\alpha = 0.1$ .

Table 5.1. Comparative average forces and specific energy for dry and saturated sandstone using long bladed single disc cutter.

	Average $F_N$	Average $F_R$	Average $F_S$	$SE_A$	$SE_N$
	kN	kN	kN	kW-hr/m <sup>3</sup>	kW-hr/m <sup>3</sup>
Dry sandstone	68.9	16.3	4.80	2.02	2.31
Saturated sandstone	49.9	9.14	2.49	1.85	2.08
Percent change	27.5%	44%	48.2%	8.42%	9.95%
$p$ -value (at $\alpha=0.1$ )	0.0002	0.0000	0.009	0.4527	0.4350
$F_N$ – normal force, $F_R$ – rolling force, $F_S$ – side force, $SE_A$ – actual specific energy, $SE_N$ – nominal specific energy.					

### 5.1. EFFECT OF CUT SPACING ON CUTTING FORCES

The effect of spacing on the cutting forces for dry and saturated rock is shown in Figures 5.1 and 5.2. The increase in the normal and rolling forces with the increase in the cut spacing is expected and is usually accompanied with a decrease in the specific energy as shown in Figures 5.5 and 5.6. The anomalous data point with exceptionally high normal and rolling forces occurred during dry cutting at spacing of 254 mm and penetration of 19 mm. The possible explanation for this is a zone of increased cementation of the rock grains, presenting more resistance to fragmentation than the rest of that rock block as well as all the other blocks. Unfortunately, this could not be verified since linear rock cutting destroys the tested portion of the sample. The outlier was not identified until the data analysis stage.

The normal and rolling forces appear to level off at very wide spacings, especially at shallower penetrations, for both dry and saturated tests. This is attributed the adjacent cuts being too far apart for the fractures induced by the cutter to meet and create chips. The effect of spacing on the side forces is much more prominent in the saturated rock than in the dry rock. In saturated rock, the side forces are clearly decreasing as the cut spacing increases, for the same reason (Figure 5.2). In dry rock, the side forces change very little (Figure 5.1). Since the wider spacing cuts in the dry rock were conducted at much deeper penetration of 25 mm, an increase in the side force was expected.

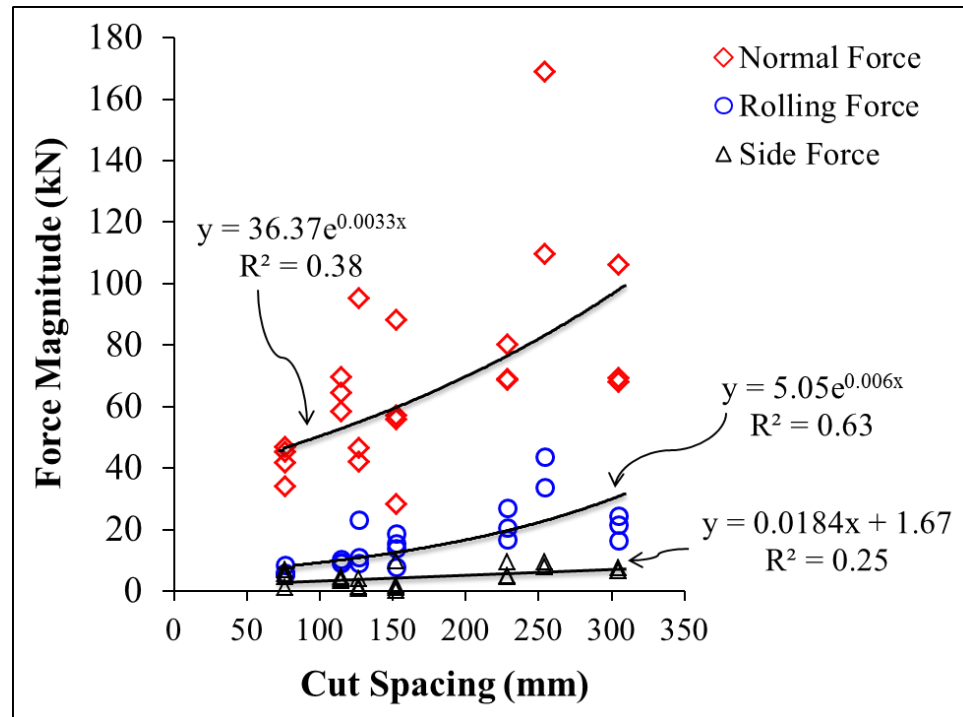


Figure 5.1. Force magnitude variation with cut spacing for dry rock.

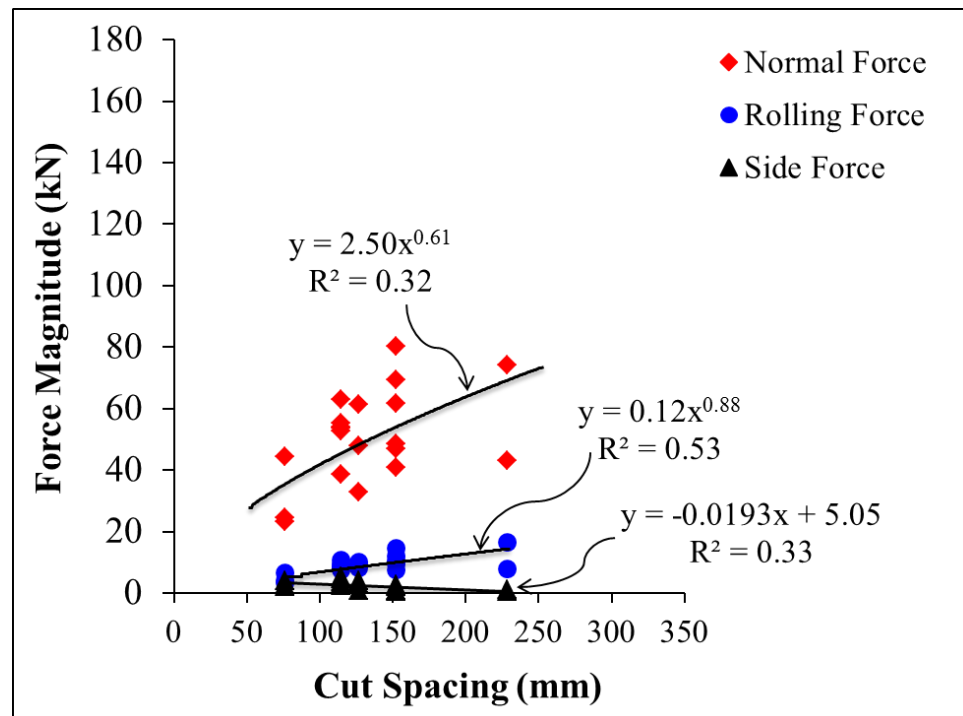


Figure 5.2. Force magnitude variation with cut spacing for saturated rock.

## 5.2. EFFECT OF CUTTER PENETRATION ON CUTTING FORCES

The effect of increasing cutter penetration on normal and rolling forces (Figures 5.3 and 5.4) shows a similar upward trend, as expected, for both dry and saturated rock cuts. This trend holds for all the cutter spacings tested.

An anomalous increase in the normal and rolling force for dry rock cuts is visible at cutter penetration of 19.05 mm; the probable reasons for this increase explained earlier. The side forces response with the increasing cutter penetration is very much in congruence with the response of the side forces with increasing cut spacing for both dry and saturated rock tests. For dry rock tests, very low side forces are experienced for shallower cutter penetrations (from 6.35 mm to 12.7 mm) which then increase with the increase in the cutter penetration (from 15.875 mm to 25.4 mm).

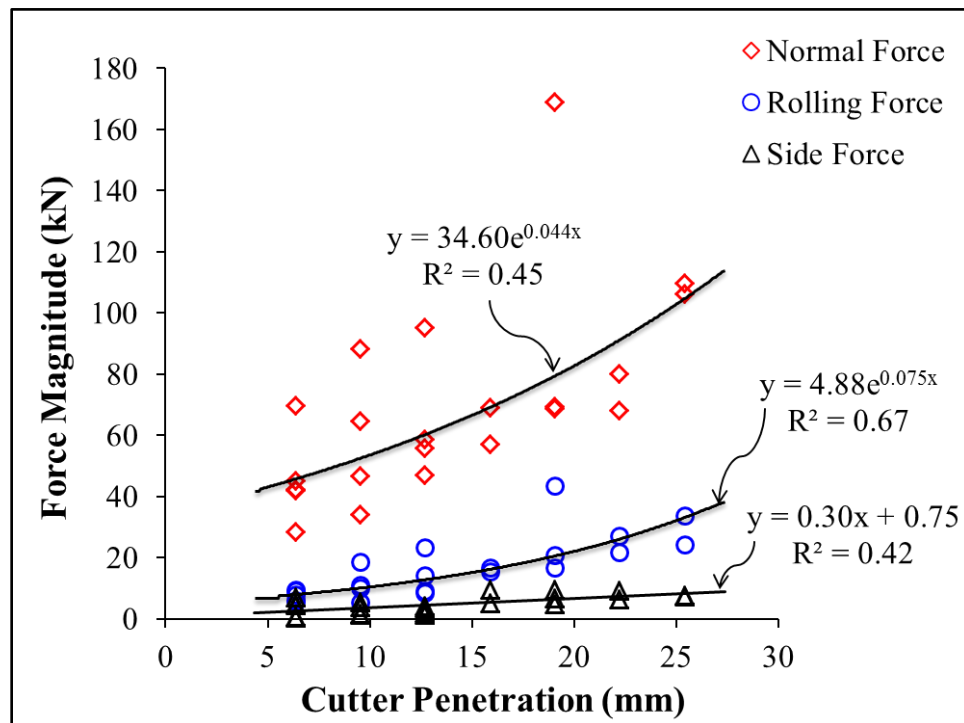


Figure 5.3. Force magnitude variation with cutter penetration for dry rock.

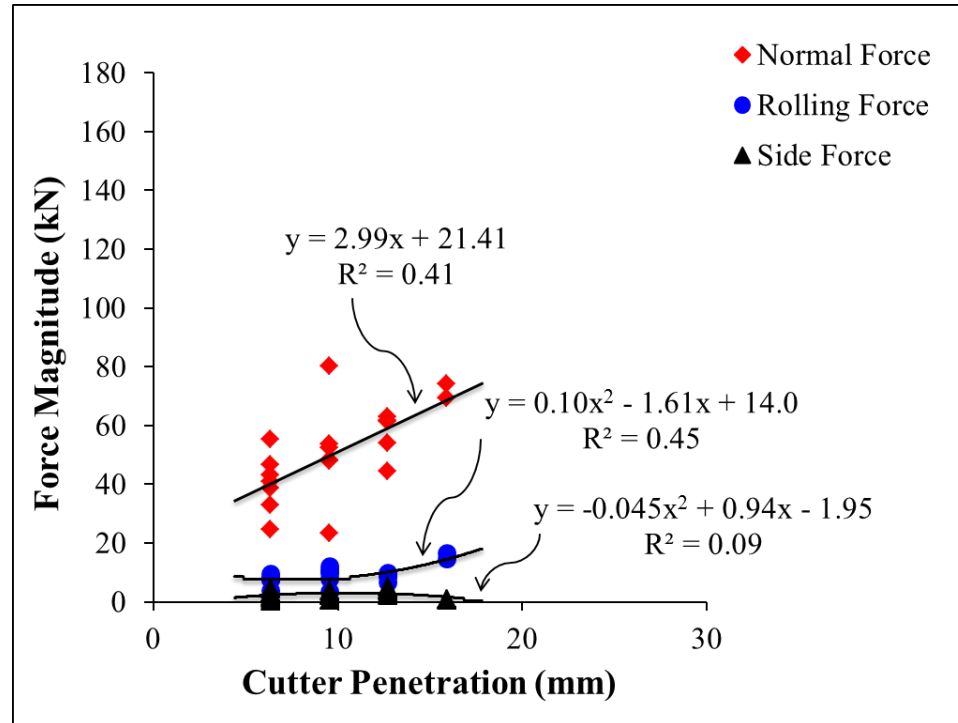


Figure 5.4. Force magnitude variation with cutter penetration for saturated rock.

### 5.3. EFFECT OF CUT SPACING ON SPECIFIC ENERGY

An increase in cut spacing coupled with an increase in cutter penetration increases the excavated volume. Both dry and saturated cutting (Figure 5.5 and Figure 5.6) show reduced  $SE$  (both  $SE_N$  and  $SE_A$ ) with increasing cut spacing.  $SE$  for dry rock reacts differently to spacing compared with the saturated rock. For dry rock tests, an  $SE$  minimum can be seen at a cut spacing of 305 mm and cutter penetration of 19 mm ( $s/p$  ratio of 16). The response of the saturated rock to the increase in the cut spacing is somewhat different to that of the dry rock tests.  $SE$  values vary widely between 114 mm and 152 mm cut spacings. A significant drop in  $SE$  is noticeable at the much wider cut spacing of 229 mm for all the penetrations tested. An anomalously high  $SE$  occurs at a cut spacing of 229 mm and a cutter penetration of 6 mm ( $s/p = 36$ ) clearly showing the lack of interaction between the adjacent cut grooves and hence very little excavated volume resulting in very high  $SE$ .

Large variability between the  $SE_N$  and  $SE_A$  is also evident in these plots, showing both the effect of heterogeneity in natural materials and the stochastic nature of rock chipping mechanisms. In addition, for both the dry and saturated tests, the  $SE_N$  is higher than the  $SE_A$ , showing that most of the cutting experiments excavated more volume than expected. The likely explanation for the overbreak is the bedded nature of the rock tested. Exploration of the effect of wider cut spacings and deeper cutter penetrations merits more cutting tests of saturated rock as well as dry rock, as does quantitative evaluation of the effects of bedding thickness in both situations.

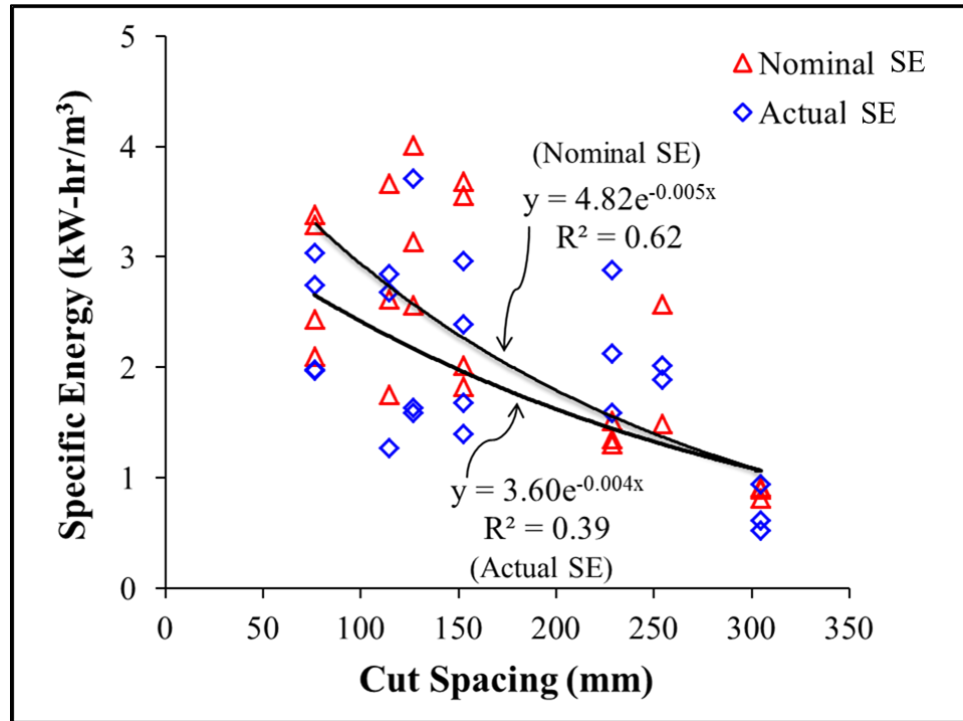


Figure 5.5. Specific energy variation with cut spacing for dry rock.

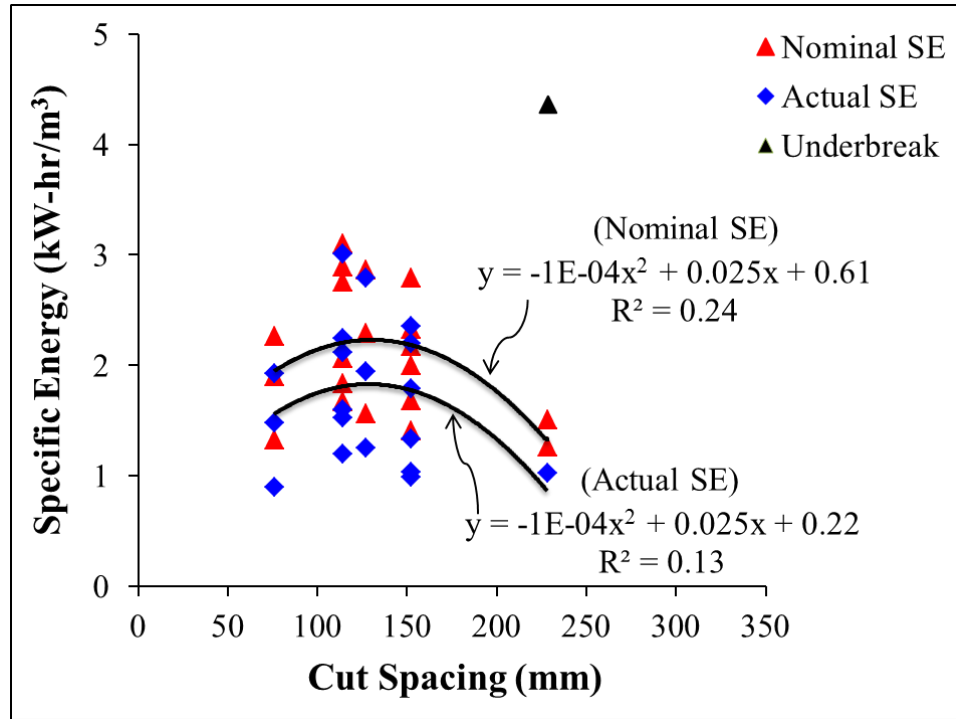


Figure 5.6. Specific energy variation with cut spacing for saturated rock.

#### 5.4. EFFECT OF CUTTER PENETRATION ON SPECIFIC ENERGY

The  $SE$  decreases with deeper cutter penetration for both dry and saturated rock. This holds for all the cut spacings tested (Figures 5.7 and 5.8). This drop in  $SE$  with increased cutter penetration is expected, since larger volumes of rock are excavated with deeper cutter penetrations, especially if coupled with wider cut spacings. Although wider cut spacings also increase the cutter forces, this is usually compensated by a decrease in the overall specific energy of fragmentation. For dry rock, cutter penetrations of 22 mm and deeper it can be observed (Figure 5.7) that the curves for  $SE_N$  and actual  $SE_A$  merge. Increases in  $SE$  are clear manifestation of the underbreak that is expected at very wide cut spacings and deep cutter penetrations, resulting in reduced fragmentation and hence higher actual  $SE$ .



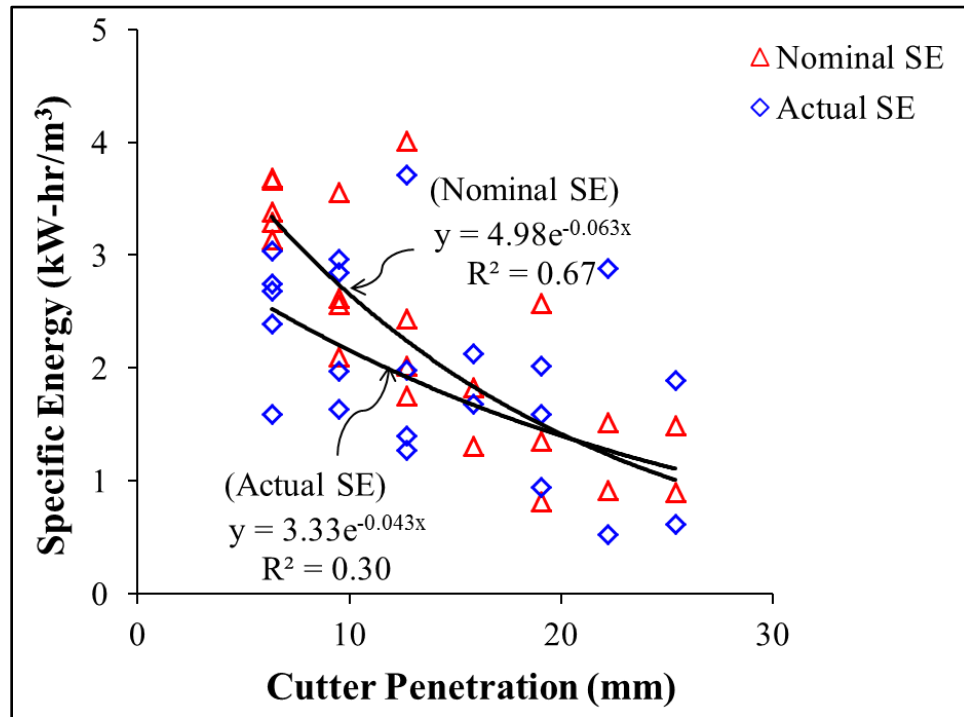


Figure 5.7. Specific energy variation with cutter penetration for dry rock.

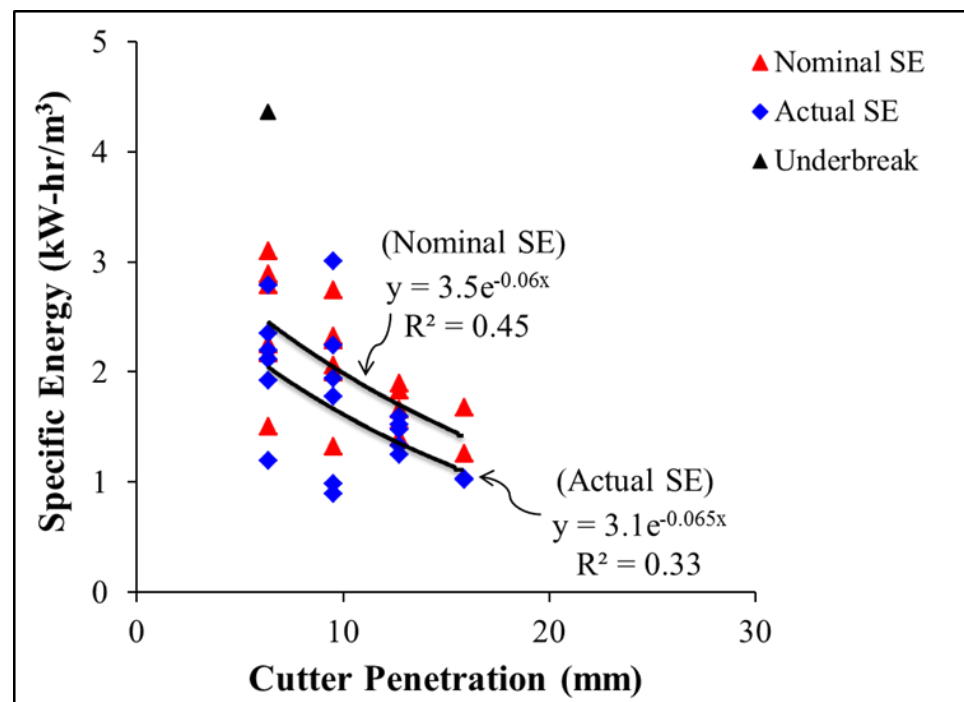


Figure 5.8. Specific energy variation with cutter penetration for saturated rock.

## 5.5. EFFECT OF $s/p$ RATIO ON SPECIFIC ENERGY

The variation of  $SE$  with  $s/p$  ratio (Figures 5.9 and 5.10) is not very clear for either saturated or dry rock, though there is slightly less variability in the saturated rock  $SE$  than in the dry rock  $SE$ . Some of the variability in  $SE$  at some  $s/p$  ratios may be due to  $s/p$  ratio not being the only determinant of  $SE$ . Some tests using the same  $s/p$  ratios actually used different spacing and penetration values that resulted in the same ratios but were different factors of average sand grain size, for example. This resulted in differences in the fragmented volume and hence the  $SE$  values. The wide variability in  $SE$  values with change in  $s/p$  ratio also may be attributed partially to the weak and heterogeneous nature of the sandstone tested.

The 3-D surface plots of nominal and actual  $SE$  values against cut spacing and cutter penetration (Figures 5.11-5.14) for dry and saturated disc cutting tests further explain the variability of  $SE$  values as seen in Figures 5.9 and 5.10. It is interesting to note from Figures 5.11 and 5.12 that the nominal and actual  $SE$  values for dry rock tests are in close agreement, except a few values at very wide cut spacings and deeper cutter penetrations (at spacings from 228.6 mm to 304.8 mm and penetrations from 15.9 mm to 25.4 mm). Flat rectangular surface areas at very wide cut spacings and too shallow cutter penetrations (from 6.4 mm to 12.7 mm) do not truly represent the actual tested  $s/p$  ratios. These areas are selected by the default rectangular shape made by the plotting software (Minitab 16).

For saturated rock cuts (Figures 5.13 and 5.14) the nominal and actual  $SE$  values at close cut spacings (from 76.2 mm to 152.4 mm) and shallower cutter penetrations (from 6.4 mm to 12.7 mm) correspond with each other. Regions at close cut spacings (from 76.2 mm to 152.4 mm) and very deep cutter penetration (15.9 mm) are flat rectangular in shape, constrained by the plotting program.  $SE$  values shown in these regions of very small  $s/p$  ratios are merely approximations. At very wide cut spacing and shallow cutter penetrations; the difference in nominal and actual  $SE$  values is visible. The very high actual  $SE$  value is attributed to too little rock yield at very high  $s/p$  ratios ( $s/p = 36$ ) resulting in ridge-formation (an underbreak situation), affecting the actual  $SE$  value.

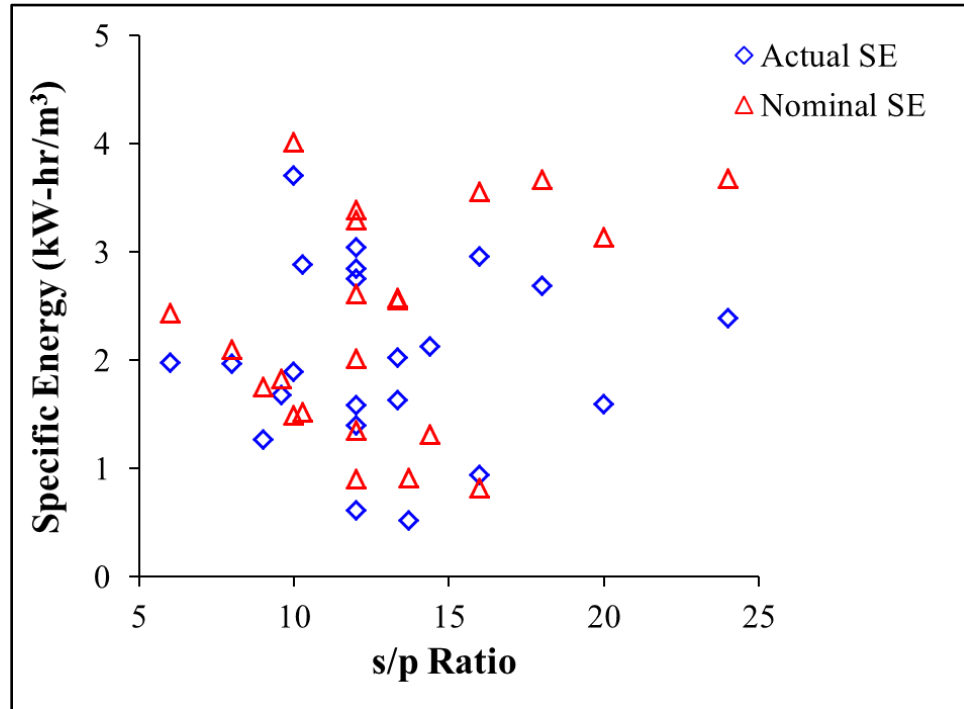


Figure 5.9. Specific energy variation with  $s/p$  ratio for dry rock tests.

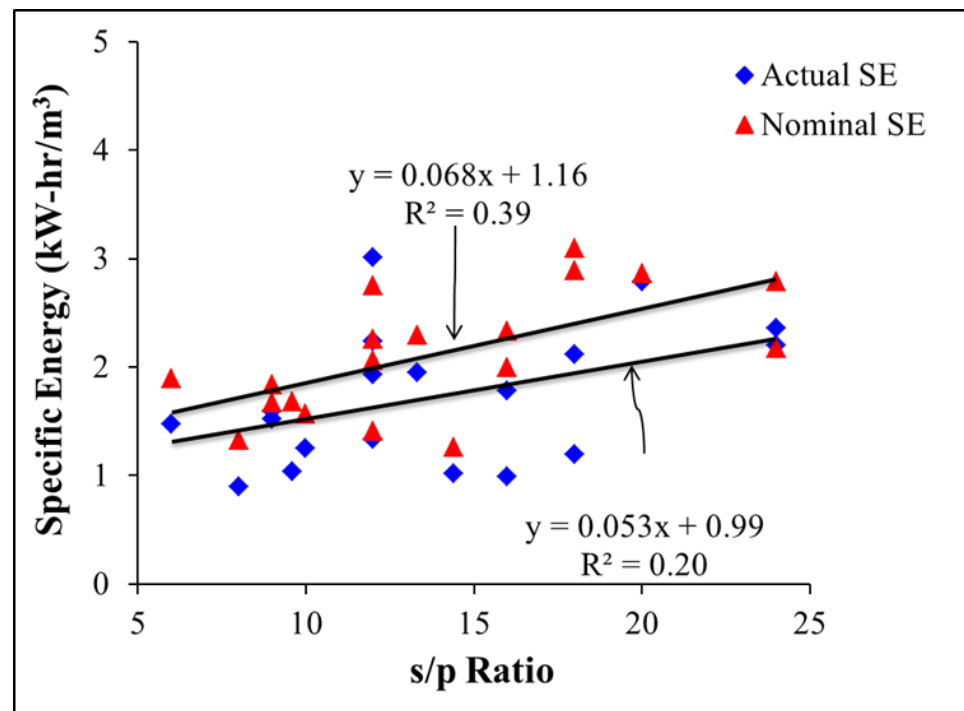


Figure 5.10. Specific energy variation with  $s/p$  ratio for saturated rock tests.

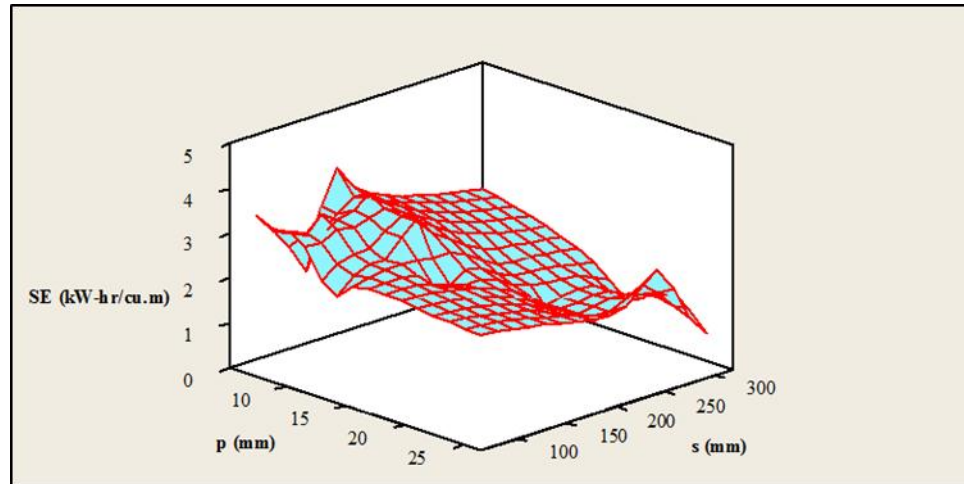


Figure 5.11. 3-D surface plot of nominal  $SE$  vs cut spacing and cutter penetration for dry rock cuts with disc cutter.

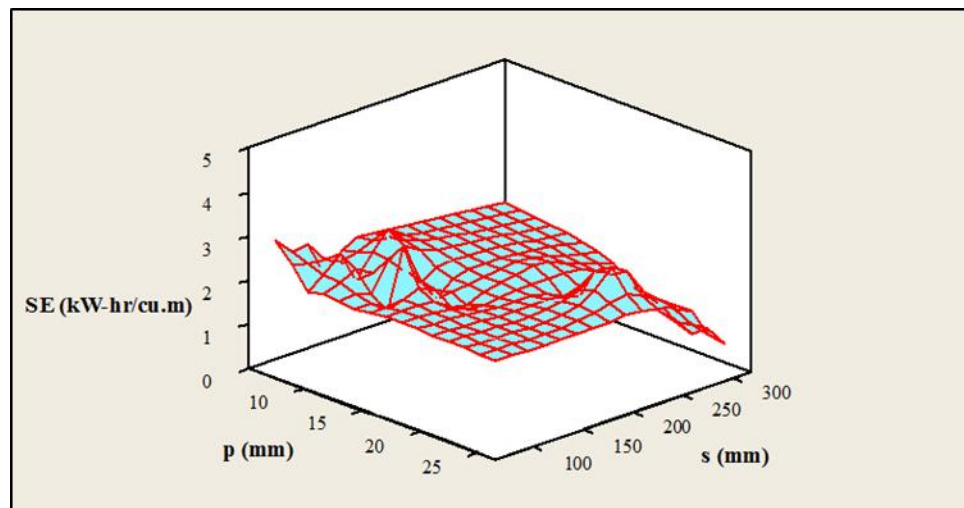


Figure 5.12. 3-D surface plot of actual  $SE$  vs cut spacing and cutter penetration for dry rock cuts with disc cutter.

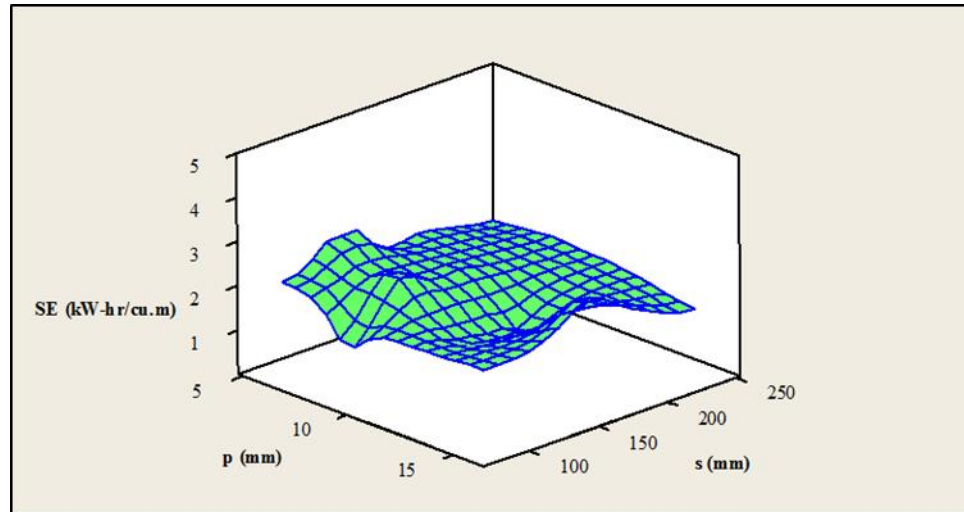


Figure 5.13. 3-D surface plot of nominal  $SE$  vs cut spacing and cutter penetration for saturated rock cuts with disc cutter.

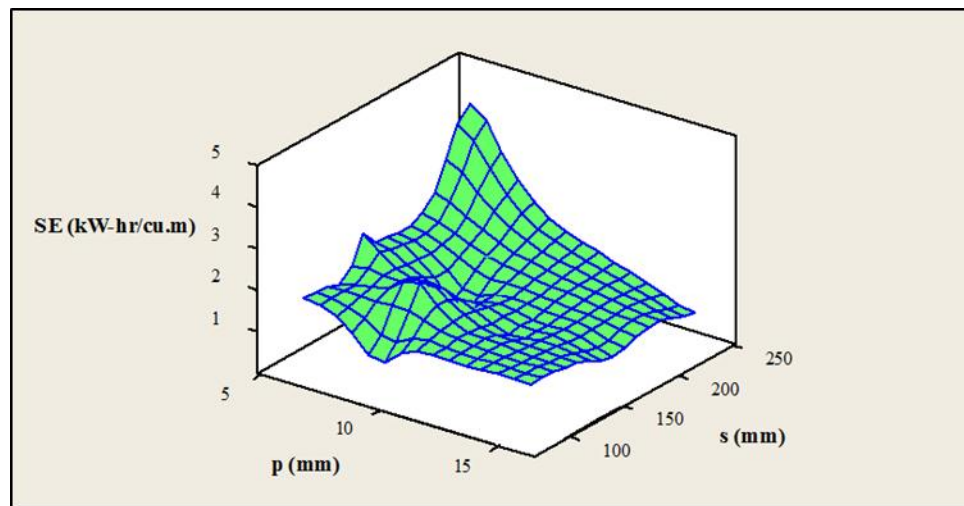


Figure 5.14. 3-D surface plot of actual  $SE$  vs cut spacing and cutter penetration for saturated rock cuts with disc cutter.

## 5.6. EFFECT OF CUTTER PENETRATION ON CUTTING COEFFICIENT

The cutting coefficient ( $CC$ ) is known as an indicator of the TBM torque requirement and has been reported to increase linearly with increasing depth of cutter penetration. The higher the  $CC$ , the higher the torque needed by the tunnel boring machine (Rostami and Ozdemir, 1993; Rostami, 1997; Gertsch et al., 2007). An overall

increasing trend in the *CC* with increasing cutter penetration was also observed in the dry sandstone blocks in this study, depicting the expected higher torque requirement at deeper cutter penetrations (Figure 5.15). This is due to the increase in the rolling force component from the increased contact length of the disc with the rock, thus requiring more bite.

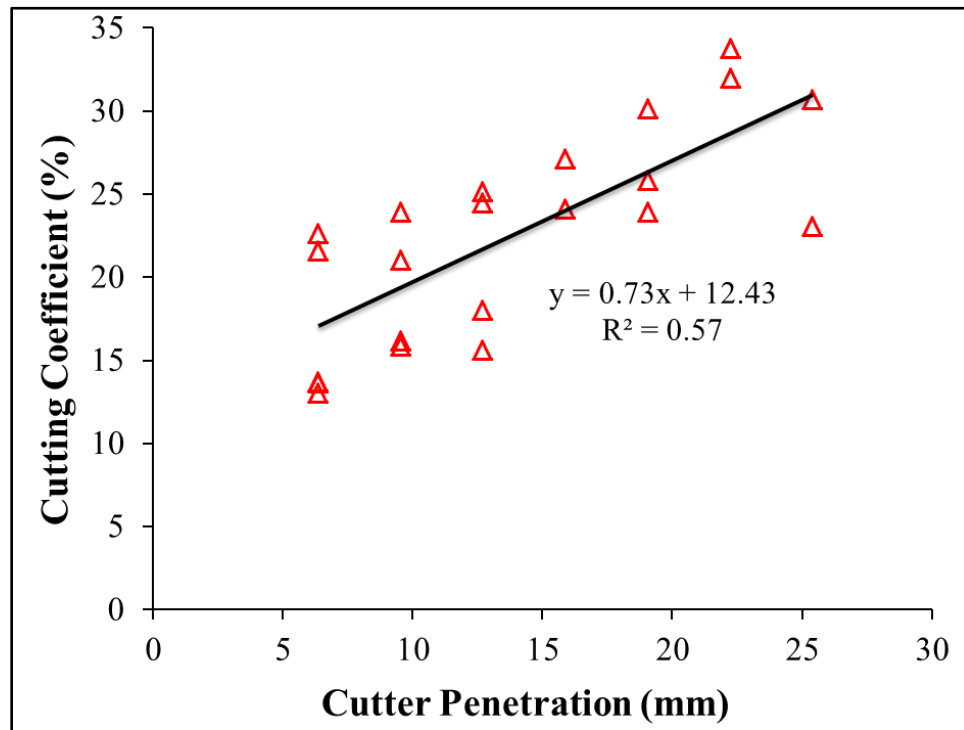


Figure 5.15. Cutting coefficient variation with cutter penetration for dry rock.

For saturated rock cutting tests, elimination of two data points causes an overall drop in the *CC* with the increased depth of cutter penetration (Figure 5.16). This behavior is contrary to the dry rock cutting results. At much deeper penetration of 16 mm, a slight increase in *CC* was observed, but still this increase was much less than some of the *CC* values obtained at shallower penetrations. The reasons for this drop in *CC* are still not fully clear. Initially it was believed that this drop in *CC* at deeper cutter penetrations is probably due to excess porewater pressure affecting the breakage process. The load-

indentation tests with porewater pressure measurement were designed to verify the presence of excess porewater pressure (Section 8). The porewater pressure quantities measured in those tests were not high enough to support the idea of excess porewater pressure affecting the breakage process and hence reducing the overall *CC* values in saturated rock.

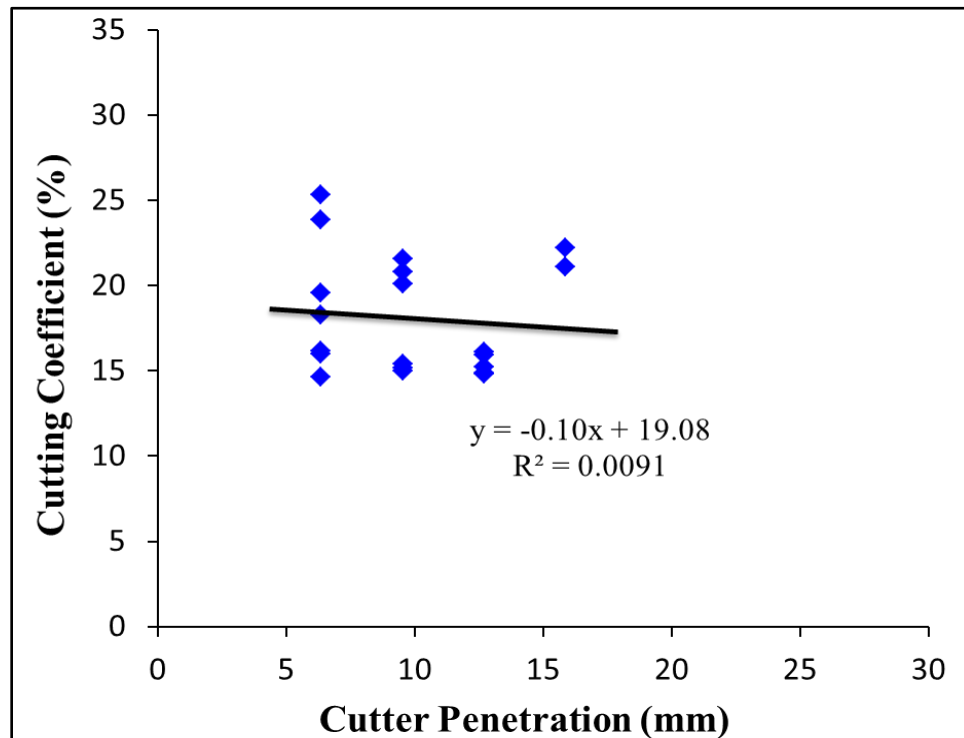


Figure 5.16. Cutting coefficient variation with cutter penetration for saturated rock.

### 5.7. EFFECT OF CUT SPACING ON CUTTING COEFFICIENT

The effect of cut spacing on dry rock *CC* also shows an upward trend for all the penetrations tested, except for very wide spacings of 305 mm, where the *CC* curve may have reached its maximum (Figure 5.17). The increasing trend in the *CC* as the cut spacing increases is due to the interaction between adjacent cuts, which is also evident in the plots of different forces against cut spacings showing an increasing trend in the

normal and rolling forces with increase in cut spacings (Figure 5.1). The reason for drop in *CC* at very wide spacings is that the disc is in effect operating in isolation (unrelieved cutting mode), resulting in reduced forces.

The effect of spacing on *CC* for saturated blocks was of similar nature to the dry cutting (Figure 5.18), except that the *CC* ranges from 15% to 25% for saturated rock, whereas it varies from 13% to 34% for dry rock cuts. An overall increase in the *CC* is evident up to 152 mm spacing for deeper cutter penetrations, whereas a slight drop in *CC* can be seen at spacing of 229 mm. More tests at wider spacings are required in saturated rock to understand if the cessation of interaction between adjacent cuts has any noticeable effect on the *CC*. Gertsch and Ozdemir (1992) and others have noted that the capacity of excavators operating in softer formations resulting in high *CC* are limited by their torque or power capabilities, rather than limited by their thrust capacity. The high *CC* obtained for both dry and saturated rock tests indicates high torque requirements for mechanical excavators in this type of rock under any saturation.

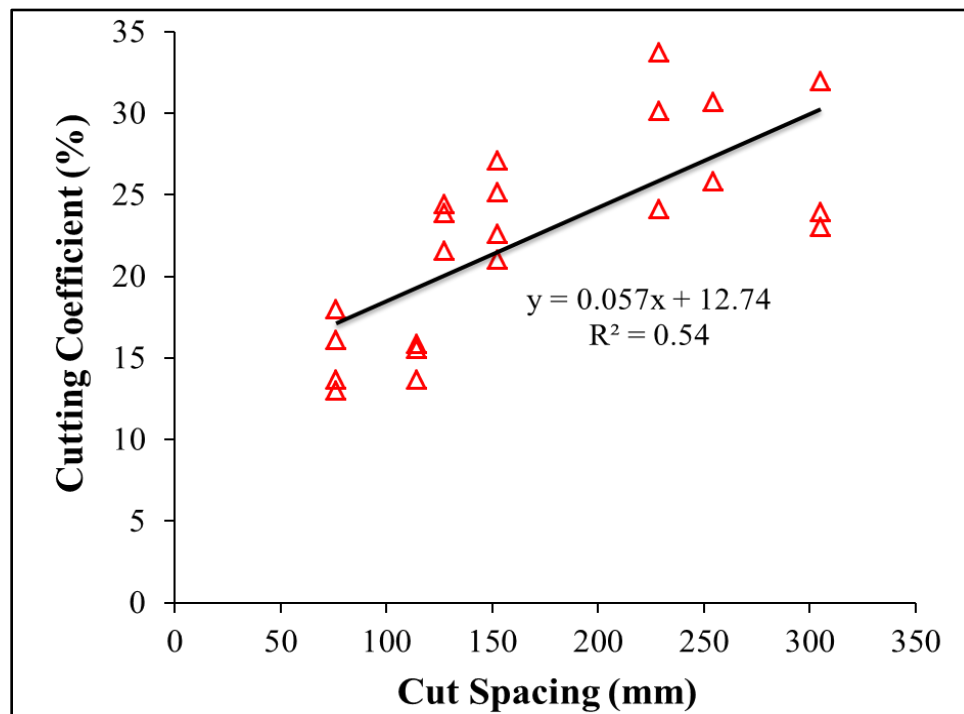


Figure 5.17. Cutting coefficient variation with cut spacing for dry rock.



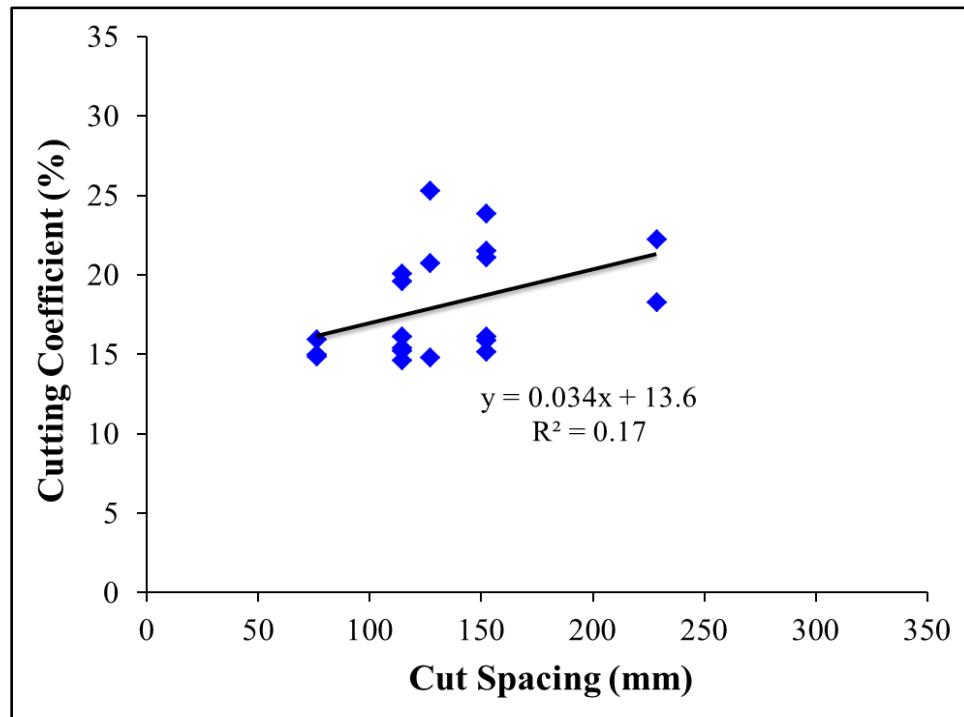


Figure 5.18. Cutting coefficient variation with cut spacing for saturated rock.

## 6. DISCUSSION: SATURATION EFFECTS ON DRAG PICK CUTTING

This section offers the discussion on the full scale drag pick cutting tests conducted on dry and saturated samples of Roubidoux Sandstone. The experimental results of 50 data passes, incorporating 350 data cuts, are evaluated in this section. Experimental procedures are outlined in Section 3, whereas detailed results are presented in Section 4.

### 6.1. OVERALL EFFECTS OF SATURATION

An overall comparison of the cutting forces and specific energy values (Table 6.1) shows slight increases in the cutting and normal forces when cutting in saturated rock as compared to dry rock cutting. The change in the side forces is negligible. It is interesting to note that the  $SE_A$  and  $SE_N$  values increase almost 28% and 9%, respectively, in saturated rock over dry rock.

Table 6.1. Comparative average forces and specific energies with related statistical parameters.

	Cutting Force, $F_d$ (kN)	Normal Force, $F_n$ (kN)	Side Force, $F_s$ (kN)	Actual Specific Energy, $SE_A$ (kW-hr/m <sup>3</sup> )	Nominal Specific Energy, $SE_N$ (kW-hr/m <sup>3</sup> )
Dry Sandstone	4.65	7.66	1.12	5.41	6.23
Saturated Sandstone	5.11	8.38	1.11	6.91	6.79
Percent change	9.90	9.40	0.90	27.73	8.99
z-value (observed)	-0.668	-0.695	0.0557	-1.460	-0.5501
z-value (critical)	-1.284	-1.284	1.284	-1.284	-1.284
p-value (at $\alpha=0.1$ )	0.252	0.244	0.522	0.072	0.291

To determine whether the pick forces and the specific energies are truly different when the rock is saturated with water, hypothesis testing about the means was performed.



Saturated rock cutting seems to experience higher forces and be more energy intensive, contrary to disc cutting experience, but statistically at the 10% significance level, only the increase in  $SE_A$  is valid. The increase in the saturated rock forces appears to have been caused by the presence of a more resistant rock layer in one of the saturated rock blocks (Figure 6.1 and 6.2). The outlier at  $s=88.9$  mm and  $d=6.4$  mm shows abnormally high values of cutting and normal forces, even for saturated rock. It can be seen that the cutting and normal force values for dry and saturated rock cutting tests are overlapping in most of the cases.

Figure 6.3 and 6.4 show the typical rock layer at  $s=88.9$  mm and  $d=6.4$  mm before and after cutting; note the difference in the chip sizes of the reddish brown and white layer; the smaller size of the brown chips suggests less resistance to cutting than white layer.

## 6.2. EFFECT OF CUT SPACING ON CUTTING FORCES

The effect of increasing cut spacing in both dry and saturated rock shows a similar upward trend (see Figures 6.5 and 6.6). A few low force values (especially at shallower depths of cut) indicate a lack of interaction between adjacent grooves and, hence, a drop in the cutting forces. An increase in the cut spacing, coupled with an increase in depth of cut, increases the cutting and the normal forces in both dry and saturated rock. This increase in the cutting forces is coupled with an increase in the amount of cuttings produced. The specific energy, being the quotient of mean drag force divided by the amount of cuttings, has been theorized to reach a minimum value when the interaction between the grooves is at its greatest (Fowell, 1993). The side forces in the saturated rock cuts seem to be of a similar magnitude for all cut spacings tested, however, although the decreasing trend with increasing cut spacing is more prominent in dry rock.

## 6.3. EFFECT OF DEPTH OF CUT ON SPECIFIC ENERGY

Figure 6.7 shows the effect of increase in the depth of cut on the actual specific energy  $SE_A$ . The  $SE$  curves for dry and saturated cutting merge as the depth of cut increases.

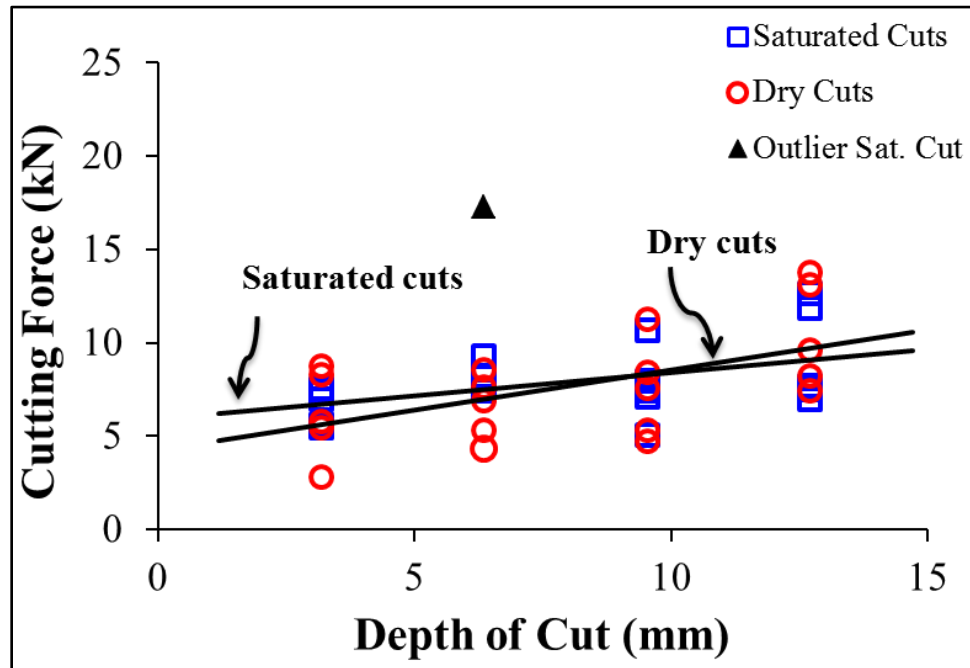


Figure 6.1. Effect of depth of cut on cutting forces.

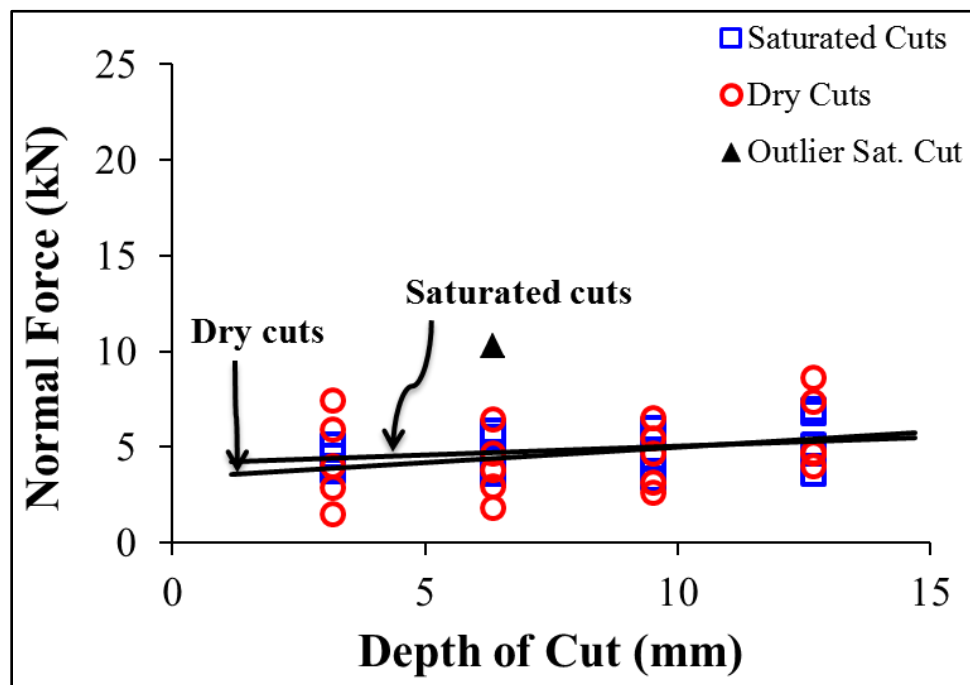


Figure 6.2. Effect of depth of cut on normal forces.



Figure 6.3. Conditioned rock surface for data pass at  $s=88.9$  mm,  $d=6.4$  mm before cutting; variation in rock lithology is visible.



Figure 6.4. Rock surface after cutting; compare smaller chip sizes of reddish layer with the relatively large chip sizes of white layer.

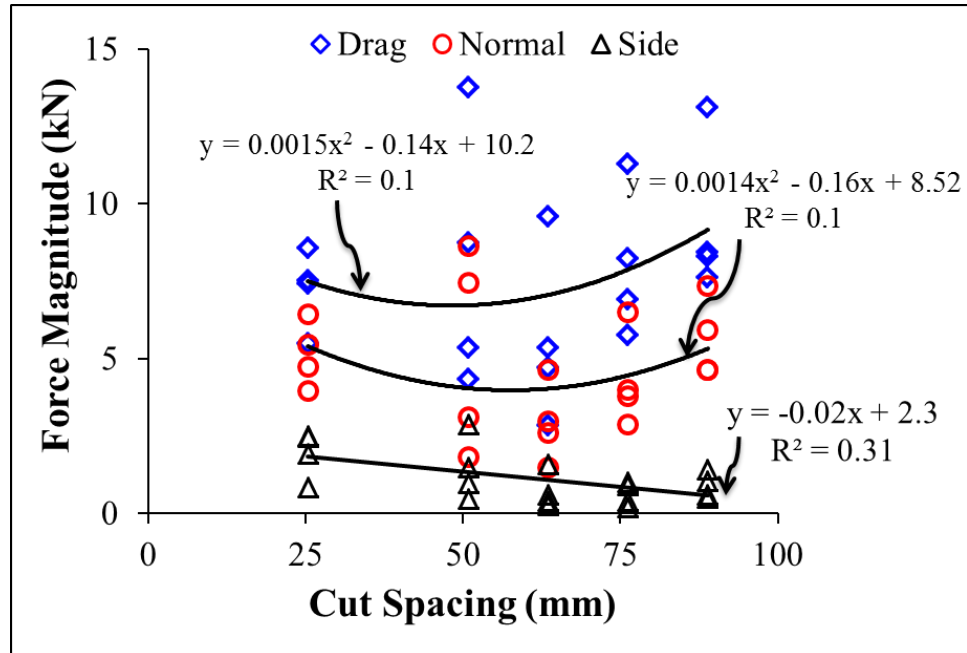


Figure 6.5. Force magnitude variation with cut spacing for dry rock cuts.

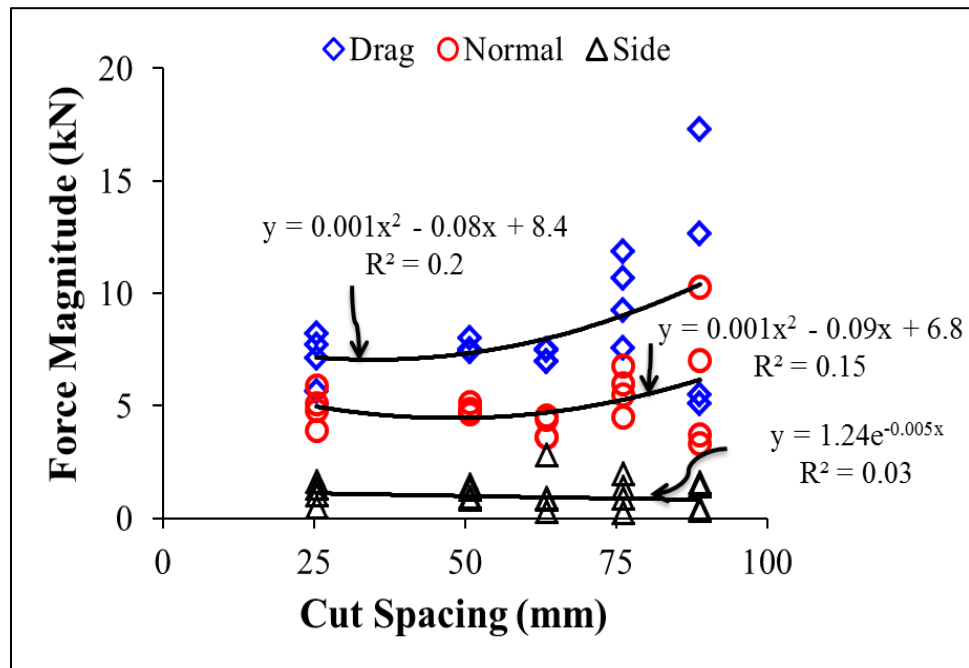


Figure 6.6. Force magnitude variation with cut spacing for saturated rock cuts.

This shows that at greater depths of cut, there is more interaction between the adjacent cuts (relieved cutting action) producing larger volumes of the broken rock. Note that there is less variation in  $SE$  values with increasing depths of cut. This relates to the boundary effects; surface roughness or asperities vary the mass of the broken chips more at shallow depths of cut than at deeper depths of cut. As the depth of cut increases there is less variability in the mass of the broken chips, hence making  $SE$  less variable.

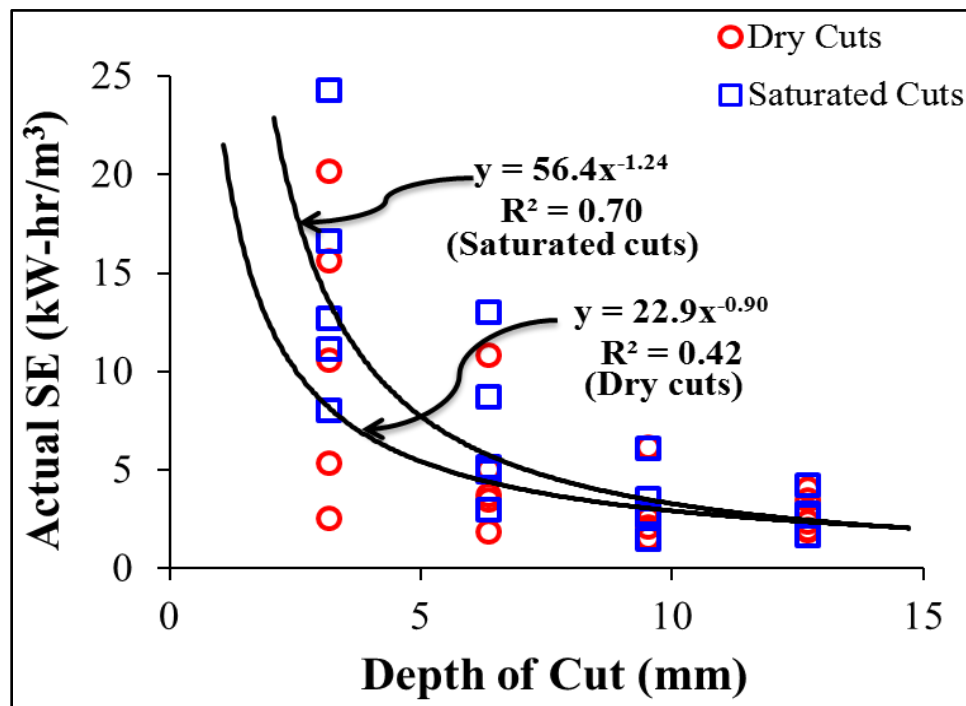


Figure 6.7. Actual specific energy variation with depth of cut for dry and saturated rock.

The variation between nominal and actual  $SE$  with increasing depth of cut can be seen in Figures 6.8 and 6.9 for dry and saturated cuts respectively. In both cases it is evident that the  $SE_A$  is higher than the  $SE_N$  at shallow depths of cut, showing lack of interaction between adjacent cuts. As the depth of cut increases, the  $SE_A$  decreases, showing that relatively more rock is being fragmented resulting in a more efficient cutting process.



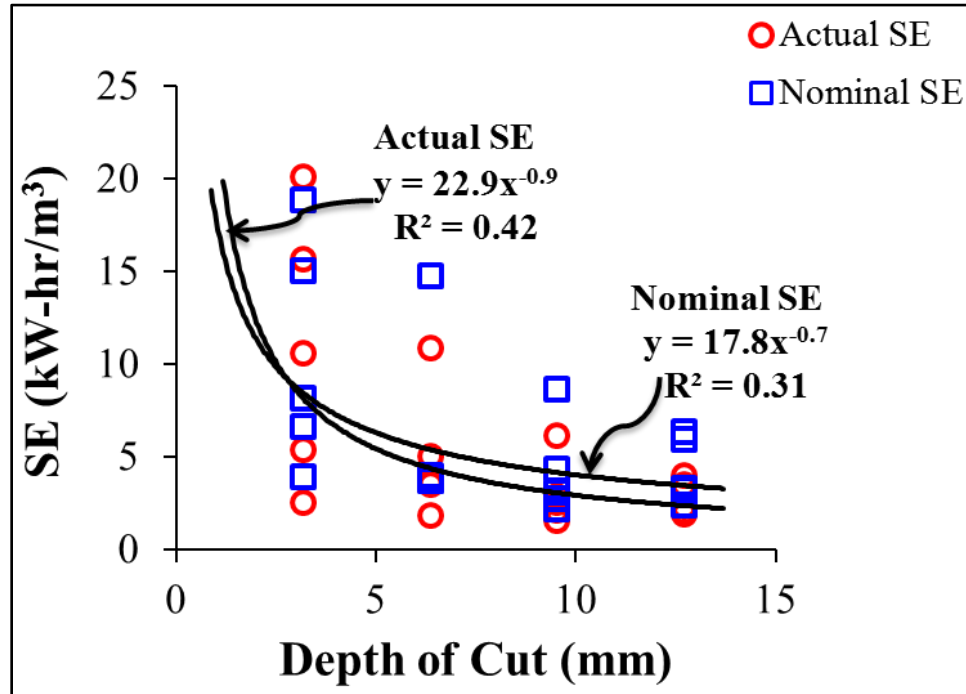


Figure 6.8. Variation in actual and nominal  $SE$  with depth of cut for dry rock cuts.

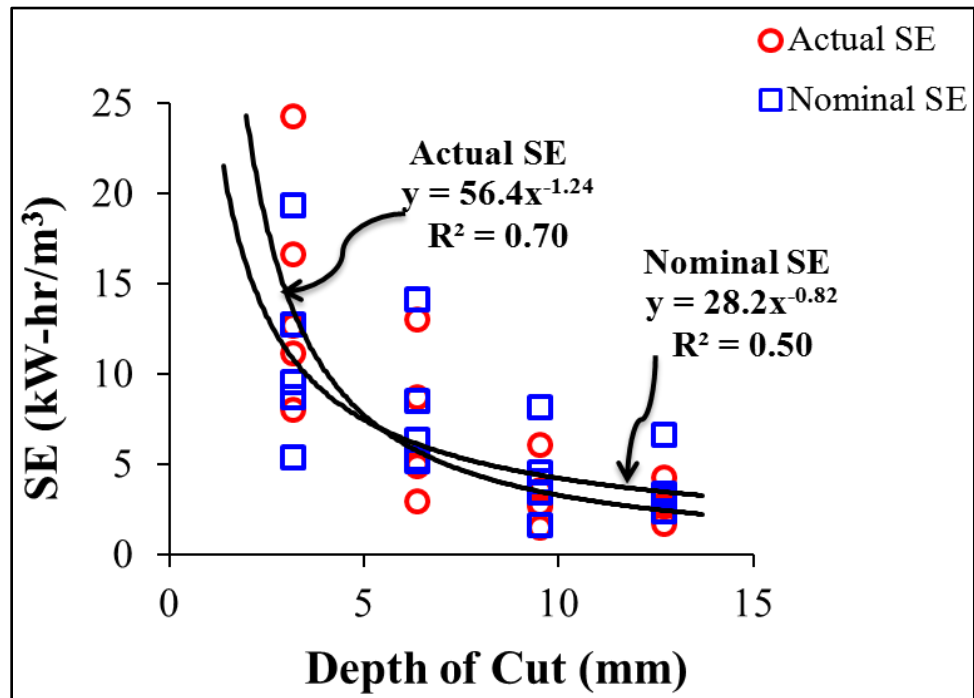


Figure 6.9. Variation in actual and nominal  $SE$  with depth of cut for saturated rock cuts.

#### 6.4. EFFECT OF CUT SPACING ON SPECIFIC ENERGY

Specific energy ( $SE$ ), which measures the efficiency of a cutting operation, has a direct relationship with cut spacing. Increased cut spacing, coupled with an increase in the depth of cut, expands the excavated volume. Hence, the  $SE$  of the cutting operation decreases if the forces simultaneously either decrease or increase by a lesser amount. Figure 6.10 and Figure 6.11 show that dry rock responded differently than saturated rock. The  $SE$  of dry rock shows a minimum at a spacing of 60 mm, but no clear minimum has been reached for saturated rock. Exceptionally high  $SE$  values can be expected at very wide cut spacings, especially at shallow depths of cut, along with too much fines and too few large chips. Very wide cut spacing results in a cut-deepening (ridge-building) situation. Cut-deepening produces very high forces and specific energy levels, with the cutter eventually just removing the volume swept by the tool (Roxborough, 1988).

Photographs of typical data passes at very wide cut spacings and shallow depths, in both dry and saturated rock, are illustrated in Figures 6.12 and 6.13, respectively. It is evident that the adjacent cuts did not interact with each other and the pick was in effect moving in isolation. This resulted in cut-deepening situation. Although the  $SE_A$  coincided with the  $SE_N$  in most cases, it is interesting to note that some  $SE_A$  values were quite higher than the  $SE_N$  values. This occurred in both dry and saturated rock cuts due to the heterogeneity of the rock.

In the context of rock cutting, specific energy should not be thought of as a fundamental property of the rock. Rather, it is a function also of cutting tool design and the geometry of its interaction with the rock (Breeds and Conway, 1992). Rock properties, such as the type of cementing material, bedding planes, and discontinuities, play roles in creating the mass of chips in a cutting operation.

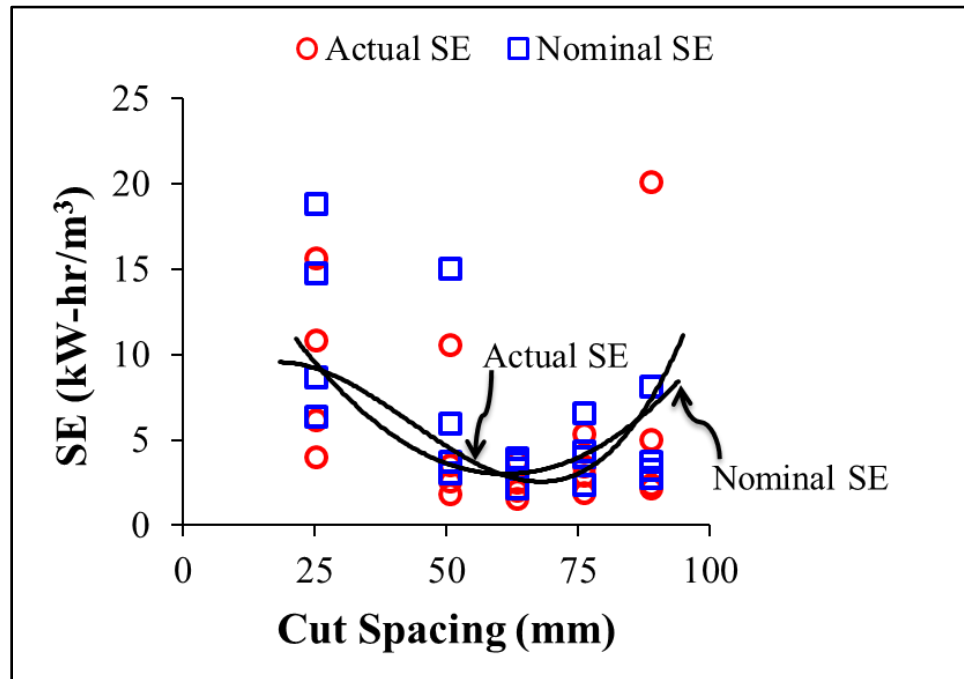


Figure 6.10. Specific energy variation with cut spacing for dry rock cuts.

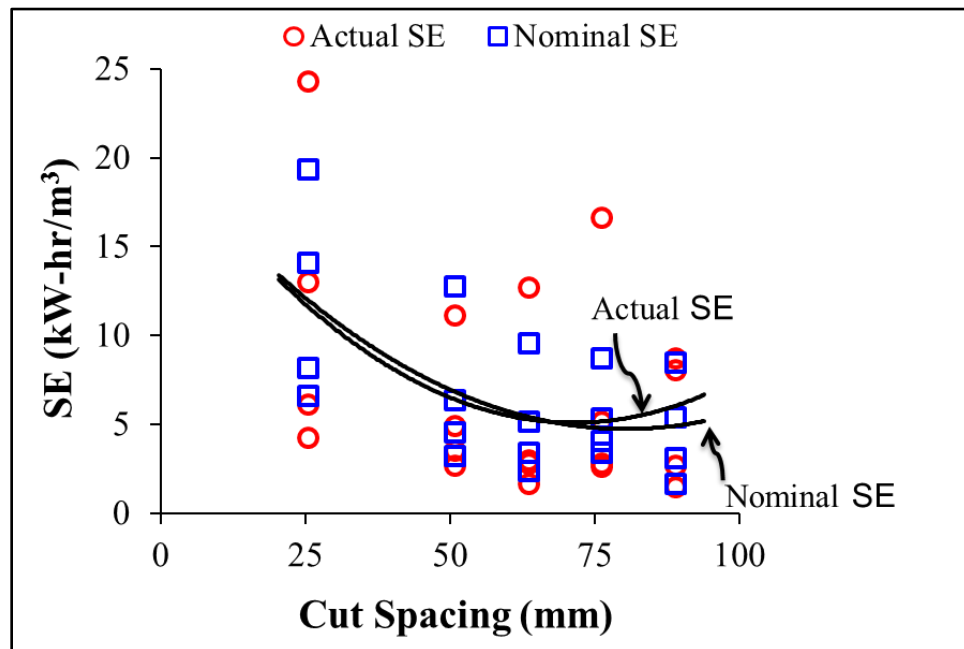


Figure 6.11. Specific energy variation with cut spacing for saturated rock cuts.

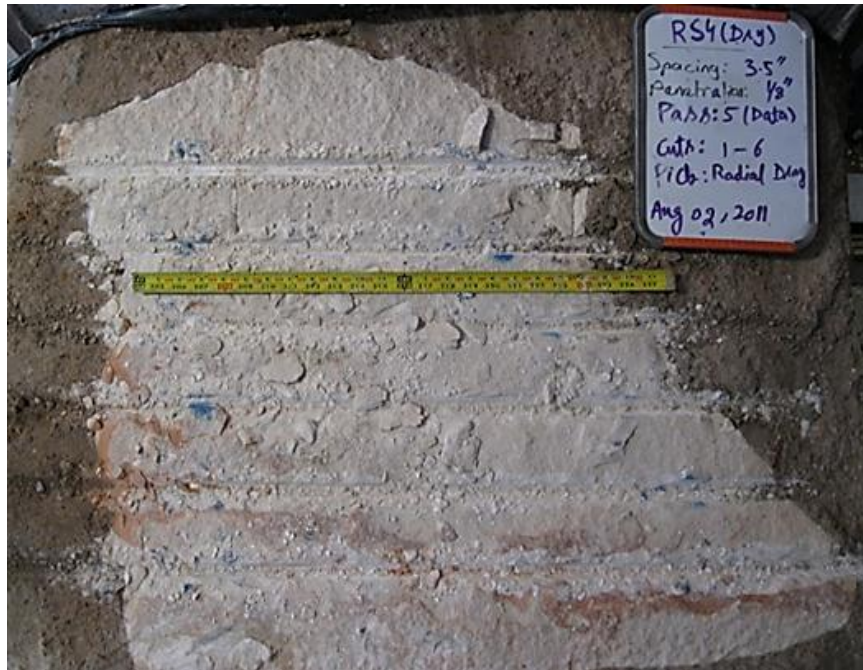


Figure 6.12. A typical dry rock data pass at wide cut spacing and shallow depth of cut before chip collection. Note the small chip sizes and the relatively few chips that break out beyond the cut.



Figure 6.13. A typical saturated rock data pass at wide cut spacing and shallow depth of cut before chip collection.

## 6.5. EFFECTS OF $s/d$ RATIO ON SPECIFIC ENERGY

The optimum ratio of spacing to depth of cut ( $s/d$ ) is the ratio at which the cutting operation gives the minimum specific energy values. This parameter has been used frequently in past studies in mining and tunneling machine design. The optimum  $s/d$  ratio for pointed tools has been reported to lie between 1.5 and 3 depending upon the rock type (Hood and Roxborough, 1992; Speight, 1997), whereas for drag picks it is between 1 and 5 (Copur et al., 2001; Balci and Bilgin, 2007). The optimum for disc cutters is approximately within the spacing-to-penetration ratios of 10-20, and for brittle rocks it can be as high as 30 (Ozdemir et al., 1978). Roxborough and Rispin (1973) report this ratio of 2-2.5 and 1-1.5 for dry and wet chalk respectively in their cutting experiments using chisel type drag tools. According to Nelson (1993) for a wide variety of rock lithologies, it appears that the optimum  $s/d$  ratio is similar, indicating that the nature of kerf interaction is more a characteristic of geometry than rock properties as long as chipping is occurring. For typical machine designs with set cutter spacings, an  $s/d$  ratio less than optimum occurs in weaker rock with high penetrations at lower cutter forces. Although such operation is less efficient than at optimum  $s/d$  ratios, resulting advance rates are usually adequate to satisfy project schedules. However, for strong rock, reduced penetration and effectively increased  $s/d$  ratios can occur even at elevated normal force levels.

Figure 6.14 and Figure 6.15 show the pattern of the  $SE_N$  and  $SE_A$  values with variation in  $s/d$  ratio for dry and saturated rock. The optimum  $s/d$  ratio for dry rock tests lies between 6 and 8 whereas for saturated rock cuts this value is found to lie between 5 and 9. A scatter in  $SE$  values can be observed after  $s/d$  ratio of 20 for both saturated and dry tests. This is attributed to very little rock yield resulting from lack of interaction between adjacent grooves especially at shallower depths of cut and very wide cut spacings.

Some fairly high  $SE$  values are also present at very small  $s/d$  ratios. When the cuts are too close, excessive crushing occurs; as the spacing widens, crushing and chipping come into an optimum balance. As the spacing becomes excessively wide, cut-to-cut interaction degrades (Gertsch et al., 2007). The relationship between  $SE$  and the overall production rate (Figure 6.16) clearly indicates that higher production rates usually

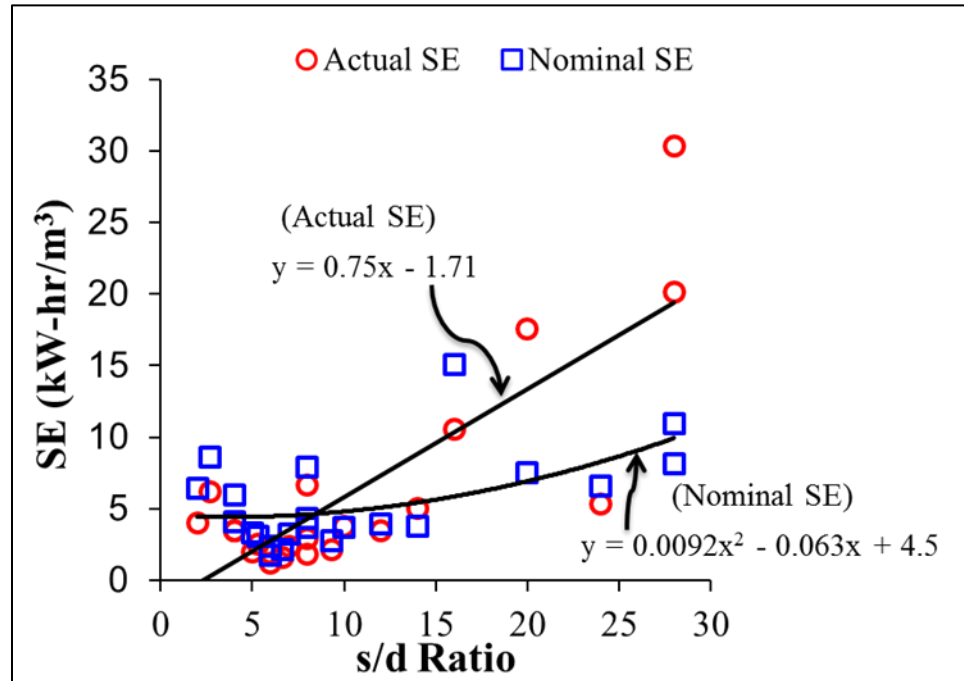


Figure 6.14. Variation in actual and nominal *SE* with *s/d* ratio for dry rock cuts.

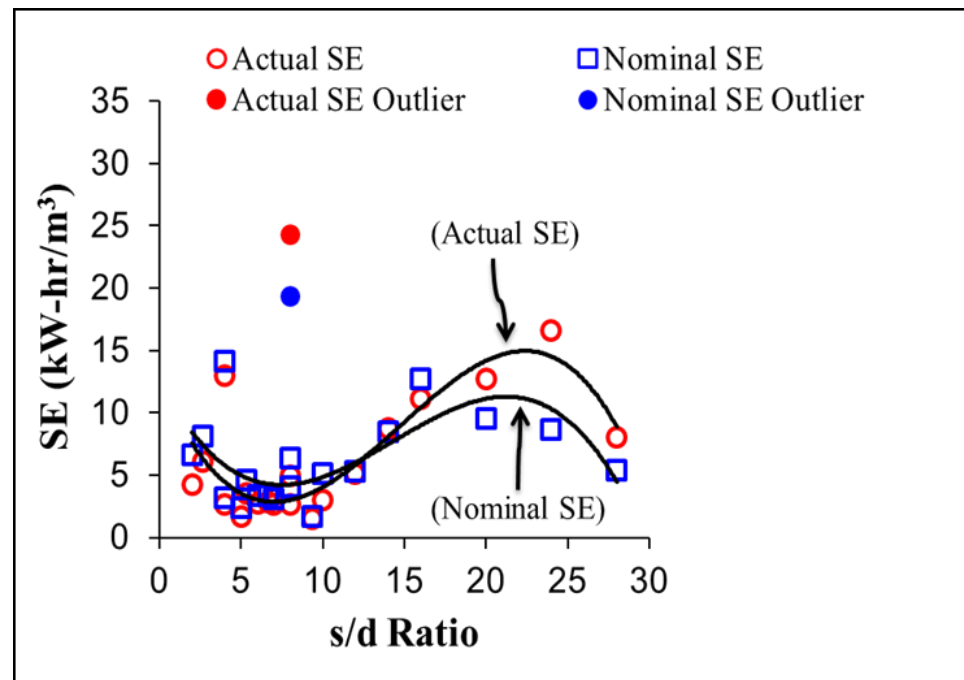


Figure 6.15. Variation in actual and nominal *SE* with *s/d* ratio for saturated rock cuts.

correspond with the minimum SE values. The highest SE value (24.3 kW-hr/m<sup>3</sup>) for saturated rock cuts corresponds to the outlier in Figure 6.15, which clearly indicates that very low production rate has direct bearing on the SE values.

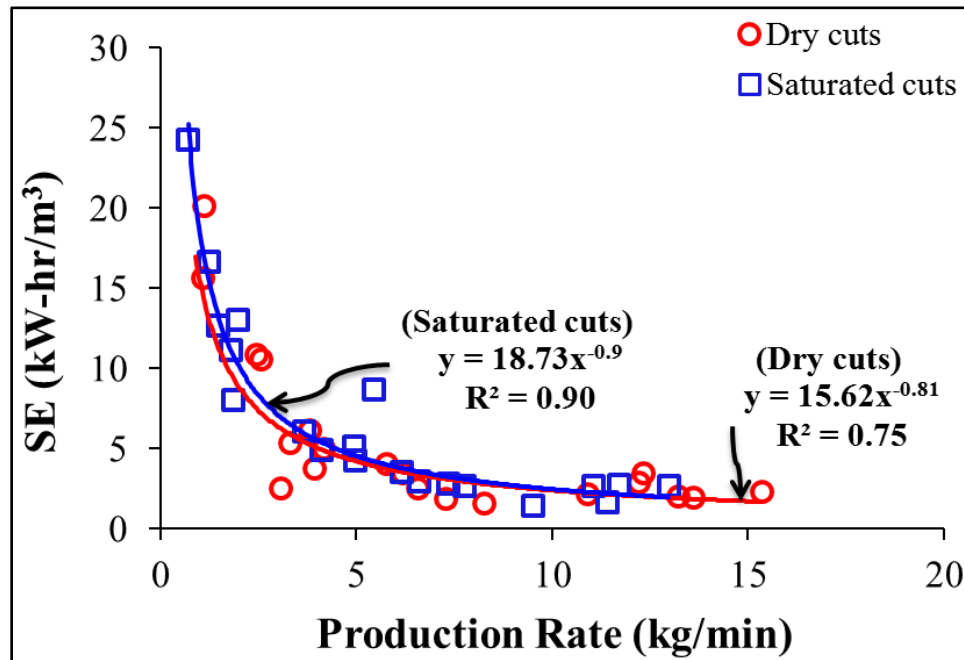


Figure 6.16. Relationship between actual specific energy and production rate.

The 3-D surface plots of nominal and actual *SE* values against cut spacing and depth of cut for dry and saturated tests (Figures 6.17- 6.20) further elucidate the variability of *SE* values with change in *s/d* ratio. It is interesting to note from Figures 6.17 and 6.18 that the nominal and actual *SE* values for dry rock tests are in close agreement at close cut spacings (from 25.4 mm to 50.8 mm). Very wide cuts (at spacings from 63.5 mm to 88.9 mm) and shallow depths of cuts (from 3.2 mm to 6.4 mm) result in a ridge-formation (or underbreak) situation resulting in very high actual *SE* values as shown in Figure 6.18. Very high actual *SE* values are also present at close cut spacings (from 25.4 mm to 50.8 mm) and very shallow depths of cut (from 3.2 mm to 6.4 mm). These high

values of actual  $SE$  are due to excessive crushing and smaller chips produced at very high  $s/d$  ratios for drag picks, directly affecting the  $SE$  values.

For saturated rock cuts (Figures 6.19 and 6.20) the nominal and actual  $SE$  values correspond very well with each other at varying cut spacings and depths of cuts. It is interesting to note that the ridge-formation at very wide cut spacings and shallow depths of cut resulting in very high actual  $SE$  values as seen for dry rock cuts (Figure 6.18) is not very prominent in the case of saturated rock cuts, though not absent. As shown in Figure 6.13 for a saturated rock pass at  $s = 88.9$  mm,  $d = 3.2$  mm, the ridges were formed between adjacent cuts but the overall drag force was lower than the dry rock pass at same  $s/d$  ratio. This resulted in lower  $SE$  values despite the lower chip mass produced.

It is pertinent to recall from Section 5.5 that there was wide scatter between nominal and actual  $SE$  values with varying  $s/p$  ratios for both dry and saturated disc cutting tests, which was partially attributed to the weak, thinly bedded, and heterogeneous nature of the Roubidoux Sandstone. For drag pick cutting tests, the  $SE$  values are less variable except at very high  $s/d$  ratios (Figure 6.14 and Figure 6.15). This difference of  $SE$  variability between disc cutter and drag pick tests may be attributed to the very wide cut spacings and deeper cutter penetrations used for disc cutting tests. At very wide cut spacings and deeper cutter penetrations, the discontinuities and heterogeneities in the rock mass have much higher effect on the size and mass of the chips produced between the adjacent cuts, directly affecting the  $SE$  values.



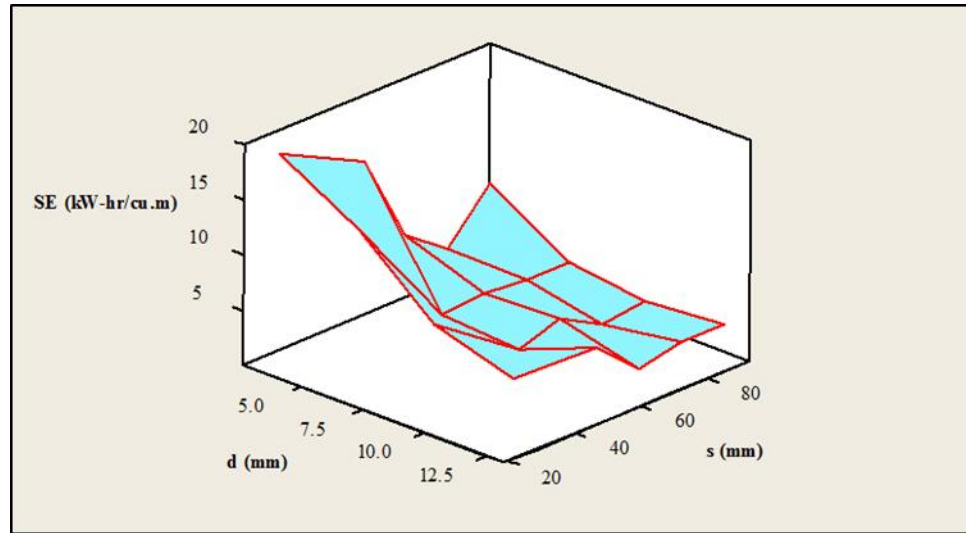


Figure 6.17. 3-D surface plot of nominal  $SE$  vs cut spacing and depth of cut for dry rock cuts with drag pick.

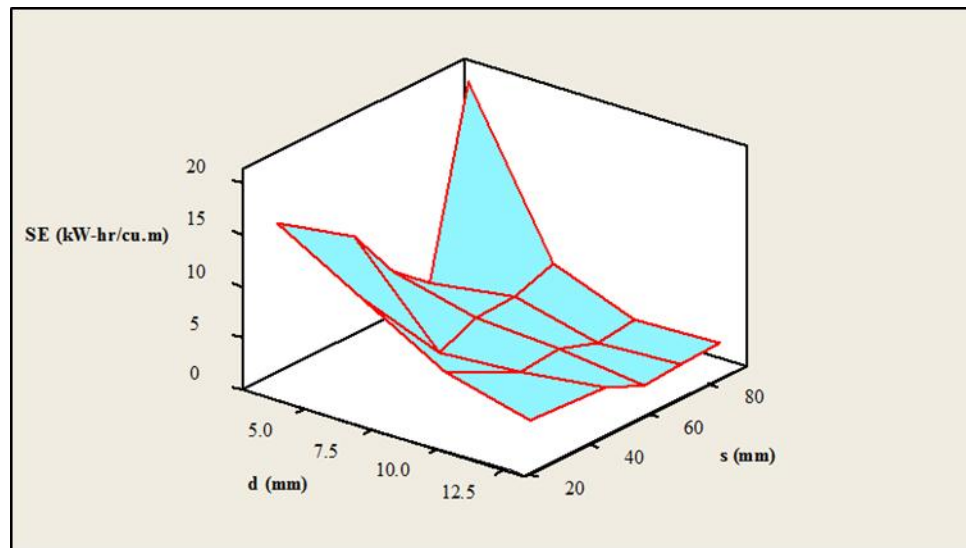


Figure 6.18. 3-D surface plot of actual  $SE$  vs cut spacing and depth of cut for dry rock cuts with drag pick.

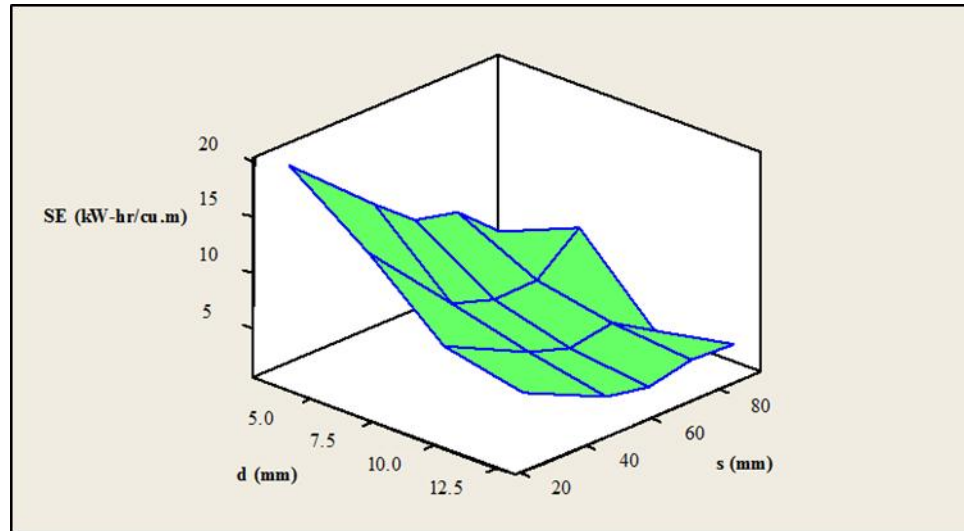


Figure 6.19. 3-D surface plot of nominal  $SE$  vs cut spacing and depth of cut for saturated rock cuts with drag pick.

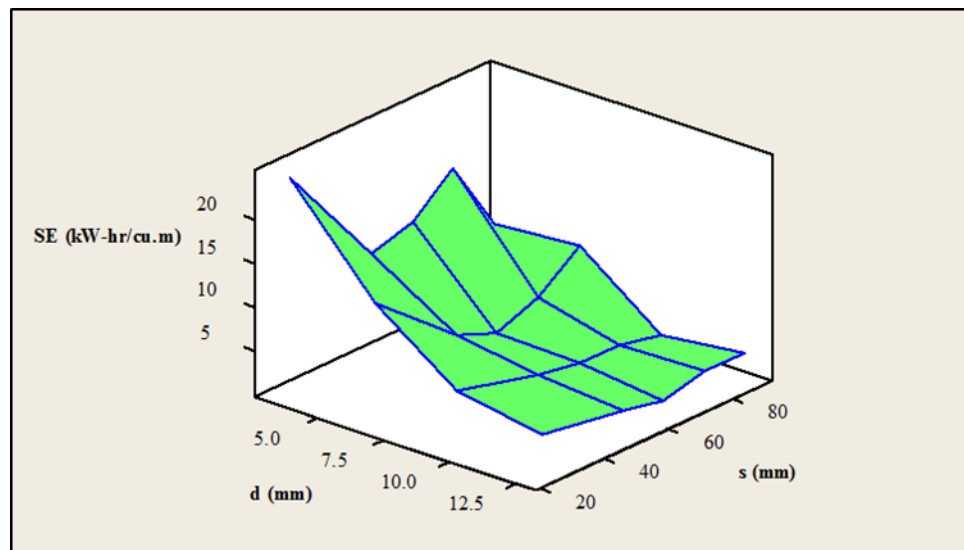


Figure 6.20. 3-D surface plot of actual  $SE$  vs cut spacing and depth of cut for saturated rock cuts with drag pick.

## 7. DISCUSSION: EVALUATION OF CUTTINGS

This section offers analysis of the results of grain size distribution of the fragments from disc cutter and drag pick cutting tests and their relationship with specific energy and cutting geometry.

### 7.1. BACKGROUND

The muck generated in full scale cutting tests and samples obtained from the tunnel face have been analyzed in several ways to get insights into mechanical excavators' performance. Coarseness index (*CI*), which is related to specific energy of cutting and thus the production rate and Instantaneous cutting rate (*ICR*) are two indicators that can be used as empirical performance indicators.

*CI* gives a measure of the production of large chips from the cumulative mass percentages of chips retained on each sieve. Production of large sized chips has direct bearing on production rate and specific energy of cutting operation. A number of investigators have reported *CI* as a useful indicator of the cutting efficiency of mechanical cutting operations. Barker (1964) reported increased mass and coarseness of the point attack pick cutting fragments with the increase in depth of cut, slowly at narrow spacings and more rapidly at wider spacings. Roxborough and Rispin (1973) used *CI* for the evaluation of the muck generated from drag picks, roller cutters and disc cutters on wet and dry chalk. The *CI* values for the wet chalk were always lower than for the dry chalk. Roxborough et al. (1981) noted an upward trend in *CI* values with increasing cut spacing in their cutting experiments on coal in connection with the performance prediction of continuous miners. Altindag (2003, 2004) and Kahraman et al. (2004) used *CI* for rock drillability studies and found reasonable correlations with the penetration rates of different blasthole drills. Tuncdemir et al. (2008) report an inverse power relationship between specific energy and *CI* for most of the rock types tested with drag and disc cutters. Jung et al. (2011) report linear cutting tests on the samples collected from the excavation zone of a shield TBM. An increase in the *CI* values with the increase in the depth of cut from 2 mm to 4 mm at fixed spacing was noted, allowing to choose 4 mm/rev as optimum advance rate.

*ICR* was first introduced by McFeat-Smith and Fowell (1977) and later was modified by Rostami et al. (1994). It is the effective average advance per cutterhead revolution and can be estimated from laboratory specific energy determined from intact rock block tests. Specific energy (*SE*), which is defined as the amount of energy consumed for excavation of unit volume (weight) of the rock has extensively been used to represent the efficiency of cutting and has also been used to estimate machine performance or *ICR*. The *ICR* introduced by McFeat-Smith and Fowell relates the cutting head power of the mechanical excavator to the optimum specific energy as determined from laboratory testing and is given as:

$$SE = \frac{HP}{ICR} \quad (7.1)$$

Where

*SE* = specific energy

*HP* = cutting head power

The Rostami et al. *ICR* (Equation 7.2) introduces an additional parameter *k* which is the coefficient of mechanical efficiency depending on the type of mechanical excavator used.

$$ICR = k \left( \frac{HP}{SE_{opt}} \right) \quad (7.2)$$

Where

*SE<sub>opt</sub>* = optimum specific energy

Bilgin et al. (1988), Gehring (1989) and Thuro and Plinninger (1999) also have developed empirical equations for *ICR* calculation based on uniaxial compressive strength of rocks and performance data of roadheaders working on different mining and tunneling projects. Models developed to compute *ICR* based on laboratory specific energy do not take discontinuities into account. In the above mentioned methods, *ICR* can be estimated from *SE* and the model is so generic that can work for full or partial face machines. Obviously, *ICR* can be translated to rate of penetration (*ROP*) or Penetration Rate (*PR*) of the machine once it is divided by area of the excavation (face area). In other words, once *ICR* is estimated from *SE* or other formulas, it can be used for estimation of

machine advance rate, and one of the objectives of the current study is to look at the possibility of estimating *SE*, *ICR* and thus machine performance based on the size distribution of the muck in dry and wet conditions.

However, *ICR* can also be calculated if the penetration per revolution of the disc cutter is known. Balci (2009) calculates the *ICR* for full face tunneling by a TBM or similar machine using the following equation:

$$ICR = p \times RPM \times A \quad (7.3)$$

Where

$p$  = penetration (mm/rev)

$RPM$  = revolutions per minute and

$A$  = tunnel face area in  $m^2$

It is often useful to fit specific algebraic functions to particle size distribution data. Typically, these functions have two parameters that can be adjusted to provide best fit to a set of experimental data. The values of the parameters provide an improved means of summarizing the actual distribution as compared to using a single, average size like  $d_{50}$ . Theoretically, there is no unique equation that can be expected to describe size distribution data. However, some functional formulas have been developed to give reasonable fit to some sets of data. These functions are simple equations that can fit data reasonably well, usually with only two adjustable parameters that can be obtained from the best fit analysis and are simple to apply (Hogg, 2003). Rosin-Rammler distribution is one of such functional forms which can be used to analyze the fragmented rock products and is very popular amongst mineral processing professionals. This technique seems to have gained very little attention in analyzing mechanized mining and tunneling muck, although its use for the analysis of blast fragmented products has been reported (Smith, 1991; Reichholf and Moser, 2000; Sanchidrian et al., 2009; Müller et al., 2010). This technique was developed to limit the coal pulverization to reach its technico-economic optimum for the coal combustion process. This technique has the advantage of reduction in the laboratory work of fineness analysis. It permits the fineness characteristics curves to be extrapolated into the range where measurements are difficult and can take a very long time (Rosin and Rammler, 1933).

Altindag (2003, 2004) used this technique to correlate mean particle size with coarseness index of drill cuttings for estimation of percussive drilling rate. He found reasonably good correlations between mean particle size of Rosin-Rammler distribution and the drilling rate. Katsunori et al. (2003) examined cuttings from five excavation machines (TBM, boomheader, rock drill, PDC rotary drill and rotary vibration drill) as well as fragments produced by blasting. The cumulative distribution function (CDF) of particle sizes of each excavation method was found to be in a reasonable agreement with the Rosin-Rammler distribution. Kezhil et al. (2008) found reasonable correlations between measured particle distributions of TBM muck with the theoretical distribution models like lognormal and Rosin-Rammler distribution. Oreste et al. (2009) applied Rosin-Rammler distribution on TBM muck and came up with a sieving curve that averaged various sieving curves of the TBM production. This curve was considered as typical for the rock products with which it was possible to obtain the optimal composition for the dimensional distribution of the aggregates to be used for concrete and shotcrete production. Therefore, the use of this technique was deemed suitable for the analysis of muck from full scale cutting tests using disc cutters and drag picks in dry and saturated sandstone samples to evaluate the impact of rock moisture conditions on cutting efficiency and machine performance.

## 7.2. DISC CUTTER CUTTINGS ANALYSES

The experimental results of 36 tests at given spacing and penetration which were completed in 58 data passes, encompassing 600 data cuts (outlined in Section-4) are evaluated. Coarseness index ( $CI$ ) and absolute size constant ( $x'$ ) determined from the grain size distribution of the disc cutting muck have been evaluated to establish their relationship with specific energy and cutting geometry.

**7.2.1. Nominal and Actual Production Rate.** The nominal (theoretical) production rate was compared with the actual production rate of chips from the cutting tests. A 45° line (1:1 line) indicates the line where predicted and actual production rates are equal. Points plotted above the 1:1 line indicate an overbreak situation (Figure 7.1 and Figure 7.2).

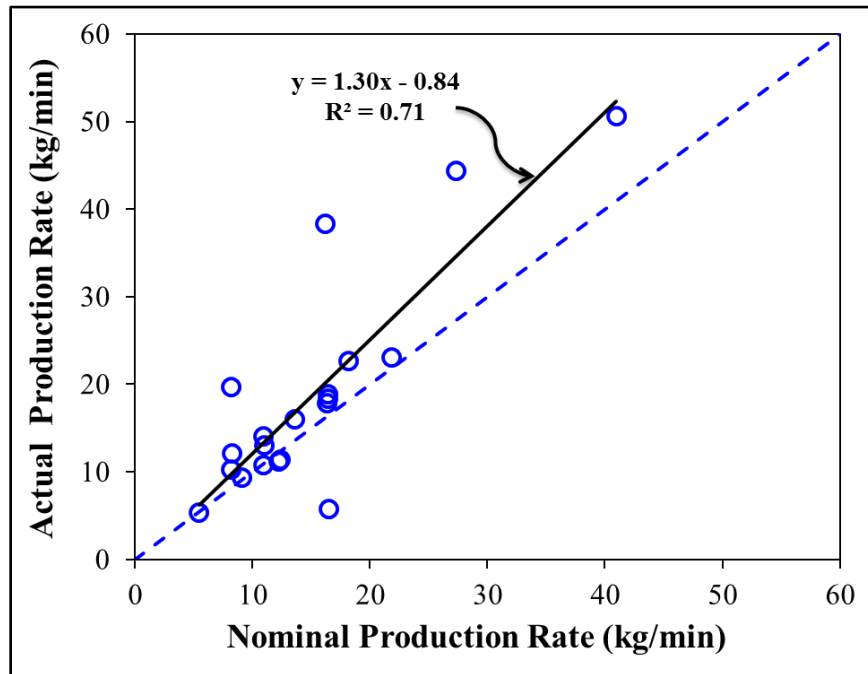


Figure 7.1. Nominal and actual production rate for saturated rock tests.

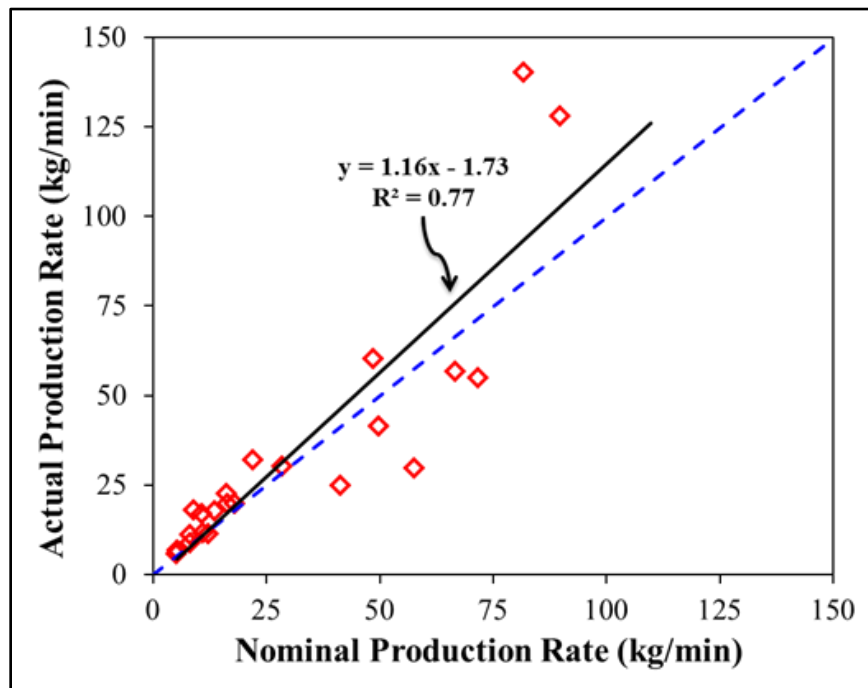


Figure 7.2. Nominal and actual production rate for dry rock tests.

For saturated rock, it can be seen (Figure 7.1) that the actual production rate corresponds well with the nominal production rate. There are some exceptions due to overbreak. This overbreak is believed to be structurally controlled because of the moderately thinly bedded nature of the sandstone tested (Figure 7.3 and Figure 7.4). It is pertinent to mention that the bedding planes of the cut blocks were oriented perpendicular to the normal force component. The cutting forces and the production rate of chips could be significantly different if the blocks are cut in different orientation. Wanner (1975) found that penetration rates when fissility or foliation was parallel to the face were twice that for perpendicular to face. Banding in gneiss acted similarly to foliation in improving penetration rate. Sanio (1985) also showed that the net rate of advance of a full-face tunneling machine in slate can be six times higher for a drive perpendicular to schistosity than for a drive parallel to schistosity.



Figure 7.3. Breakage pattern in saturated sandstone for a data pass before chip collection ( $s=230\text{mm}$ ,  $p=16\text{mm}$ ).



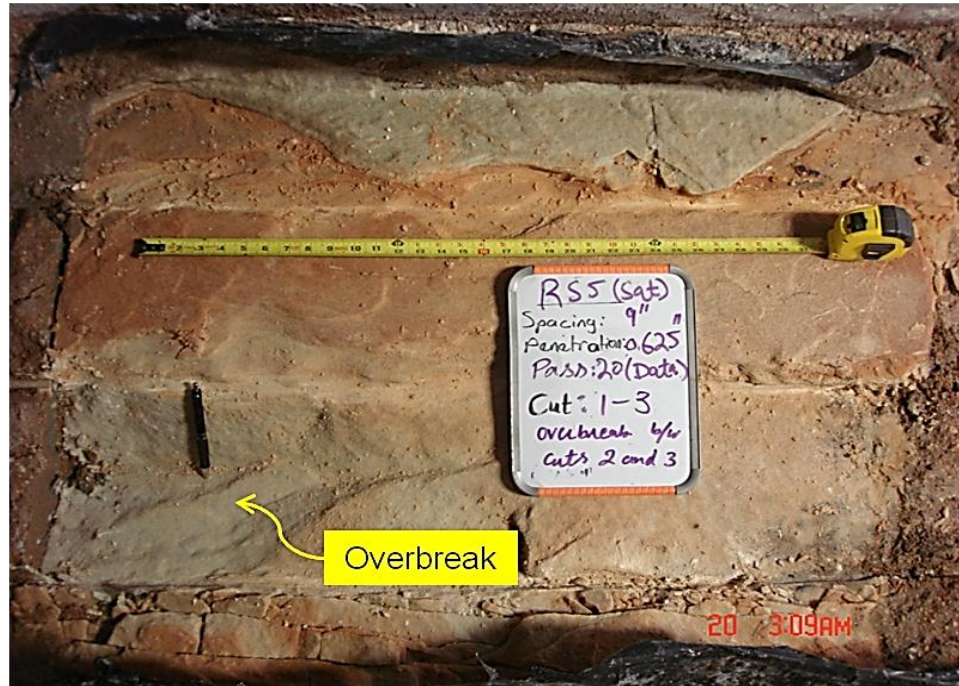


Figure 7.4. Rock surface condition after chip collection; overbreak visible in the bottom left hand side of the picture ( $s=230\text{mm}$ ,  $p=16\text{mm}$ ).

Although the overall  $CI$  for the saturated rock was less than for the dry rock, the proportion of fines produced was much higher than from the dry rock tests. A few cases of the ridge build up between cuts in the saturated rock tests is attributed to the lack of interaction between adjacent cuts due to too-shallow cutter penetration. Since the dry cutting tests were conducted at a much wider cut spacing (305 mm) than the saturated tests, ridge build up between the cuts at shallower cutter penetrations was anticipated (Figure 7.2). Overbreaks in dry rock tests are deemed to be due to the natural discontinuities already present in the rock blocks.

#### 7.2.2. Relationship between Coarseness Index and Absolute Size Constant.

Figure 7.5 shows the relationship between the  $CI$  and computed values of  $x'$  for dry and saturated cutting tests, where a strong correlation can be observed between  $CI$  and  $x'$  for both dry and saturated rock tests. The overall average  $CI$  for muck generated in cutting saturated rock is less than for dry rock due to production of large amount of fines in saturated rock cutting. This clearly indicates the saturation weakening of iron oxide and

clayey cementing material present between the quartz grains and hence a reduction in particle sizes of the muck produced. Some anomalously high values of  $CI$  exist for saturated cutting tests which are attributed to the structural variations and thinly bedded nature of sandstone tested (Abu Bakar and Gertsch, 2012). It is noteworthy that the  $x'$  values for dry and saturated muck are in close agreement for lower values of  $CI$  ( $CI < 350$ ). Shallower penetrations and closer cut spacings produce small sized rock chips due to excessive crushing of the chips, resulting in lower values of  $CI$ . For dry tests, very high values of  $x'$  and  $CI$  are present, since dry tests were performed on much wider cut spacing and deeper cutter penetrations, resulting in large sized rock chip due to relieved cutting action.

### **7.2.3. Effect of Large Sized Muck on Absolute Size Constant and Coarseness**

**Index.** From Figure 7.6, it is interesting to note that the  $x'$  has a very strong upward exponential relationship with the percentage production of large chips ( $> 51$  mm or 2 inches) for dry and saturated cutting tests. Figure 7.7 shows that  $CI$  is also very much dependent on the percentage production of large sized chips ( $> 51$  mm or 2 inches) evident in the form of a very strong upward linear trend for dry and saturated cutting tests. Overall lower values of  $CI$  for saturated rock cutting (Figure 7.7) is indicating the production of large amount of fines and fewer larger chips, although some very high  $CI$  values exist because of the structurally controlled overbreaks.

It can be deduced from Figures 7.6 and 7.7 that both  $x'$  and  $CI$  are very much dependent on the percentage production of large sized particles, though both of these respond differently to the percentage production of large chips. Large values of  $x'$  and  $CI$  would indicate an efficient disc cutting operation. According to von Rittinger's law, the net energy required in a certain process of comminution is proportional to the new surface area developed (Hukki, 1962). An excavation process producing large sized fragments/chips is considered an efficient cutting process. Whereas if an excavation process is producing large quantities of fines, it is deemed as an inefficient process (in terms of specific energy), producing new surface area. Cook and Joughin (1970) showed the relationship of specific energy of different rock breakage methods on nominal fragment size by an inverse power law; more energy was required to produce fine particles than coarse particles.

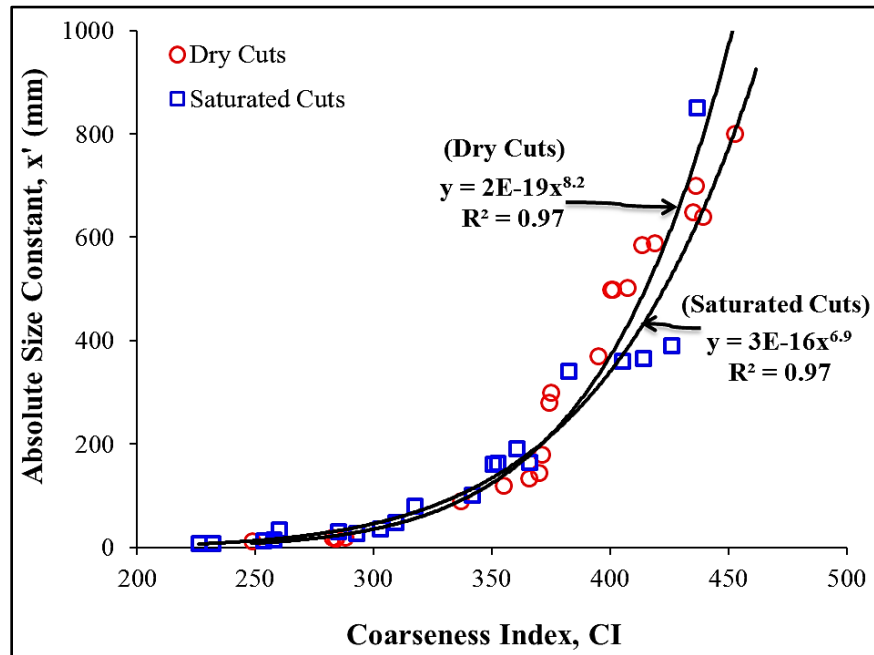


Figure 7.5. Variation of absolute size constant with coarseness index.

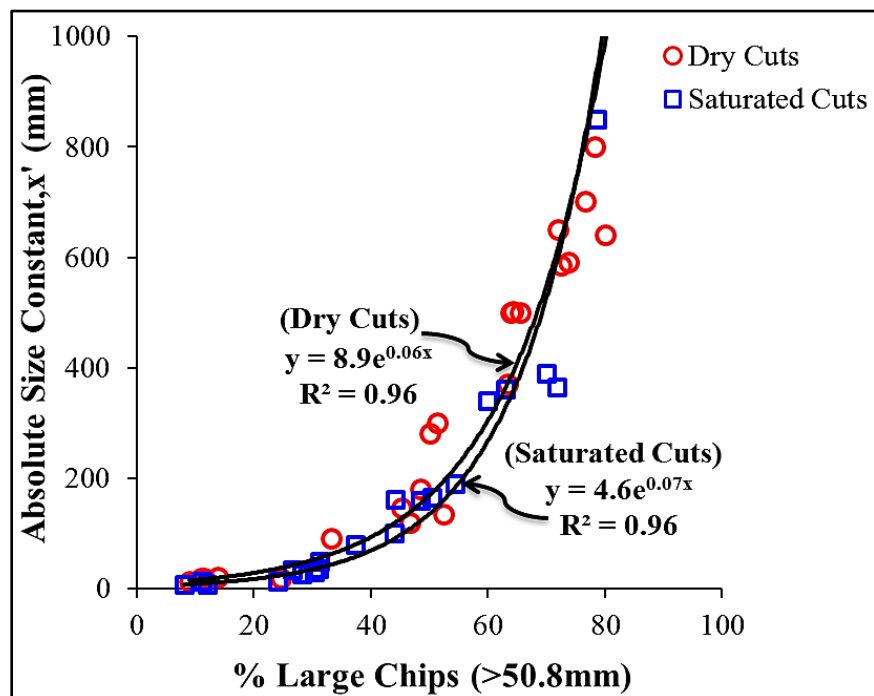


Figure 7.6. Relationship between percentage of large chips (> 51 mm or 2 inches) and  $x'$ .

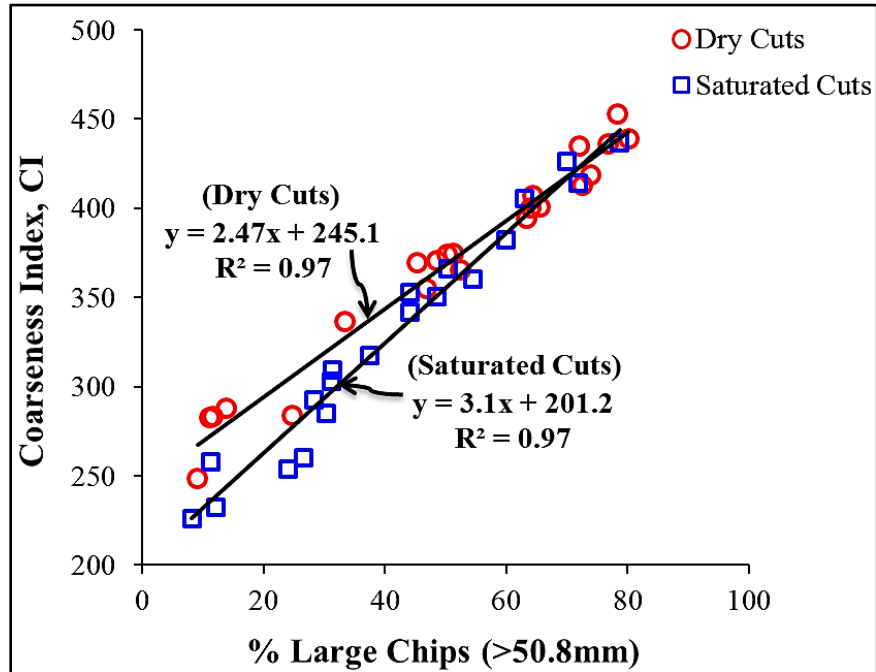


Figure 7.7. Relationship between percentage of large chips (> 51 mm or 2 inches) and *CI*.

**7.2.4. Relationship of Absolute Size Constant and Coarseness Index with Production Rate.** The estimated cutting rate or penetration rate along with the overall system performance and reliability are the aspects which are considered important for feasibility or cost effectiveness of employing a mechanical excavation system (Breeds and Conway, 1992). Figures 7.8 and 7.9 show the relationship of  $x'$  and *CI* with the overall production rate (kg/min) for dry and saturated sandstone cutting tests. There exists a moderate linear correlation between the  $x'$  and the overall production rate (Figure 7.8). Outliers in the dry cuts are attributed to the overbreaks resulting from very wide cut spacings and deeper cutter penetrations. Moderate correlation also exists between the *CI* and the overall production rate, although it is not linear. The same dry cuts outliers are also affecting the overall *CI* for those cuts.

The production rate and size of the chips determined from laboratory testing may differ from field conditions due to discontinuities and other structural features present in the rock mass. In jointed rock, the chip size can be larger due to dislocation of blocks created by crossing joints under the static or dynamic loading of the disc cutters.

Similarly, closely spaced joints and bedding, crushed zones, fault breccias, or other geological features can contribute to increased percentage of fines or smaller size muck. Moreover, cutting is more difficult when the joints are parallel to the tunnel axis, which in turn increases the cutting forces needed for penetrating into the rock surface while increasing the amount of fines and crushed material (Farrokh and Rostami, 2007).

In actual field conditions the production rate (advance rate) and coarseness of the muck produced is also very much dependent upon the overall condition of the rock mass in relation to the  $s/p$  (spacing/penetration) ratio of the disc cutters on the TBM cutterhead. For a typical machine design with set cutter spacing, an  $s/p$  ratio less than optimum occurs in weaker rock with high penetrations at lower cutter forces. Although such operation is less efficient than at optimum  $s/p$  ratios, resulting advance rates are usually adequate to satisfy most project schedules (Nelson, 1993).

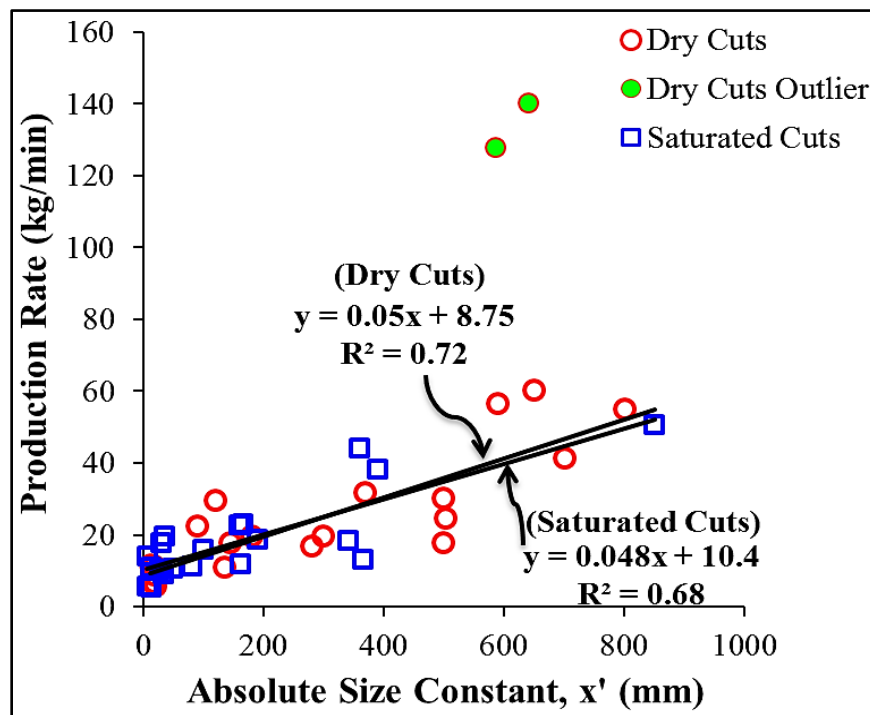


Figure 7.8. Production rate variation with absolute size constant.

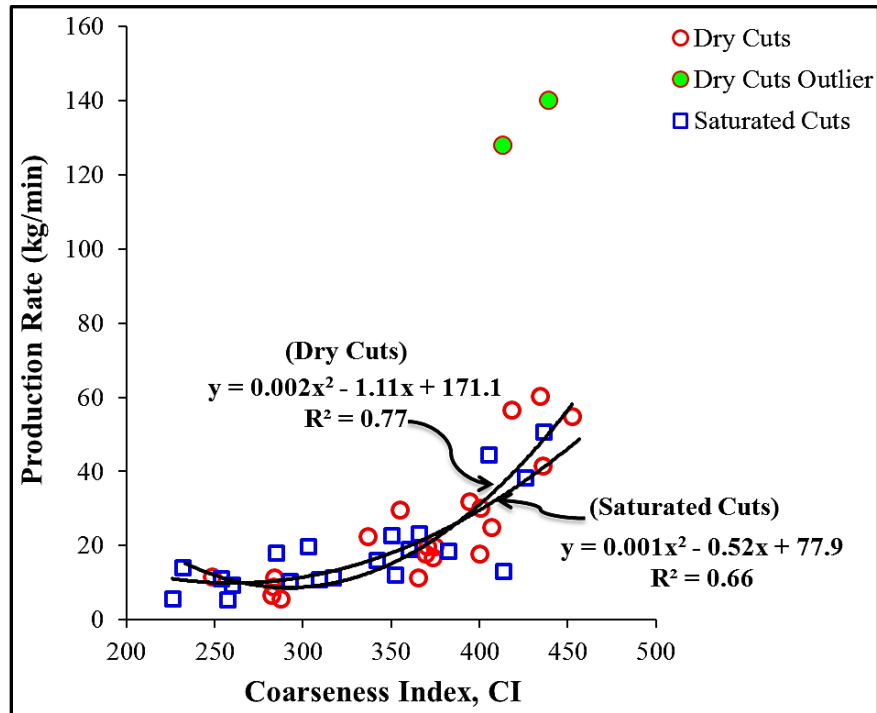


Figure 7.9. Production rate variation with coarseness index.

#### 7.2.5. Absolute Size Constant and Coarseness Index Variation with Cut

**Spacing.** Cut spacing combined with the cutter penetration has a direct bearing on the size of the chips produced. The volume of muck produced increases with cut spacing, producing a maximum as interaction between grooves is at its greatest, then drops to a constant value consistent with unrelieved cutting (Fowell, 1993). Figures 7.10 and 7.11 illustrate the relationship of  $x'$  and  $CI$  with the increasing cut spacing. It is clear that both  $x'$  and  $CI$  have an increasing upward trend with increasing cut spacing. Obviously, at very high spacings ridges will form between the cuts that prevent further advance of the machine. This phenomenon can be observed during linear cutting test but is not accounted for in the sieve analysis of the muck samples at certain combination of cut spacing and penetration.

Multiple points at the same cut spacing show the resulting  $x'$  and  $CI$  at different cutter penetration levels tested. The effect of increased cutter penetration at the same cut spacing is evident in the form of increased values of  $x'$  and  $CI$ . Deeper cuts coupled with wider cut spacing result in increased quantities of debris produced.

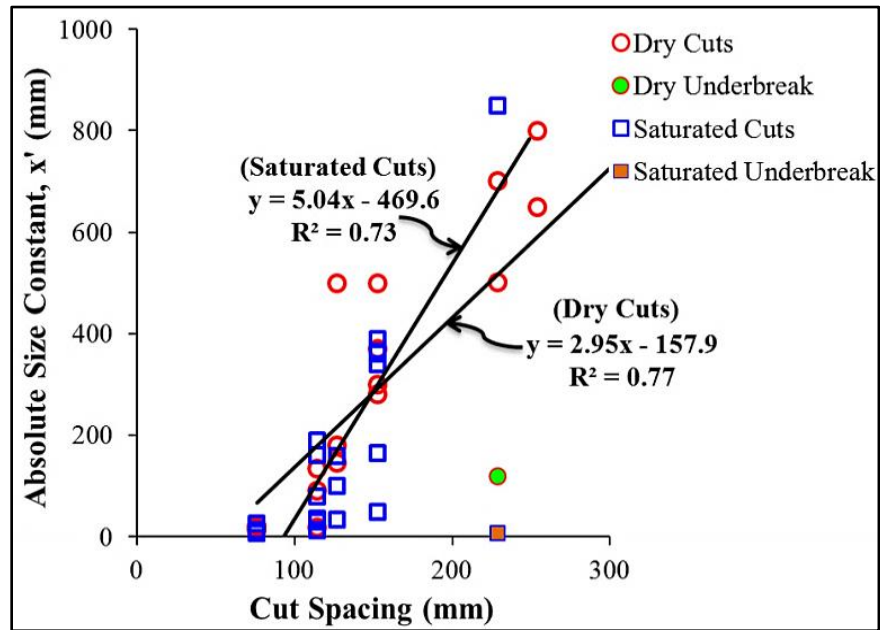


Figure 7.10. Variation of absolute size constant with cut spacing.

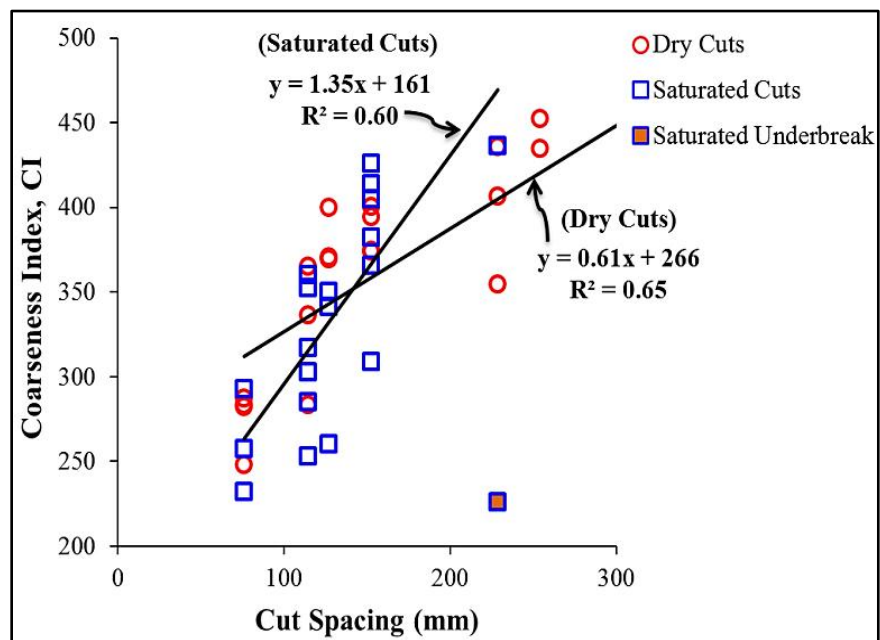


Figure 7.11. Coarseness index variation with cut spacing.



Ridges resulting from lack of interaction between the adjacent cuts especially at shallower cutter penetrations can also be seen (Figures 7.10 and 7.11), though some very high values at deeper penetrations are also present. Very close cut spacings resulting in very low values of  $x'$  and  $CI$  can also be observed as excessive crushing occurs and narrow chips are produced (Gertsch et al., 2007). Figure 7.12 shows a typical saturated rock cut at very wide cut spacing and shallow penetration before chip collection.

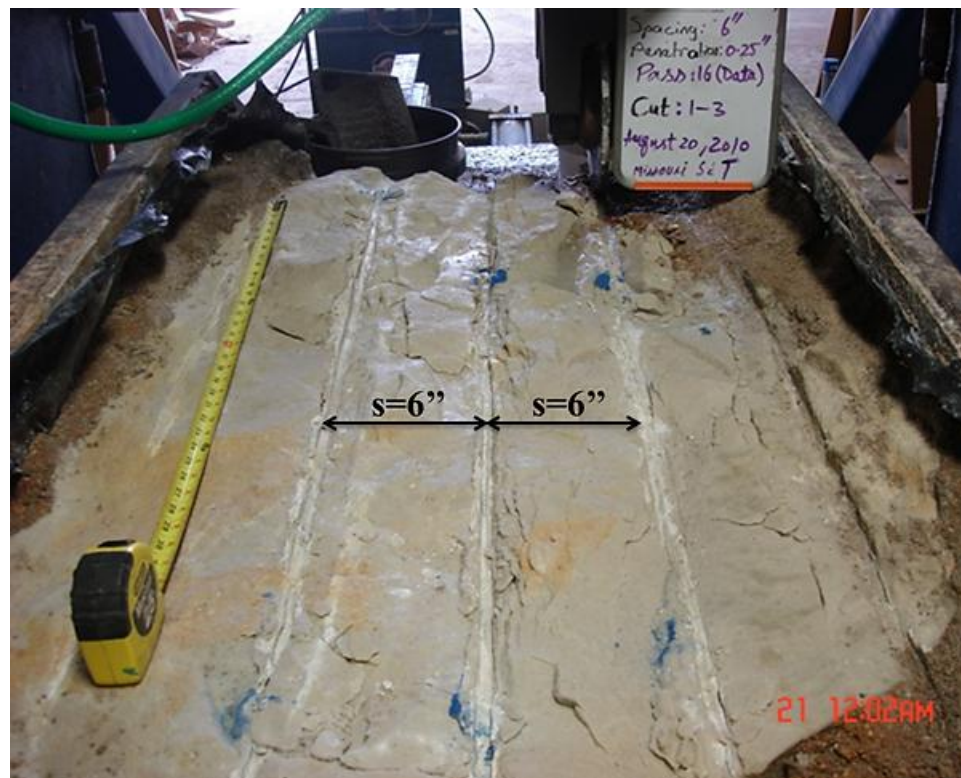


Figure 7.12. A typical saturated rock cut at wide cut spacing and shallow penetration ( $s=152.4$  mm,  $p=6.4$  mm), before chip collection; absence of large sized chips is due to unrelieved cutting mode.

**7.2.6. Relationship of Coarseness Index and Absolute Size Constant with Specific Energy.** There is strong evidence that the  $CI$  of the rock fragmented by disc cutting increases with cutting efficiency. In a given rock type an increase in the cutting efficiency (or reduction in specific energy) corresponds to increase in the coarseness of



the product and a reduction in the amount of airborne dust (Roxborough, 1973). Figure 7.13 and Figure 7.14 illustrate the relationship of  $CI$  and  $x'$  with the specific energy ( $SE$ ) of the rock cutting for dry and saturated samples. Despite a wide scatter in the data, an overall decreasing trend in  $SE$  with increasing  $CI$  and  $x'$  can be observed. Furthermore, because of poor cementation and thinly bedded nature of the sandstone, wide variability in the mass and sizes of the muck was expected, directly affecting the  $SE$  values. The  $SE$  difference between dry and saturated cutting tests is also visible. An 8.5% reduction in  $SE$  values was noted between dry and saturated disc cutting tests (Abu Bakar and Gertsch, 2011).

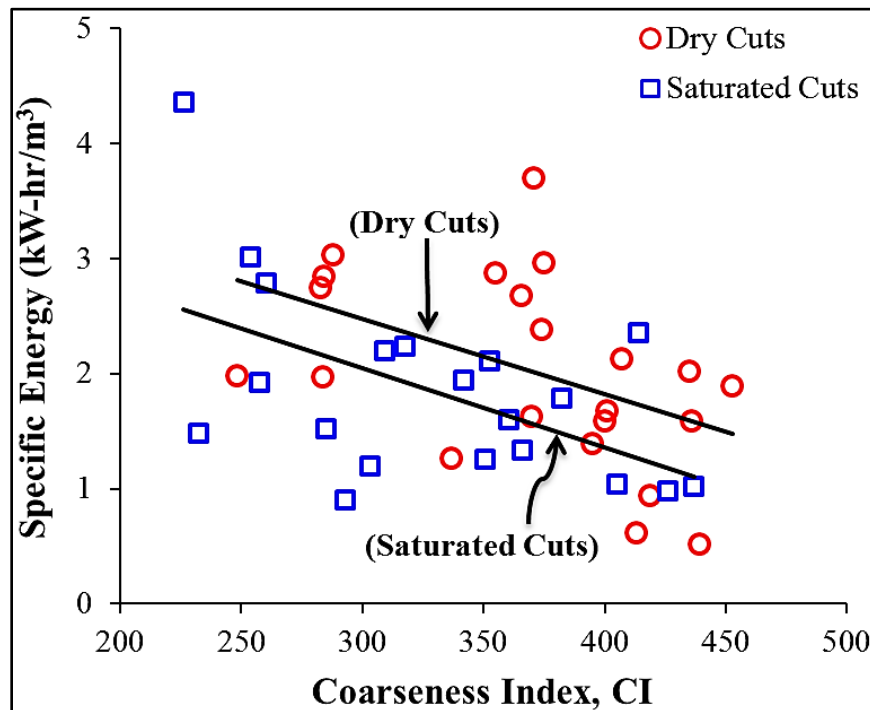


Figure 7.13. Relationship between  $CI$  and  $SE$  for dry and saturated cutting tests.

It is interesting to note the variability in  $SE$  of saturated cutting tests at lower values of  $x'$  (Figure 7.14). Very high and very low values of  $SE$  exist at lower values of  $x'$ . Very high  $SE$  values may be attributed to production of large amount of fines and

fewer larger chips resulting from very wide cut spacings and shallower cutter penetrations (large  $s/p$  ratios). Very large  $s/p$  ratios result in unrelieved cutting mode, making an inefficient cutting process (Figure 7.12). At the same time some low  $SE$  values with lower values of  $x'$  are showing the saturation weakening of sparse iron oxide and clayey cementing material present between the quartz grains decreasing the rolling force component of cutting, resulting in lower values of  $SE$ . This conclusion is also supported by the measured UCS of the rock of 51 MPa for dry versus 43 MPa in saturated samples indicating lower rock strength in saturated conditions.

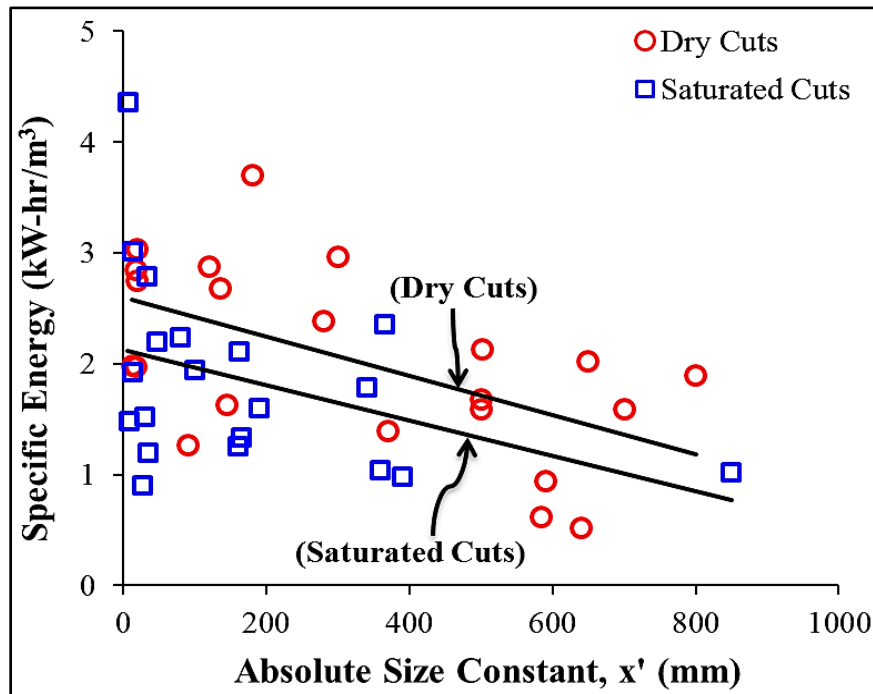


Figure 7.14. Relationship between  $x'$  and  $SE$  for dry and saturated cutting tests.

**7.2.7. Effect of  $s/p$  Ratio on Specific Energy and Coarseness Index.** Figures 7.15 and 7.16 illustrate the relationship of  $SE$  and  $CI$  to varying  $s/p$  ratio for saturated and dry cutting tests, respectively. The effect of change in  $s/p$  ratio on  $SE$  does not definitely show a single optimum  $s/p$  ratio, but there is less variability in the  $SE$  for saturated rock

than for dry rock. Some minimum  $SE$  values can be observed in the  $s/p$  ratio range of 8-16 for saturated rock tests, but there seems to be an increasing  $SE$  trend with  $s/p$  ratio. More tests at wider cut spacings are required to clearly identify the optimum  $s/p$  ratio for saturated rock. This indicates that  $s/p$  ratio may not fully capture the behavior of disc cutters.

The  $CI$  values for saturated rock cuts (Figure 7.15) clearly correspond with the  $SE$  values for same  $s/p$  ratios. Very high  $CI$  values match with the lowest  $SE$  values, showing a direct relationship between  $SE$  and  $CI$ . A trend of decreasing  $SE$  with increasing  $CI$  is also found for dry cutting tests (Figure 7.16), although there is much more scatter in the data. The variability in  $SE$  at the same  $s/p$  ratio is due to the different spacing and penetration combinations used for those tests, resulting in variations in the fragmented volume.

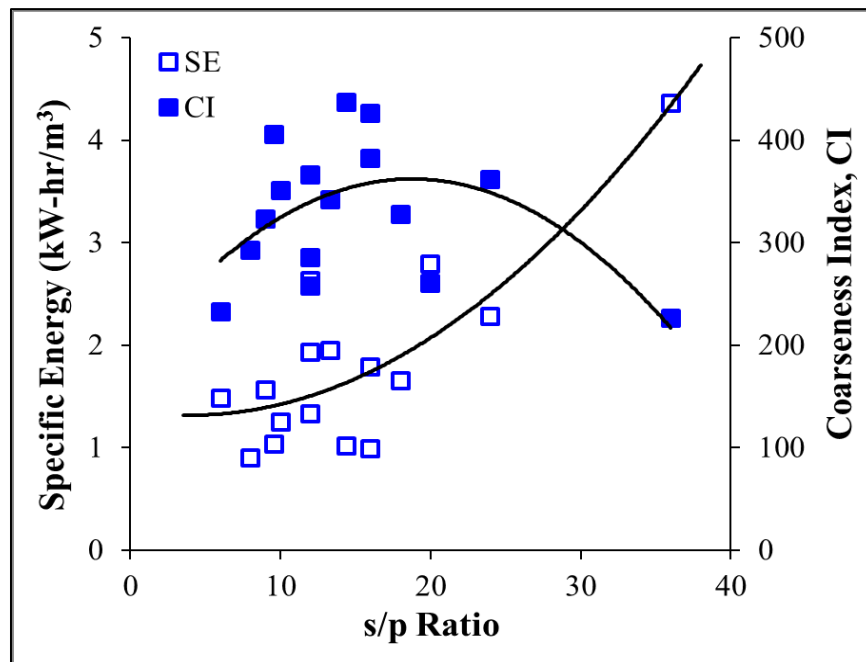


Figure 7.15. Effect of  $s/p$  ratio on  $SE$  and  $CI$  for saturated sandstone.

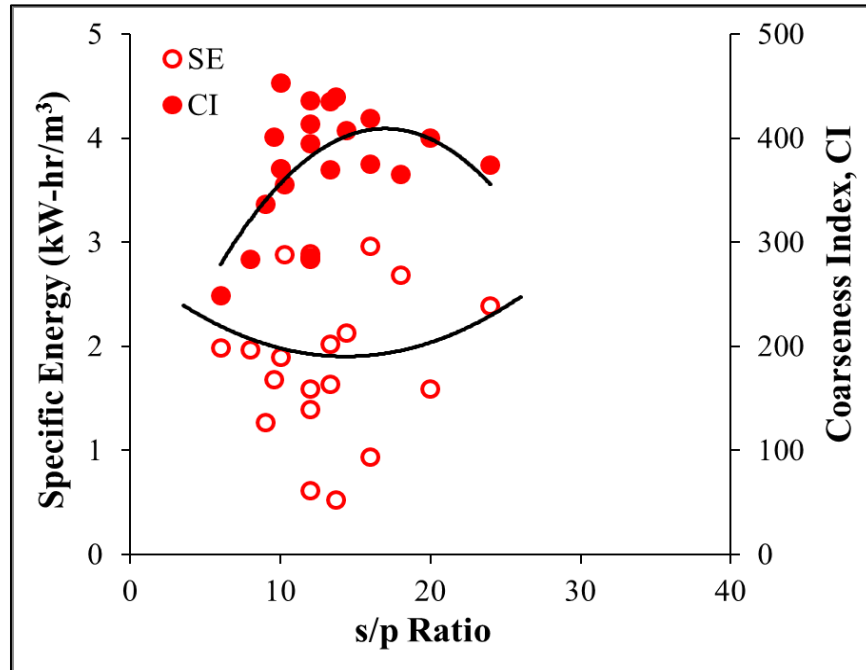


Figure 7.16. Effect of  $s/p$  ratio on  $SE$  and  $CI$  for dry sandstone.

#### 7.2.8. Effect of Cutter Penetration on Specific Energy and Production Rate.

The effect of increase in cutter penetration on  $SE$  and production rate (kg/min) is shown in Figures 7.17 and 7.18 for dry and saturated cutting. They show clear indications of an increase in the production rate with increasing cutter penetration. This behavior is consistent with the reduction in  $SE$  values, which is related inversely to the increase in cutter penetration. This observation was expected, since the increases in cutter penetration and cut spacing enlarge the cut volume, directly affecting the  $SE$  values.

It is interesting to note that there is less scatter in the  $SE$  values in saturated cutting (Figure 7.18). The deeper cutter penetrations and wider cut spacings for some of the dry tests were to evaluate different goals, and could not be matched with saturated tests at this time. These would of interest for future work.

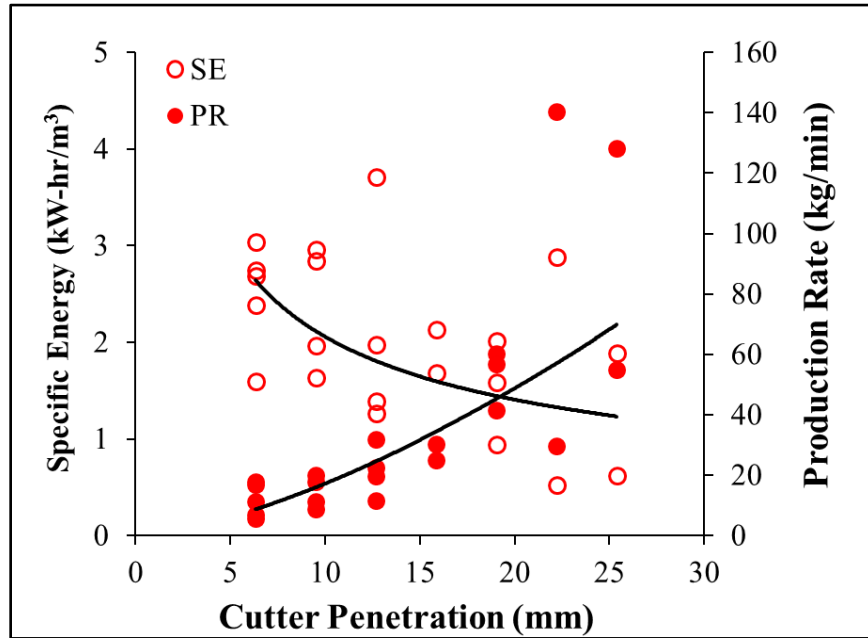


Figure 7.17. *SE* and production rate variation with cutter penetration for dry cuts.

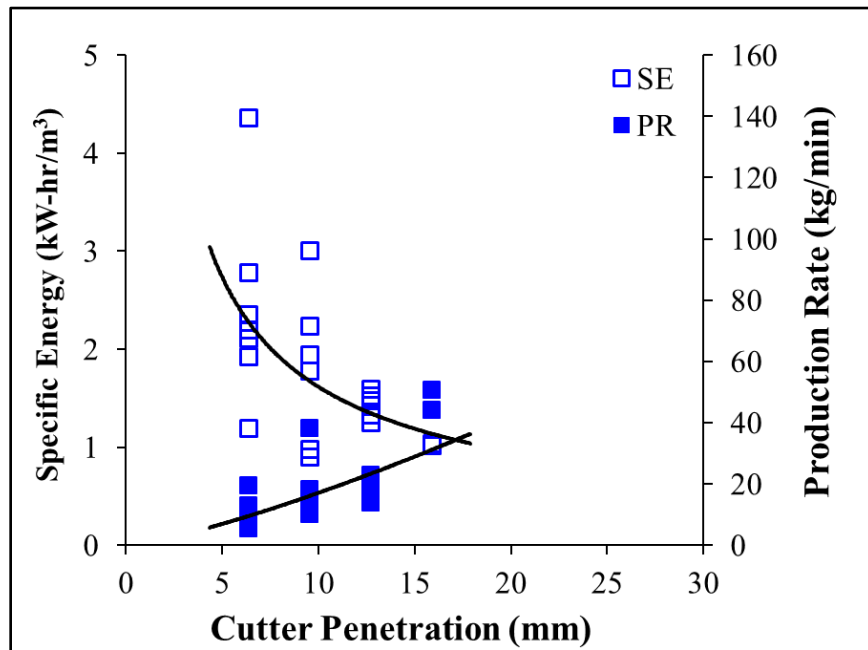


Figure 7.18. *SE* and production rate variation with cutter penetration for saturated cuts.

### 7.3. RADIAL DRAG PICK CUTTINGS ANALYSES

The overall chip mass produced in the saturated rock cuts (especially at shallower depths of cut) was less than the chip mass produced in the dry rock cuts, affecting the  $SE_A$  values. At shallow depths of cut, the amount of fines produced was quite significant, clearly showing that the cutting was not efficient due to its being unrelieved by an adjacent cut, in addition to water weakening of the clayey cementing material present in the sandstone. For porous rocks, indentation of a cutting tool results in local rock fabric collapse, causing crushing with compaction of available pore space. This compaction occurs without volume increase or dilative effects so that high stresses do not develop in the confined crushed zone, and crack propagation and chip formation are inhibited (Deliac, 1993; Roxborough, 1973). Moreover, it has been noted in saturated porous sandstones that the cutting forces are low, strain energy at failure is also low and the debris tends not to be propelled away from the cutting area in large fragments. The debris is in the form of small sandy material clinging together in the presence of water to form a highly abrasive paste near the cutter-rock contact (Roxborough, 1973).

**7.3.1. Relationship of Absolute Size Constant with Coarseness Index and Large Sized Muck.** Figure 7.19 shows the relationship between the coarseness index,  $CI$ , and computed values of the absolute size constant,  $x'$ , for muck from both dry and saturated cutting tests. Very strong correlation exists between  $CI$  and  $x'$  for both dry and saturated rock tests. The overall  $CI$  for saturated rock muck is less than for dry rock muck. Figure 7.20 shows that the absolute size constant,  $x'$ , has a very strong relationship with the percentage production of large chips ( $> 51$  mm or 2 inches). Therefore, the absolute size constant could be a good estimator of the production rate of large sized rock fragments from rock excavation.

**7.3.2. Relationship of Absolute Size Constant and Specific Energy.** A moderate correlation exists between absolute size constant  $x'$  and  $SE_A$  values for dry and saturated rock cutting tests (Figure 7.21), with drop in  $SE_A$  corresponding to increase in  $x'$ . This can be expected; as the size of the chips increases, the new surface area created diminishes, and less energy is consumed (Nelson et al., 1985).

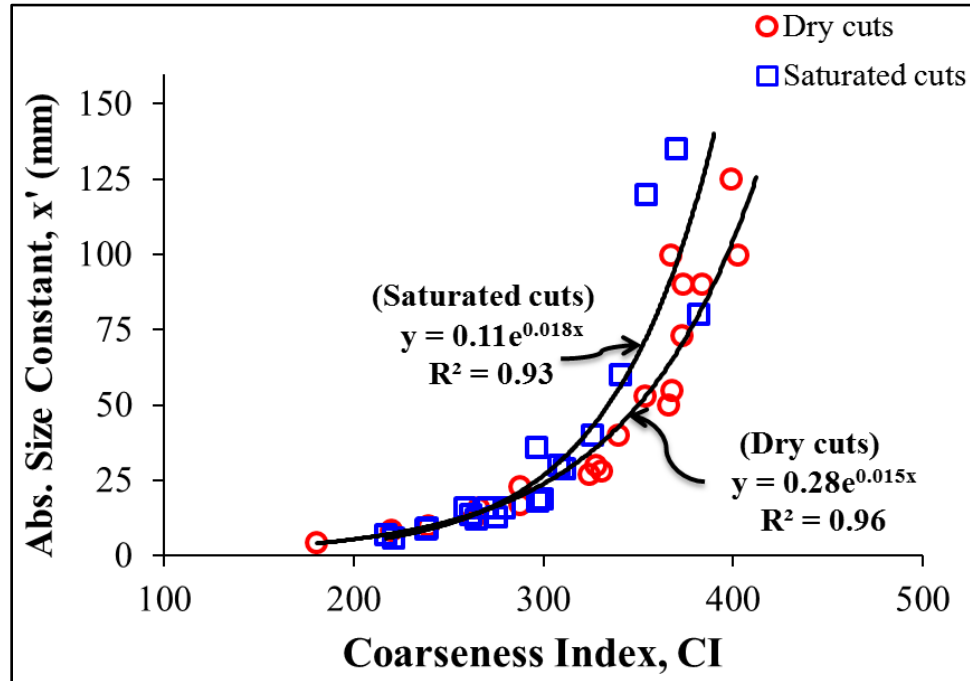


Figure 7.19. Variation of absolute size constant with coarseness index.

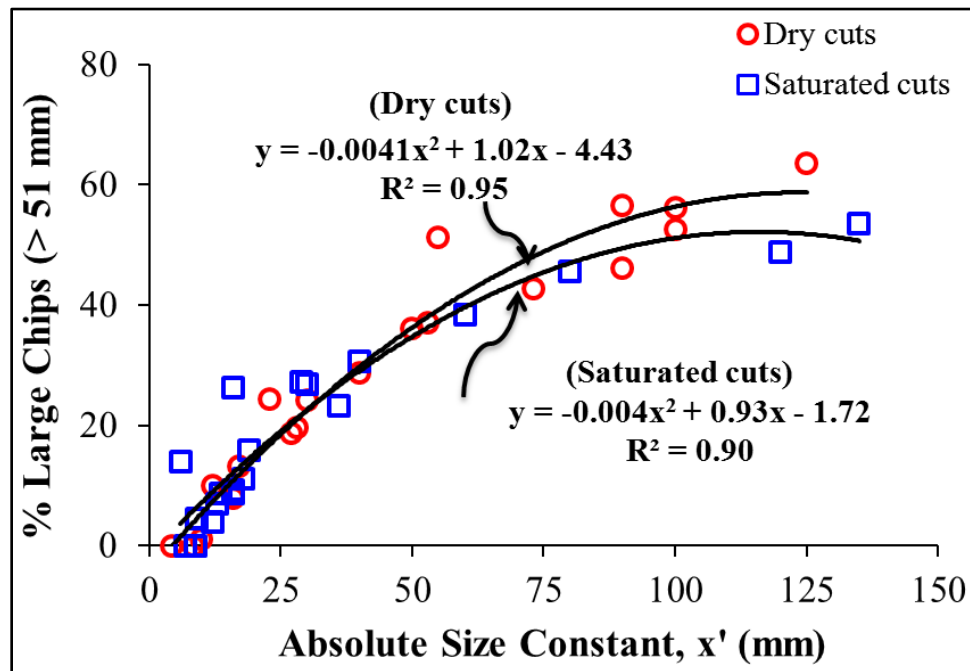


Figure 7.20. Relationship between percentage of large chips (> 51 mm or 2 inches) and absolute size constant.

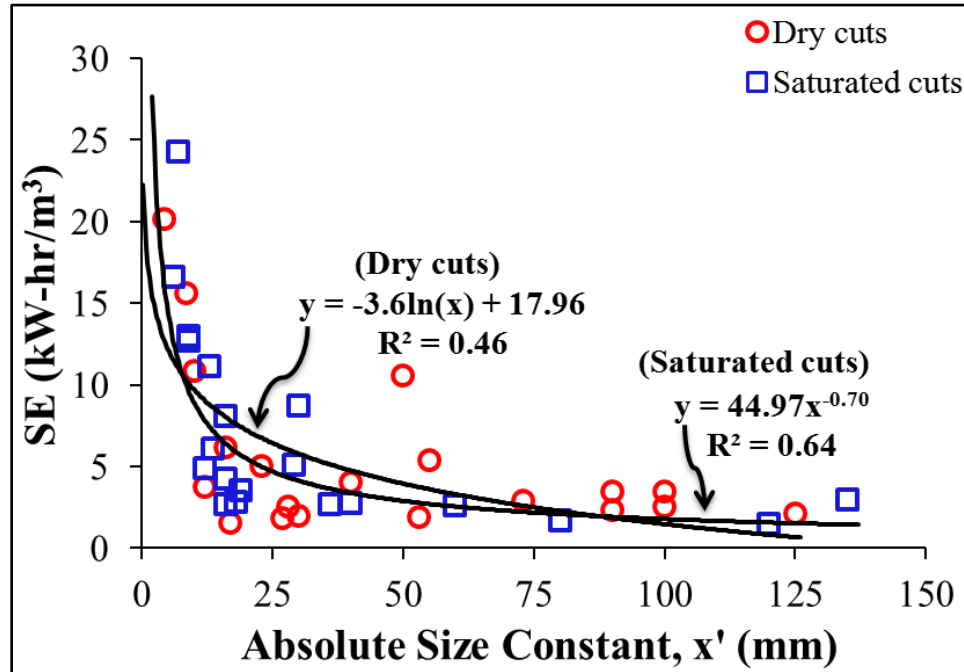


Figure 7.21. Actual  $SE$  variation with absolute size constant.

**7.3.3. Relationship of Coarseness Index and Specific Energy.** The specific energy of cutting and the size of the rock fragments are related by an inverse power law, as shown by (Tuncdemir et al., 2008; Cook and Joughin, 1970). Roxborough and Rispin (1973) also noted a reverse trend between  $CI$  and specific energy, with higher  $CI$  coinciding with lower specific energy values. The Tuncdemir et al. (2008) relationship between  $SE$  and  $CI$  is of the form of  $SE = k CI^n$  for most of the rock types and cutters used. The parameter  $k$  is a function of rock strength and cutting tool type, with  $n$  being around 1.2 for chisel picks, 1.7-3.2 for V-type disc cutters, 2.2-4.4 for conical cutters, and around 5.5 for constant cross-section (CCS) disc cutters. Interestingly, Abu Bakar and Gertsch (2012) found  $n = 1.04$  and  $n = 1.33$  for saturated and dry cutting respectively, for CCS type disc cutters.

For the chisel pick tested in this study, the  $n$  values are 2.3 and 4.1 for dry and saturated rock respectively. The relationship between  $SE$  and  $CI$  is also of the form  $SE = k CI^n$  with reasonably good correlation for saturated muck, though there is less correlation in dry chips (Figure 7.22). Both values of  $n$  are notably higher than the  $n$



value reported by Tuncdemir et al. (2008) for chisel picks. The exponent may depend on the structure and strength variation of the rock and on relationships between the dimensions of the pick/cutter used with the grain sizes of the rock.

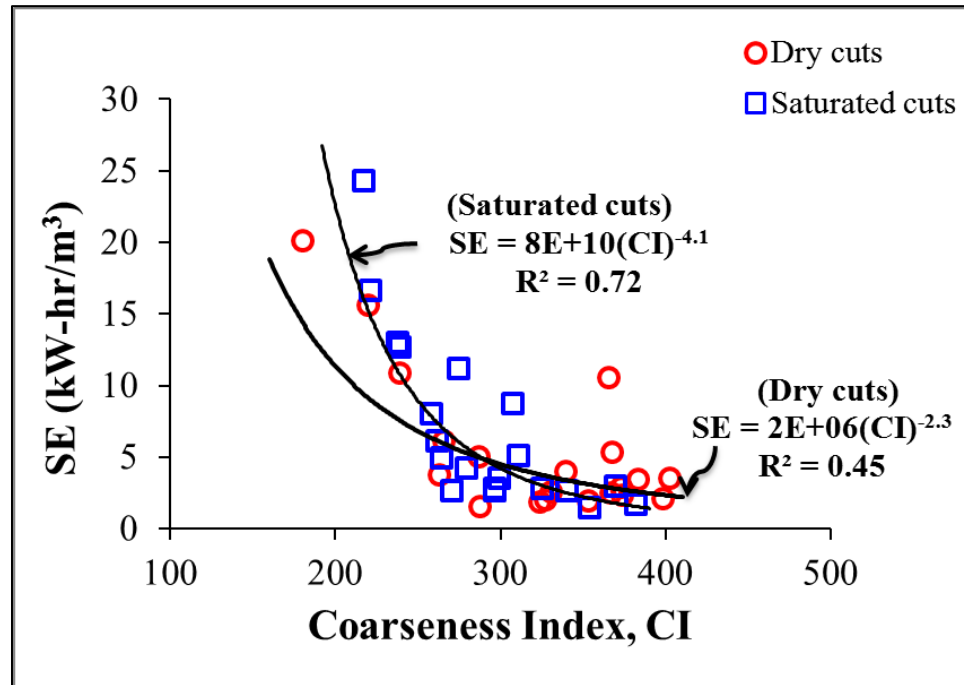


Figure 7.22. Variation in actual  $SE$  with coarseness index.

**7.3.4. Statistical Model for Drag Pick Specific Energy.** To better understand the dependence of  $SE$  on different independent variables, minimum  $R^2$  improvement method for multiple regression analysis using SAS 9.2 statistical software was adopted. Most of the statistical analysis softwares have the capability of performing forward selection method, backward elimination method and stepwise regression method for finding the most suitable multiple regression model. This software has the capability of finding more suitable models using maximum  $R^2$  and minimum  $R^2$  procedures. The maximum  $R^2$  improvement method uses the  $R^2$  criterion to try to find the best single variable model, the best two variable model, etc. The difference between the stepwise

method and the maximum  $R^2$  improvement method is that in the maximum  $R^2$  improvement method all the variable switches are evaluated before a change is made. In the stepwise method it is possible for the “worst” variable to be removed before considering what the effect of adding the “best” remaining variable would be. The minimum  $R^2$  improvement method closely resembles the maximum  $R^2$  improvement method, with the difference that at each comparison the minimum  $R^2$  improvement method makes the switch in variables that produces the smallest increase in the value of  $R^2$ . The minimum  $R^2$  improvement method potentially examines more models than the forward selection method, backward elimination method, the stepwise method and the maximum  $R^2$  improvement method (Samaranayake, 2009; SAS, 2011).

Minimum  $R^2$  improvement method was run for dry and saturated cutting tests keeping  $SE_A$  as dependent variable. The independent variables selected were spacing ( $s$ ), depth of cut ( $d$ ), spacing-to-depth ( $s/d$ ) ratio, coarseness index ( $CI$ ), absolute size constant ( $x'$ ) and the production rate ( $PR$ ). These variables were selected to check the dependence of  $SE_A$  on only the geometrical parameters of cutting ( $s$ ,  $d$ ,  $s/d$ ) and the resulting products of fragmentation ( $CI$ ,  $x'$ ,  $PR$ ). Equation 7.4 gives the best explanatory model for dry cutting tests  $SE_A$  obtained at  $\alpha=0.1$  significance level ( $p$ -value  $< 0.0003$ ,  $F$ -value = 10.67, Mallows  $C_p = 3.8$ ), whereas Equation 7.5 gives the best explanatory model for saturated cutting tests  $SE_A$  at the same level of significance ( $p$ -value  $< 0.0001$ ,  $F$ -value = 14.77, Mallows  $C_p = 3.3$ ). Table 7.1 and 7.2 show the related statistical parameters for dry and saturated tests. Appendix D gives the detailed outputs of the SAS runs.

$$SE_A = 27.98 - 0.085(s) + 0.36\left(\frac{s}{d}\right) - .074(CI), \quad R^2 = 0.74 \quad (7.4)$$

$$SE_A = 41.21 - 0.1008(s) + 1.61(d) - .073(CI), \quad R^2 = 0.80 \quad (7.5)$$

Although the selected models are the best models generated by minimum  $R^2$  improvement method (based on Mallows  $C_p$  value;  $C_p < n+1$ , where  $n$  is the number of selected variables in the model); the variable  $x'$  in the dry rocks model and  $PR$  in the saturated rocks model were not included being statistically insignificant at the selected

level of significance of  $\alpha=0.1$ . It can be deduced from these explanatory models that  $SE_A$  for dry and saturated cutting tests is very much dependent on the geometry of the adjacent cuts ( $s$ ,  $d$ ,  $s/d$ ) and also on the coarseness of the fragmented products represented in the form of  $CI$ .

Table 7.1. Parameter estimates from minimum  $R^2$  improvement method for dry tests.

Variable	Parameter Estimate	Standard Error	$F$ -value	$p$ -value
Intercept	27.986	6.095	21.08	0.0004
$s$	-0.0851	0.039	4.72	0.0463
$s/d$	0.3575	0.117	9.24	0.0086
$CI$	-0.0744	0.022	11.45	0.0041
$x'$	0.0639	0.038	2.81	0.1144

Table 7.2. Parameter estimates from minimum  $R^2$  improvement method for saturated tests.

Variable	Parameter Estimate	Standard Error	$F$ -value	$p$ -value
Intercept	41.212	7.515	30.07	<.0001
$s$	0.1008	0.051	3.96	0.0651
$d$	1.6142	0.514	9.87	0.0067
$CI$	-0.0729	0.024	8.94	0.0091
$PR$	1.0032	0.621	2.61	0.1270

## 8. DISCUSSION: LOAD-INDENTATION TESTS

### 8.1. INTRODUCTION

In saturated disc cutting tests in this study (Section 5), an unusual drop in the cutting coefficient<sup>1</sup> ( $CC$ ) values at deeper cutter penetrations was noted. This observation was contrary to the dry rock cutting tests results, where  $CC$  values increased as the cutter penetration increased. The dry rock  $CC$  response was as expected, since the increased cutter penetration increases the rolling force component due to increased contact length of the disc with the rock, thus requiring more bite. Initially it was believed that this drop in  $CC$  at deeper cutter penetrations was probably due to excess pore water pressure buildup, facilitating the breakage process and hence reducing the rolling force component. To verify the presence of excess porewater pressure during the saturated disc cutting tests, it was deemed appropriate to design load-indentation tests with porewater pressure measurement facility. The detailed equipment description is given in Section 3. Previous research studies propounded the probable role of porewater pressure in rock breakage, but none of those studies provide the ways to quantify or physically measure the porewater pressure generated under an indenter (Phillips and Roxborough, 1981; Hood and Roxborough, 1992; Van Kesteren, 1995).

**8.1.1. Load-Indentation Curves and Porewater Pressure Behavior.** The load-indentation curves obtained for both dry and saturated sandstones samples are of non-monotonic type, which is characteristic of brittle materials. Different types of load-displacement curves produced by indentation of rocks using different type of indenters have been identified by Dollinger (1978) and Thiercelin and Cook (1988) (Figure 8.1). The non-monotonic category has sharply varying slope portions. Each drop in the load (sawtooth) corresponds to the complete formation of a chip which is broken free from the specimen. A sawtooth shape, resulting from rapid loading and unloading, indicates brittle behavior, whereas a steadily increasing curve with no unloading or a more gradual drop in the force indicates a rather plastic or ductile rock. Under high confining pressures, the brittle behavior can also transform to ductile behavior, resulting in smaller or negligible

---

<sup>1</sup> Cutting coefficient is the ratio of the rolling force to the normal force component.

drops in the load-displacement curves (Cook and Thiercelin, 1989). In a brittle rock, due to force drops, less work is done during a load-indentation test, than on a non-brittle rock if the maximum cutter loads are the same. This is in agreement with the observation that brittle rocks tend to require less energy to bore than non-brittle rocks of comparable strength. The higher energy requirement in ductile or non-brittle rocks is due to the plastic deformation of ductile minerals making a very hard surface beneath the indenter (Dollinger et al., 1998). If an indenter is dragged across a face at a certain depth, simulating the action of a drag bit, it will create a sawtooth curve; however, the magnitude of forces will not increase over time, as it does in an indentation test (Rostami, 2011).

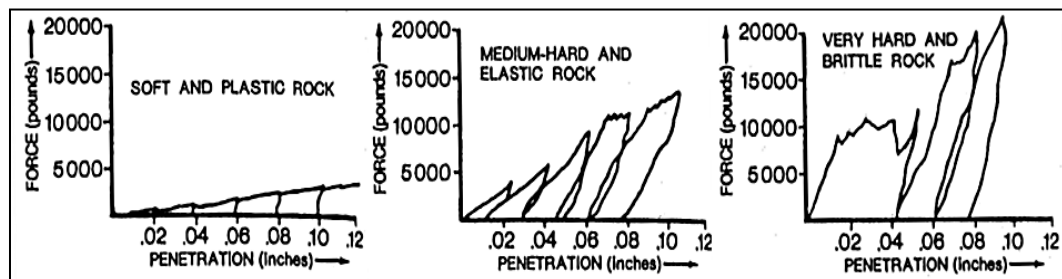


Figure 8.1. Rock failure signatures, representing (L to R) soft, plastic rock; medium hard, elastic rock; and very hard, brittle rock (after Dollinger, 1978).

Formation of a relatively large crushed zone beneath an indenter can be expected in porous rocks of high permeability. In truly brittle rocks of low porosity, where compaction is relatively minor, the crushed zone is of negligible size, with tensile cracks produced by Hertzian stress field (Swain and Lawn, 1976). In amorphous material such as glass, after a brief elastic response, Hertzian tensile cracks are initiated at the rim of the indenter base, forming a truncated cone beneath the indenter. Up to a certain load level, the cracks are known to be characterized by a stable growth with increasing load. Eventually, the cone crushes and the cracks propagate to a free surface in an unstable manner. In very dense and hard rocks, such as quartzite, there are some indications that

fracture in indentation is initiated in this manner. For porous materials such as natural sandstones with porosity ranging from 10 to 25%, failure may begin by local structural collapse beneath the indenter, leading to strain-hardening. With increasing load, the pressure transmitted to the medium through the distorted and compressed bulb (crushed zone) beneath the indenter leads to radial cracking and cratering (Ladanyi, 1968; Lindqvist and Lai, 1983).

Porous rocks also show distinctive test results characterized by reduced crushing slopes (slope of first sawtooth) and abnormally deep indenter penetration before chipping occurs. Because of this deeper-than-normal penetration prior to chipping, porous rocks generally require more energy to bore than non-porous rocks resulting in higher cutter head torque requirements. If a rock is too porous, like many volcanic pumices and scorias, the rock may not be boreable using button or disc cutters because there is insufficient strain energy stored in the rock to cause chipping to occur. In such cases, the cutters simply bury themselves in the rock (Dollinger et al., 1998).

Figure 8.2 shows the formation of the crushed rock zone in one of the saturated sandstone samples tested. The compaction of the pore space and formation of a crushed zone is evident from the shape of first sawtooth (crushing slope) of the load-indentation curves for both dry and saturated samples (Figures 8.3 and 8.5). Gertsch (2000) reported formation of primary and secondary crushed zones in load-indentation tests on Roubidoux Sandstone. The primary crushed zone was very thin, whereas secondary crushed zone exhibits more pore closure than actual crushing of individual grains of rock. The corresponding rise in the indenter pressure with increasing load explains (571 MPa in Figure 8.3) the nature of the stress buildup in the crushed zone beneath the tip of the indenter. This indenter pressure is sufficient to compress the pores and crush the rock grains. Regardless of the chip-forming failure mechanism, much higher pressures are generated under the indenter than needed for unconfined failure. Thus, the strain confinement imposed by the rock around the indentation point must be sufficient to impose confining stresses high enough to raise the triaxial strength of the material above the applied stress, as concluded by Gertsch (2000).



Figure 8.2. Formation of crushed zone under the indenter in a saturated sandstone sample.

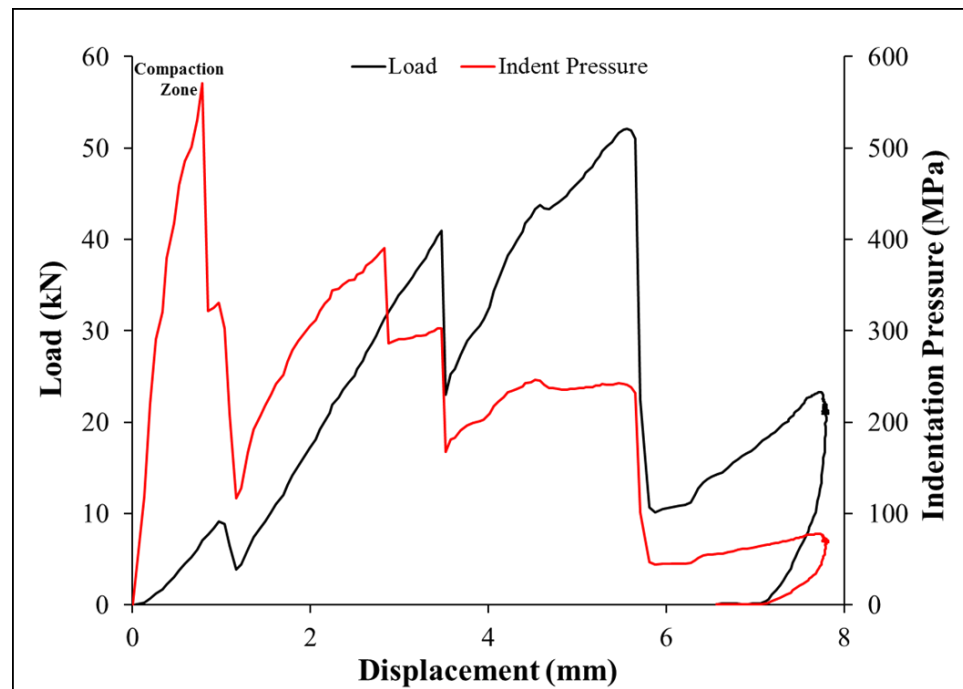


Figure 8.3. Load and indentation pressure versus displacement for a typical dry sandstone sample.

After the first major chip forming event, the rock behaves more or less elastically until the next major chip forming event. Beyond the compaction zone, it can be observed that the shape of the indenter pressure curve follows the shape of the applied load curve, although the magnitudes of both the quantities are very much different. This behavior is true for both dry and saturated samples of the Roubidoux Sandstone.

Suárez-Rivera et al. (1991) investigated the role of wetting fluids during the indentation of porous rocks. Non-wetting fluids do not fill microcracks, penetrating them only to a certain distance from their crack tips. As a result, a positive differential pressure is generated between the pore fluid pressure and the unfilled crack tip, giving rise to an effective confining stress field opposing crack propagation, which makes the rock tougher and stronger compared with its behavior when saturated with a wetting liquid. It is pertinent to mention that the wetting and non-wetting liquids used by Suárez-Rivera et al. were molten sulfur and Wood's metal (a low melting point  $\sim 70^{\circ}\text{C}$  alloy), respectively.

Podio and Gray (1965) found that saturation of rock pores with fluids of different viscosities results in more uniform indentation craters, with respect to both size and shape. Moreover, it was noted that indentation parallel and perpendicular to the bedding planes gives markedly different results at low confining pressure. These differences disappear at elevated confining pressures, reducing the effects of rock strength anisotropy.

The high permeability of the Roubidoux Sandstone and the moderate indentation velocity of the indenter ( $\sim 100$  mm/sec) resulted in very little excess porewater pressure buildup under the indenter (measured by the pressure transducer) (Figure 8.4). The indentation rate of 100mm/sec was chosen to match the cutting speed of the linear rock cutting tests. The values given in Table 4.10 (Section 4) show that the maximum porewater pressure developed in any of the tested samples was 26.1 kPa (3.8 psi) at this loading rate. Figure 8.5 illustrates that the curves for both the total load and the effective load coincide with each other. Although porewater pressure is generated under the indenter, it is not high enough to facilitate the breakage of medium strength sandstone (UCS of 43 MPa for saturated sandstone).



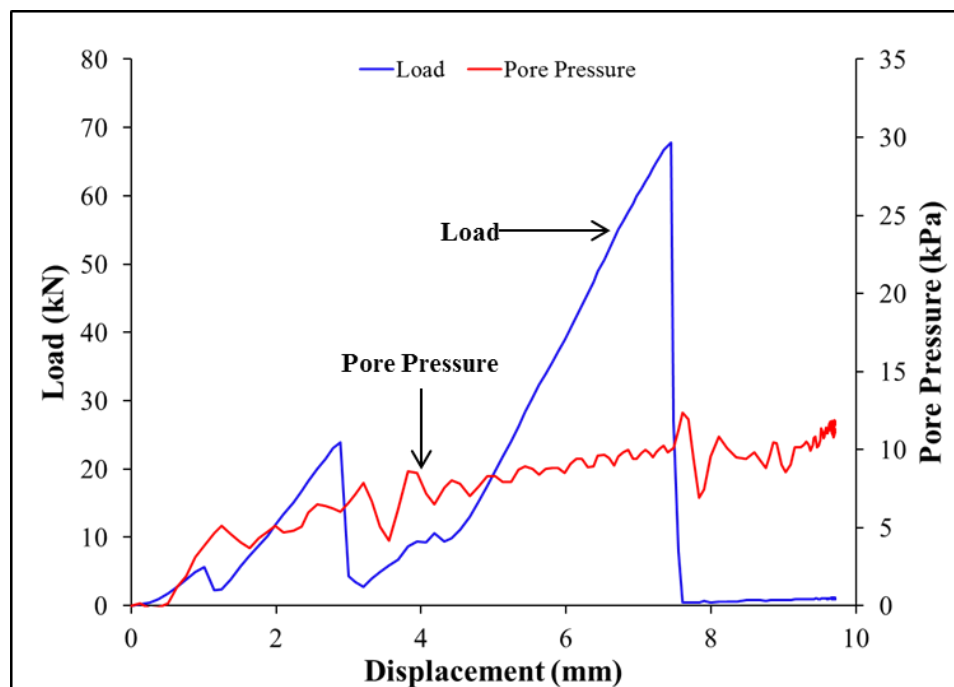


Figure 8.4. Load and porewater pressure versus displacement for a typical saturated sandstone sample.

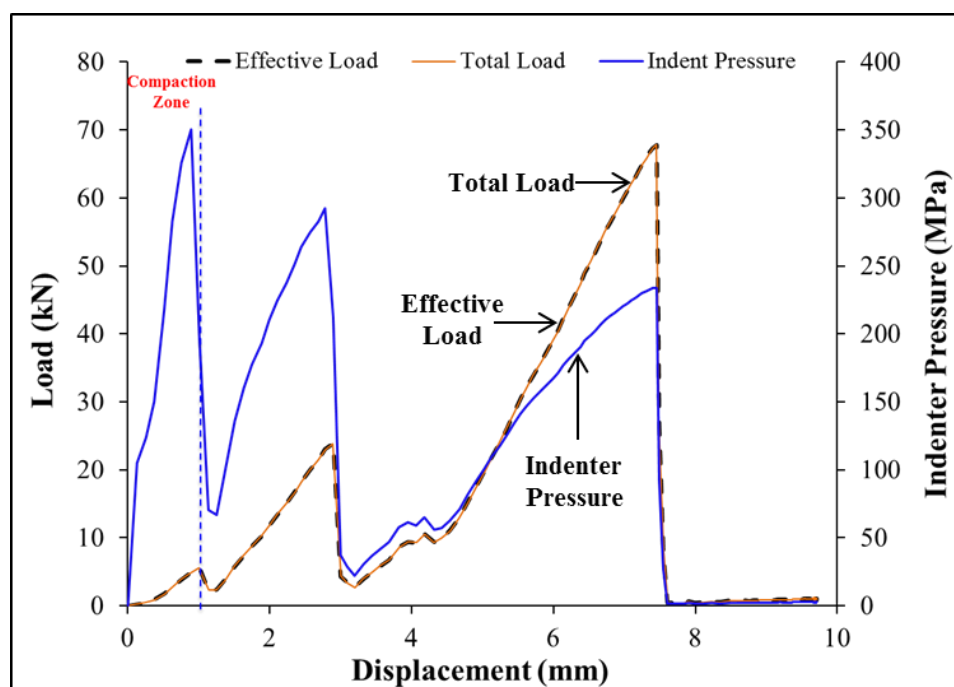


Figure 8.5. Total load, effective load and indentation pressure versus displacement calculated for the same saturated sandstone sample.

Moreover, it can be deduced that the cutting strain rate (100 mm/sec) was not high enough to make the rock stronger beyond the crushed zone and hence cause any reduction in the rock's permeability, which would have resulted in an undrained situation. Van Kesteren et al. (1992) and Van Kesteren (1995) have reported cone indentation tests on water saturated limestone of very low permeability ( $k = 10^{-7}$  m/sec) to study the effects of indentation velocity on porewater pressure. Different chip forming mechanisms were described at different indentation velocities. An intermediate velocity of indentation (100 mm/sec) resulted in the reduction of the size of the crushed zone due to the resistance of the porewater pressure. Very high indentation velocity of 1000 mm/sec was reported to have caused liquefaction in limestone of very low permeability, resulting in undrained behavior.

**8.1.2. Specific Penetration and Specific Energy.** Specific penetration (*SP*), also referred to as crushing slope or penetration index, is determined from load-indentation tests and has been used for predicting penetration rate of tunneling and raise boring machines. Penetration rates determined from *SP* have been reported to correlate very well with actual penetration rates of rock borers operating in the field (Handewith, 1970 and 1972; Dollinger, 1978). These penetration rate estimates have been found to be conservative and actual penetration rates are generally higher than the estimated ones. These differences result from the fact that the estimates are based on the testing of the small sized core samples and do not take into consideration such in-field factors as joints or cracks in the rock produced by the boring operation. Nor do they take into consideration stress interactions between the adjacent cutters, confining pressure, and natural stresses on the rock. In spite of these variables, the laboratory penetration rate estimates have been remarkably close to actual boring rates, with generally less than 15 percent variation (Dollinger, 1977).

*SP* determined from load-indentation tests on small sized core samples is very sensitive to the effectiveness of the confinement. Indentation tests are largely controlled by the boundary conditions, which, however carefully prepared, do not simulate real rock face conditions. Although indentation tests in small samples have utility for analyzing behavior in jointed rock, they are inherently more variable than indentation of intact rock. The tests on core samples suffer more internal damage than self-confined massive rock,

because the rock can expand when indented. A key element in the success of the indentation test with small samples is that the practitioners of the tests have encountered and evaluated many different rock types and have noted the behavior of the TBM's cutting them. A well-defined test conducted over and over by the same investigator tends to impart a feeling for how the rock will behave while under attack. Experience therefore becomes a key element in successful performance prediction (Gertsch, 2000).

*SP* values determined from dry and saturated samples of Roubidoux Sandstone in this study are in very close agreement (6.3 kN/mm for saturated and 6.2 kN/mm for dry samples; Table 4.10 and 4.11, Section 4; Figure 8.6). These values of *SP* are less than the range of penetration index or *SP* mentioned in the literature for rocks of intermediate strength like sandstones, coarse-grained limestones, marbles and schists. The reported values for medium strength rocks are 17.5 to 31.0 kN/mm (100,000 to 175,000 lb/in) (Dollinger, 1977 and 1978). The lower values of *SP* in this study may be attributed to several factors including, rock porosity, brittleness, cementing material between the grains, rock structure, uniaxial compressive and tensile strength of the rock, stiffness of the test equipment, loading rate, type of the indenter used, sample size tested, and confinement of the rock sample amongst others.

Although average *SP* for both dry and saturated sandstone samples is almost the same, the specific energy (*SE*) of penetration calculated from the load-indentation tests reveals more clearly the relative efficiency of the indentation process. Average *SE* value for dry rock samples is 107.1 J/cm<sup>3</sup> whereas for saturated rock samples it is 133.7 J/cm<sup>3</sup> (~25% increase in *SE* in case of saturated samples; Table 4.10 and 4.11, Section 4; Figure 8.7). Statistically this increase in saturated samples *SE* is not significant (p-value = 0.21; T-test at  $\alpha=0.1$ ). Saturated rock indentation appears to be more energy-intensive than in the dry rock samples. This is attributed to reduced chip mass produced in saturated rock tests by the same forces. The reduced chip mass and excess of fines produced in saturated samples is attributed to the water weakening the weak clayey cement present between the quartz grains in the sandstone (Figure 8.2). Production of large amounts of fines and fewer larger chips was also recorded in the saturated rock disc cutting tests in this study, which affected the disc-cutting *SE* values. Recall the almost 9% and 10% reduction in

actual and nominal specific energy values in saturated disc cutting tests, despite the lower coarseness index (*CI*) values.

The *SE* calculated from load-indentation tests should be used cautiously as a performance prediction tool. It is pertinent that in actual disc cutting operation, whether full face boring or linear cutting, the rolling force component acts in the direction of cutter motion, and is thus the major energy consumer. In disc cutting tests, the rolling force component was reduced by 44% in saturated sandstone. This reduction in rolling force resulted in lower *SE* values in saturated disc cutting tests. The *SE* calculated from load-indentation tests is based on the force which is normal to the direction of cutting or indentation. In actual rock cutting, the normal force represents very little of the cutting energy consumed in the cutting process.

The core sample size used in the indentation tests is far smaller than the sample size used in the full scale linear cutting tests, which very closely simulate actual field conditions. Moreover, full scale linear rock cutting tests incorporate the effects of interaction between adjacent cutters by varying the spacing between the cuts. In a single load-indentation test on small sized core samples, such variation of spacing is not possible. Attempts have been made by Dollinger et al. (1998) to perform indentation tests on 10 inches long core samples using sections of CCS and wedge shaped cutter rings at varying spacing. Yet, the *SE* determined from load-indentation tests is not as directly applicable as the *SE* determined from full scale cutting tests.

*SP* on the other hand has been reported as a better index for predicting boreability in the past studies by Handewith and Dollinger in various earlier citations. *SP* can be used with reasonable confidence to estimate penetration rate, provided machine specifications including load per cutter and rate of cutterhead rotation are given. In a later study, Gertsch (2000) has shown penetration tests on intact rock blocks to correlate very well with disc cutting data of various rock types as compared to the penetration tests conducted on core samples.

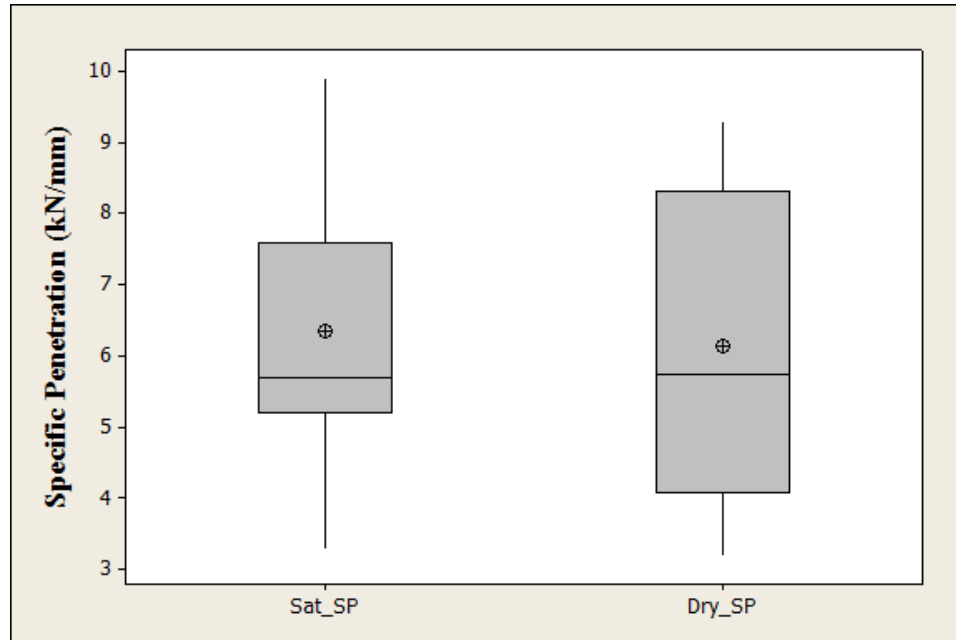


Figure 8.6. Box plot of *SP* values for dry and saturated samples showing mean, median, highest, lowest, 1<sup>st</sup> quartile, and 3<sup>rd</sup> quartile values.

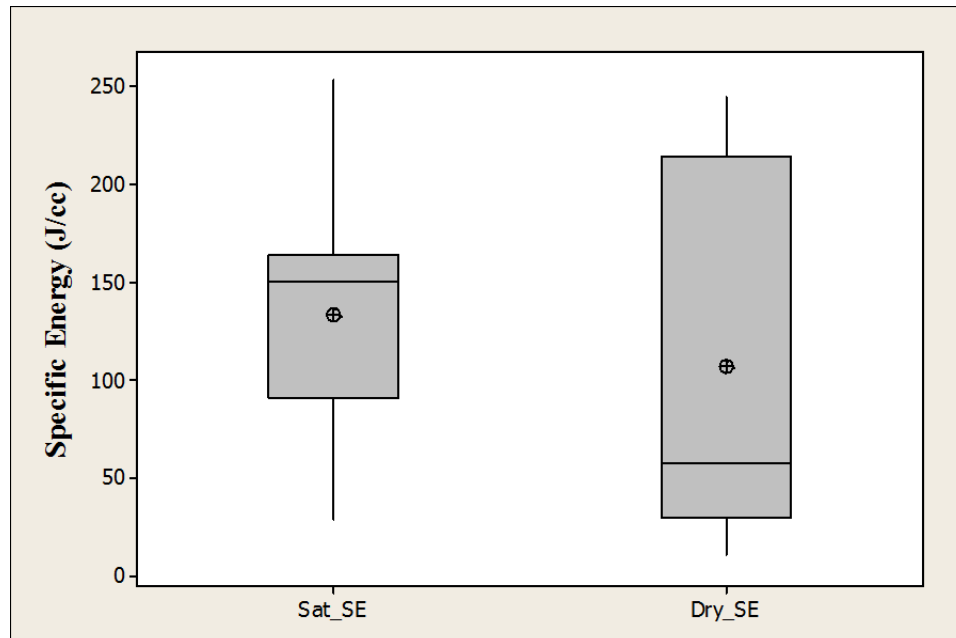


Figure 8.7. Box plot of *SE* values for dry and saturated samples showing mean, median, highest, lowest, 1<sup>st</sup> quartile, and 3<sup>rd</sup> quartile values.

## 8.2. CUTTING FORCES AND WEAR RESPONSE TO SATURATION

**8.2.1. Radial Drag Pick Cutting Tests.** For most of the dry and saturated cutting tests at the same combinations of spacing and depth of cut, the cutting forces ( $F_d$  and  $F_n$ ) were in close agreement to each other (Section 6). This observation was contrary to the water weakening of sandstone observed for disc cutting tests. One hard rock layer in one of the saturated sandstone blocks offered significant resistance to fragmentation, increasing the overall averaged drag and normal forces by almost 10% and 9.5% respectively. Even when eliminating the effect of this resistant hard layer on averaged forces, the forces in most of saturated cutting tests were similar to and in some cases were higher than in dry cuts.

In explaining this behavior of increased drag pick cutting forces with saturation, it is important to mention that the goal in any mechanical rock-cutting operation is for the tool to induce fractures in the rock to form discrete rock chips. In the process of initiating and propagating these fractures, all mechanical tools produce regions of crushed rock immediately beneath and adjacent to the tool (Figure 8.8).

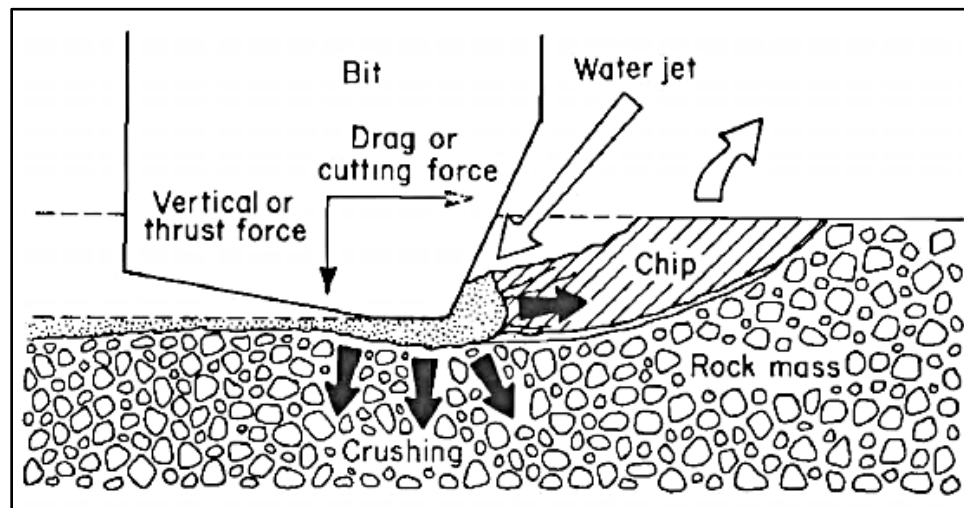


Figure 8.8. Point of impact necessary for water jet to exploit rock damage caused by drag bit (after Hood, 1985).

The stresses induced in the rock by the tool are reduced by the cushioning action of this crushed material. This increases the load that must be induced by the tool to form a rock chip (Geier et al., 1987; Hood et al., 1990). Zone of crushed rock under and adjacent to the drag pick was observed in all dry and saturated cutting tests. Removal of this crushed rock during the cutting process by, for example, high pressure water jets, significantly reduces the tool forces (Hood, 1977b; Ropchan et al., 1980; Dubugnon, 1981; Tomlin, 1982). Though no water jets were employed in this study, these findings for practice are instructive.

Some of the work of Hood (1977a) indicated that the thin layer of crushed rock between the rock and the bit could behave as a lubricating layer beneath the bit, increasing the normal force component but decreasing the coefficient of cutting friction (ratio of cutting force to normal force). By washing away this layer, the high pressure water jet removes the lubricant and thus increases the effective coefficient of friction. Relatively high pressure (70 MPa) of the water jet is required to fully remove this crushed zone ahead of the cutting tool (Geier et al., 1987; Hood et al., 1990).

The crushed rock zone in saturated drag pick tests was saturated because of the water already present in the pore spaces of the rock, which was maintained during cutting. Although the crushed rock zone was also present in dry cutting tests, it was not saturated. The regions immediately underneath and in front of the cutting tool are in a state of triaxial compression because of the strain confinement imposed by the rock around the contact footprint of the indenter (Hood, 1977c; Cook et al., 1984; Gertsch, 2000). Compaction in sandstones consists of a collapse of pore space and a subsequent readjustment of quartz grains into a denser packing. If the rock's permeability is small compared to the rate of compaction, this results in increased pore pressure (Gowd and Rummel, 1980). Transient elevated porewater pressures can also be expected in this highly confined crushed rock zone due to reduction in rock' permeability. The increase in the cutting forces ( $F_d$  and  $F_n$ ) in the saturated drag pick tests may be attributed to this increase in the porewater pressure in the confined crushed rock zone. According to Phillips and Roxborough (1981) and Hood and Roxborough (1992), if a rock remains competent after saturation, the forces required to cut it can be higher than for dry rock.

The reason for this increase is attributed to porewater dissipation of the high local stress concentrations associated with crack development.

The temperature at the rock-tool interface can exceed 1000°C (Hood, 1977a). The hardness of the tungsten carbide inserts used at the points of these tools decreases rapidly with increasing temperature. At these high temperatures, the hardness of quartz is similar to that of tungsten carbide, hence rapid wearing of localized hot spots is to be expected (Fowell, 1993). It is important to recall that the pick replacement rate in the saturated cutting tests was zero, but in the dry tests several instances of tungsten carbide tip failure were noted (Section 4). This difference in wear rate was attributed to the cooling effect caused by the dripping water (though not high pressure) in the saturated cutting tests.

Hood (1977a) in his preliminary work also showed that even a spray of low pressure water can have significant effects in cooling down the bit and hence reducing the bit wear rate. Morris and MacAndrew (1986) showed that even in situations when water jet energy was insufficient to remove the crushed material from the region adjacent to the bit, major long-term benefits of reduced bit wear rate were realized. The presence of interstitial water at the rock-tool interface, even in the absence of external sources such as water jets, can have significant effect in reducing tool wear rate. Phillips and Roxborough (1981) noted significant reduction in the tool wear rate when cutting in saturated Bunter Sandstone. Ford and Friedman (1983) attributed the water present at the rock-tool interface to behave as a lubricant thereby reducing the frictional forces while cutting limestone and sandstone with drag tools. The excess porewater pressure developed in the highly confined crushed rock underneath the tool also helps in cooling the tool and hence reduces the wear rate (Summers, 2012).

**8.2.2. Disc Cutting Tests.** Noticeable decreases of 27.5%, 44% and 48.2% in the normal, rolling and side forces (respectively) due to saturation of the rock were noted in disc cutting tests (Section 5). This behavior was opposite to that seen in the drag pick tests. Creation of excess porewater pressure in highly confined crushed rock zone ahead and underneath the drag pick explains this behavior to some extent for the increase in drag pick cutting forces with saturation. What is then different in the case of disc cutting? Why is it not influenced similarly by this excess porewater pressure buildup in the crushed rock zone?



Comparison of the footprints of these two cutter types gives part of the answer. Table 8.1 gives the disc cutter and drag pick contact areas at same penetration or depth of cut levels (Figure 8.9). Note that the frontal contact area of the drag pick is almost 85% smaller than the disc cutter contact area at the same level of penetrations. The smaller contact area of the drag pick compared with the disc results in much higher stress concentrations, especially in the direction of pick movement. Despite the commonality of the indentation process, the cutting phenomenon is drastically different between drag picks and disc cutters. In the case of drag picks, the crushed zone is small and localized, thus the developed cracks are relatively shallow. The component of the force parallel to the cutting path is relatively high, meaning low normal and significant drag forces. The concentration of stresses in the direction of cutting is very high and therefore, cracks propagate in this direction to form chips (Rostami, 1997). Disc cutters form a greater percentage of chips to the side.

Because of the smaller contact area between pick and rock, the crushed rock zone from drag pick cutting is also smaller in size than that from disc cutting. A comparison of the percentage of fines ( $< 1.65$  mm) produced for spacing of  $s = 76.2$  mm for disc cutter and drag pick at matching penetrations (6.4 mm, 9.5 mm and 12.7 mm) is given in Figure 8.10 for dry and saturated cutting tests. This also shows that the percentage of fines produced in disc cutting tests is much higher than in drag pick cutting tests. The higher percentage of fines is attributed to the mode of cutting of disc cutter, where the normal force component is much higher (10-20 times) than the rolling force.

Table 8.1. Contact area differences between disc cutter and drag pick at same penetration or depth of cut.

$p$ or $d$	Disc Cutter	Drag Pick		Difference	Difference
	$A_{disc}$	$A_{front}$	$A_{base}$	$(A_{disc} - A_{front})$	$(A_{disc} - A_{base})$
(mm)	(mm <sup>2</sup> )	(mm <sup>2</sup> )	(mm <sup>2</sup> )	(%)	(%)
6.4	477.3	59.5	163.0	87.5	65.8
9.5	582.5	87.0	270.0	85.0	53.7
12.7	674.8	111.5	353.5	83.4	47.6
p – disc cutter penetration, d – pick depth of cut, $A_{disc}$ – disc contact area, $A_{front}$ – pick frontal area, $A_{base}$ – pick base footprint area					

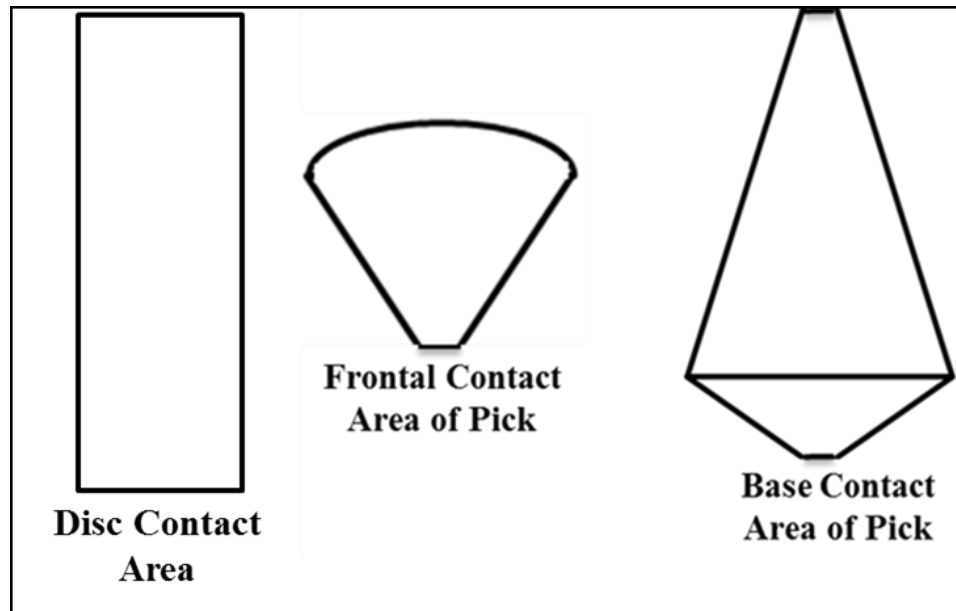


Figure 8.9. Contact shapes of the disc cutter and the drag pick used (not drawn to scale).

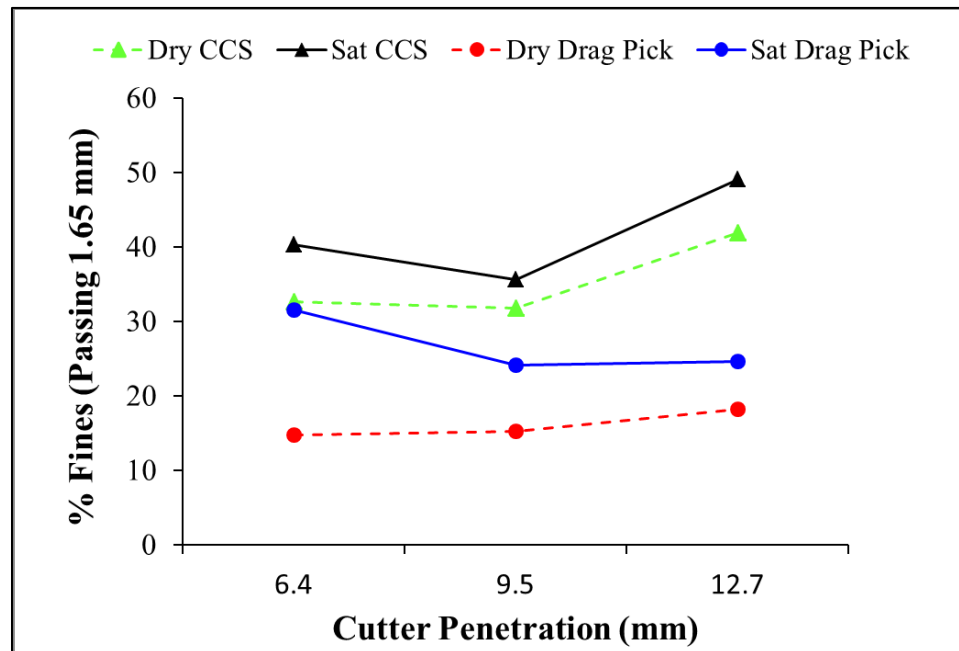


Figure 8.10. Comparison of % fines produced for data passes at  $s = 76.2$  mm for disc cutter and drag pick at matching penetration levels (6.4 mm, 9.5 mm and 12.7 mm) for dry and saturated cutting tests.

The difference of fines produced between dry and saturated cutting tests is also visible in Figure 8.10. Higher percentage of fines is produced in saturated cutting tests for both disc cutter and drag pick cutting tests, which is attributed to the saturation weakening of the weak clayey cementing material present between the quartz grains.

Because of relatively large size of the crushed rock zone in case of disc cutting, it can be hypothesized that the confined crushed rock zone under the disc cutter might not be as impermeable as in the case of drag pick cutting. Large size of the crushed rock zone might have developed several flow paths allowing the dissipation of excess porewater pressure in the confined crushed rock zone. Moreover, much larger side cracks are developed in the case of disc cutting; these may also have offered extra drainage paths for the excess porewater pressure dissipation. In case of drag pick, the side cracks are relatively smaller and major stress concentration is in the direction of pick travel. At the instant of chip formation, the drainage paths for excess porewater pressure are minimum; hence the porewater pressure drops immediately as soon as new chip is formed, falling from the maximum that developed before chip release.

The porewater pressure values measured in the load-indentation tests (Section 8.1.1) indicated that they were not high enough to have affected the cutting process of the disc cutter. As has been shown in various earlier cited work, that region immediately beneath the indenter is highly confined and is in a state of triaxial compression. This triaxial confinement can cause an excess porewater pressure situation, resulting in undrained behavior, if saturated with water. Measured pressure values do not indicate this excess porewater pressure situation. This could be attributed to the dissipation of excess porewater pressure through radial cracks generated immediately outside the crushed rock zone. The values of pressure measured by the pressure transducer are the result of water draining away from the crushed zone through the pores and cracks generated by the indentation process. The porewater pressure values immediately beneath the indenter may be orders of magnitude higher than what is being measured by the pressure transducer.

## 9. CONCLUSIONS AND RECOMMENDED FUTURE WORK

### 9.1. CONCLUSIONS

The research presented in this dissertation was conducted to provide a better understanding of the performance differences of selected type of rock cutting tools in dry and saturated rocks. The study characterized the performance of rolling disc cutters (CCS cutter) and drag picks (radial pick) in a quartzose sandstone of moderate strength and relatively high permeability. These types of cutters are widely employed on rock excavation machines like TBMs, raise and shaft borers, roadheaders, drum shearers, continuous miners, cutter suction dredgers and several other excavators. The study, through a comprehensive set of full scale linear rock cutting experiments, evaluated the differences between cutting dry and saturated sandstone. Small scale load-indentation tests with porewater pressure measurement were also performed on dry and saturated samples of sandstone. These tests were conducted to measure the porewater pressure generated under an indenter.

**9.1.1. Saturation Effects on Cutting Forces.** Cutting dry and saturated blocks of sandstone with rolling disc cutters and drag picks was one of the main tasks of this study. The data collected from the cutting experiments was thoroughly processed and analyzed to find the differences in the cutting performance of these two rock cutting tools in dry and saturated conditions. Significant drops of 27%, 44% and 48% in the disc cutter's normal, rolling and side forces, respectively, were recorded when cutting in the saturated rock as compared to cutting in dry rock. This reduction in the disc cutting forces indicated that water saturation significantly affects the performance of disc cutters, in this type of sandstone. It is believed that this reduction in the disc cutting forces was due to the reduction in the uniaxial compressive strength (UCS) of the sandstone tested. The reduction in strength of the tested sandstone when saturated was also confirmed through the differences of UCS in dry and saturated samples. An average reduction of 16% was recorded between dry and saturated UCS values.

Contrary to the observations of the disc cutting tests, the linear cutting tests with drag picks showed that the saturation actually increased cutting (drag) forces by 9.9% and normal forces by 9.4%. A negligible drop in the side forces was also observed. Force

variability in the drag pick cutting seemed to be subdued by saturation, though this could be an artifact of variability of the fabric of the samples tested, as well. The drop in the cutting forces with one type of cutter and increase in the cutting forces with other type of cutter raises a question. What is the different in the disc cutting which is not happening in the drag pick cutting? This question can be explained to some extent by the effects due to different fragmentation mechanisms of these two types of rock cutting tools.

The regions immediately underneath and in front of the cutting tool are in a state of triaxial compression because of the strain confinement imposed by the rock around the contact of the indenter (Hood, 1977c; Cook et al., 1984; Gertsch, 2000). If the rock is saturated, very high porewater pressures can be expected in this highly confined crushed rock zone due to reduction in rock' permeability. These elevated porewater pressures can dissipate local stress concentrations in the highly confined crushed rock zone ahead of the drag pick (Hood and Roxborough, 1992). Increased cutting forces in saturated drag pick tests, were hypothesized to have been effected with this excess porewater pressure build-up in the confined crushed rock zone underneath and ahead of the drag pick. It is believed that the excess porewater pressure may have caused reduction in the effective stress imposed by the drag pick, thereby increasing drag and normal forces.

If this phenomenon is considered to be valid, then why excess porewater pressure is not increasing the disc cutting forces? To explain this, it is necessary to understand the mode of action of drag picks and the disc cutters. Even though the disc and drag cutters break rock through an indentation process, the cutting phenomenon of the two tools is very much different. In case of drag picks, the crushed zone is small and localized, thus the developed cracks are relatively shallow. The component of the force parallel to the cutting path (drag force) is relatively high. The concentration of stresses in the direction of drag force is very high and, therefore, cracks propagate in this direction to form chips. Whereas in case of disc cutters, the normal force component is much higher than the rolling force component. Because of this higher normal force and relatively larger contact area than drag picks, a relatively bigger crushed zone is formed under the disc cutter, which results in much longer side cracks.

In case of the drag pick, since the side cracks are relatively small and shallow and the main stress concentration is in the direction of pick movement, it is assumed that

relatively fewer drainage paths are available for the excess porewater pressure, before any major chip formation event. Once a chip is formed in the direction of cutting, the porewater pressure drops, then immediately starts rising as the pick advances for the formation of next chip. Whereas, in case of the disc cutter, due to the relatively large size of the crushed rock zone and much larger side cracks, the rock immediately beneath and adjacent to the disc cutter might not be as impermeable as it was in the case of drag pick. The large size of the crushed rock zone and larger side cracks may offer more flow paths allowing the dissipation of excess porewater pressure in the confined crushed rock zone. Creation of relatively large sized crushed zone and much bigger chip sizes was confirmed through observation of the cut surfaces and size analyses of the collected chips.

To validate the hypothesis of excess porewater pressure generation under an indenter, small scale load-indentation tests with porewater pressure measurements were conducted using a conical indenter. Porewater pressure measurements were made on saturated core samples of the sandstone tested. Maximum porewater pressure measured was 26.1 kPa (3.8 psi) at the indenter loading rate of 100 mm/sec. From the values of the pressure measured, initially it was inferred that the indenter loading rate (100 mm/sec) was not high enough to cause any reduction in rock's permeability, and as a consequence resulting in an undrained situation.

These low values of the porewater pressures measured from load-indentation tests were in contradiction with what has been argued about the excess porewater generation under an indenter affecting the breakage process. To answer this discrepancy, it is important to note that the values of pressure as measured by the pressure transducer are those which are the result of water draining through the pores and cracks generated due to indentation process. The porewater pressure values immediately beneath the indenter, being a highly confined space, may be orders of magnitude higher than what is being measured by the pressure transducer. Moreover effects of small sample size, shape of the indenter used, and indentation speed cannot be discounted when comparing porewater pressures generated in load-indentation tests with indenters of different shapes such as disc cutters and drag picks.

**9.1.2. Saturation Effects on Specific Energy.** Along with the cutting forces, another important parameter which measures the efficiency of a cutting process is the specific energy ( $SE$ ). In disc cutting tests the  $SE$  of fragmentation was reduced by 10% and 8.4%, when calculated according to the nominal cut volume (nominal  $SE$  or  $SE_N$ ) and the actual fragmented rock mass (actual  $SE$  or  $SE_A$ ), respectively, when cutting in saturated rock as compared to cutting in dry rock. Compared to the reduction in the cutting forces, the drop in the actual  $SE$  was relatively small, since the mass of chips from both dry and saturated rock for the same cut spacing and cutter penetration combinations varied significantly.

Interestingly, in drag pick cutting tests, saturation increased the  $SE$  of cutting by 28% as measured by the actual volume of chips produced (actual  $SE$  or  $SE_A$ ) and 9% as measured by the nominal cut volume (nominal  $SE$  or  $SE_N$ ). This increase in the drag pick cutting  $SE$  was due to higher drag forces and relatively fewer larger chips produced in saturated drag pick cutting tests. Apart from the differences in the disc cutter and drag pick cutting forces affecting the  $SE$  values, the difference of  $SE$  variability was also due to very wide cut spacings and deeper cutter penetrations used for disc cutting tests. At very wide cut spacings and deeper cutter penetrations, the discontinuities and heterogeneities in the rock mass have much greater effect on the size and mass of the chips produced between the adjacent cuts, directly affecting the  $SE$  values.

The variation of  $SE$  with  $s/p$  ratio was not very clear for either saturated or dry rock disc cutting tests, though there was slightly less variability in the saturated rock  $SE$  than in the dry rock  $SE$ . Because of wide scatter in the  $SE$  values, an optimum value of  $s/p$  ratio could not be determined for disc cutting tests. For drag pick tests, the  $SE$  values with varying  $s/d$  ratios were less variable except at very high  $s/d$  ratios. For drag pick, the optimum  $s/d$  ratio for dry rock tests was noted between 6 and 8 whereas for saturated rock cuts this value was between 5 and 9. The optimum  $s/d$  ratios for drag pick cutting tests were slightly higher than the values (optimum  $s/d = 1$  to 5) reported elsewhere (Copur et al., 2001; Balci and Bilgin, 2007). The variability observed in the nominal and actual  $SE$  values for disc cutter and drag pick cutting in both dry and saturated rock conditions, reiterates that  $SE$  should not be treated as a basic property of the rock, rather,

it is a function of rock mechanical properties, cutting tool type, and the interaction between the adjacent cuts.

Apart from the porewater pressure measurements, the load-indentation tests data was also used to compute performance parameters like specific penetration (*SP*) and specific energy (*SE*) of indentation. Average *SP* calculated for both dry and saturated sandstone samples was almost the same (6.3 kN/mm for saturated and 6.2 kN/mm for dry samples), though the *SE* of indentation differed for dry and saturated tests. Average *SE* value for dry rock was 107.1 J/cm<sup>3</sup>; whereas for saturated rock it was 133.7 J/cm<sup>3</sup> (~25% increase in *SE* in case of saturated samples). Due to increased *SE* in case of saturated rock, the indentation appeared to be more energy intensive than the dry rock samples.

Increased indentation *SE* in saturated rock was due to reduced chip mass produced in saturated rock tests, directly affecting the *SE* values. Similar behavior of reduced chip mass with saturation was also noted for full scale cutting tests, nevertheless *SE* of indentation cannot be compared directly with the *SE* calculated from full scale linear cutting tests. In linear cutting or full face boring, the rolling force (drag force in case of drag picks) component acting in the direction of cutter motion is actually involved in performing real work, whereas *SE* of indentation is calculated from force of indentation (normal force).

In actual rock cutting, normal force component represents very little of the cutting energy consumed in the cutting process. Moreover, the *SE* computed from full scale cutting takes interaction between adjacent cuts into account, which is not possible in small scale core based load-indentation tests. Therefore, *SE* calculated from load-indentation tests should be used cautiously as a performance indicator. *SP*, on the other hand, can be used for estimation of advance rate or boreability. In the computed values of boreability, an allowance should be given for in-field factors such as joints or cracks in the rock already present or produced by the boring operation, interactions between the adjacent cutters, confining pressure, and natural stresses in the rock.

**9.1.3. Relationships between Specific Energy, Production Rate and Chip Size Indices.** The muck produced from the disc cutter and drag pick cutting experiments was analyzed using the absolute size constant ( $x'$ ) of the Rosin-Rammler distribution and the coarseness index (*CI*). Though *CI* has been frequently used in the past for analysis of



muck from tunnel face and full scale linear cutting tests, use of Rosin-Rammler distribution to analyze the mechanized mining and tunneling muck has been reported rarely. Interestingly,  $x'$  and  $CI$  were found to be very strongly correlated with each other. Both of these indices correlated very well with the proportion of large sized ( $> 51\text{mm}$ ) muck, though both  $x'$  and  $CI$  responded differently. In general the response of  $CI$  and  $x'$  was somewhat mixed but generally higher in saturated rocks, perhaps due to generation of additional fines in weaker rock.

Cut spacing and interaction between adjacent cuts were found to affect the values of  $x'$  and  $CI$ .  $CI$  and  $x'$  also showed reasonable relationships with specific energy and hence with the machine production rate; increasing values of  $x'$  and  $CI$  corresponded with increasing production rate. Although there was a wide scatter in specific energy values when relating with  $x'$  and  $CI$ , the overall decreasing trend confirmed that coarser fragments increase the efficiency of the cutting operation.

A relationship of the form  $SE = k CI^n$  was confirmed between specific energy ( $SE$ ) and coarseness index ( $CI$ ) of the disc cutter and drag pick cutting muck. However, the values of the exponent  $n$  were notably lower for disc cutter and higher for drag pick than reported elsewhere for CCS disc cutters and drag picks, such as Tuncdemir et al. (2008). The exponent  $n$  may depend on the structure and strength variation of the rock and on relationships between the dimensions of the pick/cutter used with the grain sizes of the rock.

The actual chip mass seemed to be in agreement with the nominal chip mass (calculated from theoretical cut volume), especially in saturated rock. Ridge build-up (underbreak) between adjacent cuts was observed at very high  $s/p$  ( $s/d$ ) ratios. The production rate or yield influenced the efficiency of the cutting operation and was shown to relate directly with the  $SE$  of the operation for both dry and saturated cutting tests. Higher production rate or yield usually corresponded with the lower  $SE$  values.

Minimum  $R^2$  improvement method for multiple regression model selection suggested that the geometrical parameters of cutting ( $s$ ,  $d$  and  $s/d$  ratio) and the coarseness of the fragmented product (in terms of  $CI$ ) explain 74% and 80% variation, respectively, in actual specific energy of drag pick cutting under both dry and saturated conditions (Equations 9.1 and 9.2).

$$\text{Dry: } SE_A = 27.98 - 0.085(s) + 0.36\left(\frac{s}{d}\right) - .074(CI), R^2 = 0.74 \quad (9.1)$$

$$\text{Saturated: } SE_A = 41.21 - 0.1008(s) + 1.61(d) - .073(CI), R^2 = 0.80 \quad (9.2)$$

## 9.2. RECOMMENDED FUTURE WORK

The contrasts in the findings of this study emphasize the need for better comprehension of the rock fragmentation process. This necessitates implementation of a coordinated, comprehensive program of rock cutting characterization. Based on the conclusions of this dissertation, some potentially useful research directions are proposed below:

- Conduct more full scale linear cutting tests on different rock types of contrasting permeability. It will be beneficial for better understanding of saturated rock fragmentation mechanisms. Different sedimentary rock types of high to low permeability would be of special interest. Testing some porous varieties of igneous rocks like volcanic tuff, scoria and pumice would also be useful.
- Investigate the use of other types of cutters in full scale cutting tests, including disc cutters of different diameters and tip widths, and other drag pick shapes and geometries including point attack picks.
- Perform underwater cutting tests to simulate dredging and subaqueous mining operations. Different types of underwater cutting tests have been reported in the literature (Larson et al., 1987; Steeghs et al., 1989; Cools, 1990, Van Kesteren, 1995). The rotary rock cutting machine (RRCM) at RMERC is capable of simulating underwater cutting at a depth of 20 m (2 bar back pressure) (Summers, 2009). By utilizing this test setup, it would be possible to evaluate the effects of hydrostatic pressure on underwater cutting of drag picks. Moreover, the effects of relative mismatch of excavator linear advance versus cutterhead rotational speed can also be further clarified using the RRCM.

- Evaluate the interactions of cutting speed and rock permeability with brittleness/ductility. Previous studies have shown that the range of cutting speeds achievable by mechanical excavator cutterheads is not sufficiently high enough to affect an excavator's performance (Evans and Pomeroy, 1966; Roxborough, 1973; Roxborough et al., 1981; Fowell, 1993; Van Kesteren, 1995 among others). Water saturation of rock changes its cutting characteristics as has been demonstrated in this study. If the cutting speed is high enough that excess porewater pressure buildup cannot be dissipated quickly enough by the rock's permeability, the energy supplied by the cutting tool is less effective at fragmenting the rock. Therefore, when fragmenting saturated rock, a maximum cutting speed is expected above which the rock-weakening effects of saturation will be offset by the reduction in effective stress.
- Perform saturated load-indentation tests at very high indentation speeds ( $\sim 1000$  mm/sec) using rocks of very high to low permeability to study the effects of excess porewater pressure buildup under an indenter and hence its impact on the rock fracture process. An effort to use indenters of different shapes including sections of actual disc or drag cutters would also be worthwhile (Dollinger et al., 1998). Using sections of actual cutters would enable to simulate the field conditions very closely.
- Use 3-D finite element method (FEM) software for simulating the action of linear rock cutting, building on the work of Cho et al. (2010). In 2D simulations, crack propagation and fragmentation by chipping can only be simulated by vertical indentation or thrust force. The horizontal or rolling force of the disc cutter has not been taken into account. In addition the amount of rock chips produced cannot be estimated on observation of one dimensional crack propagation. Modern 3-D FEM codes are capable of simulating non-linear and dynamic fracturing phenomenon associated with rock cutting tools. Use of 3-D FEM software to calculate cutter performance parameters and to correlate them with LRCM results would be of great value. This will help in minimizing the number of LRCM tests, which are expensive and time consuming.

## APPENDIX A.

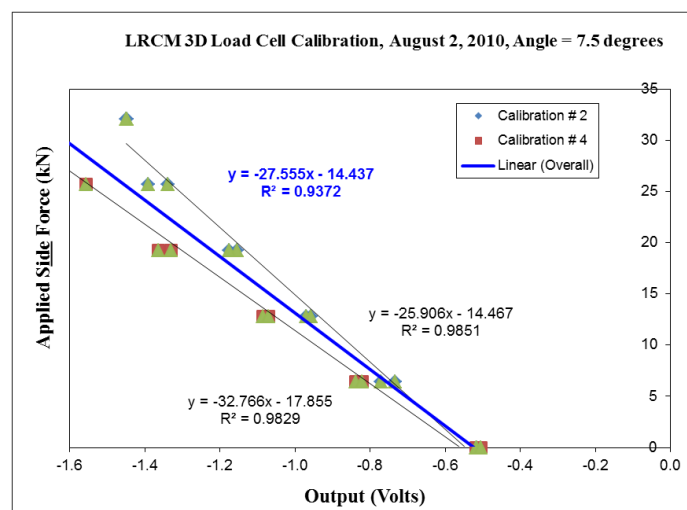
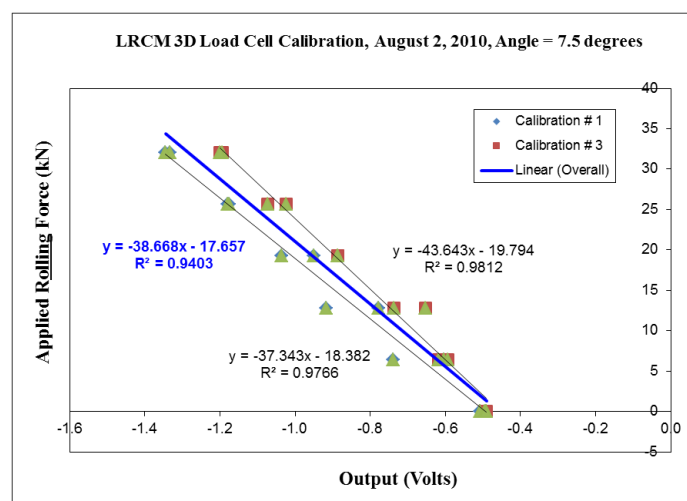
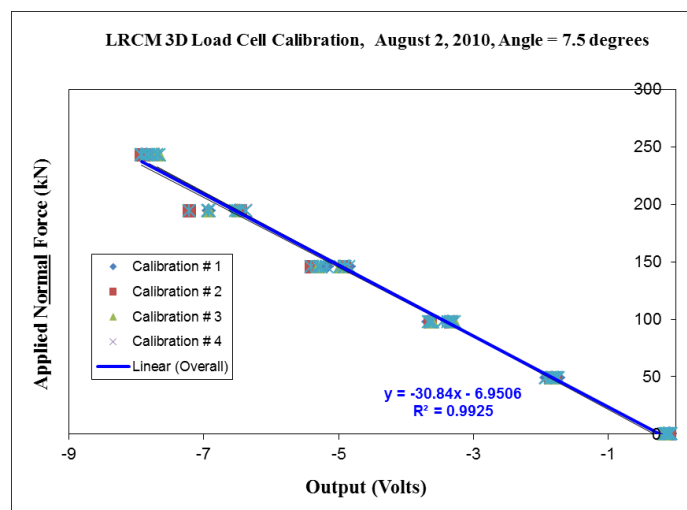
### 3-D LOAD CELL CALIBRATIONS FOR DISC CUTTER AND DRAG PICK TESTS

### Long Bladed Disc Cutter Calibrations

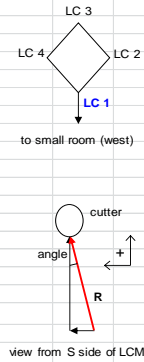
LRCM Load Cell Calibration August 2, 2010, with all penetration spacers in place									
	Normal Force			Rolling Force			Side Force		
Post	Slope	Intercept	R <sup>2</sup>	Slope	Intercept	R <sup>2</sup>	Slope	Intercept	R <sup>2</sup>
LC1	-3.234E-02	-2.373E-01	0.994842	-2.615E-02	-5.023E-01	0.976564	-3.000E-02	-5.533E-01	0.98289
LC2	-3.259E-02	-2.547E-01	0.990631						
LC3	-3.178E-02	-2.803E-01	0.991757	-2.248E-02	-4.605E-01	0.981171	-3.802E-02	-5.677E-01	0.98507
LC4	-3.202E-02	-2.470E-01	0.993833						

LRCM Load Cell Calibration 02 August 2010, with minimum penetration spacers in place									
	Normal Force			Rolling Force			Side Force		
Post	Slope	Intercept	R <sup>2</sup>	Slope	Intercept	R <sup>2</sup>	Slope	Intercept	R <sup>2</sup>
LC1	-3.221E-02	-2.384E-01	0.993432	-4.298E-02	-5.838E-01	0.998346	-2.079E-02	-3.450E-01	0.964036
LC2	-3.257E-02	-2.428E-01	0.989881						
LC3	-3.206E-02	-3.268E-01	0.991987	-3.578E-02	-3.030E-01	0.989414	-3.303E-02	-3.362E-01	0.992445
LC4	-3.284E-02	-1.958E-01	0.995689						

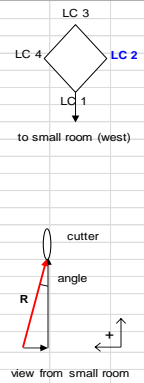
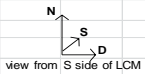
## Long Bladed Disc Cutter Calibration Constants- Maximum Penetration with Beams



LC1 Summary		angle = 7.5 degrees			0.1308997 radians			orientation = normal-rolling				date = 2-Aug-10		
	Resultant Load (R)	Normal	(lb) Rolling	Side	Normal	(kN) Rolling	Side	LC1	Avg. output (Volts) LC2	LC3	LC4	Normal	Rolling	Side
UP-load	0	0	0		0.0	0.0		-0.42514	0.38996	0.407439	-0.47495	-0.102695	-0.507467	
	11,040	10,946	1,441		48.7	6.4		-1.16875	0.317666	0.045125	-0.93933	-1.745285	-0.73987	
	22,080	21,891	2,882		97.4	12.8		-1.82018	0.21375	-0.31569	-1.44957	-3.371686	-0.917009	
	33,120	32,837	4,323		146.1	19.2		-2.35187	0.101108	-0.65082	-1.94562	-4.847204	-1.03681	
	44,160	43,782	5,764		194.7	25.6		-2.95963	-0.04388	-1.0235	-2.4963	-6.523297	-1.180094	
	55,200	54,728	7,205		243.4	32.0		-3.50074	-0.17533	-1.31264	-2.8552	-7.843919	-1.333674	
DOWN-load	55,200	54,728	7,205		243.4	32.0		-3.53125	-0.187	-1.3237	-2.87053	-7.912487	-1.345531	
	44,160	43,782	5,764		194.7	25.6		-3.05957	-0.10191	-1.13226	-2.62843	-6.922167	-1.174722	
	33,120	32,837	4,323		146.1	19.2		-2.34194	0.040595	-0.7836	-2.08323	-5.168173	-0.949829	
	22,080	21,891	2,882		97.4	12.8		-1.74422	0.15809	-0.46826	-1.60767	-3.662057	-0.777708	
	11,040	10,946	1,441		48.7	6.4		-1.06231	0.280329	-0.07268	-1.05769	-1.912349	-0.603191	
	0	0	0		0.0	0.0		-0.40175	0.37536	0.402968	-0.45352	-0.076938	-0.490486	
calibration ram area =		11.04 in <sup>2</sup>												
moment arm ratio =		0.609512												

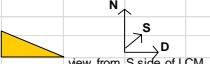


LC2 Summary		angle = 7.5 degrees			0.1309 radians			orientation = normal-side				date = 2-Aug-10			
	Resultant Load (R)	Normal	(lb)		Side	(kN)		Side	Avg. output (Volts)				Output (Volts)		
			Rolling			Normal	Rolling		LC1	LC2	LC3	LC4	Normal	Rolling	Side
UP-load	0	0		0	0.0		0.0	-0.42841	0.362254	0.394453	-0.48377	-0.55473		-0.515662	
	11,040	10,946		1,441	48.7	6.4	-0.99902	0.156744	0.159907	-1.10938	-1.791744		-0.771716		
	22,080	21,891		2,882	97.4	12.8	-1.59352	-0.05065	-0.05748	-1.64082	-3.342463		-0.96923		
	33,120	32,837		4,323	146.1	19.2	-2.19475	-0.27949	-0.2716	-2.17348	-4.919322		-1.154409		
	44,160	43,782		5,764	194.7	25.6	-2.76181	-0.50204	-0.49557	-2.69768	-6.457105		-1.338271		
	55,200	54,728		7,205	243.4	32.0	-3.28947	-0.7617	-0.66326	-3.13588	-7.850317		-1.447089		
DOWN-load	55,200	54,728		7,205	243.4	32.0	-3.32114	-0.77701	-0.67299	-3.15475	-7.925877		-1.449261		
	44,160	43,782		5,764	194.7	25.6	-3.01295	-0.66564	-0.58433	-2.9481	-7.211023		-1.391185		
	33,120	32,837		4,323	146.1	19.2	-2.3159	-0.41083	-0.34274	-2.33917	-5.408651		-1.175347		
	22,080	21,891		2,882	97.4	12.8	-1.63421	-0.167	-0.10495	-1.7394	-3.645561		-0.958394		
	11,040	10,946		1,441	48.7	6.4	-0.97441	0.089193	0.145335	-1.11267	-1.852552		-0.732552		
	0	0		0	0.0	0.0	-0.40798	0.368517	0.406887	-0.45911	-0.091683		-0.504449		
calibration ram area = moment arm ratio =		11.04 in <sup>2</sup> 0.609512						(kN)				Slope Intercept R <sup>2</sup>			
												-3.259E-02 -2.547E-01 9.906E-01			
												-3.000E-02 -5.533E-01 9.829E-01			

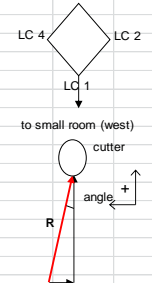


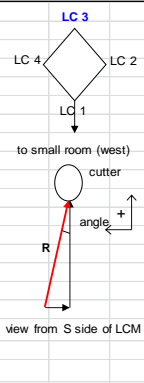
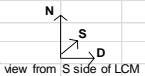
LC3 Summary		angle = 7.5 degrees			0.1309 radians			orientation = normal-rolling			date = 2-Aug-10				
	Resultant Load (R)	Normal	Rolling	Side	Normal	Rolling	Side	LC1	Avg. output (Volts)	LC2	LC3	LC4	Normal	Rolling	Side
UP-load	0	0	0		0.0	0.0		-0.42791	0.3682	0.383075	-0.4962	-0.17283	-0.494303		
	11,040	10,946	1,441		48.7	6.4		-0.96298	0.271299	0.050617	-1.13751	-1.77858	-0.617802		
	22,080	21,891	2,882		97.4	12.8		-1.35545	0.100978	-0.28493	-1.73671	-3.276116	-0.652493		
	33,120	32,837	4,323		146.1	19.2		-2.06225	0.017976	-0.60788	-2.31955	-4.971699	-0.886455		
	44,160	43,782	5,764		194.7	25.6		-2.59327	-0.12455	-0.91401	-2.86179	-6.493615	-1.023529		
	55,200	54,728	7,205		243.4	32.0		-3.09138	-0.25991	-1.13292	-3.17313	-7.657344	-1.193708		
DOWN-load	55,200	54,728	7,205		243.4	32.0		-3.10963	-0.2668	-1.14	-3.18076	-7.697188	-1.20051		
	44,160	43,782	5,764		194.7	25.6		-2.75853	-0.19441	-0.99666	-2.97598	-6.92589	-1.073698		
	33,120	32,837	4,323		146.1	19.2		-2.13593	-0.05389	-0.68278	-2.42292	-5.295519	-0.885716		
	22,080	21,891	2,882		97.4	12.8		-1.54938	0.08376	-0.3415	-1.79929	-3.606409	-0.736219		
	11,040	10,946	1,441		48.7	6.4		-0.94775	0.226562	0.025597	-1.12544	-1.82103	-0.593269		
	0	0	0		0.0	0.0		-0.40428	0.372847	0.401128	-0.4574	-0.087701	-0.490906		
calibration ram area = 11.04 in <sup>2</sup> moment arm ratio = 0.609512									(kN)			Slope -3.178E-02 -2.248E-02 Intercept -2.803E-01 -4.605E-01 R <sup>2</sup> 9.918E-01 9.812E-01			

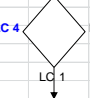
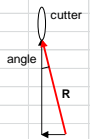
view from S side of LCM

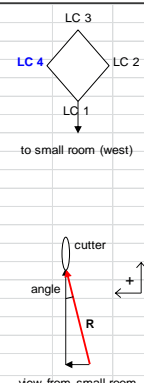
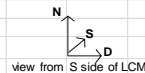


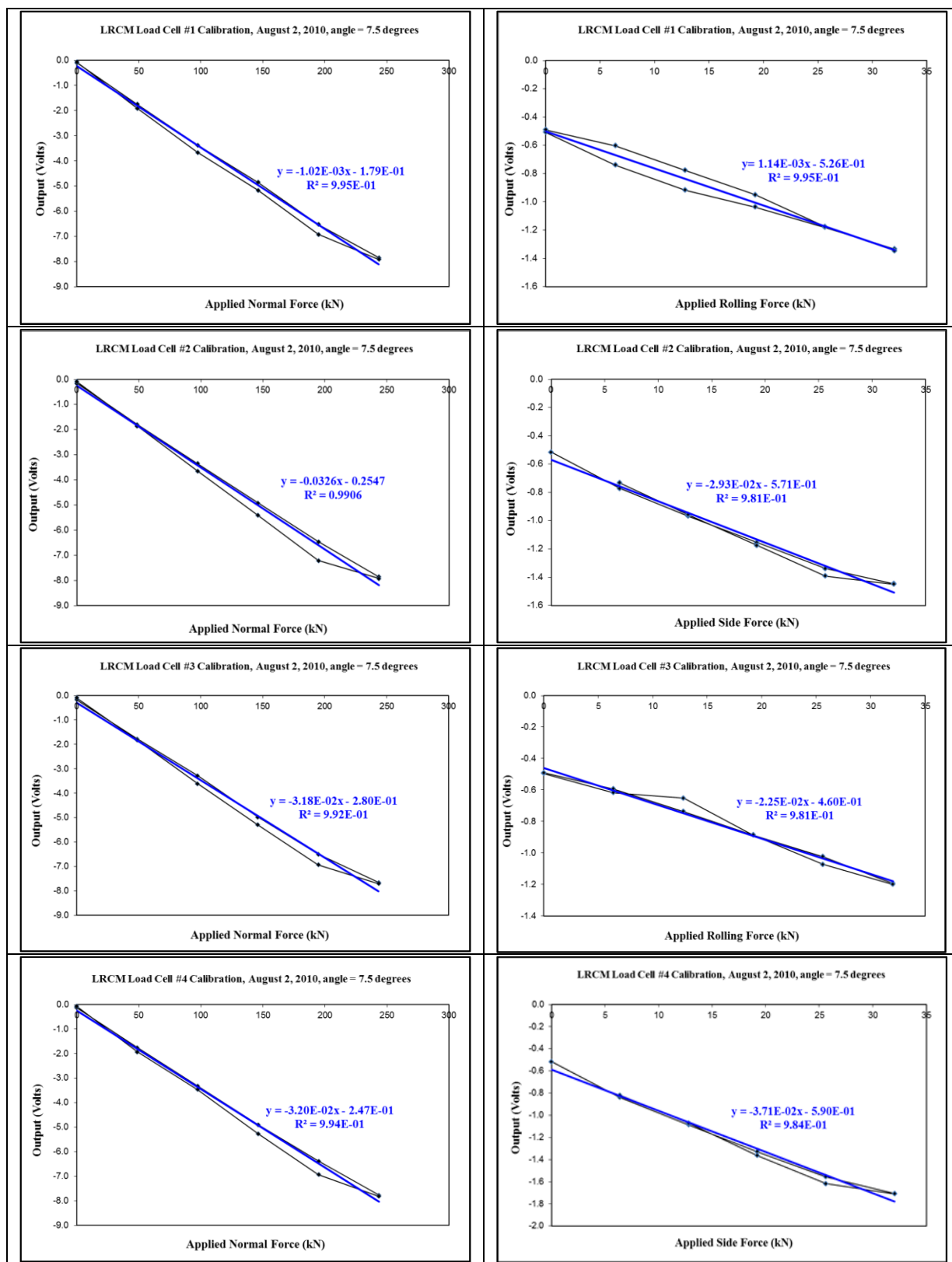
view from S side of LCM





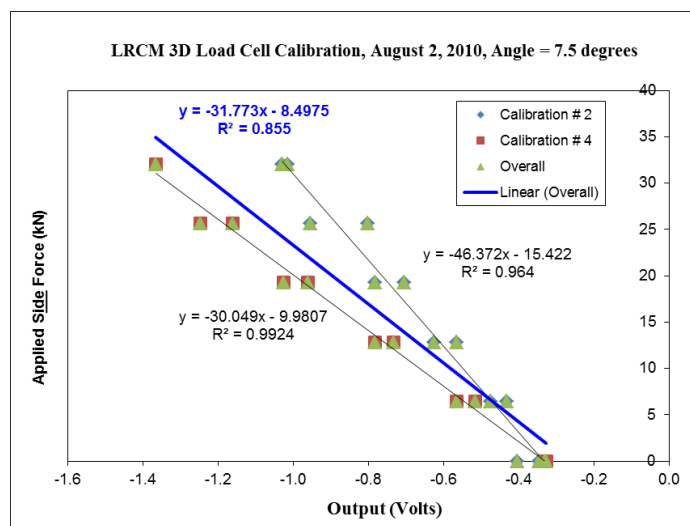
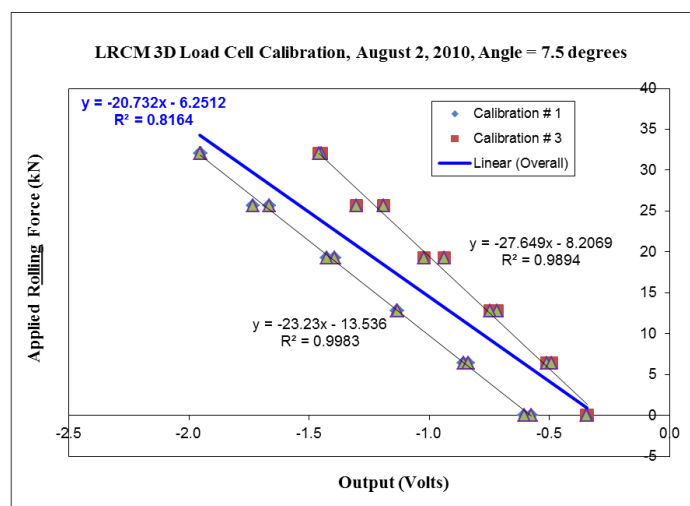
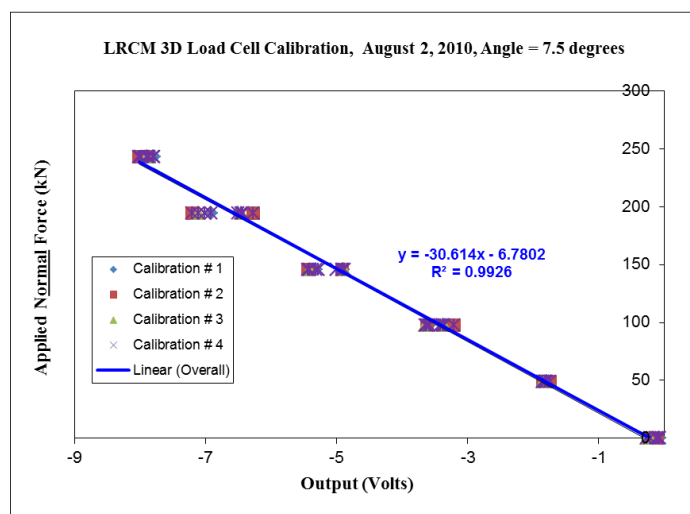
LC4 Summary		angle = 7.5 degrees			0.1309 radians			orientation = normal-side				date = 2-Aug-10					
	Resultant Load (R)	Normal	(lb) Rolling	Side	Normal	(kN) Rolling	Side	LC1	LC2	Avg. output (Volts)	LC3	LC4	Output (Volts)			LC 3	LC 2
													Normal	Rolling	Side		
UP-load	0	0		0	0.0			0.0	-0.41584	0.373614	0.387135	-0.47468	-0.129778		-0.517047		to small room (west)
	11,040	10,946		1,441	48.7		6.4	-1.02223	0.316468	0.006858	-1.05946	-1.758365		-0.838647			
	22,080	21,891		2,882	97.4		12.8	-1.65472	0.242778	-0.36781	-1.5392	-3.318947		-1.086135			
	33,120	32,837		4,323	146.1		19.2	-2.27252	0.152889	-0.7528	-2.02826	-4.900691		-1.329436			
	44,160	43,782		5,764	194.7		25.6	-2.82449	0.044835	-1.08969	-2.50988	-6.379236		-1.557133			
	55,200	54,728		7,205	243.4		32.0	-3.41437	-0.07986	-1.39262	-2.88151	-7.768362		-1.707636			
DOWN-load	55,200	54,728		7,205	243.4		32.0	-3.4327	-0.08638	-1.40137	-2.89182	-7.812265		-1.709956		cutter	
	44,160	43,782		5,764	194.7		25.6	-3.01481	-0.02771	-1.2056	-2.68148	-6.9296		-1.617507			
	33,120	32,837		4,323	146.1		19.2	-2.3449	0.074885	-0.83472	-2.16201	-5.266743		-1.363413			
	22,080	21,891		2,882	97.4		12.8	-1.64783	0.182102	-0.4184	-1.57534	-3.459472		-1.071181			
	11,040	10,946		1,441	48.7		6.4	-1.06219	0.265189	-0.05288	-1.08117	-1.931047		-0.820621			
	0	0		0	0.0		0.0	-0.40354	0.375756	0.404154	-0.45243	-0.076059		-0.50479			
calibration ram area = 11.04 in <sup>2</sup> moment arm ratio = 0.6095123									(kN)				Slope Intercept R <sup>2</sup>				
													-3.202E-02 -2.470E-01 9.938E-01				
													-3.802E-02 -5.677E-01 9.851E-01				
																view from small room	



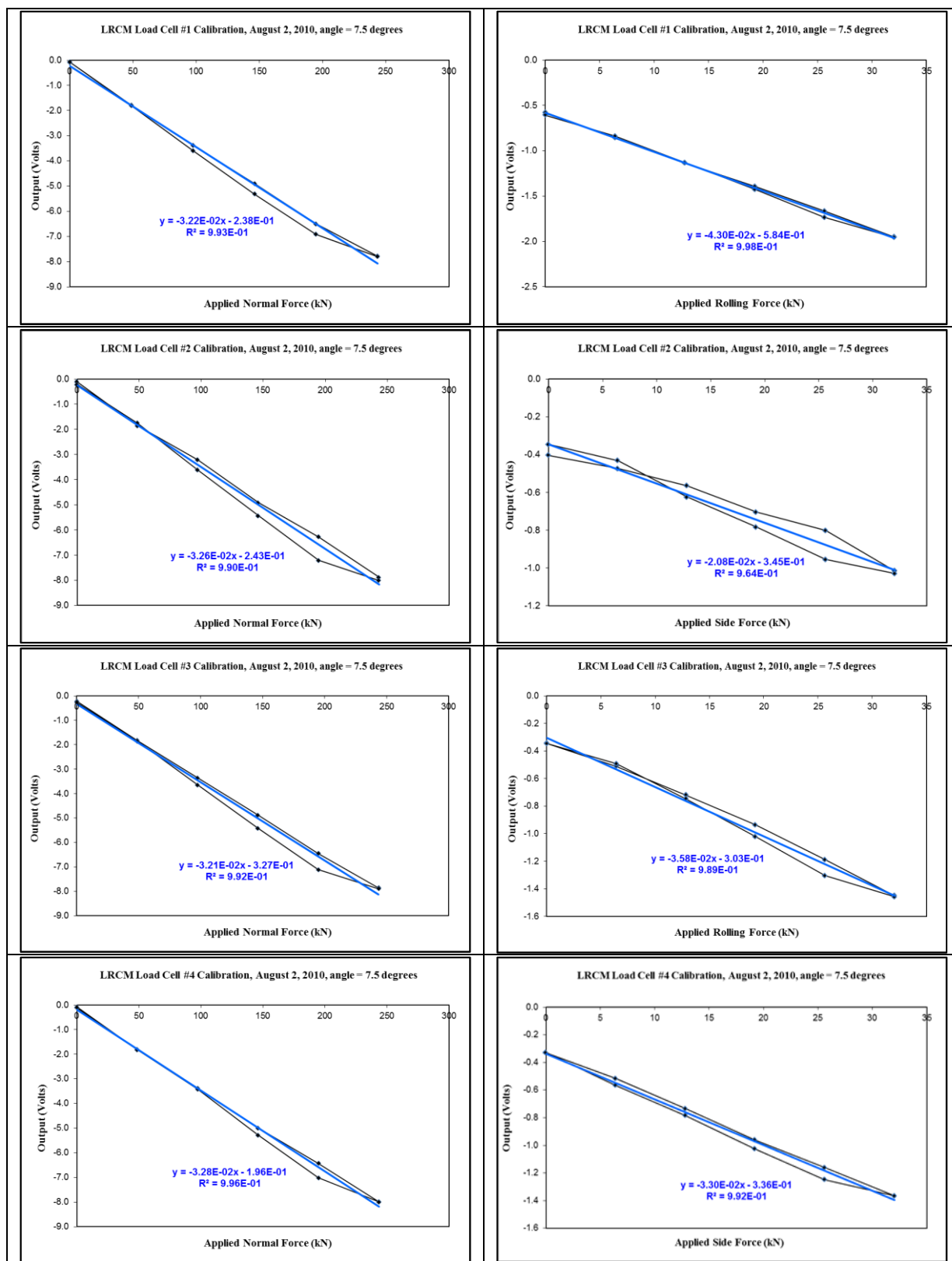




## Long Bladed Disc Cutter Calibration Constants- Minimum Penetration with Beams



LC1 Summary		angle = 7.5 degrees			0.1309 radians			orientation = normal-rolling				date = 2-Aug-10				
UP-Load	Resultant Load (R)	(lb)			(kN)			LC1	Avg. output (Volts) LC2	LC3	LC4	Output (Volts)				
	Normal	Rolling	Side	Normal	Rolling	Side	Normal					Rolling	Side			
	0	0	0	0.0	0.0	0.0	-0.47577					0.462795	0.471615	-0.5429	-0.084263	-0.577442
	11,040	10,946	1,441	48.7	6.4	6.4	-1.22872					0.374172	0.179203	-1.11421	-1.789563	-0.858148
	22,080	21,891	2,882	97.4	12.8	12.8	-1.92467					0.269242	-0.06396	-1.65545	-3.37484	-1.134122
	33,120	32,837	4,323	146.1	19.2	19.2	-2.58603					0.159042	-0.30041	-2.17247	-4.899863	-1.393118
	44,160	43,782	5,764	194.7	25.6	25.6	-3.27385					0.022624	-0.54197	-2.70577	-6.498971	-1.665115
DOWN-Load	55,200	54,728	7,205	243.4	32.0	32.0	-3.9222	-0.10434	-0.71969	-3.03308	-7.779315	-1.951967				
				0.0												
	55,200	54,728	7,205	243.4	32.0	32.0	-3.92858	-0.1079	-0.72039	-3.03674	-7.793617	-1.95543				
	44,160	43,782	5,764	194.7	25.6	25.6	-3.44325	-0.02406	-0.59896	-2.84481	-6.91108	-1.733628				
	33,120	32,837	4,323	146.1	19.2	19.2	-2.70051	0.107316	-0.36097	-2.36123	-5.315387	-1.42598				
	22,080	21,891	2,882	97.4	12.8	12.8	-1.94657	0.240433	-0.09116	-1.79024	-3.587535	-1.1309				
	11,040	10,946	1,441	48.7	6.4	6.4	-1.17574	0.366353	0.198638	-1.19352	-1.804274	-0.837703				
	0	0	0	0.0	0.0	0.0	-0.49708	0.494287	0.497314	-0.56682	-0.072297	-0.606095				
calibration ram area = 11.04 in <sup>2</sup>																
moment arm ratio = 0.609512																
								</								

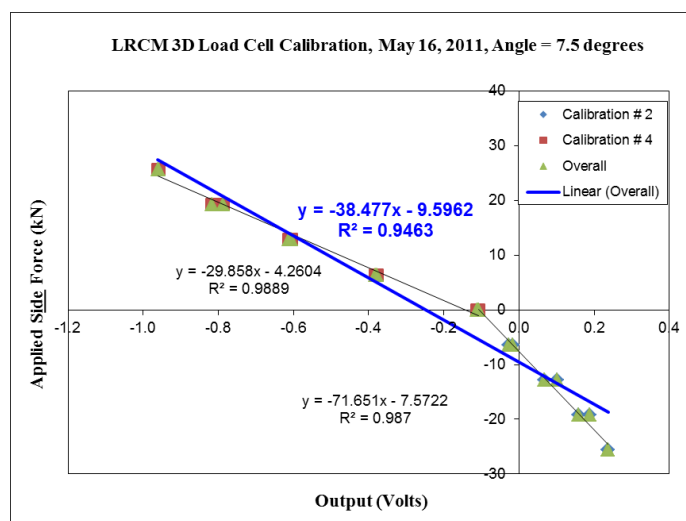
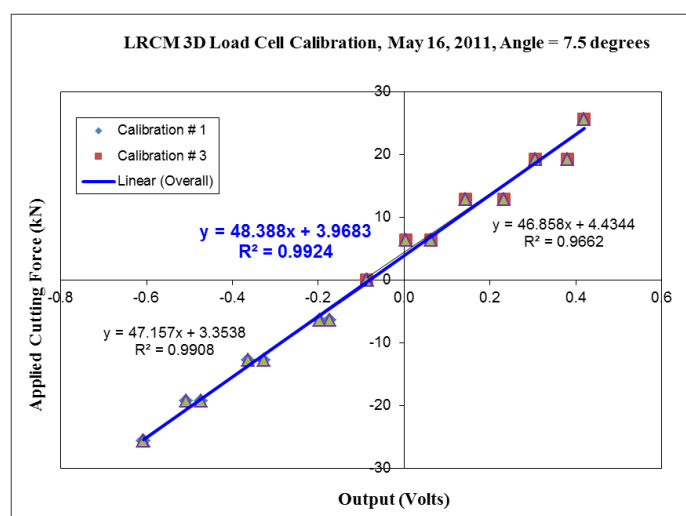
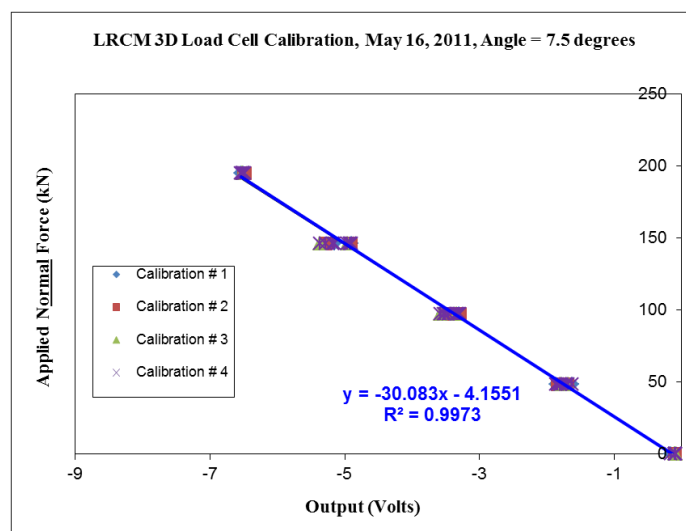


## Radial Drag Pick Calibrations

LRCM Load Cell Calibration 06 May 2011, with maximum penetration spacers in place									
Post	Normal Force			Cutting Force			Side Force		
	Slope	Intercept	R <sup>2</sup>	Slope	Intercept	R <sup>2</sup>	Slope	Intercept	R <sup>2</sup>
LC1	-3.300E-02	-1.558E-01	0.9979301	2.101E-02	-7.362E-02	0.99081019			
LC2	-3.306E-02	-1.522E-01	0.99690256				-1.378E-02	-1.034E-01	0.9870314
LC3	-3.343E-02	-1.406E-01	0.99609638	2.062E-02	-8.538E-02	0.96617829			
LC4	-3.312E-02	-1.385E-01	0.99860319				-3.312E-02	-1.475E-01	0.9888638

LRCM Load Cell Calibration 06 May 2011, with minimum penetration spacers in place									
Post	Normal Force			Rolling Force			Side Force		
	Slope	Intercept	R <sup>2</sup>	Slope	Intercept	R <sup>2</sup>	Slope	Intercept	R <sup>2</sup>
LC1	-3.306E-02	-1.774E-01	0.99812709	1.000E-02	-8.539E-02	0.993039408			
LC2	-3.280E-02	-2.047E-01	0.99518568				-9.654E-03	-9.969E-02	0.963104896
LC3	-3.292E-02	-1.829E-01	0.99360184	2.169E-02	-7.094E-02	0.949995393			
LC4	-3.335E-02	-1.528E-01	0.99827523				-2.497E-02	-1.157E-01	0.994743901

## Radial Drag Pick Calibration Constants- Maximum Penetration with Beams

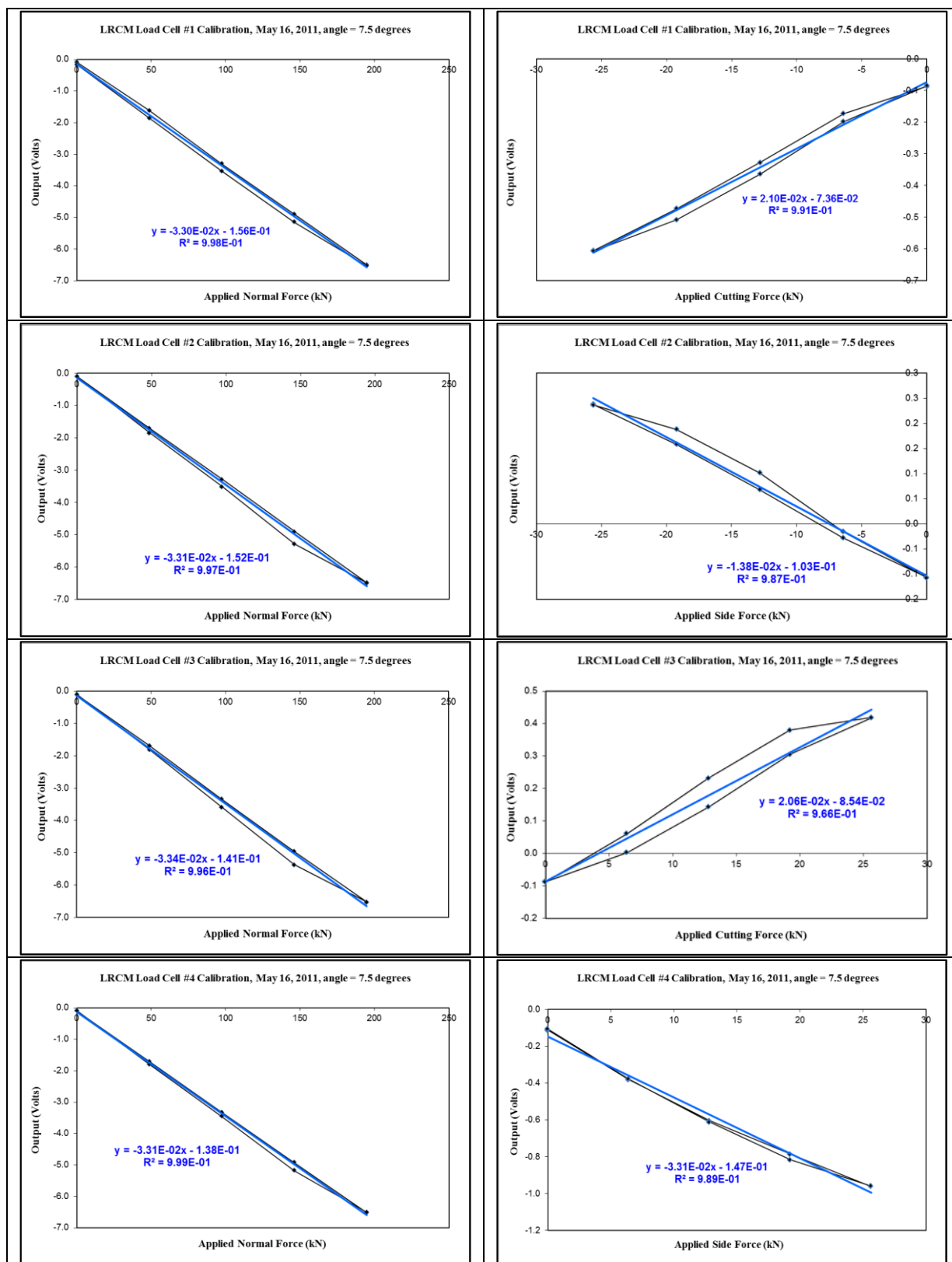


LC1 Summary		angle = 7.5 degrees			0.1309 radians			orientation = normal-rolling				date = 16-May-11						
	Resultant Load (R)	(lb)			(kN)			Avg. output (Volts)				Output (Volts)						
		Normal	Cutting	Side	Normal	Cutting	Side	LC1	LC2	LC3	LC4	Normal	Cutting	Side				
UP-Load	0	0	0		0.0	0.0		-0.27227	0.242598	-0.10923	0.041737	-0.0971715	-0.0869598		<p>LC 3</p> <p>LC 4</p> <p>LC 2</p> <p>LC 1</p> <p>to small room (west)</p> <p>cutter</p> <p>angle</p> <p>+</p> <p>R</p> <p>view from S side of LCM</p>			
	11,040	10,946	-1,441		48.7	-6.4		-0.78219	-0.0589	-0.45745	-0.32668	-1.6252159	-0.1732013					
	22,080	21,891	-2,882		97.4	-12.8		-1.39705	-0.40985	-0.78323	-0.71822	-3.3083575	-0.3273949					
	33,120	32,837	-4,323		146.1	-19.2		-1.96305	-0.74937	-1.07555	-1.11279	-4.9007625	-0.4733638					
	44,160	43,782	-5,764		194.7	-25.6		-2.5072	-1.09729	-1.3713	-1.53157	-6.5073539	-0.6058544					
DOWN-Load																		
	44,160	43,782	-5,764		194.7	-25.6		-2.51515	-1.10445	-1.37617	-1.54161	-6.537377	-0.607494					
	33,120	32,837	-4,323		146.1	-19.2		-2.05688	-0.78814	-1.1038	-1.20067	-5.1494883	-0.5083473					
	22,080	21,891	-2,882		97.4	-12.8		-1.47348	-0.46127	-0.79075	-0.81126	-3.5367577	-0.3641491					
	11,040	10,946	-1,441		48.7	-6.4		-0.84046	-0.11857	-0.46947	-0.43103	-1.8595368	-0.1978771					
	0	0	0		0.0	0.0		-0.26198	0.202939	-0.10265	-0.004	-0.1656847	-0.0849829					
calibration ram area = 11.04 in <sup>2</sup>																	<p>view from S side of LCM</p>	
moment arm ratio = 0.533369																		

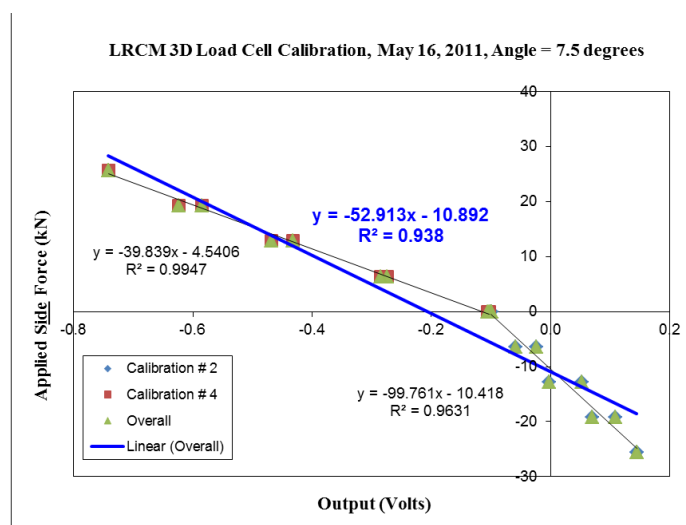
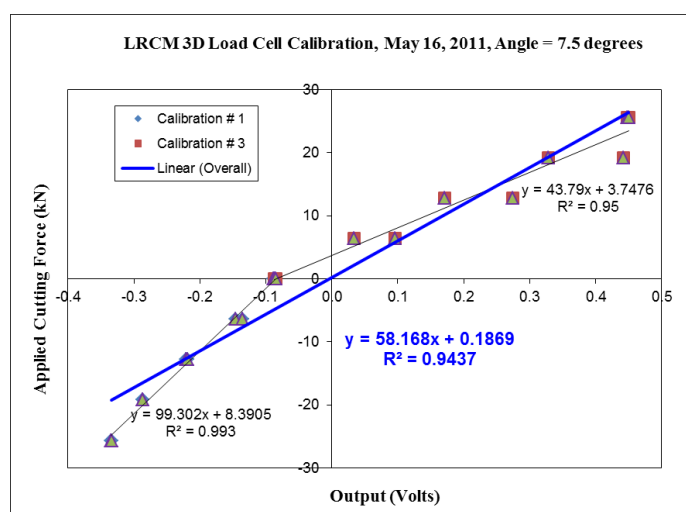
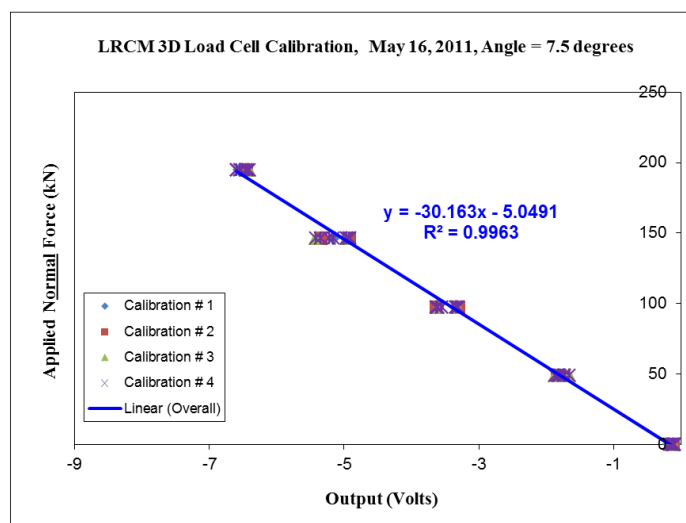
LC2 Summary		angle = 7.5 degrees			0.1309 radians			orientation = normal-side				date = 16-May-11				
	Resultant Load (R)	(lb)			(kN)			Avg. output (Volts)				Output (Volts)				
	Normal	Cutting	Side	Normal	Cutting	Side	LC1	LC2	LC3	LC4	Normal	Cutting	Side			
UP-load	0	0		0	0.0		0.0	-0.25663	0.224158	-0.09393	0.024518	-0.101879		-0.106482	<p>view from small room</p>	
	11,040	10,946		-1,441	48.7		-6.4	-0.67755	-0.18482	-0.6034	-0.23707	-1.70284		-0.027866		
	22,080	21,891		-2,882	97.4		-12.8	-1.05584	-0.61497	-1.12946	-0.48722	-3.287488		0.0681385		
	33,120	32,837		-4,323	146.1		-19.2	-1.39883	-1.05862	-1.6862	-0.76229	-4.905936		0.1580529		
	44,160	43,782		-5,764	194.7		-25.6	-1.70567	-1.50252	-2.22526	-1.0569	-6.490352		0.2376793		
DOWN-load															<p>view from small room</p>	
	44,160	43,782		-5,764	194.7		-25.6	-1.70388	-1.50143	-2.22356	-1.05793	-6.48681		0.2365465		
	33,120	32,837		-4,323	146.1		-19.2	-1.42696	-1.1779	-1.85534	-0.82563	-5.285825		0.1878889		
	22,080	21,891		-2,882	97.4		-12.8	-1.02996	-0.70881	-1.25083	-0.51846	-3.508053		0.101529		
	11,040	10,946		-1,441	48.7		-6.4	-0.65351	-0.24075	-0.68206	-0.27013	-1.846455		-0.015671		
	0	0		0	0.0		0.0	-0.25411	0.223589	-0.09128	0.022008	-0.099799		-0.107517		
calibration ram area =		11.04 in <sup>2</sup>														
moment arm ratio =		0.533369														

LC3 Summary		angle = 7.5 degrees			0.1309 radians			orientation = normal-rolling				date = 16-May-11				
	Resultant Load (R)	(lb)			(kN)			Avg. output (Volts)				Output (Volts)				
	Normal	Cutting	Side	Normal	Cutting	Side	LC1	LC2	LC3	LC4	Normal	Cutting	Side			
UP-load	0	0	0		0.0	0.0		-0.25595	0.226772	-0.09344	0.0243	-0.098321	-0.086679		<p>view from S side of LCM</p>	
	11,040	10,946	1,441		48.7	6.4		-0.62169	-0.07969	-0.62767	-0.35023	-1.679278	0.0031875			
	22,080	21,891	2,882		97.4	12.8		-0.96731	-0.38987	-1.2358	-0.74471	-3.337693	0.1432035			
	33,120	32,837	4,323		146.1	19.2		-1.27248	-0.69649	-1.8455	-1.13956	-4.954036	0.3056327			
	44,160	43,782	5,764		194.7	25.6		-1.59397	-1.02929	-2.37856	-1.52087	-6.522692	0.4184765			
DOWN-load															<p>view from S side of LCM</p>	
	44,160	43,782	5,764		194.7	25.6		-1.5925	-1.02979	-2.37783	-1.52045	-6.520568	0.4188691			
	33,120	32,837	4,323		146.1	19.2		-1.31552	-0.79104	-2.02814	-1.23122	-5.365919	0.3800862			
	22,080	21,891	2,882		97.4	12.8		-0.94705	-0.4576	-1.3822	-0.79773	-3.584593	0.2320957			
	11,040	10,946	1,441		48.7	6.4		-0.5947	-0.11892	-0.71038	-0.37443	-1.798443	0.0616994			
	0	0	0		0.0	0.0		-0.25386	0.226882	-0.09043	0.025214	-0.092188	-0.08717			
calibration ram area = 11.04 in <sup>2</sup>															<p>view from S side of LCM</p>	
moment arm ratio = 0.533369																

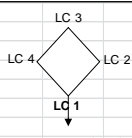
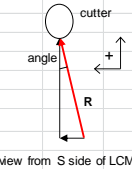
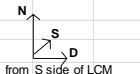
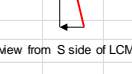
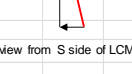
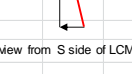
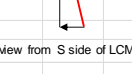
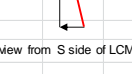
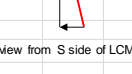
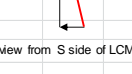
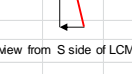
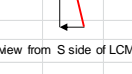
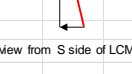
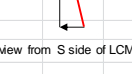
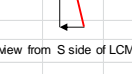
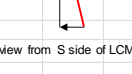
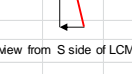
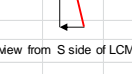
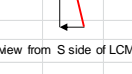
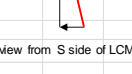
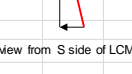
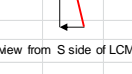
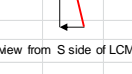
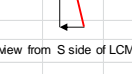
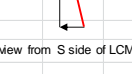
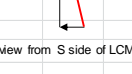
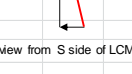
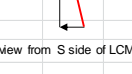
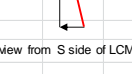
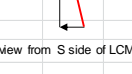
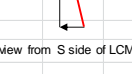
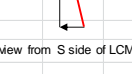
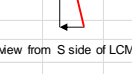
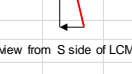
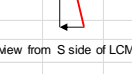
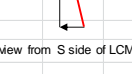
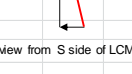
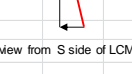
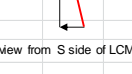
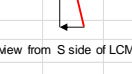
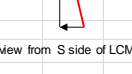
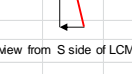
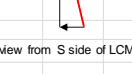
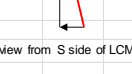
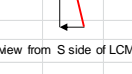
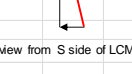
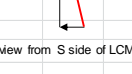
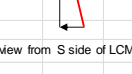
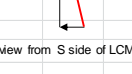
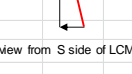
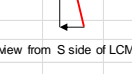
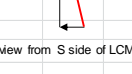
LC4 Summary		angle = 7.5 degrees			0.1309 radians			orientation = normal-side				date = 16-May-11				
	Resultant Load (R)	(lb)			(kN)			Avg. output (Volts)				Output (Volts)				
		Normal	Cutting	Side	Normal	Cutting	Side	LC1	LC2	LC3	LC4	Normal	Cutting	Side		
UP-load	0	0		0	0.0		0.0	-0.25653	0.228754	-0.09211	0.017538	-0.10234		-0.112656	<p>view from small room</p>	
	11,040	10,946		1,441	48.7		6.4	-0.70421	0.108622	-0.51203	-0.60779	-1.71541		-0.382111		
	22,080	21,891		2,882	97.4		12.8	-1.1316	-0.05905	-0.94921	-1.19296	-3.332823		-0.604792		
	33,120	32,837		4,323	146.1		19.2	-1.55982	-0.25092	-1.38929	-1.7256	-4.925627		-0.786548		
	44,160	43,782		5,764	194.7		25.6	-1.97839	-0.44653	-1.84549	-2.2489	-6.519308		-0.96133		
DOWN-load															<p>view from small room</p>	
	44,160	43,782		5,764	194.7		25.6	-1.97501	-0.44605	-1.84283	-2.24383	-6.507718		-0.958881		
	33,120	32,837		4,323	146.1		19.2	-1.59934	-0.28044	-1.48704	-1.81306	-5.179867		-0.817453		
	22,080	21,891		2,882	97.4		12.8	-1.12442	-0.0846	-1.01669	-1.23134	-3.457047		-0.611636		
	11,040	10,946		1,441	48.7		6.4	-0.68789	0.079202	-0.56567	-0.63026	-1.804622		-0.378403		
	0	0		0	0.0		0.0	-0.25296	0.224873	-0.08879	0.025209	-0.091669		-0.106494		
calibration ram area = 11.04 in <sup>2</sup>																
moment arm ratio = 0.533369																

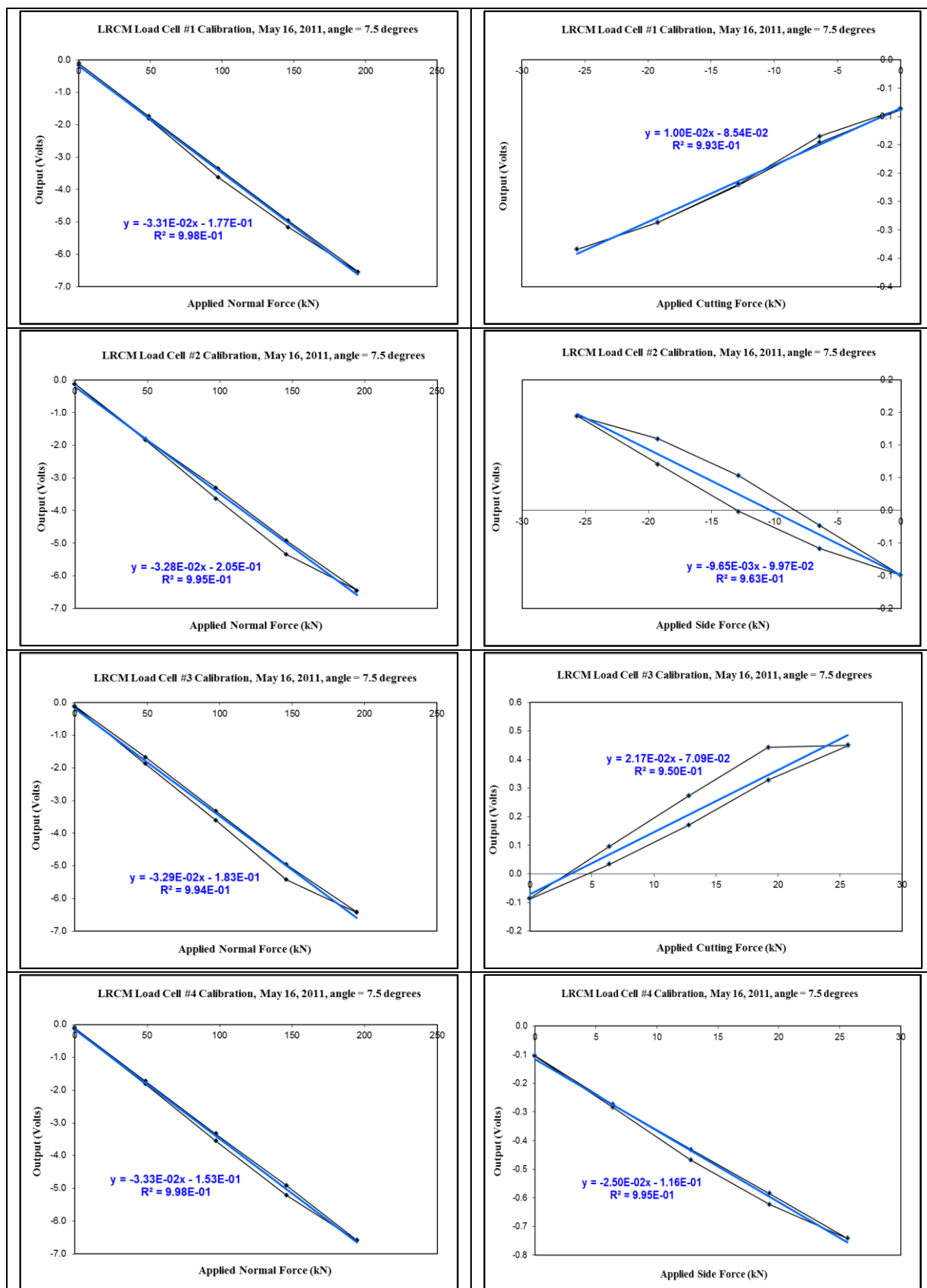


## Radial Drag Pick Calibration Constants- Minimum Penetration with Beams





LC1 Summary		angle = 7.5 degrees			0.1309 radians			orientation = normal-rolling				date = 2-Aug-10					
Resultant Load (R)		(lb)			(kN)			Avg. output (Volts)				Output (Volts)					
		Normal	Cutting	Side	Normal	Cutting	Side	LC1	LC2	LC3	LC4	Normal	Cutting	Side			
UP-Load	0	0	0		0.0	0.0		-0.33954	0.302524	-0.17499	0.107748	-0.104248	-0.087766				
	11,040	10,946	-1,441		48.7	-6.4		-0.90608	0.071642	-0.63301	-0.26895	-1.736394	-0.145647				
	22,080	21,891	-2,882		97.4	-12.8		-1.48053	-0.17489	-1.0668	-0.61952	-3.341733	-0.22067				
	33,120	32,837	-4,323		146.1	-19.2		-2.041	-0.43843	-1.50419	-0.96919	-4.952809	-0.286318				
	44,160	43,782	-5,764		194.7	-25.6		-2.57217	-0.70101	-1.94512	-1.31873	-6.537034	-0.334447				
DOWN-Load																	
	44,160	43,782	-5,764		194.7	-25.6		-2.57447	-0.70226	-1.94805	-1.31972	-6.54449	-0.334116				
	33,120	32,837	-4,323		146.1	-19.2		-2.10062	-0.47034	-1.56304	-1.02078	-5.154779	-0.286725				
	22,080	21,891	-2,882		97.4	-12.8		-1.55453	-0.23089	-1.14373	-0.68953	-3.618683	-0.219105				
	11,040	10,946	-1,441		48.7	-6.4		-0.90458	0.045283	-0.6512	-0.29987	-1.810359	-0.135144				
	0	0	0		0.0	0.0		-0.34494	0.279774	-0.1838	0.086139	-0.162833	-0.085948				
calibration ram area =		11.04 in <sup>2</sup>															
moment arm ratio =		0.533369															
																	
																	
																	
																	
																	
																	
																	
																	
																	
																	
																	
																	
																	
																	
																	
																	
																	
																	
																	
																	
																	
																	
																	
																	
																	
																	
																	
																	
																	
																	
																	
																	
																	
																	
																	
																	
																	
																	
																	
																	
																	
																	
																	
																	
																	
																	
																	
																	
																	



## APPENDIX B.

### DISC CUTTING FORCES AND SIEVE ANALYSIS DATA

## Disc Cutter Tests - Dry Rock

Rock= Roubidoux Sandstone			Block # 1 (Dry)										
Data Window Cuts			Spacing			3 inch							
Cutter			Penetration			0.25 inch							
	Averages			Standard Deviations			Maximums			Start Position	End Position	Speed	Length of Cut
	Normal(kN)	Rolling(kN)	Side(kN)	Normal(kN)	Rolling(kN)	Side(kN)	Normal(kN)	Rolling(kN)	Side(kN)	(inches)	(inches)	(inch/sec)	(inch)
Cut # 1	18.251	1.650	2.990	16.608	2.280	3.018	62.587	9.344	9.391	57.53	26.46	3.45	31.07
Cut # 2	42.510	7.952	0.914	25.658	5.806	4.430	95.970	21.197	10.583	57.44	24.16	3.45	33.29
Cut # 3	73.069	7.809	9.673	35.177	5.653	5.176	160.340	23.000	22.581	55.79	22.63	3.38	33.16

Rock= Roubidoux Sandstone			Block # 1 (Dry)										
Data Window Cuts			Spacing			3 inch							
Cutter			Penetration			0.375 inch							
	Averages			Standard Deviations			Maximums			Start Position	End Position	Speed	Length of Cut
	Normal(kN)	Rolling(kN)	Side(kN)	Normal(kN)	Rolling(kN)	Side(kN)	Normal(kN)	Rolling(kN)	Side(kN)	(inches)	(inches)	(inch/sec)	(inch)
Cut # 1	35.889	7.031	0.324	21.422	4.418	4.452	91.716	18.390	14.028	55.20	23.86	3.46	31.34
Cut # 2	29.426	3.602	19.650	46.557	7.872	3.956	167.392	39.136	33.935	55.09	22.46	3.46	32.62
Cut # 3	36.524	8.054	-1.380	28.581	6.013	2.843	100.916	19.960	-8.285	54.13	20.86	3.44	33.27
Cut # 4	37.129	4.471	4.009	33.229	5.379	5.636	133.609	20.767	18.960	46.79	20.86	3.44	25.92
Cut # 5	30.400	3.319	4.129	24.057	3.475	5.012	80.933	13.955	15.253	41.91	20.83	3.43	21.08

Rock= Roubidoux Sandstone			Block # 1 (Dry)										
Data Window Cuts			Spacing			3 inch							
Cutter			Penetration			0.5 inch							
	Averages			Standard Deviations			Maximums			Start Position	End Position	Speed	Length of Cut
	Normal(kN)	Rolling(kN)	Side(kN)	Normal(kN)	Rolling(kN)	Side(kN)	Normal(kN)	Rolling(kN)	Side(kN)	(inches)	(inches)	(inch/sec)	(inch)
Cut # 1	36.721	8.348	-1.640	36.754	8.599	3.310	127.437	29.024	-13.519	48.20	23.35	3.47	24.84
Cut # 2	37.471	6.816	1.211	33.012	7.289	3.568	121.814	38.238	-10.151	48.48	23.64	3.46	24.84
Cut # 3	44.503	8.053	1.778	33.132	7.077	5.404	130.464	26.478	15.152	48.04	22.40	3.45	25.64
Cut # 4	74.608	16.007	-2.089	24.901	3.956	7.279	168.909	28.724	21.366	46.14	20.53	3.42	25.61
Cut # 5	51.644	6.238	5.030	19.235	5.556	6.987	118.765	21.389	15.529	45.51	20.27	3.44	25.24
Cut # 6	34.420	4.564	3.499	19.505	2.182	5.079	81.125	8.555	15.720	40.53	19.68	3.44	20.85

Rock= Roubidoux Sandstone			Block # 1 (Dry)										
Data Window Cuts			Spacing			4.5 inch							
Cutter			Penetration			0.25 inch							
	Averages			Standard Deviations			Maximums			Start Position	End Position	Speed	Length of Cut
	Normal(kN)	Rolling(kN)	Side(kN)	Normal(kN)	Rolling(kN)	Side(kN)	Normal(kN)	Rolling(kN)	Side(kN)	(inches)	(inches)	(inch/sec)	(inch)
Cut # 1	52.713	11.161	-2.428	19.276	3.715	5.110	5.755	20.307	-12.529	52.33	22.53	3.46	29.81
Cut # 2	89.195	15.097	3.149	32.878	4.753	7.025	23.172	24.144	23.172	53.48	20.27	3.44	33.22
Cut # 3	65.528	2.243	13.054	38.688	4.401	5.845	174.425	17.959	25.574	51.92	20.49	3.43	31.43

Rock= Roubidoux Sandstone			Block # 1 (Dry)										
Data Window Cuts			Spacing			4.5 inch							
Cutter			Penetration			0.375 inch							
	Averages			Standard Deviations			Maximums			Start Position	End Position	Speed	Length of Cut
	Normal(kN)	Rolling(kN)	Side(kN)	Normal(kN)	Rolling(kN)	Side(kN)	Normal(kN)	Rolling(kN)	Side(kN)	(inches)	(inches)	(inch/sec)	(inch)
Cut # 1	48.262	9.424	0.528	28.953	6.106	3.761	10.139	51.720	10.139	51.63	19.53	3.45	32.11
Cut # 2	77.307	14.776	1.576	27.670	5.457	4.185	164.316	28.791	13.536	51.67	21.39	3.43	30.28
Cut # 3	69.784	6.273	10.333	25.982	4.057	4.787	152.724	17.592	24.120	49.16	21.45	3.44	27.72

Rock= Roubidoux Sandstone			Block # 1 (Dry)										
Data Window Cuts			Spacing			4.5 inch							
Cutter			Long Bladed Disc			Penetration	0.5 inch						
	Averages			Standard Deviations			Maximums			Start Position	End Position	Speed	Length of Cut
	Normal(kN)	Rolling(kN)	Side(kN)	Normal(kN)	Rolling(kN)	Side(kN)	Normal(kN)	Rolling(kN)	Side(kN)	(inches)	(inches)	(inch/sec)	(inch)
Cut # 1	34.353	7.644	-1.530	28.022	7.004	5.129	125.013	29.064	-15.579	52.95	23.24	3.44	29.71
Cut # 2	71.476	13.012	2.484	39.479	7.584	4.569	175.303	31.563	16.840	53.23	21.78	3.43	31.45
Cut # 3	68.824	6.624	9.366	33.252	5.115	4.626	152.984	21.839	21.739	53.26	22.37	3.43	30.89

Rock= Roubidoux Sandstone			Block # 4 (Dry)										
Data Window Cuts			Spacing			5 inch							
Cutter			Long Bladed Disc			Penetration	0.25 inch						
	Averages			Standard Deviations			Maximums			Start Position	End Position	Speed	Length of Cut
	Normal(kN)	Rolling(kN)	Side(kN)	Normal(kN)	Rolling(kN)	Side(kN)	Normal(kN)	Rolling(kN)	Side(kN)	(inches)	(inches)	(inch/sec)	(inch)
Cut # 1	33.281	9.345	-3.794	24.894	6.328	4.102	103.794	25.087	-12.517	52.03	34.36	3.43	17.67
Cut # 2	58.845	13.601	1.134	25.034	4.995	5.866	119.876	26.188	-12.716	52.39	33.71	3.43	18.68
Cut # 3	35.814	5.426	3.737	28.471	4.471	3.175	101.951	16.564	11.443	54.00	30.09	3.42	23.91

Rock= Roubidoux Sandstone			Block # 4 (Dry)										
Data Window Cuts			Spacing			5 inch							
Cutter			Long Bladed Disc			Penetration	0.375 inch						
	Averages			Standard Deviations			Maximums			Start Position	End Position	Speed	Length of Cut
	Normal(kN)	Rolling(kN)	Side(kN)	Normal(kN)	Rolling(kN)	Side(kN)	Normal(kN)	Rolling(kN)	Side(kN)	(inches)	(inches)	(inch/sec)	(inch)
Cut # 1	32.831	9.610	-4.709	24.722	7.385	5.041	92.958	25.439	-14.769	54.56	32.12	3.48	22.44
Cut # 2	38.619	9.398	-1.265	28.677	7.823	3.333	121.953	32.563	-12.151	54.50	37.10	3.47	17.40
Cut # 3	63.266	12.927	2.461	38.449	7.569	5.015	188.289	35.989	15.724	54.12	30.62	3.45	23.50
Cut # 4	50.612	12.817	-3.031	20.640	5.276	5.476	107.218	25.260	-15.340	54.37	40.80	3.44	13.56

Rock= Roubidoux Sandstone			Block # 4 (Dry)										
Data Window Cuts			Spacing			5 inch							
Cutter			Long Bladed Disc			Penetration	0.5 inch						
	Averages			Standard Deviations			Maximums			Start Position	End Position	Speed	Length of Cut
	Normal(kN)	Rolling(kN)	Side(kN)	Normal(kN)	Rolling(kN)	Side(kN)	Normal(kN)	Rolling(kN)	Side(kN)	(inches)	(inches)	(inch/sec)	(inch)
Cut # 1	127.649	31.664	-4.617	46.322	11.588	5.411	246.148	61.654	-15.322	51.61	31.78	3.44	19.82
Cut # 2	94.224	22.269	-1.046	35.724	8.181	5.468	220.369	49.899	16.466	49.51	30.75	3.41	18.76
Cut # 3	68.314	16.985	-6.177	35.564	10.011	10.267	198.699	50.060	-24.197	53.20	30.14	3.45	23.06

Rock= Roubidoux Sandstone			Block # 4 (Dry)										
Data Window Cuts			Spacing			6 inch							
Cutter			Long Bladed Disc			Penetration	0.25 inch						
	Averages			Standard Deviations			Maximums			Start Position	End Position	Speed	Length of Cut
	Normal(kN)	Rolling(kN)	Side(kN)	Normal(kN)	Rolling(kN)	Side(kN)	Normal(kN)	Rolling(kN)	Side(kN)	(inches)	(inches)	(inch/sec)	(inch)
Cut # 1	56.755	12.606	0.420	23.953	5.503	3.209	118.858	31.267	8.439	53.00	32.05	3.44	20.96
Cut # 2	84.371	18.356	0.952	28.493	7.811	6.889	161.692	34.186	19.172	47.73	31.42	3.43	16.31
Cut # 3	35.025	8.709	-0.649	23.302	4.357	2.789	109.448	21.032	8.305	54.55	33.77	3.44	20.79

Rock= Roubidoux Sandstone			Block # 4 (Dry)										
Data Window Cuts			Spacing			6 inch							
Cutter			Long Bladed Disc			Penetration	0.375 inch						
	Averages			Standard Deviations			Maximums			Start Position	End Position	Speed	Length of Cut
	Normal(kN)	Rolling(kN)	Side(kN)	Normal(kN)	Rolling(kN)	Side(kN)	Normal(kN)	Rolling(kN)	Side(kN)	(inches)	(inches)	(inch/sec)	(inch)
Cut # 1	92.254	18.258	2.474	29.809	6.943	8.600	166.988	38.009	18.619	53.11	32.77	3.47	20.35
Cut # 2	104.074	20.409	3.696	43.620	9.949	5.607	225.859	50.950	18.018	52.60	30.15	3.45	22.45
Cut # 3	68.801	17.056	-2.504	26.165	7.599	5.621	130.394	37.216	-14.761	53.50	31.18	3.45	22.32

Rock= Roubidoux Sandstone			Block # 4 (Dry)										
Data Window Cuts			Spacing			6 inch							
Cutter			Long Bladed Disc			Penetration			0.5 inch				
	Averages			Standard Deviations			Maximums			Start Position	End Position	Speed	Length of Cut
	Normal(kN)	Rolling(kN)	Side(kN)	Normal(kN)	Rolling(kN)	Side(kN)	Normal(kN)	Rolling(kN)	Side(kN)	(inches)	(inches)	(inch/sec)	(inch)
Cut # 1	56.832	12.332	0.652	28.151	8.878	6.170	115.285	32.459	-11.791	53.38	33.39	3.48	19.99
Cut # 2	52.515	16.624	-7.192	36.439	10.766	5.664	153.827	46.382	-23.579	54.76	29.64	3.46	25.12
Cut # 3	58.875	12.612	2.396	27.980	6.623	4.700	132.748	33.095	10.840	52.91	31.98	3.47	20.92

## Disc Cutter Tests - Saturated Rock

Rock= Roubidoux Sandstone			Block # 2 (Saturated)											
Data Window Cuts			Spacing 3 inch											
Cutter	Long Bladed Disc		Penetration 0.25 inch											
	Averages			Standard Deviations			Maximums			Start Position	End Position	Speed	Length of Cut	
	Normal(kN)	Rolling(kN)	Side(kN)	Normal(kN)	Rolling(kN)	Side(kN)	Normal(kN)	Rolling(kN)	Side(kN)	(inches)	(inches)	(inch/sec)	(inch)	
Cut # 1	26.101	3.808	3.123	23.795	5.180	4.218	85.539	18.405	12.906	53.76	18.82	3.44	34.94	
Cut # 2	21.432	4.333	1.395	24.467	5.532	2.838	92.143	22.036	8.921	51.74	20.37	3.45	31.37	
Cut # 3	37.640	5.037	5.066	22.731	4.723	4.420	86.815	16.143	14.198	52.72	24.10	3.45	28.62	
Cut # 4	26.513	5.055	2.408	17.162	4.118	3.087	68.036	15.053	9.599	53.04	25.03	3.45	28.01	
Cut # 5	17.250	2.176	3.045	15.722	1.671	3.188	52.266	6.219	9.857	50.34	22.41	3.46	27.93	
Cut # 6	18.675	3.146	2.145	12.132	2.469	2.425	36.328	8.808	8.261	49.79	21.62	3.47	28.17	

Rock= Roubidoux Sandstone			Block # 2 (Saturated)												
Data Window Cuts			Spacing 3 inch												
Cutter	Long Bladed Disc		Penetration 0.375 inch												
	Averages			Standard Deviations			Maximums			Start Position	End Position		Speed	Length of Cut	
	Normal(kN)	Rolling(kN)	Side(kN)	Normal(kN)	Rolling(kN)	Side(kN)	Normal(kN)	Rolling(kN)	Side(kN)	(inches)	(inches)		(inch/sec)	(inch)	
Cut # 1	24.146	4.459	1.365	15.475	3.938	3.717	72.833	18.665	-9.536	54.98	18.55		3.44	36.43	
Cut # 2	21.817	5.520	-0.927	22.090	5.773	2.321	98.953	25.188	-7.043	55.62	18.01		3.45	37.61	
Cut # 3	25.413	2.155	3.432	14.414	6.773	4.427	72.522	17.419	11.116	54.21	16.59		3.46	37.62	
Cut # 4	16.049	2.148	2.782	14.926	4.014	3.177	69.221	15.914	11.079	54.47	17.93		3.46	36.54	
Cut # 5	25.542	4.908	1.294	16.041	5.362	3.902	85.528	20.026	8.960	52.98	18.26		3.46	34.73	
Cut # 6	26.728	1.430	5.762	15.116	2.209	3.832	60.592	6.684	12.636	51.67	19.65		3.46	32.02	

Rock= Roubidoux Sandstone			Block # 2 (Saturated)												
Data Window Cuts			Spacing 3 inch												
Cutter	Long Bladed Disc		Penetration 0.5 inch												
										Start Position	End Position	Speed	Length of Cut		
	Averages			Standard Deviations			Maximums								
	Normal(kN)	Rolling(kN)	Side(kN)	Normal(kN)	Rolling(kN)	Side(kN)	Normal(kN)	Rolling(kN)	Side(kN)	(inches)	(inches)	(inch/sec)	(inch)		
Cut # 1	36.185	0.744	6.903	14.955	5.174	2.135	72.582	11.483	11.672	50.60	20.10	3.46	30.51		
Cut # 2	38.235	5.313	4.626	22.097	4.553	3.671	94.360	21.268	15.938	52.43	18.44	3.45	33.99		
Cut # 3	56.798	11.199	2.073	20.178	6.248	6.317	115.901	26.429	13.485	52.52	21.86	3.45	30.66		
Cut # 4	39.282	8.286	1.076	36.380	7.884	3.529	126.047	28.160	10.878	47.95	20.24	3.45	27.71		
Cut # 5	58.666	8.950	5.794	12.673	4.278	2.983	90.604	19.115	12.369	45.54	30.59	3.43	14.95		

Rock= Roubidoux Sandstone			Block # 2 (Saturated)											
Data Window Cuts			Spacing 4.5 inch											
Cutter	Long Bladed Disc		Penetration 0.25 inch											
	Averages			Standard Deviations			Maximums			Start Position	End Position	Speed	Length of Cut	
	Normal(kN)	Rolling(kN)	Side(kN)	Normal(kN)	Rolling(kN)	Side(kN)	Normal(kN)	Rolling(kN)	Side(kN)	(inches)	(inches)	(inch/sec)	(inch)	
Cut # 1	35.308	7.204	1.905	20.396	3.177	3.876	94.122	17.921	12.937	52.65	20.37	3.44	32.28	
Cut # 2	35.667	4.902	5.019	36.391	6.355	4.804	128.342	26.603	14.779	53.41	20.71	3.43	32.70	
Cut # 3	44.136	10.295	1.716	31.939	7.963	3.656	107.429	29.350	-13.143	54.95	19.41	3.43	35.55	

Rock= Roubidoux Sandstone			Block # 2 (Saturated)											
Data Window Cuts			Spacing 4.5 inch											
Cutter	Long Bladed Disc		Penetration 0.375 inch											
	Averages			Standard Deviations			Maximums			Start Position	End Position	Speed	Length of Cut	
	Normal(kN)	Rolling(kN)	Side(kN)	Normal(kN)	Rolling(kN)	Side(kN)	Normal(kN)	Rolling(kN)	Side(kN)	(inches)	(inches)	(inch/sec)	(inch)	
Cut # 1	52.708	8.110	5.629	14.277	3.974	3.351	88.134	20.426	13.887	53.25	20.03	3.43	33.22	
Cut # 2	46.797	7.112	4.853	18.670	4.798	2.381	102.135	21.979	11.840	52.92	16.28	3.43	36.63	
Cut # 3	61.583	17.062	-3.512	20.723	6.542	4.961	130.403	36.778	-21.302	54.17	18.71	3.43	35.46	

Rock= Roubidoux Sandstone			Block # 2 (Saturated)										
Data Window Cuts			Spacing			4.5 inch							
Cutter			Long Bladed Disc			Penetration	0.5 inch						
	Averages			Standard Deviations			Maximums			Start Position	End Position	Speed	Length of Cut
	Normal(kN)	Rolling(kN)	Side(kN)	Normal(kN)	Rolling(kN)	Side(kN)	Normal(kN)	Rolling(kN)	Side(kN)	(inches)	(inches)	(inch/sec)	(inch)
Cut # 1	65.183	12.126	4.908	17.582	5.208	3.435	118.437	27.263	15.743	53.97	16.40	3.44	37.57
Cut # 2	57.087	7.615	6.609	17.334	5.589	4.459	103.900	23.965	17.414	53.41	17.55	3.44	35.86
Cut # 3	39.649	6.264	4.298	16.127	4.505	3.712	90.002	21.417	10.873	55.40	18.79	3.44	36.61

Rock= Roubidoux Sandstone			Block # 3 (Saturated)										
Data Window Cuts			Spacing			5 inch							
Cutter			Long Bladed Disc			Penetration	0.25 inch						
	Averages			Standard Deviations			Maximums			Start Position	End Position	Speed	Length of Cut
	Normal(kN)	Rolling(kN)	Side(kN)	Normal(kN)	Rolling(kN)	Side(kN)	Normal(kN)	Rolling(kN)	Side(kN)	(inches)	(inches)	(inch/sec)	(inch)
Cut # 1	47.394	12.897	-7.202	22.424	5.980	5.680	102.784	25.339	-17.092	49.40	19.37	3.44	30.04
Cut # 2	34.065	7.960	-1.333	14.167	4.536	4.763	80.610	18.797	-13.417	54.48	19.23	3.44	35.25
Cut # 3	12.466	2.984	-0.636	14.333	3.688	1.593	58.991	14.672	-6.234	51.72	28.16	3.44	23.56

Rock= Roubidoux Sandstone			Block # 3 (Saturated)										
Data Window Cuts			Spacing			5 inch							
Cutter			Long Bladed Disc			Penetration	0.375 inch						
	Averages			Standard Deviations			Maximums			Start Position	End Position	Speed	Length of Cut
	Normal(kN)	Rolling(kN)	Side(kN)	Normal(kN)	Rolling(kN)	Side(kN)	Normal(kN)	Rolling(kN)	Side(kN)	(inches)	(inches)	(inch/sec)	(inch)
Cut # 1	55.246	10.610	1.151	19.859	7.152	6.830	116.029	30.705	14.594	56.79	21.37	3.44	35.42
Cut # 2	60.222	12.788	1.549	33.855	5.275	5.134	151.125	27.235	17.226	52.53	21.26	3.43	31.27
Cut # 3	19.131	4.969	-0.933	20.580	4.963	1.910	83.373	18.447	-5.987	49.14	27.08	3.42	22.06

Rock= Roubidoux Sandstone			Block # 3 (Saturated)										
Data Window Cuts			Spacing			5 inch							
Cutter			Long Bladed Disc			Penetration	0.5 inch						
	Averages			Standard Deviations			Maximums			Start Position	End Position	Speed	Length of Cut
	Normal(kN)	Rolling(kN)	Side(kN)	Normal(kN)	Rolling(kN)	Side(kN)	Normal(kN)	Rolling(kN)	Side(kN)	(inches)	(inches)	(inch/sec)	(inch)
Cut # 1	84.430	11.760	6.544	27.438	6.909	5.642	169.045	34.156	24.930	54.32	16.91	3.44	37.40
Cut # 2	38.981	3.857	4.463	22.515	5.826	3.228	126.621	32.200	12.175	53.50	19.69	3.44	33.81
Cut # 3	55.585	13.334	-1.718	38.755	8.939	5.228	138.436	29.205	-15.364	53.09	35.08	3.44	18.01

Rock= Roubidoux Sandstone			Block # 3 (Saturated)										
Data Window Cuts			Spacing			6 inch							
Cutter			Long Bladed Disc			Penetration	0.25 inch						
	Averages			Standard Deviations			Maximums			Start Position	End Position	Speed	Length of Cut
	Normal(kN)	Rolling(kN)	Side(kN)	Normal(kN)	Rolling(kN)	Side(kN)	Normal(kN)	Rolling(kN)	Side(kN)	(inches)	(inches)	(inch/sec)	(inch)
Cut # 1	57.757	8.064	3.876	35.425	5.746	5.214	156.398	20.347	17.713	56.45	16.91	3.45	39.53
Cut # 2	57.476	10.722	0.387	36.531	7.848	5.038	136.417	23.556	12.685	56.84	28.13	3.45	28.71
Cut # 3	16.571	3.016	1.100	11.038	2.275	1.949	55.140	9.534	5.429	53.17	28.78	3.45	24.39

Rock= Roubidoux Sandstone			Block # 3 (Saturated)										
Data Window Cuts			Spacing			6 inch							
Cutter			Long Bladed Disc			Penetration	0.375 inch						
	Averages			Standard Deviations			Maximums			Start Position	End Position	Speed	Length of Cut
	Normal(kN)	Rolling(kN)	Side(kN)	Normal(kN)	Rolling(kN)	Side(kN)	Normal(kN)	Rolling(kN)	Side(kN)	(inches)	(inches)	(inch/sec)	(inch)
Cut # 1	82.006	4.571	10.888	29.381	6.184	3.852	193.051	26.196	25.180	55.95	19.93	3.43	36.03
Cut # 2	98.788	20.815	-1.999	33.826	7.435	4.975	217.347	45.416	-14.459	54.57	22.22	3.41	32.35
Cut # 3	42.680	11.801	-5.168	15.928	3.629	2.621	93.166	27.072	-10.655	50.35	32.51	3.41	17.83



Rock= Roubidoux Sandstone			Block # 3 (Saturated)										
Data Window Cuts			Spacing 6 inch										
Cutter Long Bladed Disc			Penetration 0.5 inch										
	Averages			Standard Deviations			Maximums			Start Position	End Position	Speed	Length of Cut
	Normal(kN)	Rolling(kN)	Side(kN)	Normal(kN)	Rolling(kN)	Side(kN)	Normal(kN)	Rolling(kN)	Side(kN)	(inches)	(inches)	(inch/sec)	(inch)
Cut # 1	100.701	12.018	9.014	38.559	7.589	4.153	222.003	39.043	21.476	54.18	25.90	3.44	28.27
Cut # 2	54.215	13.785	-4.825	35.962	10.284	5.022	145.906	37.310	-17.698	55.84	33.53	3.45	22.32
Cut # 3	0.781	0.010	0.467	1.056	0.283	0.501	6.390	1.382	1.970	51.85	36.41	3.46	15.45

Rock= Roubidoux Sandstone			Block # 5 (Saturated)										
Data Window Cuts			Spacing 4.5 inch										
Cutter Long Bladed Disc			Penetration 0.25 inch										
	Averages			Standard Deviations			Maximums			Start Position	End Position	Speed	Length of Cut
	Normal(kN)	Rolling(kN)	Side(kN)	Normal(kN)	Rolling(kN)	Side(kN)	Normal(kN)	Rolling(kN)	Side(kN)	(inches)	(inches)	(inch/sec)	(inch)
Cut # 1	67.729	6.220	8.310	24.328	4.723	2.728	143.654	23.652	12.955	49.29	26.13	3.47	23.17
Cut # 2	61.751	11.183	2.870	28.525	5.452	2.514	125.158	23.567	9.481	50.45	20.38	3.47	30.07
Cut # 3	40.389	6.527	3.335	28.506	5.876	2.210	98.383	21.246	10.046	52.32	20.61	3.47	31.72

Rock= Roubidoux Sandstone			Block # 5 (Saturated)										
Data Window Cuts			Spacing 4.5 inch										
Cutter Long Bladed Disc			Penetration 0.375 inch										
	Averages			Standard Deviations			Maximums			Start Position	End Position	Speed	Length of Cut
	Normal(kN)	Rolling(kN)	Side(kN)	Normal(kN)	Rolling(kN)	Side(kN)	Normal(kN)	Rolling(kN)	Side(kN)	(inches)	(inches)	(inch/sec)	(inch)
Cut # 1	59.617	8.404	4.866	26.291	5.730	2.557	119.634	21.289	10.487	51.32	21.82	3.48	29.49
Cut # 2	33.449	3.356	4.782	27.725	4.194	3.286	98.684	14.985	11.198	50.54	22.69	3.47	27.85
Cut # 3	64.305	12.496	1.651	22.646	7.770	3.913	122.445	28.036	8.248	52.05	24.31	3.47	27.73

Rock= Roubidoux Sandstone			Block # 5 (Saturated)										
Data Window Cuts			Spacing 4.5 inch										
Cutter Long Bladed Disc			Penetration 0.5 inch										
	Averages			Standard Deviations			Maximums			Start Position	End Position	Speed	Length of Cut
	Normal(kN)	Rolling(kN)	Side(kN)	Normal(kN)	Rolling(kN)	Side(kN)	Normal(kN)	Rolling(kN)	Side(kN)	(inches)	(inches)	(inch/sec)	(inch)
Cut # 1	58.201	3.746	8.440	37.201	5.992	5.485	138.945	18.121	19.121	51.32	21.82	3.46	29.49
Cut # 2	35.283	7.281	-0.173	21.138	6.842	5.873	93.621	21.470	-13.510	50.54	23.98	3.45	26.56
Cut # 3	94.719	18.003	-0.110	43.842	10.670	4.674	191.497	45.373	-12.862	52.05	24.31	3.45	27.73

Rock= Roubidoux Sandstone			Block # 5 (Saturated)										
Data Window Cuts			Spacing 6 inch										
Cutter Long Bladed Disc			Penetration 0.25 inch										
	Averages			Standard Deviations			Maximums			Start Position	End Position	Speed	Length of Cut
	Normal(kN)	Rolling(kN)	Side(kN)	Normal(kN)	Rolling(kN)	Side(kN)	Normal(kN)	Rolling(kN)	Side(kN)	(inches)	(inches)	(inch/sec)	(inch)
Cut # 1	37.296	8.759	0.856	19.867	5.102	2.237	83.670	21.634	7.728	51.79	21.92	3.49	29.86
Cut # 2	41.489	9.115	0.179	12.832	3.683	2.977	85.416	18.584	5.657	51.55	18.43	3.48	33.12
Cut # 3	43.411	11.336	-2.531	12.675	2.651	2.579	82.211	17.920	7.108	51.58	21.17	3.48	30.40

Rock= Roubidoux Sandstone			Block # 5 (Saturated)										
Data Window Cuts			Spacing 6 inch										
Cutter Long Bladed Disc			Penetration 0.375 inch										
	Averages			Standard Deviations			Maximums			Start Position	End Position	Speed	Length of Cut
	Normal(kN)	Rolling(kN)	Side(kN)	Normal(kN)	Rolling(kN)	Side(kN)	Normal(kN)	Rolling(kN)	Side(kN)	(inches)	(inches)	(inch/sec)	(inch)
Cut # 1	62.506	14.257	-1.125	19.988	3.813	3.782	118.711	24.021	-11.154	50.53	21.53	3.45	29.00
Cut # 2	38.881	7.447	-0.980	20.796	7.376	4.682	111.538	30.125	-12.271	45.10	19.20	3.45	25.91
Cut # 3	41.278	8.947	-0.061	18.228	6.172	4.494	88.151	24.430	9.741	44.16	21.42	3.46	22.74

Rock= Roubidoux Sandstone			Block # 5 (Saturated)										
Data Window Cuts			Spacing 6 inch										
Cutter Long Bladed Disc			Penetration 0.625 inch										
	Averages			Standard Deviations			Maximums			Start Position	End Position	Speed	Length of Cut
	Normal(kN)	Rolling(kN)	Side(kN)	Normal(kN)	Rolling(kN)	Side(kN)	Normal(kN)	Rolling(kN)	Side(kN)	(inches)	(inches)	(inch/sec)	(inch)
Cut # 1	89.271	20.436	-2.648	43.168	17.058	9.844	193.459	52.802	-23.994	49.29	26.13	3.46	23.17
Cut # 2	70.243	17.996	-2.271	27.283	9.775	7.773	164.906	46.088	-23.532	50.45	20.38	3.44	30.07
Cut # 3	54.065	7.237	6.499	22.576	8.562	3.919	116.502	33.288	13.366	52.32	20.61	3.45	31.72

Rock= Roubidoux Sandstone			Block # 5 (Saturated)										
Data Window Cuts			Spacing 9 inch										
Cutter Long Bladed Disc			Penetration 0.25 inch										
	Averages			Standard Deviations			Maximums			Start Position	End Position	Speed	Length of Cut
	Normal(kN)	Rolling(kN)	Side(kN)	Normal(kN)	Rolling(kN)	Side(kN)	Normal(kN)	Rolling(kN)	Side(kN)	(inches)	(inches)	(inch/sec)	(inch)
Cut # 1	20.293	3.624	-0.187	14.956	2.137	3.253	50.775	10.269	7.643	51.96	27.52	3.49	24.44
Cut # 2	56.742	10.617	1.395	19.741	4.426	1.646	104.503	20.190	7.446	53.66	29.84	3.48	23.82
Cut # 3	56.191	10.024	2.936	18.575	3.840	2.589	106.862	21.560	12.130	43.32	25.53	3.48	17.79

Rock= Roubidoux Sandstone			Block # 5 (Saturated)										
Data Window Cuts			Spacing 9 inch										
Cutter Long Bladed Disc			Penetration 0.625 inch										
	Averages			Standard Deviations			Maximums			Start Position	End Position	Speed	Length of Cut
	Normal(kN)	Rolling(kN)	Side(kN)	Normal(kN)	Rolling(kN)	Side(kN)	Normal(kN)	Rolling(kN)	Side(kN)	(inches)	(inches)	(inch/sec)	(inch)
Cut # 1	72.672	6.903	9.566	19.071	6.087	4.292	140.845	22.999	19.754	52.63	20.72	3.47	31.91
Cut # 2	109.146	28.360	-2.661	43.048	11.638	5.135	204.439	57.730	-17.567	52.66	19.17	3.44	33.49
Cut # 3	39.385	13.632	-8.569	15.318	5.406	6.322	76.860	26.098	-21.467	54.03	21.62	3.44	32.41

### Sieve Analysis Data for Dry CCS Disc Cutter Tests

<i>s</i>	<i>p</i>	<i>s/p</i>	Caught on 50.8 mm	Caught on 25.4 mm	Caught on 9.42 mm	Caught on 1.65 mm	Passing 1.65 mm	Total
(mm)	(mm)		(kg)	(kg)	(kg)	(kg)	(kg)	(kg)
76.2	6.4	12	0.493	1.269	0.561	0.287	1.263	3.872
76.2	9.5	8	0.704	1.886	1.133	0.437	1.932	6.092
76.2	12.7	6	0.742	1.824	1.51	0.678	3.426	8.18
114.3	6.4	18	2.68	0.57	0.465	0.193	1.198	5.106
114.3	9.5	12	1.216	0.848	0.678	0.276	1.898	4.916
114.3	12.7	9	3.355	2.174	1.645	0.571	2.307	10.052
127	6.4	20	3.346	0.555	0.254	0.116	0.953	5.224
127	9.5	13.3	2.965	1.336	0.732	0.346	1.173	6.552
127	12.7	10	2.852	0.926	0.71	0.299	1.087	5.874
152.4	6.4	24	2.371	0.767	0.482	0.205	0.903	4.728
152.4	9.5	16	3.178	0.979	0.537	0.282	1.215	6.191
152.4	12.7	12	6.394	0.808	0.723	0.295	1.872	10.092
152.4	15.9	9.6	6.783	1.013	0.491	--	2.067	10.353
228.6	15.9	14.4	3.562	0.722	0.295	--	0.959	5.537
228.6	19.05	12	7.191	0.690	0.327	--	1.166	9.374
228.6	22.23	10.3	3.438	1.127	0.789	--	1.988	7.341
254	19.05	13.3	8.837	1.364	0.801	--	1.259	12.260
254	25.4	10	12.130	1.423	0.907	--	1.023	15.483
304.8	22.23	13.7	16.047	0.922	0.485	--	2.568	20.021
304.8	19.05	16	9.931	0.818	0.330	--	2.365	13.444
304.8	25.4	12	18.109	1.466	0.676	--	4.713	24.964

**Sieve Analysis Data for Saturated CCS Disc Cutter Tests**

<i>s</i>	<i>p</i>	<i>s/p</i>	Caught on 50.8 mm	Caught on 25.4 mm	Caught on 9.42 mm	Caught on 1.65 mm	Passing 1.65 mm	Total
(mm)	(mm)		(kg)	(kg)	(kg)	(kg)	(kg)	(kg)
76.2	6.4	12	0.526	1.161	0.66	0.443	1.873	4.663
76.2	9.5	8	3.019	1.653	1.342	0.866	3.797	10.677
76.2	12.7	6	1.126	1.404	1.381	0.848	4.567	9.326
114.3	6.4	18	2.588	1.234	0.752	0.403	2.288	7.264
114.3	9.5	12	1.557	0.627	0.523	0.282	2.191	5.180
114.3	12.7	9	3.521	1.114	0.482	0.352	3.105	8.573
127	6.4	20	1.07	0.789	0.688	0.266	1.199	4.012
127	9.5	13.3	3.034	0.937	0.693	0.319	1.903	6.886
127	12.7	10	4.762	1.108	0.918	0.344	2.664	9.796
152.4	6.4	24	2.854	0.570	0.461	0.161	1.283	5.329
152.4	9.5	16	7.705	1.197	0.640	0.304	1.653	11.498
152.4	12.7	12	3.713	1.157	0.475	0.306	1.709	7.36
152.4	15.9	9.6	11.471	2.079	1.444	0.512	2.683	18.189
228.6	6.35	36	0.148	0.38	0.217	0.11	0.95	1.805
228.6	15.9	14.4	18.835	1.164	0.838	0.092	3.005	23.934

## APPENDIX C.

### DRAG PICK CUTTING FORCES AND SIEVE ANALYSIS DATA

## Radial Drag Pick Tests - Dry Rock

Rock= Roubidoux Sandstone			Block # 1 (Dry)																
Data Window Cuts			Spacing			1 inch													
Cutter	Radial Pick		Depth of cut			0.125 inch													
	Averages			Standard Deviations			Maximums			Start Position	End Position	Speed	Length of Cut						
	Normal(kN)	Cutting(kN)	Side(kN)	Normal(kN)	Cutting(kN)	Side(kN)	Normal(kN)	Cutting(kN)	Side(kN)	(inches)	(inches)	(inch/sec)	(inch)						
Cut # 1	4.473	8.236	-1.742	2.311	4.902	1.441	13.309	27.837	-5.774	48.43	24.67	3.46	23.75						
Cut # 2	3.489	5.378	1.042	2.227	3.950	0.881	11.712	21.297	4.652	48.34	25.95	3.46	22.38						
Cut # 3	3.685	5.592	1.587	2.273	3.975	1.215	10.525	20.388	5.350	47.58	26.55	3.46	21.03						
Cut # 4	3.004	4.433	0.719	2.287	3.824	0.653	12.096	21.046	3.226	47.88	24.99	3.45	22.89						
Cut # 5	3.256	4.963	0.662	2.388	4.040	0.812	12.104	21.191	4.417	47.46	24.31	3.46	23.16						
Cut # 6	3.005	3.992	0.650	2.274	3.340	0.673	11.159	16.651	3.061	47.25	25.29	3.45	21.96						
Cut # 7	2.656	3.368	0.885	2.349	3.257	0.869	11.811	15.577	3.898	46.89	25.41	3.49	21.48						
Cut # 8	2.607	3.314	0.437	2.422	3.306	0.666	11.815	16.186	3.089	47.09	25.46	3.49	21.63						
Cut # 9	2.842	3.546	1.112	2.291	3.083	0.873	9.818	14.202	4.120	47.14	25.71	3.48	21.43						
Cut # 10	5.303	7.169	0.852	3.955	5.569	0.625	18.638	25.407	3.969	46.40	25.61	3.47	20.79						
Cut # 11	4.073	5.265	1.198	3.266	4.513	1.037	17.301	24.059	4.999	47.26	25.11	3.47	22.14						
Cut # 12	5.004	6.637	1.162	3.086	4.548	0.977	17.839	25.475	5.641	47.01	26.13	3.47	20.88						
Cut # 13	4.386	5.101	1.379	2.997	3.891	1.025	16.095	20.137	5.025	46.59	25.58	3.47	21.00						
Cut # 14	5.372	6.785	0.706	2.770	4.044	0.706	15.908	22.804	3.685	46.46	26.34	3.46	20.12						
Cut # 15	5.659	7.074	1.244	3.215	4.481	0.807	16.442	22.826	4.135	46.76	26.59	3.46	20.17						
Cut # 16	5.337	7.846	1.134	4.238	5.906	0.912	24.098	34.766	4.883	44.85	24.70	3.46	20.15						
Cut # 17	3.689	4.461	1.374	3.082	3.964	0.769	13.070	18.870	4.347	45.08	26.46	3.46	18.63						

Rock= Roubidoux Sandstone			Block # 1 (Dry)																
Data Window Cuts			Spacing			1 inch													
Cutter	Radial Pick		Depth of cut			0.25 inch													
	Averages			Standard Deviations			Maximums			Start Position	End Position	Speed	Length of Cut						
	Normal(kN)	Cutting(kN)	Side(kN)	Normal(kN)	Cutting(kN)	Side(kN)	Normal(kN)	Cutting(kN)	Side(kN)	(inches)	(inches)	(inch/sec)	(inch)						
Cut # 1	5.131	7.663	0.404	2.600	4.412	0.841	18.014	28.817	3.760	47.65	22.69	3.47	24.96						
Cut # 2	5.137	7.635	1.792	2.709	4.372	1.170	18.775	29.314	6.806	47.70	22.64	3.46	25.06						
Cut # 3	5.465	7.943	1.345	3.576	5.792	1.134	20.730	31.910	6.170	47.56	23.32	3.45	24.24						
Cut # 4	5.535	7.842	3.023	3.793	5.468	1.922	23.288	32.986	8.561	47.82	23.74	3.45	24.08						
Cut # 5	6.535	9.686	1.887	3.728	6.067	1.338	24.543	43.206	7.700	46.81	23.79	3.44	23.02						
Cut # 6	7.369	8.712	3.086	4.317	5.491	2.046	22.806	29.247	10.849	47.58	23.88	3.44	23.70						
Cut # 7	7.175	9.135	1.732	4.438	5.620	1.200	22.177	29.006	6.344	46.83	23.59	3.43	23.24						
Cut # 8	7.234	8.954	2.419	5.103	6.745	1.769	26.221	34.612	8.741	46.68	23.81	3.42	22.88						
Cut # 9	6.926	9.239	3.237	4.695	6.269	2.497	26.530	34.666	10.485	46.78	24.45	3.43	22.34						
Cut # 10	6.754	8.584	2.731	4.123	5.617	1.785	25.388	34.418	8.551	46.69	25.55	3.43	21.14						
Cut # 11	7.011	8.381	2.553	4.097	5.550	1.735	21.560	28.464	8.871	46.74	25.98	3.43	20.76						
Cut # 12	5.299	7.551	0.870	3.926	5.881	0.882	20.740	33.492	4.848	46.60	25.25	3.43	21.35						
Cut # 13	4.314	5.336	1.614	3.401	4.527	1.429	20.927	24.422	8.067	45.66	25.87	3.43	19.79						
Cut # 14	6.450	7.995	1.550	3.584	4.857	0.933	22.520	30.299	5.969	46.85	25.84	3.43	21.00						
Cut # 15	6.682	8.363	3.905	4.059	5.435	2.380	26.137	32.984	11.349	45.99	27.46	3.42	18.53						
Cut # 16	6.328	8.016	2.015	4.201	5.822	1.448	24.455	37.423	7.920	46.00	24.89	3.42	21.11						
Cut # 17	10.934	15.288	9.293	4.660	6.107	1.799	32.245	44.356	15.149	44.57	26.14	3.40	18.44						

Rock= Roubidoux Sandstone			Block # 1 (Dry)																
Data Window Cuts			Spacing			1 inch													
Cutter	Radial Pick		Depth of cut			0.375 inch													
	Averages			Standard Deviations			Maximums			Start Position	End Position	Speed	Length of Cut						
	Normal(kN)	Cutting(kN)	Side(kN)	Normal(kN)	Cutting(kN)	Side(kN)	Normal(kN)	Cutting(kN)	Side(kN)	(inches)	(inches)	(inch/sec)	(inch)						
Cut # 1	-89.078	-89.444	-19.091	15.614	12.526	6.156	-54.945	-62.763	-42.673	88.74	88.44	0.02	0.30						
Cut # 2	10.325	14.989	6.135	5.271	8.207	3.557	30.798	52.099	18.531	48.27	24.16	3.34	24.11						
Cut # 3	9.295	13.249	4.992	6.557	9.915	3.205	39.391	62.986	15.219	47.83	24.13	3.47	23.71						
Cut # 4	8.078	11.701	4.949	4.298	7.014	2.286	30.594	44.393	13.825	47.97	24.54	3.46	23.43						
Cut # 5	6.764	10.150	3.066	4.487	7.072	2.270	25.925	42.581	12.702	47.10	24.06	3.46	23.04						
Cut # 6	6.947	8.858	2.587	4.381	5.984	1.672	24.931	35.848	7.772	47.44	24.31	3.45	23.13						
Cut # 7	10.421	11.128	4.503	7.324	7.169	2.084	41.968	49.052	12.037	46.64	24.65	3.42	21.98						
Cut # 8	9.379	11.455	3.562	6.991	9.289	2.144	40.354	55.345	12.121	46.99	25.20	3.43	21.78						
Cut # 9	6.991	9.253	2.379	6.914	9.747	2.340	37.223	54.250	11.193	46.70	26.88	3.41	19.82						
Cut # 10	1.116	2.303	0.463	1.335	2.933	0.593	8.582	18.247	3.638	46.53	25.13	3.45	21.40						
Cut # 11	1.372	2.267	0.573	1.390	2.644	0.649	10.347	18.324	3.572	46.43	25.11	3.49	21.32						
Cut # 12	1.795	3.097	0.593	1.939	3.587	0.743	15.489	25.540	5.244	46.99	25.42	3.48	21.57						
Cut # 13	1.968	3.014	0.804	1.698	3.132	0.799	11.978	20.559	4.465	46.53	26.88	3.48	19.65						
Cut # 14	2.493	3.847	1.137	1.988	3.677	1.136	11.394	21.798	7.189	46.30	27.00	3.48	19.30						
Cut # 15	2.823	4.356	1.116	2.098	3.773	1.000	12.584	21.813	5.312	46.30	25.90	3.47	20.40						
Cut # 16	2.161	3.212	0.744	2.004	3.499	0.768	11.814	21.206	4.293	45.50	26.21	3.31	19.29						
Cut # 17	2.536	3.767	0.964	1.914	3.504	1.021	10.591	19.504	5.161	47.14	26.71	3.47	20.43						
Load Cell Not Excited-Values Discarded																			

Rock= Roubidoux Sandstone			Block # 1 (Dry)													
Data Window Cuts			Spacing		1 inch											
Cutter      Radial Pick			Depth of cut		0.5 inch											
	Averages			Standard Deviations			Maximums			Start Position	End Position	Speed	Length of Cut			
	Normal(kN)	Cutting(kN)	Side(kN)	Normal(kN)	Cutting(kN)	Side(kN)	Normal(kN)	Cutting(kN)	Side(kN)	(inches)	(inches)	(inch/sec)	(inch)			
Cut # 1	6.984	13.538	-0.109	6.338	11.212	1.457	41.973	59.094	7.289	47.26	22.51	3.48	24.75			
Cut # 2	2.875	4.937	1.310	2.507	4.588	1.671	14.721	30.491	9.477	47.40	22.54	3.48	24.85			
Cut # 3	3.652	6.380	1.853	3.740	6.818	2.002	28.426	50.855	11.054	47.00	23.30	3.44	23.70			
Cut # 4	4.226	7.406	1.945	3.858	7.473	2.080	30.568	50.750	13.300	47.45	23.53	3.46	23.93			
Cut # 5	4.244	7.009	2.829	2.868	5.664	2.464	17.595	33.354	11.240	47.03	23.87	3.46	23.15			
Cut # 6	5.587	9.176	2.803	4.314	7.492	2.529	26.013	39.929	11.641	46.54	23.76	3.45	22.78			
Cut # 7	3.882	6.258	1.700	4.010	6.718	2.189	24.547	38.031	11.976	46.45	25.13	3.45	21.31			
Cut # 8	6.048	8.665	2.513	6.260	8.887	2.460	39.451	50.626	12.141	46.50	26.92	3.46	19.59			
Cut # 9	6.603	9.058	2.698	7.375	9.456	2.984	40.226	51.459	16.203	46.79	26.68	3.41	20.10			
Cut # 10	4.938	7.222	1.996	5.107	6.813	1.799	31.575	40.463	11.114	46.58	27.03	3.45	19.54			
Cut # 11	6.127	7.919	2.562	6.274	8.088	2.687	30.961	37.243	13.229	46.33	26.72	3.45	19.61			
Cut # 12	8.667	10.433	2.203	9.423	11.108	2.341	37.298	45.035	12.751	46.51	29.12	3.45	17.39			
Cut # 13	4.850	7.312	2.416	5.837	8.645	2.206	30.528	47.552	10.658	45.97	26.69	3.45	19.28			
Cut # 14	2.708	4.707	1.414	2.403	4.808	1.510	17.646	29.185	7.274	46.30	26.45	3.44	19.85			
Cut # 15	4.031	6.488	2.121	3.774	5.536	1.685	23.989	33.872	9.508	45.64	26.82	3.44	18.82			
Cut # 16	2.023	3.325	0.748	1.806	3.146	0.884	11.640	16.348	4.704	45.22	28.06	3.43	17.16			
Cut # 17	2.951	4.849	1.798	1.473	2.852	0.963	9.260	16.351	5.063	45.27	28.25	3.41	17.02			

Rock= Roubidoux Sandstone			Block # 1 (Dry)											
Data Window Cuts			Spacing			2 Inch								
Cutter			Radial Pick			Depth of cut			0.125 inch					
	Averages			Standard Deviations			Maximums			Start Position	End Position	Speed	Length of Cut	
	Normal(kN)	Cutting(kN)	Side(kN)	Normal(kN)	Cutting(kN)	Side(kN)	Normal(kN)	Cutting(kN)	Side(kN)	(inches)	(inches)	(inch/sec)	(inch)	
Cut # 1	6.789	8.013	-0.290	8.239	9.328	1.291	46.476	48.344	-4.739	48.59	22.79	3.44	25.80	
Cut # 2	8.451	11.072	3.156	9.581	12.535	3.229	55.810	68.767	12.939	47.61	22.92	3.43	24.69	
Cut # 3	7.818	9.519	1.549	9.931	11.810	2.204	47.389	55.047	11.497	47.68	23.84	3.44	23.84	
Cut # 4	8.500	9.918	1.396	13.254	14.480	1.874	93.382	90.160	10.401	47.57	25.77	3.44	21.80	
Cut # 5	5.799	6.872	0.379	6.186	8.023	1.161	29.288	34.377	-5.845	46.83	25.67	3.44	21.16	
Cut # 6	8.830	8.884	1.905	9.186	9.462	1.812	46.130	40.451	8.878	46.96	27.55	3.44	19.41	
Cut # 7	6.749	7.544	1.313	8.522	9.605	1.237	47.406	51.343	6.717	47.22	26.68	3.43	20.54	
Cut # 8	5.657	6.320	0.921	6.901	8.018	0.996	48.431	50.503	5.043	47.36	27.04	3.43	20.32	
Cut # 9	8.627	10.202	3.464	7.660	8.655	2.180	42.932	42.057	10.174	46.86	29.06	3.43	17.80	

Rock= Roubidoux Sandstone			Block # 1 (Dry)														
Data Window Cuts			Spacing 2 inch														
Cutter Radial Pick			Depth of cut 0.25 inch														
	Averages			Standard Deviations			Maximums				Start Position	End Position		Speed	Length of Cut		
	Normal(kN)	Cutting(kN)	Side(kN)	Normal(kN)	Cutting(kN)	Side(kN)	Normal(kN)	Cutting(kN)	Side(kN)		(inches)	(inches)		(inch/sec)	(inch)		
Cut # 1	6.874	13.969	0.165	12.201	16.187	2.713	87.141	95.311	15.736		47.97	23.06		3.44	24.91		
Cut # 2	0.792	2.366	0.370	1.286	3.520	0.679	10.305	27.774	5.460		46.94	23.19		3.47	23.75		
Cut # 3	0.632	2.231	0.284	0.728	2.494	0.425	6.795	17.126	2.305		47.49	23.53		3.43	23.96		
Cut # 4	0.731	2.321	0.405	0.682	2.148	0.495	4.062	11.968	2.547		46.84	24.95		3.43	21.89		
Cut # 5	1.061	3.268	0.627	0.880	2.953	0.613	6.303	19.517	4.564		46.90	24.95		3.45	21.96		
Cut # 6	1.149	2.787	0.558	1.011	2.665	0.506	6.690	17.561	3.466		46.64	24.77		3.45	21.87		
Cut # 7	1.276	3.302	0.363	1.257	3.163	0.513	8.616	21.390	2.389		46.76	26.27		3.44	20.49		
Cut # 8	1.379	3.194	0.647	1.317	3.082	0.553	9.791	21.887	2.994		45.66	26.80		3.40	18.86		
Cut # 9	1.871	4.389	0.984	1.421	3.738	0.701	9.790	21.187	4.249		46.35	27.86		3.43	18.48		

Rock= Roubidoux Sandstone		Block #1 (Dry)															
Data Window Cuts		Spacing 2 inch															
Cutter	Radial Pick	Depth of cut 0.375 inch															
		Averages			Standard Deviations			Maximums			Start Position	End Position	Speed	Length of Cut			
		Normal(kN)	Cutting(kN)	Side(kN)	Normal(kN)	Cutting(kN)	Side(kN)	Normal(kN)	Cutting(kN)	Side(kN)	(inches)	(inches)	(inch/sec)	(inch)			
Cut # 1		2.045	3.879	0.221	1.902	3.690	0.503	11.882	21.806	2.607	48.63	22.26	3.46	26.38			
Cut # 2		2.433	4.979	1.211	2.976	5.805	1.374	20.790	37.337	7.139	48.15	22.53	3.46	25.62			
Cut # 3		2.825	5.172	1.497	2.931	5.259	1.545	18.532	30.314	7.348	47.60	23.48	3.44	24.12			
Cut # 4		4.036	7.191	0.719	4.231	7.452	0.977	25.953	44.318	5.221	46.64	24.54	3.44	22.10			
Cut # 5		3.379	6.311	1.239	4.656	7.739	1.671	34.297	48.821	11.040	46.78	24.89	3.43	21.89			
Cut # 6		4.008	5.593	1.781	4.378	5.945	1.730	23.056	30.463	8.814	47.54	25.68	3.43	21.86			
Cut # 7		3.270	5.037	0.802	4.516	6.544	0.858	30.913	37.958	6.090	46.25	26.48	3.43	19.77			
Cut # 8		3.201	5.092	1.057	3.249	5.299	1.129	18.165	29.225	5.569	45.89	26.44	3.42	19.46			
Cut # 9		3.176	5.125	0.343	4.088	6.513	0.752	31.271	43.012	3.205	45.94	27.06	3.42	18.87			

Rock= Roubidoux Sandstone			Block # 1 (Dry)																
Data Window Cuts			Spacing			2 inch													
Cutter			Radial Pick			Depth of cut			0.5 inch										
	Averages						Standard Deviations			Maximums			Start Position	End Position	Speed	Length of Cut			
	Normal(kN)	Cutting(kN)	Side(kN)	Normal(kN)	Cutting(kN)	Side(kN)	Normal(kN)	Cutting(kN)	Side(kN)	(inches)	(inches)	(inch/sec)	(inch)						
Cut # 1	15.168	27.573	0.678	13.863	23.987	2.625	76.157	112.699	10.789	47.36	22.10	3.45	25.25						
Cut # 2	3.162	5.658	1.894	3.585	6.747	1.753	30.803	53.072	11.341	47.51	23.47	3.46	24.04						
Cut # 3	6.784	10.977	3.168	7.140	11.622	2.948	35.219	54.590	12.880	47.56	25.87	3.45	21.69						
Cut # 4	4.929	9.020	2.883	4.599	8.810	2.304	28.613	49.944	12.320	47.23	25.96	3.45	21.27						
Cut # 5	8.042	13.705	3.133	7.419	12.291	2.136	43.738	58.577	11.846	44.88	26.97	3.44	17.92						
Cut # 6	8.851	12.684	2.795	9.521	12.270	2.364	50.034	62.261	13.014	46.01	24.91	3.42	21.10						
Cut # 7	8.949	12.702	3.036	11.290	13.755	2.693	78.199	79.845	16.585	45.31	25.22	3.43	20.09						
Cut # 8	11.186	15.703	3.668	12.154	15.459	2.871	55.540	62.250	14.708	44.14	27.12	3.42	17.02						
Cut # 9	10.821	14.877	5.840	10.530	13.081	2.565	52.921	63.263	13.650	45.53	26.98	3.42	18.55						

Rock= Roubidoux Sandstone			Block # 1 (Dry)																
Data Window Cuts			Spacing			3 inch													
Cutter			Radial Pick			Depth of cut			0.125 inch										
	Averages			Standard Deviations			Maximums			Start Position	End Position	Speed	Length of Cut						
	Normal(kN)	Cutting(kN)	Side(kN)	Normal(kN)	Cutting(kN)	Side(kN)	Normal(kN)	Cutting(kN)	Side(kN)	(inches)	(inches)	(inch/sec)	(inch)						
Cut # 1	1.563	3.343	-0.393	1.914	4.041	0.940	15.088	25.437	-6.986	49.61	23.70	3.46	25.92						
Cut # 2	2.537	5.453	-1.058	2.061	4.632	1.101	14.284	31.396	-6.606	48.11	23.12	3.46	24.99						
Cut # 3	5.211	10.133	-0.852	4.809	8.649	2.148	22.966	39.311	-12.633	47.14	26.59	3.13	20.56						
Cut # 4	4.323	8.148	2.128	4.257	7.178	1.804	30.502	47.755	10.867	47.33	26.61	3.44	20.72						
Cut # 5	2.062	4.311	-1.055	1.835	3.789	1.041	11.570	21.304	-6.342	47.14	26.92	3.45	20.22						
Cut # 6	1.734	3.506	-1.120	1.493	2.977	0.945	7.215	15.457	-4.520	46.24	27.84	3.45	18.40						

Rock= Roubidoux Sandstone			Block # 1 (Dry)																
Data Window Cuts			Spacing			3 inch													
Cutter			Radial Pick			Depth of cut			0.25 inch										
	Averages			Standard Deviations			Maximums			Start Position	End Position	Speed	Length of Cut						
	Normal(kN)	Cutting(kN)	Side(kN)	Normal(kN)	Cutting(kN)	Side(kN)	Normal(kN)	Cutting(kN)	Side(kN)	(inches)	(inches)	(inch/sec)	(inch)						
Cut # 1	8.122	13.484	0.363	8.655	12.430	1.448	54.525	64.379	8.108	48.18	23.05	3.43	25.13						
Cut # 2	4.882	9.156	0.288	5.020	8.891	0.817	23.348	39.500	3.942	47.58	24.14	3.44	23.44						
Cut # 3	3.468	6.827	-0.083	3.953	7.336	0.718	25.126	42.318	-5.853	47.52	26.10	3.44	21.43						
Cut # 4	2.052	4.053	-0.003	3.041	5.748	0.413	20.482	35.698	-2.132	47.03	26.68	3.44	20.35						
Cut # 5	1.650	3.414	0.311	2.142	4.171	0.562	14.102	27.232	3.112	47.03	27.15	3.44	19.87						
Cut # 6	1.175	2.255	0.249	1.191	2.145	0.395	6.984	12.464	1.857	45.86	26.66	3.43	19.20						

Rock= Roubidoux Sandstone			Block # 1 (Dry)																
Data Window Cuts			Spacing			3 inch													
Cutter			Radial Pick			Depth of cut			0.375 inch										
	Averages			Standard Deviations			Maximums				Start Position	End Position		Speed	Length of Cut				
	Normal(kN)	Cutting(kN)	Side(kN)	Normal(kN)	Cutting(kN)	Side(kN)	Normal(kN)	Cutting(kN)	Side(kN)	(inches)	(inches)	(inch/sec)	(inch)						
Cut # 1	8.544	14.786	0.451	8.746	13.391	1.530	38.055	55.520	6.857	47.63	22.83	3.46	24.80						
Cut # 2	3.072	6.551	1.001	3.839	7.197	1.222	20.210	35.622	5.680	47.80	25.56	3.47	22.23						
Cut # 3	4.625	8.197	1.523	5.229	8.373	1.263	31.371	43.945	5.387	47.39	26.56	3.46	20.82						
Cut # 4	5.736	10.188	0.799	8.143	12.051	1.145	51.500	64.541	5.857	46.46	26.96	3.45	19.50						
Cut # 5	4.990	9.416	0.783	6.044	10.007	1.236	29.275	46.233	6.585	45.92	29.59	3.45	16.33						
Cut # 6	12.301	18.824	1.608	12.891	15.934	1.397	66.005	70.959	8.878	45.58	27.95	3.43	17.64						

Rock= Roubidoux Sandstone			Block # 1 (Dry)																
Data Window Cuts			Spacing			3 inch													
Cutter			Radial Pick			Depth of cut			0.5 inch										
	Averages			Standard Deviations			Maximums			Start Position	End Position	Speed	Length of Cut						
	Normal(kN)	Cutting(kN)	Side(kN)	Normal(kN)	Cutting(kN)	Side(kN)	Normal(kN)	Cutting(kN)	Side(kN)	(inches)	(inches)	(inch/sec)	(inch)						
Cut # 1	7.305	13.350	1.515	11.288	17.084	2.186	58.205	78.922	8.885	47.73	27.37	3.46	20.36						
Cut # 2	3.363	6.726	0.937	7.369	13.138	1.390	41.671	70.119	8.134	47.22	27.90	3.46	19.32						
Cut # 3	0.970	3.265	0.643	1.366	2.942	0.784	9.041	21.272	3.882	47.80	27.03	3.45	20.77						
Cut # 4	0.662	1.687	-0.019	0.896	1.879	0.360	7.055	12.712	2.091	47.86	30.08	3.45	17.78						
Cut # 5	2.356	5.040	0.882	3.257	6.365	0.834	23.706	43.601	3.758	46.12	29.24	3.44	16.88						



Rock= Roubidoux Sandstone			Block # 1 (Dry)												
Data Window Cuts			Spacing			3 inch									
Cutter	Radial Pick		Depth of cut			0.5 inch	Repeat								
	Averages			Standard Deviations			Maximums			Start Position	End Position	Speed	Length of Cut		
	Normal(kN)	Cutting(kN)	Side(kN)	Normal(kN)	Cutting(kN)	Side(kN)	Normal(kN)	Cutting(kN)	Side(kN)	(inches)	(inches)	(inch/sec)	(inch)		
Cut # 1	5.430	9.726	0.504	6.247	9.952	1.491	33.756	50.647	6.574	48.33	28.77	3.48	19.56		
Cut # 2	2.809	6.359	0.890	3.258	6.427	1.028	18.896	32.467	6.214	48.41	28.68	3.48	19.72		
Cut # 3	2.712	5.938	0.655	2.667	5.465	0.696	14.625	27.272	4.588	47.41	29.17	3.48	18.24		
Cut # 4	2.609	5.806	0.545	2.830	5.839	0.863	17.068	31.681	3.692	46.52	30.85	3.48	15.67		
Cut # 5	6.525	13.696	2.082	6.544	11.928	2.223	32.528	56.071	9.446	46.87	30.71	3.47	16.16		

Rock= Roubidoux Sandstone			Block # 4 (Dry)											
Data Window Cuts			Spacing			1 inch								
Cutter	Radial Pick		Depth of cut			0.125 inch								
	Averages			Standard Deviations			Maximums			Start Position	End Position	Speed	Length of Cut	
	Normal(kN)	Cutting(kN)	Side(kN)	Normal(kN)	Cutting(kN)	Side(kN)	Normal(kN)	Cutting(kN)	Side(kN)	(inches)	(inches)	(inch/sec)	(inch)	
Cut # 1	1.894	2.990	-0.295	1.406	2.226	0.525	7.075	11.100	-2.222	45.84	27.04	3.04	18.80	
Cut # 2	1.167	1.942	0.588	1.064	1.964	0.658	5.549	9.803	3.051	44.91	26.92	3.04	17.99	
Cut # 3	1.421	2.247	0.314	1.075	1.856	0.425	5.869	9.647	2.246	44.57	26.76	3.04	17.81	
Cut # 4	1.610	2.587	0.286	1.098	1.934	0.428	6.292	10.550	1.899	44.21	26.15	3.04	18.06	
Cut # 5	1.366	2.247	0.258	1.086	1.930	0.489	7.466	12.413	2.190	42.76	26.35	3.05	16.40	
Cut # 6	1.391	2.005	0.313	1.125	1.726	0.436	5.785	8.744	1.922	42.55	26.52	3.05	16.02	
Cut # 7	1.637	2.328	0.326	1.128	1.776	0.436	6.460	9.723	1.882	42.50	26.18	3.05	16.32	
Cut # 8	1.458	2.164	0.282	1.193	1.835	0.429	6.166	9.642	2.265	43.09	26.71	3.05	16.38	
Cut # 9	1.417	2.117	0.587	0.988	1.535	0.457	6.052	8.531	2.545	42.36	26.99	3.05	15.37	

Rock= Roubidoux Sandstone			Block # 4 (Dry)												
Data Window Cuts			Spacing			1 inch									
Cutter	Radial Pick		Depth of cut			0.25 inch									
	Averages			Standard Deviations			Maximums			Start Position	End Position	Speed	Length of Cut		
	Normal(kN)	Cutting(kN)	Side(kN)	Normal(kN)	Cutting(kN)	Side(kN)	Normal(kN)	Cutting(kN)	Side(kN)	(inches)	(inches)	(inch/sec)	(inch)		
Cut # 1	2.255	3.648	-0.362	1.723	2.864	0.792	9.554	18.304	-3.412	44.55	27.49	3.05	17.07		
Cut # 2	1.123	1.917	0.496	1.038	1.891	0.722	5.758	9.450	3.987	44.04	26.84	3.05	17.20		
Cut # 3	1.535	2.565	0.345	1.287	2.247	0.449	7.666	12.542	2.121	42.86	27.30	3.05	15.56		
Cut # 4	1.467	2.426	0.423	1.096	1.967	0.551	5.508	10.187	2.863	42.41	27.10	3.05	15.31		
Cut # 5	1.141	1.897	0.286	1.036	1.849	0.445	5.919	10.089	3.036	42.34	27.10	3.05	15.24		
Cut # 6	1.411	2.020	0.336	1.091	1.720	0.372	5.551	8.202	1.749	41.74	27.39	3.05	14.35		
Cut # 7	1.667	2.399	0.484	1.082	1.695	0.610	5.364	7.835	2.335	41.94	27.63	3.05	14.31		
Cut # 8	1.480	2.102	0.197	1.112	1.717	0.433	5.460	8.194	1.947	41.92	26.99	3.05	14.92		
Cut # 9	1.596	2.313	0.702	1.025	1.645	0.523	5.318	8.701	2.653	41.97	27.52	3.04	14.45		

Rock= Roubidoux Sandstone			Block # 4 (Dry)												
Data Window Cuts			Spacing			2.5 inch									
Cutter	Radial Pick		Depth of cut			0.125 inch									
	Averages			Standard Deviations			Maximums			Start Position	End Position	Speed	Length of Cut		
	Normal(kN)	Cutting(kN)	Side(kN)	Normal(kN)	Cutting(kN)	Side(kN)	Normal(kN)	Cutting(kN)	Side(kN)	(inches)	(inches)	(inch/sec)	(inch)		
Cut # 1	1.542	2.620	0.131	1.110	1.829	0.308	6.570	9.803	1.457	46.93	28.95	3.03	17.98		
Cut # 2	1.455	2.663	0.210	0.981	1.796	0.309	5.557	9.344	1.438	45.31	28.23	3.03	17.08		
Cut # 3	1.452	2.724	0.163	1.031	1.917	0.392	6.371	10.867	1.868	43.57	27.67	3.04	15.90		
Cut # 4	1.493	2.918	0.819	0.948	1.833	1.094	5.480	9.235	4.072	42.83	27.39	3.04	15.43		
Cut # 5	1.593	2.888	0.558	1.372	2.502	0.537	12.201	20.563	3.194	41.46	27.32	3.05	14.15		
Cut # 6	1.431	3.214	0.520	1.504	2.886	0.572	12.613	20.868	4.204	40.43	25.87	3.04	14.56		

Rock= Roubidoux Sandstone			Block # 4 (Dry)												
Data Window Cuts			Spacing			2.5 inch									
Cutter	Radial Pick		Depth of cut			0.125 inch		Repeat							
	Averages			Standard Deviations			Maximums			Start Position	End Position		Speed	Length of Cut	
	Normal(kN)	Cutting(kN)	Side(kN)	Normal(kN)	Cutting(kN)	Side(kN)	Normal(kN)	Cutting(kN)	Side(kN)	(inches)	(inches)		(inch/sec)	(inch)	
Cut # 1	3.167	5.165	0.462	2.172	3.195	0.547	9.002	14.298	2.481	47.24	29.36		3.04	17.88	
Cut # 2	3.784	6.719	0.436	2.800	4.539	0.820	12.607	21.413	2.534	45.28	28.54		3.04	16.74	
Cut # 3	3.376	6.151	0.610	2.488	4.107	0.676	10.818	17.953	2.872	42.64	27.77		3.05	14.87	
Cut # 4	3.280	5.903	0.357	2.440	3.954	0.677	11.661	17.840	2.802	41.99	28.04		3.04	13.95	
Cut # 5	2.440	4.428	-0.643	1.996	3.441	0.615	10.081	16.279	-2.876	42.11	28.37		3.00	13.74	
Cut # 6	2.365	4.065	0.663	1.913	2.965	0.528	10.931	15.657	2.440	41.49	26.97		3.00	14.51	

Rock= Roubidoux Sandstone			Block # 4 (Dry)										
Data Window Cuts			Spacing			2.5 inch							
Cutter	Radial Pick		Depth of cut			0.25 inch							
	Averages			Standard Deviations			Maximums			Start Position	End Position	Speed	Length of Cut
	Normal(kN)	Cutting(kN)	Side(kN)	Normal(kN)	Cutting(kN)	Side(kN)	Normal(kN)	Cutting(kN)	Side(kN)	(inches)	(inches)	(inch/sec)	(inch)
Cut # 1	3.320	5.711	-0.058	2.409	3.866	0.535	14.937	26.213	2.196	44.53	28.61	3.03	15.92
Cut # 2	2.985	5.525	0.428	2.201	3.908	0.577	11.565	19.667	3.179	44.61	27.84	3.03	16.76
Cut # 3	3.044	5.598	0.530	2.293	4.034	0.692	12.871	21.700	3.061	43.34	27.36	3.00	15.97
Cut # 4	3.103	5.665	0.234	2.256	3.976	0.528	11.193	19.603	2.290	42.87	26.70	3.03	16.17
Cut # 5	2.639	4.813	0.123	2.171	3.790	0.444	11.567	19.589	1.779	42.71	26.88	3.03	15.83
Cut # 6	2.724	4.750	0.352	2.046	3.252	0.444	10.340	16.085	2.236	43.28	26.66	3.03	16.62

Rock= Roubidoux Sandstone			Block # 4 (Dry)										
Data Window Cuts			Spacing			2.5 inch							
Cutter	Radial Pick		Depth of cut			0.375 inch							
	Averages			Standard Deviations			Maximums			Start Position	End Position	Speed	Length of Cut
	Normal(kN)	Cutting(kN)	Side(kN)	Normal(kN)	Cutting(kN)	Side(kN)	Normal(kN)	Cutting(kN)	Side(kN)	(inches)	(inches)	(inch/sec)	(inch)
Cut # 1	2.295	3.994	0.443	2.241	3.441	0.534	14.910	22.082	2.602	47.18	29.52	3.03	17.66
Cut # 2	2.722	4.851	0.807	2.259	3.910	0.701	11.239	20.296	3.151	45.25	28.97	2.95	16.28
Cut # 3	2.507	4.620	0.573	2.356	4.207	0.637	12.656	23.814	3.030	43.08	28.31	3.04	14.77
Cut # 4	2.404	4.652	0.612	2.289	4.182	0.621	13.109	22.011	3.327	42.56	27.61	3.04	14.95
Cut # 5	2.914	5.430	0.706	2.610	4.577	0.635	14.736	25.465	3.484	41.62	28.58	3.04	13.04
Cut # 6	2.935	4.940	0.536	2.428	3.988	0.686	13.571	20.086	-3.103	43.19	28.16	3.04	15.02

Rock= Roubidoux Sandstone			Block # 4 (Dry)										
Data Window Cuts			Spacing			2.5 inch							
Cutter	Radial Pick		Depth of cut			0.5 inch							
	Averages			Standard Deviations			Maximums			Start Position	End Position	Speed	Length of Cut
	Normal(kN)	Cutting(kN)	Side(kN)	Normal(kN)	Cutting(kN)	Side(kN)	Normal(kN)	Cutting(kN)	Side(kN)	(inches)	(inches)	(inch/sec)	(inch)
Cut # 1	8.288	15.180	1.218	8.629	14.100	1.505	36.998	60.157	6.518	46.32	28.08	3.04	18.24
Cut # 2	2.973	7.105	1.829	3.426	7.622	2.352	15.295	35.721	12.684	44.97	27.52	3.05	17.46
Cut # 3	4.872	9.327	2.255	5.320	9.463	1.860	27.153	45.878	8.423	43.50	27.60	3.05	15.90
Cut # 4	4.000	9.493	1.415	4.152	8.280	1.977	18.378	35.508	7.544	41.03	27.23	3.06	13.80
Cut # 5	3.813	8.428	1.928	5.935	10.110	1.804	31.511	53.981	7.566	41.61	27.68	3.05	13.93
Cut # 6	2.981	6.788	0.766	3.246	5.684	1.089	20.098	31.499	3.827	40.75	27.74	3.05	13.01

Rock= Roubidoux Sandstone			Block # 4 (Dry)										
Data Window Cuts			Spacing			3.5 inch							
Cutter	Radial Pick		Depth of cut			0.125 inch							
	Averages			Standard Deviations			Maximums			Start Position	End Position	Speed	Length of Cut
	Normal(kN)	Cutting(kN)	Side(kN)	Normal(kN)	Cutting(kN)	Side(kN)	Normal(kN)	Cutting(kN)	Side(kN)	(inches)	(inches)	(inch/sec)	(inch)
Cut # 1	6.092	7.743	1.201	3.677	5.063	1.191	18.028	24.053	6.228	49.28	30.30	3.01	18.99
Cut # 2	6.085	8.629	-1.056	3.574	5.726	1.320	15.873	26.189	-5.432	47.57	29.35	3.01	18.22
Cut # 3	6.654	9.821	0.644	3.895	6.021	1.159	17.016	28.875	5.832	43.54	28.26	3.03	15.28
Cut # 4	6.091	8.855	1.611	3.526	5.631	1.024	16.359	26.612	5.088	42.67	28.66	3.03	14.01
Cut # 5	5.418	8.102	0.361	3.779	6.147	1.031	17.056	26.313	4.052	39.96	27.94	3.04	12.02
Cut # 6	4.772	5.979	0.388	3.093	4.121	0.847	14.410	20.780	2.785	39.23	28.41	3.04	10.83

Rock= Roubidoux Sandstone			Block # 4 (Dry)										
Data Window Cuts			Spacing			3.5 inch							
Cutter	Radial Pick		Depth of cut			0.125 inch	Repeat						
	Averages			Standard Deviations			Maximums			Start Position	End Position	Speed	Length of Cut
	Normal(kN)	Cutting(kN)	Side(kN)	Normal(kN)	Cutting(kN)	Side(kN)	Normal(kN)	Cutting(kN)	Side(kN)	(inches)	(inches)	(inch/sec)	(inch)
Cut # 1	8.158	12.526	2.324	3.810	6.118	1.743	20.385	31.800	6.852	49.11	30.48	3.03	18.63
Cut # 2	6.173	9.051	4.773	3.026	4.494	1.488	13.918	21.479	8.874	47.53	29.09	3.02	18.44
Cut # 3	6.822	12.260	0.622	4.001	7.328	0.905	20.748	37.043	3.529	45.06	28.86	3.03	16.21
Cut # 4	7.255	11.861	0.965	4.344	7.371	1.144	18.167	32.607	5.494	42.93	29.00	3.03	13.93
Cut # 5	6.945	11.715	1.203	4.376	7.951	1.516	21.394	39.064	6.333	40.80	28.55	3.04	12.25
Cut # 6	5.842	8.832	0.765	3.264	5.345	1.006	17.625	28.132	4.279	39.10	28.02	3.04	11.08

Rock= Roubidoux Sandstone			Block # 4 (Dry)										
Data Window Cuts			Spacing			3.5 inch							
Cutter	Radial Pick		Depth of cut			0.25 inch							
	Averages			Standard Deviations			Maximums			Start Position	End Position	Speed	Length of Cut
	Normal(kN)	Cutting(kN)	Side(kN)	Normal(kN)	Cutting(kN)	Side(kN)	Normal(kN)	Cutting(kN)	Side(kN)	(inches)	(inches)	(inch/sec)	(inch)
Cut # 1	5.751	8.821	0.939	3.684	5.743	1.308	30.956	47.842	6.328	47.04	28.69	3.02	18.36
Cut # 2	4.759	7.914	1.111	3.420	5.858	1.062	15.652	27.671	5.482	45.96	27.93	3.02	18.03
Cut # 3	5.519	9.132	-0.524	3.779	6.593	0.936	21.062	36.345	-3.968	43.25	28.28	3.03	14.97
Cut # 4	4.856	8.098	1.293	2.988	5.180	1.750	16.674	28.273	6.154	41.36	28.34	3.03	13.02
Cut # 5	3.395	6.428	0.295	3.829	6.419	0.862	25.016	44.426	3.487	41.97	26.94	3.04	15.03
Cut # 6	2.390	3.256	0.190	1.890	2.858	0.425	8.606	13.119	2.273	40.03	31.23	3.02	8.80

Rock= Roubidoux Sandstone			Block # 4 (Dry)										
Data Window Cuts			Spacing			3.5 inch							
Cutter	Radial Pick		Depth of cut			0.375 inch							
	Averages			Standard Deviations			Maximums			Start Position	End Position	Speed	Length of Cut
	Normal(kN)	Cutting(kN)	Side(kN)	Normal(kN)	Cutting(kN)	Side(kN)	Normal(kN)	Cutting(kN)	Side(kN)	(inches)	(inches)	(inch/sec)	(inch)
Cut # 1	5.244	9.178	0.361	3.934	5.988	1.164	20.828	31.690	4.408	42.17	29.34	3.05	12.83
Cut # 2	7.806	12.275	0.919	5.366	8.523	1.241	34.641	47.045	5.477	45.07	28.42	3.03	16.65
Cut # 3	7.656	12.572	4.678	6.725	10.652	3.610	45.904	71.188	17.836	41.90	28.25	3.04	13.65
Cut # 4	3.140	7.091	1.284	3.284	5.295	1.847	15.872	28.050	8.901	41.46	27.41	3.05	14.06
Cut # 5	1.409	4.237	1.218	2.452	3.922	1.274	15.436	25.648	5.546	41.04	27.02	3.04	14.02
Cut # 6	2.088	4.824	0.137	2.555	3.723	1.064	16.827	25.863	4.107	40.66	26.29	3.04	14.36

Rock= Roubidoux Sandstone			Block # 4 (Dry)										
Data Window Cuts			Spacing			3.5 inch							
Cutter	Radial Pick		Depth of cut			0.5 inch							
	Averages			Standard Deviations			Maximums			Start Position	End Position	Speed	Length of Cut
	Normal(kN)	Cutting(kN)	Side(kN)	Normal(kN)	Cutting(kN)	Side(kN)	Normal(kN)	Cutting(kN)	Side(kN)	(inches)	(inches)	(inch/sec)	(inch)
Cut # 1	17.933	28.332	0.311	14.873	20.982	1.831	77.536	98.812	8.914	47.70	29.17	2.99	18.54
Cut # 2	11.206	16.781	2.110	8.866	13.633	2.443	47.554	72.330	11.248	46.29	28.24	3.01	18.04
Cut # 3	4.518	9.596	1.874	4.191	8.051	1.271	26.955	47.093	7.167	43.12	27.94	3.03	15.18
Cut # 4	1.989	5.861	0.261	2.385	5.224	0.926	19.406	38.049	4.741	42.32	27.98	3.03	14.34
Cut # 5	3.090	7.608	0.917	3.952	7.240	0.868	26.617	48.065	4.022	41.68	28.10	3.03	13.58
Cut # 6	0.627	4.322	0.562	1.006	2.848	0.665	5.491	16.695	2.958	39.83	26.71	3.04	13.13

## Radial Drag Pick Tests - Saturated Rock

Rock= Roubidoux Sandstone			Block # 2 (Saturated)											
Data Window Cuts			Spacing 1 inch											
Cutter	Radial Pick		Depth of cut 0.125 inch											
	Averages			Standard Deviations			Maximums			Start Position	End Position	Speed	Length of Cut	
	Normal(kN)	Cutting(kN)	Side(kN)	Normal(kN)	Cutting(kN)	Side(kN)	Normal(kN)	Cutting(kN)	Side(kN)	(inches)	(inches)	(inch/sec)	(inch)	
Cut # 1	5.751	9.043	-1.415	3.716	6.006	2.395	20.930	34.497	-8.989	53.50	30.34	2.71	23.16	
Cut # 2	3.300	5.312	0.477	2.538	4.549	0.887	15.222	27.405	3.541	53.16	30.54	3.43	22.63	
Cut # 3	3.970	6.639	0.633	2.518	4.690	0.941	16.645	28.477	4.445	52.67	30.48	3.43	22.19	
Cut # 4	3.667	5.771	0.655	2.245	4.040	0.817	17.044	26.754	4.712	53.30	30.24	3.42	23.06	
Cut # 5	3.841	6.306	0.089	2.705	4.801	0.576	14.938	25.158	2.835	53.66	30.57	3.43	23.09	
Cut # 6	3.127	4.311	0.668	2.237	3.373	0.654	12.640	18.643	2.944	53.36	30.37	3.43	22.99	
Cut # 7	4.228	6.042	0.356	2.850	4.325	0.597	20.033	30.504	2.338	53.50	30.31	3.43	23.19	
Cut # 8	4.077	5.594	0.365	2.855	4.276	0.622	17.858	26.951	2.837	54.15	30.42	3.43	23.73	
Cut # 9	3.273	4.318	0.413	2.273	3.474	0.595	15.697	23.309	2.586	53.62	30.11	3.43	23.51	
Cut # 10	3.765	5.327	0.150	2.457	3.758	0.581	14.618	20.438	2.768	53.65	30.24	3.43	23.40	
Cut # 11	4.023	5.492	-0.048	3.164	4.218	1.248	19.497	24.709	6.437	53.53	30.17	3.43	23.36	
Cut # 12	3.751	5.152	0.799	3.020	4.249	0.891	19.953	29.318	4.834	53.58	30.46	3.43	23.12	
Cut # 13	3.861	5.205	1.164	2.770	3.798	0.802	17.133	23.122	5.058	54.57	30.33	3.43	24.24	
Cut # 14	3.385	4.459	0.882	2.580	3.706	0.919	18.604	26.144	5.293	54.30	29.78	3.43	24.52	
Cut # 15	3.607	4.624	1.050	2.413	3.231	0.644	14.419	19.989	3.345	53.85	30.01	3.43	23.84	
Cut # 16	4.544	6.415	1.972	2.925	4.110	0.777	18.579	25.974	5.485	53.48	30.20	3.43	23.28	

Rock= Roubidoux Sandstone			Block # 2 (Saturated)												
Data Window Cuts			Spacing 1 inch												
Cutter	Radial Pick		Depth of cut 0.25 inch												
	Averages			Standard Deviations			Maximums			Start Position	End Position	Speed	Length of Cut		
	Normal(kN)	Cutting(kN)	Side(kN)	Normal(kN)	Cutting(kN)	Side(kN)	Normal(kN)	Cutting(kN)	Side(kN)	(inches)	(inches)	(inch/sec)	(inch)		
Cut # 1	6.512	9.043	0.759	3.730	5.574	0.977	20.379	30.444	5.189	55.40	32.10	3.44	23.31		
Cut # 2	4.975	7.960	1.113	3.933	6.705	1.647	19.011	34.942	8.099	54.95	31.63	3.45	23.32		
Cut # 3	5.415	8.502	1.076	3.715	6.265	1.389	20.706	37.884	6.431	55.14	31.73	3.44	23.40		
Cut # 4	5.888	9.358	1.419	3.904	6.665	1.762	19.831	35.996	8.576	55.16	31.32	3.43	23.83		
Cut # 5	6.252	9.931	1.763	3.756	6.468	1.564	19.187	34.037	6.633	55.08	31.76	3.44	23.32		
Cut # 6	6.434	8.932	0.836	4.530	6.802	1.338	30.103	48.108	6.115	55.03	31.48	3.49	23.56		
Cut # 7	6.087	7.986	0.566	4.141	5.972	1.249	20.288	30.266	6.146	55.38	31.89	3.48	23.49		
Cut # 8	5.860	7.767	1.074	4.118	5.945	1.558	21.094	32.256	6.524	55.02	31.02	3.48	23.99		
Cut # 9	5.767	7.789	0.637	4.423	6.534	1.000	22.709	35.620	5.769	54.87	30.47	3.48	24.40		
Cut # 10	6.315	8.580	1.549	4.609	6.636	1.860	21.222	31.437	9.584	54.43	31.28	3.47	23.15		
Cut # 11	5.676	7.329	0.753	4.742	6.516	1.083	23.120	31.968	5.112	54.43	31.38	3.48	23.05		
Cut # 12	6.003	7.837	1.270	4.248	5.834	1.547	23.038	32.003	7.226	54.65	30.59	3.47	24.06		
Cut # 13	6.586	8.813	0.155	4.132	6.211	0.963	22.178	31.097	4.289	54.38	31.43	3.46	22.95		
Cut # 14	5.466	7.217	1.189	4.552	6.183	1.343	21.751	31.091	6.439	54.67	30.97	3.45	23.70		
Cut # 15	5.193	7.037	1.097	3.646	5.170	1.287	17.007	25.076	5.884	54.16	30.54	3.44	23.62		
Cut # 16	5.281	7.164	1.073	4.102	5.641	1.457	21.470	28.545	6.470	54.79	31.05	3.44	23.74		

Rock= Roubidoux Sandstone			Block # 2 (Saturated)												
Data Window Cuts			Spacing 1 inch												
Cutter	Radial Pick		Depth of cut 0.375 inch												
	Averages			Standard Deviations			Maximums			Start Position	End Position	Speed	Length of Cut		
	Normal(kN)	Cutting(kN)	Side(kN)	Normal(kN)	Cutting(kN)	Side(kN)	Normal(kN)	Cutting(kN)	Side(kN)	(inches)	(inches)	(inch/sec)	(inch)		
Cut # 1	8.756	15.418	-1.316	5.912	9.275	1.607	33.835	50.785	-6.430	55.35	30.93	3.47	24.42		
Cut # 2	3.019	4.992	1.171	2.740	4.224	1.142	14.440	23.215	5.811	54.90	30.95	3.48	23.95		
Cut # 3	4.029	6.618	0.979	3.732	5.977	1.174	21.303	37.408	5.318	54.96	31.17	3.47	23.79		
Cut # 4	3.716	6.478	1.871	3.153	5.265	1.743	20.174	34.578	8.381	55.10	31.06	3.47	24.03		
Cut # 5	4.030	6.796	1.464	3.401	5.814	2.164	18.019	30.903	13.608	55.80	30.15	3.47	25.65		
Cut # 6	3.697	5.076	1.198	3.505	5.009	1.212	24.767	35.805	6.807	55.60	30.49	3.48	25.11		
Cut # 7	3.644	4.907	1.865	2.892	4.052	1.312	18.131	26.416	6.400	55.64	31.09	3.47	24.55		
Cut # 8	4.929	6.650	0.948	4.844	6.412	1.179	25.437	34.291	5.437	55.20	30.78	3.48	24.42		
Cut # 9	4.632	6.354	1.181	3.839	5.378	1.074	22.458	31.197	5.545	56.07	30.49	3.47	25.58		
Cut # 10	4.996	6.759	2.410	3.981	5.603	1.791	22.303	31.489	8.382	56.18	30.86	3.47	25.32		
Cut # 11	4.927	6.814	0.710	3.885	5.633	1.053	24.653	36.651	5.275	55.83	30.66	3.47	25.17		
Cut # 12	5.068	6.674	1.950	3.493	4.785	1.637	21.344	30.277	7.038	55.85	30.56	3.46	25.29		
Cut # 13	5.678	7.712	0.984	4.906	6.595	1.015	24.285	36.118	5.613	55.36	30.56	3.46	24.80		
Cut # 14	4.358	5.663	1.421	3.979	5.225	1.602	22.427	28.208	8.166	55.22	30.52	3.46	24.70		
Cut # 15	5.741	7.937	1.097	4.039	5.858	1.195	20.533	32.880	6.003	55.20	30.57	3.46	24.62		
Cut # 16	5.701	9.017	3.361	3.958	6.012	2.529	24.999	38.071	11.909	55.37	30.29	3.45	25.08		

Rock= Roubidoux Sandstone			Blk # 2 (Saturated)														
Data Window Cuts			Spacing 1 inch														
Cutter Radial Pick			Depth of cut 0.5 inch														
	Averages			Standard Deviations			Maximums			Start Position	End Position	Speed	Length of Cut				
	Normal(kN)	Cutting(kN)	Side(kN)	Normal(kN)	Cutting(kN)	Side(kN)	Normal(kN)	Cutting(kN)	Side(kN)	(inches)	(inches)	(inch/sec)	(inch)				
Cut # 1	6.438	14.012	0.573	6.829	12.604	1.413	31.256	63.475	6.670	50.96	29.46	3.03	21.50				
Cut # 2	2.126	4.170	0.876	2.593	4.570	0.903	13.751	24.087	5.340	51.52	30.07	3.03	21.45				
Cut # 3	2.696	4.561	0.904	2.443	3.791	1.114	12.362	20.950	5.040	51.51	29.77	3.02	21.74				
Cut # 4	3.687	6.544	2.378	3.678	6.343	2.411	20.984	39.057	14.276	51.49	29.35	3.02	22.15				
Cut # 5	3.749	6.490	1.713	3.739	6.307	2.329	18.721	33.060	10.508	50.83	29.14	3.02	21.69				
Cut # 6	3.898	6.359	2.383	4.291	6.425	2.847	21.469	29.996	14.844	51.48	29.61	3.02	21.87				
Cut # 7	4.148	6.203	1.975	5.225	7.542	2.138	24.870	37.076	10.822	50.99	29.47	3.02	21.52				
Cut # 8	6.288	8.333	2.083	6.590	8.621	1.991	35.136	43.432	10.665	50.42	28.98	3.02	21.44				
Cut # 9	6.543	9.901	2.222	7.756	10.829	2.551	37.779	54.778	13.311	50.57	29.29	3.02	21.28				
Cut # 10	5.938	8.013	1.777	7.710	9.260	1.834	43.257	49.644	8.973	50.36	29.27	3.02	21.09				
Cut # 11	6.408	8.289	1.554	6.539	8.304	1.744	33.461	43.972	10.841	50.63	29.26	3.01	21.38				
Cut # 12	7.260	9.356	1.670	7.428	9.238	1.799	38.126	48.304	10.189	51.02	29.43	3.01	21.59				
Cut # 13	6.620	8.440	0.976	8.841	9.678	1.541	51.907	49.420	10.430	50.43	27.45	3.01	22.98				
Cut # 14	4.931	6.554	2.395	5.108	6.231	2.415	29.373	38.668	14.096	50.95	28.81	3.01	22.14				
Cut # 15	5.788	8.126	0.883	6.523	7.651	1.621	36.664	45.083	6.638	50.43	29.26	3.00	21.17				

Rock= Roubidoux Sandstone			Block # 2 (Saturated)												
Data Window Cuts			Spacing 2 inch												
Cutter	Radial Pick		Depth of cut 0.125 inch												
											Start Position	End Position	Speed	Length of Cut	
	Averages			Standard Deviations			Maximums								
	Normal(kN)	Cutting(kN)	Side(kN)	Normal(kN)	Cutting(kN)	Side(kN)	Normal(kN)	Cutting(kN)	Side(kN)	(inches)	(inches)	(inch/sec)	(inch)		
Cut # 1	4.554	6.259	0.786	2.052	3.191	0.925	12.290	18.185	4.878	50.39	29.16	3.02	21.23		
Cut # 2	4.736	7.403	0.819	2.059	3.565	0.917	12.032	20.529	3.576	50.30	28.72	3.02	21.58		
Cut # 3	5.064	8.526	0.662	2.776	4.935	1.184	18.172	31.970	4.567	50.49	28.83	3.01	21.67		
Cut # 4	5.277	8.713	1.468	2.866	5.066	1.470	18.373	30.064	4.923	50.31	28.20	3.02	22.11		
Cut # 5	5.147	7.360	0.915	2.706	4.582	0.924	15.363	26.796	4.402	50.40	28.58	3.01	21.81		
Cut # 6	4.871	5.949	0.765	3.179	4.234	1.052	15.661	21.564	4.817	49.90	28.44	3.01	21.46		
Cut # 7	5.820	8.018	1.792	3.727	5.668	2.040	21.293	31.967	8.968	49.79	31.12	3.00	18.68		
Cut # 8	5.775	6.863	0.441	5.209	6.756	1.073	32.861	39.129	4.476	49.13	30.93	3.00	18.20		

Rock= Roubidoux Sandstone			Block # 2 (Saturated)												
Data Window Cuts			Spacing 2 inch												
Cutter	Radial Pick		Depth of cut 0.25 inch												
	Averages			Standard Deviations			Maximums			Start Position	End Position	Speed	Length of Cut		
	Normal(kN)	Cutting(kN)	Side(kN)	Normal(kN)	Cutting(kN)	Side(kN)	Normal(kN)	Cutting(kN)	Side(kN)	(inches)	(inches)	(inch/sec)	(inch)		
Cut # 1	5.827	8.868	0.079	5.661	7.594	0.779	33.757	44.398	3.633	49.60	28.05	3.03	21.55		
Cut # 2	3.928	6.204	1.757	3.782	5.591	1.304	31.132	41.611	6.114	49.03	28.65	3.03	20.38		
Cut # 3	5.014	8.454	0.748	3.490	5.952	0.823	20.437	33.821	4.279	49.83	28.53	3.02	21.30		
Cut # 4	4.504	7.492	0.943	3.724	6.049	1.007	20.078	33.821	5.030	49.15	28.62	3.02	20.53		
Cut # 5	5.045	8.099	0.430	4.478	6.448	1.082	32.691	38.801	6.036	49.52	28.92	3.02	20.60		
Cut # 6	4.022	5.767	0.749	3.330	4.780	0.749	19.336	28.969	3.220	49.74	28.63	3.02	21.11		
Cut # 7	4.701	7.159	0.712	3.694	5.265	0.873	21.324	30.944	4.079	49.57	27.92	3.02	21.65		
Cut # 8	4.681	7.073	1.278	3.854	5.185	1.373	21.807	30.370	5.518	48.88	28.76	3.01	20.12		

Rock= Roubidoux Sandstone			Block # 2 (Saturated)												
Data Window Cuts			Spacing 2 inch												
Cutter	Radial Pick		Depth of cut 0.375 inch												
	Averages			Standard Deviations			Maximums			Start Position	End Position	Speed	Length of Cut		
	Normal(kN)	Cutting(kN)	Side(kN)	Normal(kN)	Cutting(kN)	Side(kN)	Normal(kN)	Cutting(kN)	Side(kN)	(inches)	(inches)	(inch/sec)	(inch)		
Cut # 1	5.294	9.064	0.468	5.107	7.902	0.971	34.672	49.145	5.003	50.197	29.245	3.01	20.95		
Cut # 2	3.935	6.901	1.278	3.462	6.096	1.549	19.632	32.589	8.201	50.976	28.199	3.01	22.78		
Cut # 3	5.263	9.088	1.772	4.060	6.914	1.441	23.416	38.139	7.145	49.851	28.650	3.01	21.20		
Cut # 4	6.004	10.373	1.975	5.299	8.735	1.754	30.916	46.553	8.188	50.560	28.125	3.00	22.44		
Cut # 5	4.957	8.536	1.504	4.359	6.992	1.273	29.641	41.041	5.733	50.306	28.270	3.00	22.04		
Cut # 6	4.157	6.359	0.843	4.683	6.439	1.082	32.064	37.882	5.833	50.678	27.486	3.00	23.19		
Cut # 7	4.701	6.845	1.391	4.452	6.107	1.175	28.903	33.793	6.455	50.551	29.101	2.99	21.45		
Cut # 8	4.558	6.822	0.864	4.627	6.586	0.958	31.626	37.696	5.988	49.620	26.939	3.00	22.68		

Rock= Roubidoux Sandstone			Block # 2 (Saturated)										
Data Window Cuts			Spacing 2 inch										
Cutter	Radial Pick		Depth of cut 0.5 inch										
	Averages			Standard Deviations			Maximums			Start Position	End Position	Speed	Length of Cut
	Normal(kN)	Cutting(kN)	Side(kN)	Normal(kN)	Cutting(kN)	Side(kN)	Normal(kN)	Cutting(kN)	Side(kN)	(inches)	(inches)	(inch/sec)	(inch)
Cut # 1	7.278	11.685	0.812	6.327	9.829	1.456	31.384	49.017	7.870	49.62	27.93	3.04	21.68
Cut # 2	3.563	6.389	1.580	3.448	5.833	1.828	16.839	27.159	9.127	49.90	27.61	3.04	22.28
Cut # 3	4.526	7.741	1.950	3.959	6.629	2.150	21.893	35.725	13.525	50.02	27.24	3.03	22.79
Cut # 4	4.319	7.446	1.760	3.972	6.431	2.039	19.546	30.375	10.393	50.11	27.60	3.03	22.51
Cut # 5	4.961	8.155	2.898	4.692	7.451	2.803	23.390	34.890	15.334	50.34	27.41	3.03	22.93
Cut # 6	4.546	6.713	1.162	4.264	5.798	1.333	21.718	29.285	7.817	49.55	27.16	3.03	22.39
Cut # 7	4.164	6.181	0.797	3.482	4.821	0.823	20.857	23.502	4.173	49.76	26.77	3.03	22.98
Cut # 8	3.811	5.776	0.827	2.751	4.123	0.897	15.712	22.903	5.147	49.93	27.32	3.02	22.61

Rock= Roubidoux Sandstone			Block # 2 (Saturated)										
Data Window Cuts			Spacing 3 inch										
Cutter	Radial Pick		Depth of cut 0.125 inch										
	Averages			Standard Deviations			Maximums			Start Position	End Position	Speed	Length of Cut
	Normal(kN)	Cutting(kN)	Side(kN)	Normal(kN)	Cutting(kN)	Side(kN)	Normal(kN)	Cutting(kN)	Side(kN)	(inches)	(inches)	(inch/sec)	(inch)
Cut # 1	4.086	6.318	1.989	2.046	3.331	1.258	12.454	20.471	6.010	50.21	29.02	3.04	21.19
Cut # 2	4.824	8.767	0.391	2.595	4.576	0.755	16.726	30.151	3.802	51.05	29.25	3.03	21.80
Cut # 3	4.076	7.358	2.574	2.265	4.089	1.448	13.780	24.209	6.881	50.47	29.11	3.03	21.36
Cut # 4	4.606	7.827	2.319	2.567	4.647	1.476	14.715	25.489	6.661	50.32	28.16	3.03	22.16
Cut # 5	4.042	6.396	2.455	1.855	3.346	1.524	13.064	22.419	7.015	50.35	28.51	3.03	21.83
Cut # 6	5.441	8.741	2.166	2.865	4.531	1.364	15.887	24.943	6.040	50.35	28.41	3.03	21.94

Rock= Roubidoux Sandstone			Block # 2 (Saturated)										
Data Window Cuts			Spacing 3 inch										
Cutter	Radial Pick		Depth of cut 0.25 inch										
	Averages			Standard Deviations			Maximums			Start Position	End Position	Speed	Length of Cut
	Normal(kN)	Cutting(kN)	Side(kN)	Normal(kN)	Cutting(kN)	Side(kN)	Normal(kN)	Cutting(kN)	Side(kN)	(inches)	(inches)	(inch/sec)	(inch)
Cut # 1	5.843	9.426	-0.754	3.651	5.618	1.158	23.457	35.786	-4.771	50.14	29.14	3.02	21.00
Cut # 2	4.358	7.544	0.359	2.725	4.917	0.909	16.761	29.837	4.711	50.68	28.90	3.02	21.79
Cut # 3	4.878	8.648	0.488	3.077	5.411	0.850	18.238	31.210	3.987	50.47	27.82	3.02	22.65
Cut # 4	5.147	8.946	0.673	3.470	6.094	0.887	17.872	31.059	4.656	50.61	27.97	3.02	22.64
Cut # 5	6.480	11.295	-0.409	4.249	7.301	2.606	25.217	42.800	-6.956	50.67	27.99	3.01	22.68
Cut # 6	6.231	9.598	1.225	4.369	6.712	1.406	24.416	36.392	7.254	49.84	28.15	3.01	21.69

Rock= Roubidoux Sandstone			Block # 2 (Saturated)										
Data Window Cuts			Spacing 3 inch										
Cutter	Radial Pick		Depth of cut 0.375 inch										
	Averages			Standard Deviations			Maximums			Start Position	End Position	Speed	Length of Cut
	Normal(kN)	Cutting(kN)	Side(kN)	Normal(kN)	Cutting(kN)	Side(kN)	Normal(kN)	Cutting(kN)	Side(kN)	(inches)	(inches)	(inch/sec)	(inch)
Cut # 1	8.983	15.713	-1.686	6.598	10.647	2.283	35.256	56.084	-9.904	49.85	28.44	3.01	21.41
Cut # 2	5.342	9.366	2.169	3.363	6.028	1.594	20.147	33.813	9.005	50.67	28.26	3.01	22.41
Cut # 3	4.999	9.613	-0.226	4.854	8.649	1.666	29.709	49.702	-6.981	50.18	28.45	3.01	21.73
Cut # 4	4.251	8.059	1.526	3.888	6.955	2.057	23.592	39.607	9.919	50.30	27.81	3.01	22.49
Cut # 5	5.533	10.251	0.451	5.227	9.027	1.097	30.598	47.675	5.809	50.09	28.77	3.01	21.32
Cut # 6	6.864	11.319	3.003	5.392	8.116	2.413	31.136	42.697	13.570	49.55	28.57	3.01	20.98

Rock= Roubidoux Sandstone			Block # 2 (Saturated)										
Data Window Cuts			Spacing 3 inch										
Cutter	Radial Pick		Depth of cut 0.5 inch										
	Averages			Standard Deviations			Maximums			Start Position	End Position	Speed	Length of Cut
	Normal(kN)	Cutting(kN)	Side(kN)	Normal(kN)	Cutting(kN)	Side(kN)	Normal(kN)	Cutting(kN)	Side(kN)	(inches)	(inches)	(inch/sec)	(inch)
Cut # 1	10.132	17.273	-0.733	8.303	12.643	2.187	41.574	60.356	-10.119	48.78	28.44	3.03	20.34
Cut # 2	5.157	9.219	2.646	4.301	7.062	1.812	21.479	35.555	9.031	49.14	28.00	3.03	21.14
Cut # 3	6.259	11.025	1.577	5.603	9.508	2.041	31.591	49.674	10.844	49.13	28.00	3.03	21.12
Cut # 4	6.604	12.037	1.594	5.567	9.194	1.879	32.257	48.785	8.769	49.23	27.90	3.03	21.34
Cut # 5	6.177	11.157	1.581	5.440	8.826	1.742	38.141	51.068	6.681	49.10	28.02	3.03	21.09
Cut # 6	6.280	10.191	1.519	5.224	7.771	1.043	28.145	42.559	5.409	50.62	33.62	3.01	17.01

Rock= Roubidoux Sandstone			Block # 3 (Saturated)										
Data Window Cuts			Spacing 2.5 inch										
Cutter	Radial Pick		Depth of cut 0.125 inch										
	Averages			Standard Deviations			Maximums			Start Position	End Position	Speed	Length of Cut
	Normal(kN)	Cutting(kN)	Side(kN)	Normal(kN)	Cutting(kN)	Side(kN)	Normal(kN)	Cutting(kN)	Side(kN)	(inches)	(inches)	(inch/sec)	(inch)
Cut # 1	4.811	6.701	-0.662	2.325	3.453	0.699	12.510	18.930	-2.857	51.30	27.40	3.01	23.89
Cut # 2	5.493	8.457	-0.373	2.941	4.781	0.829	15.222	23.235	-3.989	51.18	27.61	2.97	23.56
Cut # 3	4.688	7.763	0.844	2.640	4.671	1.324	13.861	22.727	5.017	50.09	27.83	3.01	22.26
Cut # 4	3.430	5.527	0.410	2.194	3.981	1.694	12.073	21.189	5.395	49.76	28.01	3.01	21.76
Cut # 5	4.400	7.796	-0.161	2.357	4.635	0.780	14.385	25.869	-2.817	48.88	27.68	3.01	21.20
Cut # 6	4.429	5.973	1.259	2.346	3.614	1.237	13.182	19.335	5.191	47.85	28.22	3.01	19.63
Cut # 7	4.324	6.038	0.990	2.668	4.093	1.279	14.976	21.882	6.355	47.50	28.43	3.01	19.08

Rock= Roubidoux Sandstone			Block # 3 (Saturated)										
Data Window Cuts			Spacing 2.5 inch										
Cutter	Radial Pick		Depth of cut 0.25 inch										
	Averages			Standard Deviations			Maximums			Start Position	End Position	Speed	Length of Cut
	Normal(kN)	Cutting(kN)	Side(kN)	Normal(kN)	Cutting(kN)	Side(kN)	Normal(kN)	Cutting(kN)	Side(kN)	(inches)	(inches)	(inch/sec)	(inch)
Cut # 1	3.577	7.753	-0.626	2.795	4.547	1.086	17.266	30.683	-5.579	51.77	27.89	3.03	23.88
Cut # 2	4.400	8.543	5.033	2.529	5.081	4.014	15.317	26.929	14.289	50.84	27.30	3.02	23.54
Cut # 3	2.858	8.397	3.560	1.761	4.672	2.595	10.809	25.122	11.930	49.19	27.85	3.03	21.35
Cut # 4	2.902	5.037	2.904	1.918	3.643	1.290	10.767	20.744	7.772	49.63	27.67	3.03	21.96
Cut # 5	2.878	6.573	0.740	2.351	4.395	2.389	16.518	30.568	8.774	48.05	27.81	2.17	20.24
Cut # 6	4.936	8.491	5.282	2.316	4.208	1.633	16.157	28.590	8.803	48.47	27.60	3.02	20.87

Rock= Roubidoux Sandstone			Block # 3 (Saturated)										
Data Window Cuts			Spacing 2.5 inch										
Cutter	Radial Pick		Depth of cut 0.375 inch										
	Averages			Standard Deviations			Maximums			Start Position	End Position	Speed	Length of Cut
	Normal(kN)	Cutting(kN)	Side(kN)	Normal(kN)	Cutting(kN)	Side(kN)	Normal(kN)	Cutting(kN)	Side(kN)	(inches)	(inches)	(inch/sec)	(inch)
Cut # 1	5.466	9.833	-0.099	3.541	6.114	1.031	26.709	50.042	4.237	50.38	25.91	3.04	24.47
Cut # 2	3.209	5.768	1.607	2.158	4.054	1.443	14.367	24.905	6.851	50.39	26.09	3.04	24.30
Cut # 3	4.311	7.669	1.070	1.828	3.145	1.525	29.598	50.924	8.637	48.54	25.78	3.04	22.76
Cut # 4	4.059	6.756	1.039	3.444	6.349	1.328	32.007	57.460	7.447	48.06	25.87	3.04	22.19
Cut # 5	3.677	6.162	0.388	2.619	4.741	1.092	21.471	37.868	-5.183	48.25	26.32	3.04	21.94
Cut # 6	5.807	8.500	1.532	4.350	6.582	1.183	26.740	39.170	6.311	47.48	27.31	3.04	20.18

Rock= Roubidoux Sandstone			Block # 3 (Saturated)										
Data Window Cuts			Spacing 2.5 inch										
Cutter	Radial Pick		Depth of cut 0.5 inch			Test 1							
	Averages			Standard Deviations			Maximums			Start Position	End Position	Speed	Length of Cut
	Normal(kN)	Cutting(kN)	Side(kN)	Normal(kN)	Cutting(kN)	Side(kN)	Normal(kN)	Cutting(kN)	Side(kN)	(inches)	(inches)	(inch/sec)	(inch)
Cut # 1	5.216	11.645	-0.517	3.881	6.745	1.817	22.195	37.333	-6.426	50.41	25.54	3.02	24.87
Cut # 2	2.786	5.587	0.568	2.694	4.661	0.939	15.402	26.948	3.809	49.41	25.58	3.03	23.83
Cut # 3	2.154	4.103	1.347	2.029	3.969	1.420	10.358	18.072	6.027	48.99	25.59	3.03	23.41
Cut # 4	3.032	5.343	0.985	3.245	5.438	1.335	19.466	29.989	6.140	49.30	25.69	3.03	23.61
Cut # 5	3.599	7.108	0.614	2.851	4.817	1.498	21.660	36.896	7.088	48.31	27.08	3.02	21.23
Cut # 6	5.002	7.950	2.318	3.719	5.608	1.190	24.977	35.758	5.634	48.33	30.11	3.01	18.22

Rock= Roubidoux Sandstone			Block # 3 (Saturated)										
Data Window Cuts			Spacing 2.5 inch										
Cutter	Radial Pick		Depth of cut 0.5 inch			Test 2							
	Averages			Standard Deviations			Maximums			Start Position	End Position	Speed	Length of Cut
	Normal(kN)	Cutting(kN)	Side(kN)	Normal(kN)	Cutting(kN)	Side(kN)	Normal(kN)	Cutting(kN)	Side(kN)	(inches)	(inches)	(inch/sec)	(inch)
Cut # 1	4.966	12.674	0.197	4.659	7.722	1.104	27.060	48.584	4.933	50.39	25.48	3.04	24.91
Cut # 2	2.346	3.306	0.227	2.132	3.126	0.602	10.210	17.173	3.647	50.81	25.99	3.03	24.82
Cut # 3	2.315	4.144	1.859	1.520	2.595	1.499	9.533	16.494	7.388	48.95	26.21	3.05	22.74
Cut # 4	2.386	4.835	1.393	1.550	3.046	1.326	10.530	20.379	6.260	48.75	26.13	3.04	22.62
Cut # 5	2.927	5.251	1.502	1.912	3.363	1.225	11.574	19.857	5.720	48.19	26.08	3.04	22.11
Cut # 6	5.614	9.558	4.361	2.838	4.878	2.502	17.323	26.843	10.379	48.21	26.57	3.04	21.64

Rock= Roubidoux Sandstone			Block # 3 (Saturated)										
Data Window Cuts			Spacing 2.5 inch										
Cutter	Radial Pick		Depth of cut 0.5 inch			Test 3							
	Averages			Standard Deviations			Maximums			Start Position	End Position	Speed	Length of Cut
	Normal(kN)	Cutting(kN)	Side(kN)	Normal(kN)	Cutting(kN)	Side(kN)	Normal(kN)	Cutting(kN)	Side(kN)	(inches)	(inches)	(inch/sec)	(inch)
Cut # 1	7.138	13.821	-0.764	9.417	12.591	1.280	53.812	68.422	-7.128	49.92	25.40	3.04	24.52
Cut # 2	2.135	5.206	1.880	3.037	5.253	1.702	18.974	32.042	9.294	50.04	26.15	3.04	23.89
Cut # 3	2.503	5.924	0.558	3.736	5.984	1.627	22.702	35.243	7.486	49.79	26.10	3.04	23.69
Cut # 4	2.700	6.230	0.963	5.436	8.225	1.871	39.029	51.681	9.926	48.50	26.87	2.84	21.63
Cut # 5	1.936	4.413	1.182	3.040	5.540	1.791	21.612	39.808	6.738	47.96	26.21	3.04	21.75
Cut # 6	3.101	9.910	5.784	2.446	6.257	3.091	16.540	41.397	13.026	48.19	27.15	3.03	21.05

Rock= Roubidoux Sandstone			Block # 3 (Saturated)										
Data Window Cuts			Spacing 3.5 inch										
Cutter	Radial Pick		Depth of cut 0.125 inch										
	Averages			Standard Deviations			Maximums			Start Position	End Position	Speed	Length of Cut
	Normal(kN)	Cutting(kN)	Side(kN)	Normal(kN)	Cutting(kN)	Side(kN)	Normal(kN)	Cutting(kN)	Side(kN)	(inches)	(inches)	(inch/sec)	(inch)
Cut # 1	2.559	2.951	0.442	1.807	2.244	0.965	9.783	11.332	3.863	47.63	31.93	3.04	15.71
Cut # 2	2.699	4.130	0.153	2.604	3.897	0.650	11.180	19.142	-2.747	50.87	27.49	3.04	23.38
Cut # 3	4.278	6.608	0.052	2.254	3.830	1.564	14.418	23.188	5.577	49.06	26.31	3.04	22.75
Cut # 4	4.133	6.698	1.762	2.292	3.936	2.065	12.856	21.760	6.127	47.52	27.18	3.04	20.33
Cut # 5	4.188	6.314	0.103	2.606	4.375	1.579	13.738	22.333	4.707	47.25	29.00	3.04	18.25
Cut # 6	4.422	5.767	0.330	3.173	4.636	1.126	17.309	25.912	4.440	46.34	29.88	3.04	16.46

Rock= Roubidoux Sandstone			Block # 3 (Saturated)										
Data Window Cuts			Spacing 3.5 inch										
Cutter	Radial Pick		Depth of cut 0.25 inch										
	Averages			Standard Deviations			Maximums			Start Position	End Position	Speed	Length of Cut
	Normal(kN)	Cutting(kN)	Side(kN)	Normal(kN)	Cutting(kN)	Side(kN)	Normal(kN)	Cutting(kN)	Side(kN)	(inches)	(inches)	(inch/sec)	(inch)
Cut # 1	10.515	16.002	0.711	6.817	10.175	1.923	34.371	49.455	12.119	48.28	27.08	3.03	21.20
Cut # 2	9.574	16.592	1.975	7.879	13.221	2.533	45.391	66.382	12.574	50.71	27.18	3.02	23.53
Cut # 3	9.418	16.691	1.782	6.258	10.643	2.219	30.050	52.425	7.948	49.34	27.43	3.02	21.91
Cut # 4	9.891	17.443	1.402	6.443	11.109	2.329	30.379	49.713	8.621	47.88	26.99	3.02	20.89
Cut # 5	11.231	19.573	1.476	8.559	14.095	1.807	42.566	68.289	6.928	47.65	28.21	3.02	19.44
Cut # 6	11.215	17.739	1.170	7.090	10.450	1.544	32.962	49.663	6.397	47.06	27.42	3.02	19.64

Rock= Roubidoux Sandstone			Block # 3 (Saturated)										
Data Window Cuts			Spacing 3.5 inch										
Cutter	Radial Pick		Depth of cut 0.375 inch										
	Averages			Standard Deviations			Maximums			Start Position	End Position	Speed	Length of Cut
	Normal(kN)	Cutting(kN)	Side(kN)	Normal(kN)	Cutting(kN)	Side(kN)	Normal(kN)	Cutting(kN)	Side(kN)	(inches)	(inches)	(inch/sec)	(inch)
Cut # 1	3.438	4.514	1.079	2.149	3.162	1.467	12.344	18.252	6.150	48.81	32.74	3.03	16.07
Cut # 2	4.027	6.417	0.702	3.813	6.487	1.160	22.952	37.493	6.253	48.47	28.42	3.04	20.05
Cut # 3	1.934	3.073	-0.277	2.266	3.237	0.680	13.634	20.132	-2.809	48.15	27.72	3.04	20.43
Cut # 4	2.446	3.934	0.375	2.244	3.673	1.029	13.742	22.841	4.316	47.03	27.39	3.05	19.64
Cut # 5	3.330	5.481	0.200	2.385	4.006	0.967	11.473	20.137	-4.107	46.19	26.76	3.05	19.43
Cut # 6	4.903	7.040	0.116	2.567	3.963	0.540	13.740	20.869	1.990	46.14	27.62	3.04	18.52

Rock= Roubidoux Sandstone			Block # 3 (Saturated)										
Data Window Cuts			Spacing 3.5 inch										
Cutter	Radial Pick		Depth of cut 0.5 inch										
	Averages			Standard Deviations			Maximums			Start Position	End Position	Speed	Length of Cut
	Normal(kN)	Cutting(kN)	Side(kN)	Normal(kN)	Cutting(kN)	Side(kN)	Normal(kN)	Cutting(kN)	Side(kN)	(inches)	(inches)	(inch/sec)	(inch)
Cut # 1	9.976	15.570	-0.105	6.387	9.497	1.559	34.371	46.380	-6.278	49.76	31.20	3.01	18.56
Cut # 2	8.189	14.605	2.276	6.176	10.286	1.818	32.374	53.605	9.243	50.69	27.48	3.02	23.21
Cut # 3	7.177	13.132	1.609	6.321	10.671	1.611	29.188	50.312	7.126	49.00	27.55	3.03	21.45
Cut # 4	6.642	12.362	2.491	6.494	10.925	2.216	30.253	49.026	9.288	47.13	27.04	3.03	20.10
Cut # 5	4.508	10.130	-0.210	5.406	9.367	1.352	30.201	52.893	-5.194	46.17	27.35	3.04	18.83
Cut # 6	5.229	9.615	3.265	4.359	6.948	1.943	28.332	42.408	8.157	45.94	26.89	3.03	19.05



**Sieve Analysis Data for Dry Radial Drag Pick Tests**

<i>s</i>	<i>d</i>	<i>s/d</i>	Caught on 50.8 mm	Caught on 25.4 mm	Caught on 9.42 mm	Caught on 1.65 mm	Passing 1.65 mm	Total
(mm)	(mm)		(kg)	(kg)	(kg)	(kg)	(kg)	(kg)
25.4	3.2	8	0	0.225	0.631	0.376	0.696	1.928
25.4	6.4	4	0.049	0.525	1.979	0.506	1.431	4.49
25.4	9.5	2.7	0.504	1.331	1.945	0.634	1.952	6.366
25.4	12.7	2	2.825	2.19	2.473	0.788	1.584	9.86
50.8	3.2	16	0.883	0.775	0.221	0.194	0.371	2.444
50.8	6.4	8	1.301	2.269	1.461	0.61	1.302	6.943
50.8	9.5	5.3	1.255	2.168	1.355	0.507	1.105	6.39
50.8	12.7	4	5.886	2.359	1.275	0.627	1.035	11.182
63.5	3.2	20	0.908	0.09	0.142	0.121	0.353	1.614
63.5	6.4	10	0.211	0.434	0.484	0.312	0.664	2.105
63.5	9.5	6.7	0.551	1.111	0.912	0.472	1.13	4.176
63.5	12.7	5	1.608	2.01	1.141	0.422	1.489	6.67
76.2	3.2	24	1.09	0.128	0.37	0.198	0.337	2.123
76.2	6.4	12	2.205	0.261	0.579	0.273	0.573	3.891
76.2	9.5	8	3.055	1.723	0.854	0.432	1.091	7.155
76.2	12.7	6	2.157	1.358	0.81	0.448	1.059	5.832
88.9	3.2	28	0	0.042	0.112	0.097	0.306	0.557
88.9	6.4	14	0.494	0.261	0.436	0.177	0.665	2.033
88.9	9.5	9.3	3.257	0.349	0.491	0.263	0.77	5.13
88.9	12.7	7	3.634	1.583	0.95	0.384	1.332	7.883

### Sieve Analysis Data for Saturated Radial Drag Pick Tests

<i>s</i>	<i>d</i>	<i>s/d</i>	Caught on 50.8 mm	Caught on 25.4 mm	Caught on 9.42 mm	Caught on 1.65 mm	Passing 1.65 mm	Total
(mm)	(mm)		(kg)	(kg)	(kg)	(kg)	(kg)	(kg)
25.4	3.2	8	0	0.053	0.547	0.277	0.431	0
25.4	6.4	4	0	0.257	1.786	0.615	0.937	0
25.4	9.5	2.7	0.606	1.037	2.53	0.727	2.098	0.606
25.4	12.7	2	0.772	2.119	2.847	0.857	2.329	0.772
50.8	3.2	16	0.115	0.567	0.305	0.156	0.531	0.115
50.8	6.4	8	0.152	1.382	0.593	0.322	1.36	0.152
50.8	9.5	5.3	0.952	1.721	1.279	0.49	1.591	0.952
50.8	12.7	4	0.707	2.338	1.33	0.63	2.696	0.707
63.5	3.2	20	0.057	0.213	0.336	0.2	0.447	0.057
63.5	6.4	10	2.694	0.426	0.594	0.316	0.996	2.694
63.5	9.5	6.7	0.61	1.903	1.041	0.554	1.372	0.61
63.5	12.7	5	3.878	2.048	0.93	0.436	1.203	3.878
76.2	3.2	24	0.126	0.093	0.119	0.067	0.494	0.126
76.2	6.4	12	0.986	0.869	0.454	0.168	1.138	0.986
76.2	9.5	8	3.07	1.464	1.012	0.517	1.924	3.07
76.2	12.7	6	2.414	1.663	1.27	0.598	1.937	2.414
88.9	3.2	28	0.315	0.079	0.153	0.104	0.552	0.315
88.9	6.4	14	1.019	0.698	0.71	0.316	1.061	1.019
88.9	9.5	9.3	2.91	0.88	0.306	0.249	1.611	2.91
88.9	12.7	7	2.015	1.737	1.447	0.849	2.616	2.015

## APPENDIX D.

### SAS OUTPUTS FOR STEPWISE AND MINIMUM $R^2$ IMPROVEMENT VARIABLE SELECTION METHODS

## Stepwise Variable Selection Method for Dry Cutting Tests

Stepwise Selection: Step 5

Variable x Removed: R-Square = 0.6912 and C(p) = 4.3946

The SAS System 19  
10:33 Wednesday, November 30, 2011

The REG Procedure  
Model: MODEL1  
Dependent Variable: SE

Stepwise Selection: Step 5

Analysis of Variance

Source	DF	Sum of Squares	Mean Square	F Value	Pr > F
Model	3	334.03208	111.34403	11.94	0.0002
Error	16	149.23742	9.32734		
Corrected Total	19	483.26950			

Variable	Parameter Estimate	Standard Error	Type II SS	F Value	Pr > F
Intercept	19.91025	3.93877	238.33589	25.55	0.0001
s	-0.07185	0.04050	29.35872	3.15	0.0951
sdratio	0.38528	0.12286	91.72852	9.83	0.0064
CI	-0.04335	0.01246	112.90156	12.10	0.0031

Bounds on condition number: 1.6789, 13.458

All variables left in the model are significant at the 0.1000 level.

The stepwise method terminated because the next variable to be entered was just removed.

### Summary of Stepwise Selection

Step	Variable Entered	Variable Removed	Number Vars In	Partial R-Square	Model R-Square	C(p)	F Value	Pr > F
1	CI		1	0.5012	0.5012	10.4791	18.09	0.0005
2	sdratio		2	0.1292	0.6304	5.6199	5.94	0.0260
3	s		3	0.0608	0.6912	4.3946	3.15	0.0951
4	x		4	0.0487	0.7399	3.8086	2.81	0.1144
5		x	3	0.0487	0.6912	4.3946	2.81	0.1144

## Output Statistics

Obs	Dependent Variable	Predicted Value	Std Error Mean Predict	90% CL Predict	Residual
1	15.6000	11.6295	1.5624	5.6402 17.6188	3.9705
2	10.8000	9.2690	1.4690	3.3522 15.1858	1.5310
3	6.2000	7.6149	1.3748	1.7675 13.4623	-1.4149
4	4.0000	4.1413	1.4161	-1.7361 10.0186	-0.1413
5	10.6000	6.5701	1.5157	0.6175 12.5227	4.0299
6	1.9000	5.3000	0.7622	-0.1956 10.7956	-3.4000
7	2.5000	3.9649	0.8339	-1.5623 9.4922	-1.4649
8	3.5000	0.3599	1.2861	-5.4257 6.1454	3.1401
9	5.4000	7.7450	1.8034	1.5528 13.9373	-2.3450
10	3.5000	2.4279	1.0170	-3.1920 8.0479	1.0721
11	2.9000	1.3507	1.0184	-4.2700 6.9714	1.5493
12	1.9000	1.4299	1.1204	-4.2496 7.1094	0.4701
13	2.5000	7.1467	1.6040	1.1240 13.1694	-4.6467
14	3.7000	7.8071	1.0464	2.1707 13.4435	-4.1071
15	1.6000	5.4605	1.0200	-0.1611 11.0820	-3.8605
16	2.0000	3.0800	0.9488	-2.5035 8.6634	-1.0800
17	20.1000	16.4941	2.4132	9.6984 23.2897	3.6059
18	5.0000	6.4611	1.3432	0.6362 12.2860	-1.4611
19	2.1000	-0.1751	1.3350	-5.9943 5.6441	2.2751
20	2.3000	0.0226	1.4106	-5.8507 5.8959	2.2774
Sum of Residuals					0
Sum of Squared Residuals					149.23742
Predicted Residual SS (PRESS)					307.48153

### Stepwise Variable Selection Method for Saturated Cutting Tests

The REG Procedure  
Model: MODEL1  
Dependent Variable: SE

Stepwise Selection: Step 6

Variable sdratio Removed: R-Square = 0.7427 and C(p) = 2.9519

#### Analysis of Variance

Source	DF	Sum of Squares	Mean Square	F Value	Pr > F
Model	2	502.36006	251.18003	24.54	<.0001
Error	17	174.03794	10.23753		
Corrected Total	19	676.39800			

Variable	Parameter Estimate	Standard Error	Type III SS	F Value	Pr > F
Intercept	31.72545	4.66904	472.66715	46.17	<.0001
d	-0.79006	0.23910	111.77538	10.92	0.0042
CI	-0.06383	0.01837	123.58017	12.07	0.0029

Stepwise Selection: Step 6

Bounds on condition number: 1.3941, 5.5765

All variables left in the model are significant at the 0.1000 level.

The stepwise method terminated because the next variable to be entered was just removed.

#### Summary of Stepwise Selection

Step	Variable Entered	Variable Removed	Number Vars In	Partial R-Square	Model R-Square	C(p)	F Value	Pr > F
1	PR		1	0.5963	0.5963	10.5993	26.58	<.0001
2	CI		2	0.0657	0.6620	8.2697	3.31	0.0867
3	d		3	0.0820	0.7440	4.8653	5.13	0.0378
4		PR	2	0.0013	0.7427	2.9519	0.08	0.7780
5	sdratio		3	0.0270	0.7697	3.1747	1.87	0.1899
6		sdratio	2	0.0270	0.7427	2.9519	1.87	0.1899

## Output Statistics

Obs	Dependent Variable	Predicted Value	Std Error Mean Predict	90% CL Predict		Residual
1	24.3000	15.3476	1.4112	9.2643	21.4310	8.9524
2	13.0000	11.4827	1.0946	5.6000	17.3655	1.5173
3	6.1000	7.5096	1.0639	1.6439	13.3753	-1.4096
4	4.2000	3.8670	1.4458	-2.2409	9.9749	0.3330
5	11.2000	11.6532	1.2405	5.6835	17.6229	-0.4532
6	4.9000	9.7921	0.8299	4.0418	15.5424	-4.8921
7	3.5000	5.1203	0.7820	-0.6097	10.8502	-1.6203
8	2.7000	4.4239	1.5411	-1.7542	10.6019	-1.7239
9	16.6000	15.0891	1.3734	9.0319	21.1462	1.5109
10	5.1000	6.8187	0.9705	1.0022	12.6352	-1.7187
11	2.6000	2.4820	1.0658	-3.3848	8.3487	0.1180
12	2.8000	0.9073	1.1996	-5.0371	6.8517	1.8927
13	12.7000	13.9552	1.2471	7.9813	19.9291	-1.2552
14	3.0000	3.0670	1.8307	-3.3457	9.4798	-0.0670
15	2.8000	5.2744	0.7852	-0.4569	11.0056	-2.4744
16	1.7000	-2.6889	1.6127	-8.9220	3.5442	4.3889
17	8.1000	12.6956	1.1989	6.7516	18.6396	-4.5956
18	8.7000	7.0197	0.9374	1.2196	12.8197	1.6803
19	1.5000	1.6100	1.2501	-4.3659	7.5858	-0.1100
20	2.7000	2.7737	1.2964	-3.2319	8.7793	-0.0737

Sum of Residuals	0
Sum of Squared Residuals	174.03794
Predicted Residual SS (PRESS)	252.58663

## Minimum R<sup>2</sup> Improvement Procedure for Dry Cutting Tests

The SAS System 28  
12:31 Saturday, December 3, 2011

The REG Procedure  
Model: MODEL1  
Dependent Variable: SE

Minimum R-Square Improvement: Step 19

Bounds on condition number: 5.8436, 70.341

---

Minimum R-Square Improvement: Step 20

Variable PR Removed: R-Square = 0.7399 and C(p) = 3.8086  
Variable x Entered

### Analysis of Variance

Source	DF	Sum of Squares	Mean Square	F Value	Pr > F
Model	4	357.57196	89.39299	10.67	0.0003
Error	15	125.69754	8.37984		
Corrected Total	19	483.26950			

The REG Procedure  
Model: MODEL1  
Dependent Variable: SE

Minimum R-Square Improvement: Step 20

Variable	Parameter Estimate	Standard Error	Type II SS	F Value	Pr > F
Intercept	27.98688	6.09586	176.63388	21.08	0.0004
s	-0.08511	0.03919	39.51883	4.72	0.0463
sdratio	0.35753	0.11762	77.42566	9.24	0.0083
CI	-0.07447	0.02200	95.98258	11.45	0.0041
x	0.06392	0.03814	23.53988	2.81	0.1144

Bounds on condition number: 4.446, 48.518

---

The above model is the best 4-variable model found.



## Output Statistics

Obs	Dependent Variable	Predicted Value	Std Error Mean Predict	90% CL Predict	Residual
1	15.6000	13.2366	2.1318	6.6943 19.7789	2.3634
2	10.8000	9.9725	1.6165	3.9108 16.0342	0.8275
3	6.2000	7.7280	1.5524	1.7191 13.7368	-1.5280
4	4.0000	3.3078	2.3014	-3.4123 10.0278	0.6922
5	10.6000	5.2626	1.7780	-0.9392 11.4644	5.3374
6	1.9000	4.6472	1.6260	-1.4224 10.7167	-2.7472
7	2.5000	2.2082	1.2757	-3.5928 8.0093	0.2918
8	3.5000	2.1271	1.7365	-4.0378 8.2919	1.3729
9	5.4000	6.3773	2.0342	-0.0667 12.8213	-0.9773
10	3.5000	2.0135	1.5675	-4.0077 8.0347	1.4865
11	2.9000	1.7647	1.3337	-4.0772 7.6065	1.1353
12	1.9000	1.2905	1.3806	-4.5853 7.1664	0.6095
13	2.5000	8.8441	1.8905	2.5387 15.1494	-6.3441
14	3.7000	6.7116	1.3238	0.8769 12.5464	-3.0116
15	1.6000	4.6790	1.1316	-1.0276 10.3855	-3.0790
16	2.0000	2.9627	1.7012	-3.1712 9.0967	-0.9627
17	20.1000	17.8917	2.7406	10.6734 25.1099	2.2083
18	5.0000	4.1780	2.0693	-2.3010 10.6569	0.8220
19	2.1000	1.4392	2.0408	-5.0114 7.8898	0.6608
20	2.3000	1.4579	1.6338	-4.6183 7.5341	0.8421

The REG Procedure  
Model: MODEL1  
Dependent Variable: SE

Sum of Residuals	0
Sum of Squared Residuals	118.33665
Predicted Residual SS (PRESS)	429.41272

## Minimum R<sup>2</sup> Improvement Procedure for Saturated Cutting Tests

The REG Procedure  
Model: MODEL1  
Dependent Variable: SE

Minimum R-Square Improvement: Step 10

Variable sdratio Removed: R-Square = 0.7975 and C(p) = 3.3429  
Variable s Entered

### Analysis of Variance

Source	DF	Sum of Squares	Mean Square	F Value	Pr > F
Model	4	539.41239	134.85310	14.77	<.0001
Error	15	136.98561	9.13237		
Corrected Total	19	676.39800			

Variable	Parameter Estimate	Standard Error	Type III SS	F Value	Pr > F
Intercept	41.21247	7.51500	274.65197	30.07	<.0001
s	-0.10089	0.05070	36.16258	3.96	0.0651
d	-1.61426	0.51378	90.15190	9.87	0.0067
CI	-0.07295	0.02439	81.67438	8.94	0.0091
PR	1.00318	0.62083	23.84518	2.61	0.1270

-----

The above model is the best 4-variable model found.

### Output Statistics

Obs	Dependent Variable	Predicted Value	Std Error Mean Predict	90% CL Predict	Residual
1	24.3000	18.5794	2.1941	11.7021 25.4566	5.7206
2	13.0000	13.0695	1.6522	6.6852 19.4538	-0.0695
3	6.1000	7.9962	1.4882	1.7397 14.2527	-1.8962
4	4.2000	2.9321	2.2662	-4.0181 9.8822	1.2679
5	11.2000	12.1779	1.8580	5.6187 18.7372	-0.9779
6	4.9000	10.3603	1.2094	4.2952 16.4254	-5.4603
7	3.5000	4.6514	1.2121	-1.4153 10.7182	-1.1514
8	2.7000	3.9252	1.6642	-2.4689 10.3192	-1.2252
9	16.6000	13.9358	1.9566	7.2872 20.5844	2.6642
10	5.1000	4.8486	1.8789	-1.7294 11.4266	0.2514
11	2.6000	4.1726	1.8963	-2.4210 10.7662	-1.5726
12	2.8000	0.8441	1.4982	-5.4200 7.1081	1.9559
13	12.7000	13.8306	1.4355	7.6129 20.0484	-1.1306
14	3.0000	4.9460	2.4673	-2.2157 12.1077	-1.9460
15	2.8000	4.7509	1.1720	-1.2912 10.7929	-1.9509
16	1.7000	-2.3432	2.1591	-9.1856 4.4992	4.0432
17	8.1000	10.1945	2.2177	3.2936 17.0955	-2.0945
18	8.7000	4.4054	2.1167	-2.3953 11.2061	4.2946
19	1.5000	1.5752	2.3922	-5.5062 8.6566	-0.0752
20	2.7000	3.3474	2.3053	-3.6429 10.3377	-0.6474

The REG Procedure  
Model: MODEL1  
Dependent Variable: SE

Sum of Residuals	0
Sum of Squared Residuals	133.46532
Predicted Residual SS (PRESS)	366.81326

## BIBLIOGRAPHY

- Abu Bakar, M.Z. and Gertsch, L.S., "Saturation Effects on Disc Cutting of Sandstone," *Proceedings of the 45th US Rock Mechanics/Geomechanics Symposium, San Francisco, CA, USA*, pp.1-9, June 2011.
- Abu Bakar, M.Z. and Gertsch, L.S., "Disc Cutting Tests on Dry and Saturated Sandstone: Muck as a Performance Estimator," In: *Proceedings of the SME Annual Meeting and Exhibit*, February 19-22, Seattle, WA, USA, preprint number: 12-104, 2012.
- Abramson, L.W., "50 Years of Tunnels on the Interstate Highway System," Transportation Research Circular E-C104: 50 Years of Interstate Structures: Past, Present, and Future, Transportation Research Board, *National Academies of Science*, pp. 96-108, 2006.
- Altindag, R., "Estimation of Penetration Rate in Percussive Drilling by Means of Coarseness Index and Mean Particle Size," *Rock Mechanics and Rock Engineering*, Vol. 36 (4), pp. 323-332, 2003.
- Altindag, R., "Evaluation of Drill Cuttings in Prediction of Penetration Rate by using Coarseness Index and Mean Particle Size in Percussive Drilling," *Geotechnical and Geological Engineering*, Vol. 22, pp. 417-425, 2004.
- Altinoluk, S., "Investigations into the Effects of Tungsten Carbide Composition and Geometry on the Durability of Rock Excavation Tools," *Ph.D. Thesis*, University of Newcastle upon Tyne, 1981.
- Ashar, A., "Long-Term Development Trends of US Ports," [www.trb.org/Conferences/MTS/4C%20AsharPaper.pdf](http://www.trb.org/Conferences/MTS/4C%20AsharPaper.pdf), 2004, accessed May15, 2009.
- Atkinson, B.K., "Subcritical Crack Growth in Geological Materials," *Journal of Geophysics Research*, Vol. 89, pp. 4077-4144, 1984.
- Balci, C. and Bilgin, N., "Correlative Study of Linear Small and Full Scale Rock Cutting Tests to Select Mechanized Excavation Machines," *International Journal of Rock Mechanics and Mining Sciences*, Vol. 44, pp. 468-476, 2007.
- Balci, C., "Correlation of Rock Cutting Tests with Field Performance of a TBM in a Highly Fractured Rock Formation: A Case Study in Kazyatagi-Kadikoy Metro Tunnel, Turkey," *Tunnelling and Underground Space Technology*, Vol. 24, pp. 423-435, 2009.
- Barker, J.S., "A Laboratory Investigation of Rock Cutting using Large Picks," *International Journal of Rock Mechanics and Mining Sciences & Geomechanics Abstracts*, Vol. 1(4), pp. 519-534, 1964.

- Barton, C.C., "Variable in Fracture Energy and Toughness Testing of Rock", *Proceedings of 23<sup>rd</sup> Symposium on Rock Mechanics*, Berkeley, pp. 449-462, 1982.
- Benjumea, R. and Sikarskie, D.L., "A Note on Penetration of a Rigid Wedge into a Non-Isotropic Brittle Material," *International Journal of Rock Mechanics and Mining Sciences & Geomechanics Abstracts*, Vol. 6, pp. 343-352, 1969.
- Bilgin, N., "Investigation into the Mechanical Cutting Characteristics of Some Medium and High Strength Rocks," *PhD Thesis*, University of New-Castle upon Tyne, England, 1977.
- Bilgin, N., Seyrek, T. and Shahriar, K., "Roadheader Performance in Istanbul, Golden Horn Clean-up Contributes Valuable Data," *Tunnels and Tunnelling*, pp. 41-44, 1988.
- Bilgin, N., Demircin, M.A., Copur, H., Balci, C., Tuncdemir, H. and Akcin, N., "Dominant Rock Properties Affecting the Performance of Conical Picks and the Comparison of Some Experimental and Theoretical Results," *International Journal of Rock Mechanics and Mining Sciences*, Vol. 43, pp. 139-156, 2006.
- Borodich, F.M., "Some Fractal Models of Fracture," *Journal of the Mechanics and Physics of Solids*, Vol. 45, No.2, pp. 239-259, 1996.
- Boussinesq, J., "Application des Potentiels a l'Etude de l'Equilibre et du Mouvement des Solides Elastiques," *Gauthier-Viallars*, Paris, pp. 508, 1885.
- Brace, W.F. and Martin, R.J., "A Test of the Law of Effective Stress for Crystalline Rocks of Low Porosity," *International Journal of Rock Mechanics and Mining Sciences*, Vol. 5, pp. 415-426, 1968.
- Breeds, C.D. and Conway, J.J., "Rapid Excavation," *SME Mining Engineering Handbook*, Vol. 2, pp. 1871-1907, 1992.
- Broek, D., "Elementary Engineering Fracture Mechanics," *Sijthoff and Noordhoff*, 1982.
- Broch, E., "Changes in Rock Strength Caused by Water," *Proceedings of 4th Congress of International Society for Rock Mechanics*, Montreux, Switzerland, (1), pp. 71-75, 1979.
- Cheatham, J.B. and Gnirk P.F., "The Mechanics of Rock Failure Associated with Drilling at Depth," *Proceedings of the 8<sup>th</sup> Symposium on Rock Mechanics (USRMS)*, Minneapolis, MN, pp. 410-439, 1966.

- Cho, J.W., Jeon, S., Yu, S.H. and Chang, S.H., "Optimum Spacing of TBM Disc Cutters: A Numerical Simulation using the Three-Dimensional Dynamic Fracturing Method," *Tunnelling and Underground Space Technology*, Vol. 25, pp. 230-244, 2010.
- Cigla, M. and Ozdemir, L., "Computer Modeling for Improved Production of Mechanical excavators," *Proceedings of the SME Annual Meeting*, Salt Lake City, Utah, 2000.
- Colback, P.S.B. and Wiid, B.L., "The influence of Moisture Content on the Compressive Strength of Rocks," *Proceedings of the 3<sup>rd</sup> Rock Mechanics Symposium, Toronto, Canada*, p.65-83, 1965.
- Cook, N.G.W. and Joughin, N.C., "Rock Fragmentation by Mechanical, Chemical and Thermal Methods," *Proceedings of 6<sup>th</sup> International Mining Congress*, Madrid, Spain, 1970.
- Cook, N.G.W., Hood, M.C. and Tsai, H., "Observation of Crack Growth in Hard Rock Loaded by an Indenter," *International Journal of Rock Mechanics and Mining Sciences & Geomechanics Abstracts*, Vol. 21, No.2, pp. 97-107, 1984.
- Cook, J.M. and Thiercelin, M., "Indentation Resistance of Shale: The Effects of Stress State and Strain Rate," *Proceedings of the 30th U.S. Symposium on Rock Mechanics (USRMS)*, Morgantown, WV, pp.757-764, 1989.
- Cools, P.M.C.B.M., "Research Activities on Mechanical Rock Cutting and Dredging at Delft Hydraulics," *Proceedings of the 6<sup>th</sup> International IAEG Congress*, Amsterdam, Netherlands, pp. 2889-2898, 1990.
- Copur, H., Tuncdemir, H., Bilgin, N. and Dincer, T., "Specific Energy as a Criterion for the Use of Rapid Excavation Systems in Turkish Mines," *Institution of Mining and Metallurgy*, pp.149-157, 2001.
- Dake, C.L., "The Sand and Gravel Resources of Missouri", *Missouri Bureau of Geology and Mines*, Rolla, MO, 1918.
- Deliac, E.P., "Optimization Des Machines D'abattage a Pics," *PhD Thesis*, University of Paris, IV, 1986.
- Deliac, E.P., "Theoretical and Practical Rules for Mechanical Rock Excavation," *Comprehensive Rock Engineering*, Vol. 4: J.A. Hudson, Ed., pp.177-227, 1993.
- Dollinger, G.L., "Choosing Cutters for the Best Boreability," *Compressed Air Magazine*, Vol. 82, pp. 15-19, September 1977.
- Dollinger, G.L., "Lab Tests Provide Low-Cost Method for Predicting Raise Boring Costs," *Engineering and Mining Journal*, pp. 86-89, January 1978.

- Dollinger, G.L., Handewith, H.J. and Breeds, C.D., "Use of the Punch Test for Estimating TBM Performance," *Tunnelling and Underground Space Technology*, Vol. 13, No. 4, pp. 403-408, 1998.
- Dubugnon, O., "An Experimental Study of Water-Jet-Assisted Drag Bit Cutting of Rocks," *In Proceedings of the 1<sup>st</sup> U.S. Water Jet Symposium*, Golden, CO, pp. II.4.1-II.4.11, 1981.
- Dyke, C.G. and Dobereiner, L., "Evaluating the Strength and Deformability of Sandstones," *Quarterly Journal of Engineering Geology*, Vol. 24, pp.123-134, 1991.
- Erguler, Z.A. and Ulusay, R., "Water Induced Variations in Mechanical Properties of Clay Bearing Rocks," *International Journal of Rock Mechanics and Mining Science*, Vol. 46, pp. 355-370, 2009.
- Evans, I., "A Theory on the Basic Mechanics of Coal Ploughing," *Proceedings of the International Symposium on Mining Research*, February 1961, Missouri, Vol. 2, pp. 761-798, 1962.
- Evans, I., "The Expanding Bolt Seam Tester: A Theory of Tensile Breakage," *International Journal of Rock Mechanics and Mining Sciences & Geomechanics Abstracts* Vol.1, pp. 459-474, 1964.
- Evans, I., "The Force Required to Cut Coal with Blunt Wedges," *International Journal of Rock Mechanics and Mining Sciences*, Vol. 2, pp. 1-12, 1965.
- Evans, I. and Pomeroy, C.D., "The Strength, Fracture and Workability of Coal," London, Pergamon Press, 1966.
- Evans, I., "Line Spacing of Picks for Effective Cutting," *International Journal Rock Mechanics and Mining Sciences*, Vol. 9, pp. 355-361, 1972.
- Evans, I., "Relative Efficiency of Picks and Discs for Cutting Rock," *Proceedings of the 3<sup>rd</sup> Congress on Advances in Rock Mechanics*, Denver, Colorado, Vol. 11B, pp. 1399-1405, 1974.
- Evans, I., "A Theory of the Cutting Force for Point Attack Picks," *International Journal of Mining Engineering*, Vol. 2, p. 63-71, 1984.
- Farrokh, E. and Rostami, J., "The Relationship between Tunnel Convergence and Machine Operational Parameters and Chip Size for Double Shield TBMs-A Case History of Ghomroud Water Conveyance Tunnel," *Proceedings of the Rapid Excavation and Tunnelling Conference*, Toronto, Canada, pp.1094-1108, 2007.

- Farrokhi, E., Rostami, J., and Laughton, C., "Study of Various Models for Estimation of Penetration Rate of Hard Rock TBMs," *Tunnelling and Underground Space Technology*, pp. 1-14, 2012.
- Ford, L.M. and Friedman, M., "Optimization of Rock-Cutting Tools used in Coal Mining," *Proceedings of the 24<sup>th</sup> U.S. Symposium on Rock Mechanics*, Texas, pp.725-732, June, 1983.
- Frenzel, C., "Wear Patterns and Prediction of Disc Cutter Consumption for Tunnel Boring Machines," *Proceedings of the SME Annual Meeting*, Denver, CO, Preprint Number. 11-128, 2011.
- Friant, J.E., "Disc Cutter Technology Applied to Drill Bits," *U.S. Department of Energy's Natural Gas Conference*, Houston, Texas, pp.1-16, 1997.
- Fowell, R.J., Hekimoglu, O.Z. and Altinoluk, S., "Drag Tools Employed on Shearer Drums and Roadheaders," *Proceedings 10th Turkish Mining Congress*, Ankara, pp. 529–550, 1987.
- Fowell, R.J., "The Mechanics of Rock Cutting," *Comprehensive Rock Engineering*, Vol. 4: J.A. Hudson, Ed., pp.155-176, 1993.
- Gehring, K.H., "A Cutting Comparison," *Tunnels and Tunnelling*, pp. 27-30, November, 1989.
- Geier, J.E., Hood, M. and Thimons, E.D., "Water-Jet-Assisted Drag Bit Cutting in Medium-Strength Rock," *U.S. Bureau of Mines Report*, IC-9164, 1987.
- Gertsch, R. and Ozdemir, L., "Performance Prediction of Mechanical Excavators from Linear Cutting Tests on Yucca Mountain Welded Tuffs" *SAND91-7038*, Albuquerque, New Mexico, Sandia National Laboratories, 1992.
- Gertsch, R.E., "Rock Toughness and Disc Cutting," *Ph.D. Dissertation*, University of Missouri-Rolla, USA, 2000.
- Gertsch, L.S., Gertsch, R.E. and Gustafson, R.J., "Excavatability of Lunar and Martian Regolith: Initial Laboratory Tests on JSC-1 Simulants," *Proceedings of the 41<sup>st</sup> U.S. Symposium on Rock Mechanics (USRMS)*, paper no. ARMA 06-994, 2006.
- Gertsch, L.S. and Summers, D.A., "Disc Cutting of Low-Strength Brittle Rock", *In Proceedings of the 41st U.S. Symposium on Rock Mechanics*, Golden, CO, ARMA/USRMS 06-1094, pp.1-7, June 2006.
- Gertsch, R., Gertsch, L.S., Rostami, J., "Disc Cutting Tests in Colorado Red Granite: Implications for TBM Performance Prediction," *International Journal of Rock Mechanics and Mining Sciences*, Vol. 44, pp.238-246, 2007.



- Godard, J.P., "Urban Underground Space and the Benefits of Going Underground," *World Tunnel Congress and ITA General Assembly*, Singapore, May 2004, [www.itaaites.org/fileadmin/filemounts/general/pdf/ItaAssociation/ProductAndPublication/OpenSession/JPGodard.pdf](http://www.itaaites.org/fileadmin/filemounts/general/pdf/ItaAssociation/ProductAndPublication/OpenSession/JPGodard.pdf), accessed 30 May 2012.
- Goktan, R.M., "A Suggested Improvement on Evans Cutting Theory for Conical Bits," *Proceedings of the Fourth International Symposium on Mine Mechanization and Automation*, Brisbane, Queensland, Vol.1, pp. 57-61, 1997.
- Gowd, T.N. and Rummel, F., "Effect of Confining Pressure on the Fracture Behavior of a Porous Rock," *International Journal of Rock Mechanics and Mining Sciences & Geomechanics Abstracts*, Vol. 17, pp. 225-229, 1980.
- Gupta, A. and Yan, D.S., "Mineral Processing Design and Operation: An Introduction," *Elsevier*, Netherlands, 2006.
- Handewith, H.J., "Predicting the Economic Success of Continuous Tunneling in Hard Rock," *CIM Bulletin*, pp. 595-599, May, 1970.
- Handewith, H.J., "Suggested Tunnel Investigation Criteria for Rock Boring Machines," *Proceedings of the 8<sup>th</sup> Canadian Rock Mechanics Symposium*, Toronto, pp. 177-186, 1972.
- Hardy, M.P., "Fracture Mechanics Applied to Rock," *PhD Thesis*, University of Minnesota, Michigan, 1973.
- Hawkins, A.B. and McConnell, B.J., "Sensitivity of Sandstone Strength and Deformability to Changes in Moisture Content," *Quarterly Journal of Engineering Geology*, Vol. 25, pp. 115-130, 1992.
- Herrenknecht Cutter Tools,  
[http://www.herrenknecht.com/fileadmin/redaktion/PDF\\_Downloads/07-05-02\\_CutterTools\\_E.pdf](http://www.herrenknecht.com/fileadmin/redaktion/PDF_Downloads/07-05-02_CutterTools_E.pdf), accessed June 15, 2012.
- Hignett, H.J. and Banks, D.C., "Current Issues in Rock Dredging," *Proceedings of the Conference on Dredging '84*, Florida, USA, pp.321-333, November, 1984.
- Hogg, R., "Particle Characterization," *Principles of Mineral Processing*, Fuerstenau, C. and Han, K.N. (ed.), SME, CO, USA, 2003.
- Hood, M., "A Study of Methods to Improve the Performance of Drag Bits used to Cut Hard Rock," *Ph.D. Thesis*, University of the Witwatersrand, 1977a.
- Hood, M., "Cutting Strong Rock with a Drag Bit Assisted by High Pressure Water Jets," *Journal of South African Inst. Min. and Metall.*, Vol. 77, No.1, pp. 79-90, 1977b.
- Hood, M., "Phenomena Relating to the Failure of Hard Rock Adjacent to an Indenter," *Journal of South African Inst. Min. and Metall.*, pp. 113-123, December 1977c.

- Hood, M., "Waterjet-Assisted Rock Cutting Systems-The Present State of the Art," *Int. J. Min. Eng.*, Vol.3, pp. 91-111, 1985.
- Hood, M., Knight, G.C. and Thimons, E.D., "A Review of Water-Jet-Assisted Rock Cutting," *U.S. Bureau of Mines Report*, IC-9273, 1990.
- Hood, M.C. and Roxborough, F.F., "Rock Breakage: Mechanical," *SME Mining Engineering Handbook*, 2<sup>nd</sup> Edition, Vol. 1, Ed. Howard L. Hartman, pp. 680-721, 1992.
- Hood, M.C. and Alehossein, H., "A Development in Rock Cutting Technology," *International Journal of Rock Mechanics and Mining Sciences*, Vol. 37, pp. 297-305, 2000.
- Hua Guo, "Rock Cutting using Fracture Mechanics Principles," *PhD Thesis*, University of Wollongong, N.S.W, Australia, 1990.
- Hukki, R.T., "Proposal for a Solomonic Settlement between the Theories of Von Rittinger, Kick and Bond," *AIME Transactions (Mining)*, Vol. 223, pp. 403-408, 1962.
- Hurt, K.G., "Roadheader Cutting Heads and Picks," *Colliery Guardian*, pp. 332-334, September, 1988.
- Ingraffea, A.R. and Manu, C., "Stress-Intensity Factor Computations in Three Dimensions," *International Journal of Numerical Methods in Engineering*, 15, pp.1427-1445, 1980.
- Ingraffea, A.R., "Theory of Crack Initiation and Propagation in Rock," In: *Fracture Mechanics of Rock*, Ed., Barry Kean Atkinson, Academic Press Geology Series, 1991, p. 534, 1987.
- Inyang, H.I., "Drag Bit Cutting a Conception of Rock Deformation Processes that Correspond to Observed Force-Distance Plots," *Proceedings of the 2<sup>nd</sup> International Symposium in Mine Planning and Equipment Selection in Surface Mining*, Calgary, Canada, pp. 373-378, 1990.
- Jackson, E., Devaux, M. and Machin, J., "Performance Prediction for a Subsea Mechanical Trenching Wheel," *Proceedings of the 6<sup>th</sup> International Offshore Site Investigation and Geotechnics Conference*, London, UK, pp.527-532, 2007.
- Jung, H.S., Choi, J.M., Chun, B.S., Park, J.S. and Lee, Y.J., "Causes of Reduction in Shield TBM Performance – A Case Study in Seoul," *Tunnelling and Underground Space Technology*, Vol. 26 pp. 453-461, 2011.

- Kahraman, S., Develi, K. and Yasar, E., "Predicting the Penetration Rate of Percussive Blasthole Drills using Coarseness Index and Median Particle Size," *CIM Bulletin*, Vol. 97, Paper No. 15: 1-4, 2004.
- Kaitkay, P. and Lei, S., "Experimental Study of Rock Cutting under External Hydrostatic Pressure," *Journal of Material Processing Technology*, Vol. 159, pp.206-213, 2005.
- Katsunori, F., Chen, W., Seisuke, O., and Shigeru, S., "Particle Distribution of Cuttings in Tunnel Excavation," *Journal of the Mining and Materials Processing Institute of Japan*, Vol. 119 (10/11), pp.640-646, 2003.
- Kezhil, S., Liguang, J., Dajun, Y. and Mengshu, W., "Research on Distribution Regularities of Grain Size of Rock Detritus from Discoid Cutters," *Chinese Journal of Rock Mechanics and Engineering*, Vol. 27, 2008.
- Kemeny, J., "Frictional Stability of Heterogeneous Surfaces in Contact: The Mechanics of Faulting and Earthquake Rupture," *PhD Thesis*, University of California at Berkeley, 1986.
- Kennametal Catalog,  
[www.kennametal.com/images/repositories/PDFs/B04-8\\_underground\\_mining.pdf](http://www.kennametal.com/images/repositories/PDFs/B04-8_underground_mining.pdf),  
 accessed 27 March 2012.
- Khademi, H.J., Shahriar, K., Rezai, B., and Rostami, J., "Performance Prediction of Hard Rock TBM using Rock Mass Rating (RMR) system," *Tunnelling and Underground Space Technology*, Vol. 25, No. 4, pp. 333-345, 2010.
- Ladanyi, B., "Rock Failure Under Concentrated Loading," *In Proceedings of the 10<sup>th</sup> U.S. Symposium on Rock Mechanics*, pp. 363-387, May 1968.
- Larson, D.A., Tandanand, S., Boucher, M.L., Olson, M.S., Morell, R.J., and Thill, R.E., "Physical Properties and Mechanical Cutting Characteristics of Cobalt-Rich Manganese Crusts," *Bureau of Mines Report of Investigations*, RI 9128, 1987.
- Lawn, B.R. and Swain, M.V., "Microfracture beneath Point Indentations in Brittle Solids," *Journal of Material Science*, Vol.10, pp. 113-122, 1975.
- Li, X.B., Summers, D.A., Rupert G., and Santi, P., "Experimental Investigation on the Breakage of Hard Rock by the PDC Cutters with Combined Action Modes," *Tunneling and Underground Space Technology*, Vol. 16, pp. 107-114, 2001.
- Lindqvist, P.A., and Ranman, K.E., "Mechanical Rock Fragmentation: Chipping under a Disc Cutter," *University of Lulea, Report 59T*, p. 37, 1980.
- Lindqvist, P.A., "Rock Fragmentation by Indentation and Disc Cutting," *Ph.D. Thesis*, University of Lulea, Sweden, 1982.

- Lindqvist, P.A. and Lai, H.H., "Behavior of the Crushed Zone in Rock Indentation," *Rock Mechanics and Rock Engineering*, Vol. 16, pp. 199-207, 1983.
- Lockner, D.A., "Rock Failure," *Rock Physics & Phase Relations, A Handbook of Physical Constants*, Ahrens, T.J. (ed.), pp. 127-147, 1995.
- McFeat-Smith, I and Fowell, R.J., "Correlation of Rock Properties and the Cutting Performance of Tunnelling Machines," *Proceeding: Conference on Rock Engineering*, New Castle upon Tyne, England, pp. 581-602, 1977.
- Mammen, J. Saydam, S. and Hagan, P., "A Study on the Effect of Moisture Content on Rock Cutting Performance," *Proceedings of the Coal Operators Conference*, University of Wollongong & Australian Institute of Mining and Metallurgy, ed. N. Aziz, p.340-347, 2009.
- Merchant, E.M., "Mechanics of the Metal Cutting Process," *Journal of Applied Physics*, Vol.11, p. A168, 1954.
- Miedema, S.A., "New Developments of Cutting Theories with respect to Offshore Applications, the Cutting of Sand, Clay and Rock," *International Offshore Ocean and Polar Engineering Conference*, Beijing, China, June 2010.
- Monsees, J.E., "A Very Brief History of Tunneling," *PB Network*, Issue No. 62, Vol. 21, No.1, 2006, [www.pbworld.com/pdfs/publications/pb\\_network/pbnetwork62.pdf](http://www.pbworld.com/pdfs/publications/pb_network/pbnetwork62.pdf), accessed 30 May 2012.
- Morris, A.H., "Practical Results of Cutting Harder Rocks with Picks in United Kingdom Coal Mine Tunnels," *Tunnelling '85*, IMM, Ed. M.J. Jones, 173-177, 1985.
- Morris, C.J., and MacAndrew, K.M., "A Laboratory Study of High Pressure Water Jet Assisted Cutting," *In Proceedings of the 8<sup>th</sup> International Symposium on Jet Cutting Technology*, Durham, England, pp. 1-9, 1986.
- Müller, B., Hausmann, J. and Niedzweidz, H., "Control of Rock Fragmentation and Muck Pile Geometry during Production Blasts (Environmentally Friendly Blasting Technique)," *Rock Fragmentation by Blasting*, Sanchidrian (ed), Taylor and Francis Group, London, 2010.
- Neil, D.M., "Production Estimating Techniques for Underground Mining using Roadheaders," *SME Annual Meeting*, Albuquerque NM, February, 1994.
- Nelson, P.P., "Tunnel Boring Machine Performance in Sedimentary Rocks," *Doctoral Dissertation*, Dept. of Civil Engineering, Cornell University, 1983.
- Nelson, P.P., Ingraffea, A.R. and O'Rourke, T.D., "TBM Performance Prediction using Rock Fracture Parameters," *Int. Journal of Rock Mechanics and Mining Sciences and Geomechanics Abstracts*, 22(3), 189-192, 1985.

- Nelson, P.P., "TBM Performance Analysis with Reference to Rock Properties," *Comprehensive Rock Engineering*, Vol. 4: J.A. Hudson, Ed., p.261-291, 1993.
- Nilsen, B and Ozdemir, L., "Hard Rock Tunnel Boring and Field Performance," *Proceedings of Rapid Excavation and Tunneling Conference*, Chapter. 52, pp.833-852, 1993.
- Nishimatsu, Y., "The Mechanics of Rock Cutting," *International Journal of Rock Mechanics and Mining Sciences & Geomechanics Abstracts*, Vol. 9, pp. 261-270, 1972.
- O'Reilly, M.P., Tough, S.G., Pirrie, N.D., Hignett, H.J. and Roxborough, F.F., "Tunnelling Trials in Chalk," *Proceedings of the Institution of Civil Engineers*, London, UK, Ed. J.S. Davis, Part 2, 67, pp.255-283, 1979.
- Oreste, P., Castellano, M. and Innaurato, N., "Debris Recycling in Tunnels: A Study Case Analysis," 2009, [www.ctta.org/FileUpload/ita/2009/papers/P-05/P-05-16.pdf](http://www.ctta.org/FileUpload/ita/2009/papers/P-05/P-05-16.pdf), accessed February 25, 2012.
- Ozdemir, L., Miller, R. and Wang, F., "Mechanical Tunnel Boring Prediction and Machine Design," *Colorado School of Mines, Golden, CO, Annual Report*, 1976.
- Ozdemir, L., Miller, R.J. and Wang, F.D., "Mechanical Tunnel Boring Prediction and Machine Design," *NSF APR73-07776-A03*, Colorado School of Mines, Golden, CO, USA, 1978.
- Ozdemir, L., "Mechanical Tunneling," *Short Course, Colorado School of Mines*, October 2-4, 1995.
- Parker, H., "Underground Space: Good for Sustainable Development and Vice Versa," *World Tunnel Congress and ITA General Assembly*, Singapore, May 2004, [www.itaaites.org/fileadmin/filemounts/general/pdf/ItaAssociation/ITAEvents/OpenSessions/HParker.pdf](http://www.itaaites.org/fileadmin/filemounts/general/pdf/ItaAssociation/ITAEvents/OpenSessions/HParker.pdf), accessed 30 May 2012.
- Paul, B. and Sikarskie, D.L., "A Preliminary Theory of Static Penetration by a Rigid Wedge into a Brittle Material," *SME Transactions*, pp. 372-383, 1965.
- Peng, S.S., Goldsmith, W., and Hood, M.C., "A Force Indentation Model for Brittle Rocks," *Journal of Rock Mechanics and Rock Engineering*, Vol. 22, pp. 127-148, 1989.
- Phillips, H.R. and Roxborough, F.F., "The Influence of Tool Material on the Wear Rate of Rock Cutting Picks," *Proceedings of the 34<sup>th</sup> Annual Conference of Australian Institute of Metals*, Brisbane, p.52-56, 1981.

- Podio, A. and Gray, K.E., "Single-Blow Bit-Tooth Impact Tests on Saturated Rocks under Confining Pressure: I. Zero Pore Pressure," *Society of Petroleum Engineers Journal*, pp. 211-224, September 1965.
- Pomeroy, C.D. and Brown, J.H., "Laboratory Investigations of Cutting Processes Applied to Coal Winning Machines," *Journal of Strain Analysis*, Vol.3, No.3, pp. 232-243, 1968.
- Potts, E.L.J. and Shuttleworth, P., "A Study of Ploughability of Coal with Special Reference to the Effects of Blade Shape, Direction of Planing to the Cleat, Planing Speed and the Influence of Water Infusion," *Transactions Institution of Mining Engineers*, London, 117, p. 520-548, 1958.
- Raise Boring Users Manual,  
[http://www.miningandconstruction.sandvik.com/sandvik/0120/Internet/Global/S003713.nsf/Alldocs/Products\\*5CRock\\*tools\\*and\\*systems\\*5CRaise\\*boring\\*tools\\*and\\*systems\\*2ACRH\\*4/\\$FILE/RaiseBoringUsersManual.pdf](http://www.miningandconstruction.sandvik.com/sandvik/0120/Internet/Global/S003713.nsf/Alldocs/Products*5CRock*tools*and*systems*5CRaise*boring*tools*and*systems*2ACRH*4/$FILE/RaiseBoringUsersManual.pdf), accessed June 15, 2012.
- Ranman, K.E. and Norin, J., "Static Button Indentation Tests in Granite and Limestone," *Mechanical Rock Fragmentation*, Technical Report: 57T, University of Lulea, pp.3-13, 1981.
- Rehbinder, P and Lichtman, V., "Effect of Surface Active Media on Strains and Rupture in Solids," *Proceedings 2<sup>nd</sup> International Congress on Surface Activity*, pp. 563-582, 1957.
- Reichholf, G. and Moser, P., "The Influence of Rock and Rock Parameters on the Blasting Results in Terms of Fragmentation," *Explosives and Blasting Technique*, Holmberg (ed.), Balkema, Rotterdam, 2000.
- Reichmuth, D.R., "Correlation of Force-Displacement Data with Physical Properties of Rock for Percussive Drilling Systems," *Proceedings, 5<sup>th</sup> Symposium on Rock Mechanics*, Pergamon Press, New York, pp.33-60, 1963.
- Robinson, L.H. and Holland, W.E., "Some Interpretation of Pore Fluid Effects in Rock Failure. *The 11th U.S. Symposium on Rock Mechanics (USRMS)*, Berkeley, CA, June, pp.585-597, 1969.
- Ropchan, D., Wang, F.D., and Wolgamott, J., "Application of Water Jet Assisted Drag Bit and Pick Cutter for the Cutting of Coal Measure Rocks," *U.S. DOE Contract ET-77-A-01-9082*, Colorado School of Mines, 1980.
- Rosin, P., Rammler, B., "The Laws Governing the Fineness of Powdered Coal," *Journal of Institute of Fuel*, Vol. 7, pp. 29-36, 1933.

- Rostami, J. and Ozdemir, L., "A New Model for Performance Prediction of Hardrock TBMs," *Proceedings of the Rapid Excavation and Tunnelling Conference*, Boston, MA, USA, pp. 372-383, 1993.
- Rostami, J., Ozdemir, L. and Neil, D.M., "Performance Prediction: A Key Issue in Mechanical Hard Rock Mining" *Mining Engineering*, pp.1263-1267, November 1994.
- Rostami, J. and Ozdemir, L., "Modeling for Design and Performance Analysis of Mechanical Excavators," *Proceedings of the Conference on Mechanical Excavation's Future Role in Mining*, World Rock Boring Association, Sudbury, Ontario, Canada, September;1996.
- Rostami, J., "Development of a Force Estimation Model for Rock Fragmentation with Disc Cutters through Theoretical Modeling and Physical Measurement of the Crushed Zone Pressure," *Doctorate Dissertation*, Dept. of Mining Eng., Colorado School of Mines, Golden, CO, 1997.
- Rostami, J., "Mechanical Rock Breaking," *SME Mining Engineering Handbook*, 3<sup>rd</sup> Edition, pp. 417-434, 2011.
- Roxborough, F.F., "Cutting Rock with Picks," *The Mining Engineer*, London, Vol. 132, Issue. 153, pp. 445-455, 1973.
- Roxborough, F.F. and Rispin, A., "The Mechanical Cutting Characteristics of the Lower Chalk" *Tunnels and Tunnelling*, p.45-67, January 1973.
- Roxborough, F.F. and Phillips, H.R., "Rock Excavation by Disc Cutter," *International Journal of Rock Mechanics and Mining Sciences & Geomechanics Abstracts*, Vol. 12, pp.361-366, 1975.
- Roxborough, F.F., King, P. and Pedroncelli, E.J., "Tests on the Cutting Performance of a Continuous Miner," *Journal of the South African Institute of Mining and Metallurgy*, pp. 9-25, 1981.
- Roxborough, F.F., "Research in Mechanical Rock Excavation: Progress and Prospects," In: *Proceedings of the Rapid Excavation and Tunneling Conference*, Vol. 1, pp. 225-243, 1985.
- Roxborough, F.F. and Sen G.C., "Breaking Coal and Rock," *Australasian Coal Mining Practice*, Vol. 12, pp. 130-147, 1986.
- Roxborough, F.F., "Multiple Pass Sub-Interactive Rock Cutting with Picks and Discs," *Proc. Conf. Applied Rock Engineering*, New Castle upon Tyne (Ed. M. Jones), IMM, London, pp. 183-191, 1988.



- Saouma, V.E. and Kleinosky, M., "Finite Element Simulation of Rock Cutting; A Fracture Mechanics Approach," *Proceedings of the 25<sup>th</sup> U.S. Symposium on Rock Mech.*, pp. 792-799, 1984.
- Samaranayake, V.A., "Statistical Data Analysis," *STAT-353 Course*, Missouri University of Science and Technology, Rolla, MO, USA, 2009.
- Sanchidrian, J.A., Segarral, P., Ouchterlony, F. and Lopez, L.M., "On the Accuracy of Fragment Size Measurement by Image Analysis in Combination with Some Distribution Functions," *Rock Mechanics and Rock Engineering*, Vol. 42, pp. 95–116, 2009.
- Sandvik Raise Boring Users Manual,  
[http://construction.sandvik.com/sandvik/0120/Internet/Global/S003713.nsf/Alldocs/Raise\\*boring\\*products\\*2ARaise\\*boring\\*brochure/\\$FILE/raiseboring12671a.pdf](http://construction.sandvik.com/sandvik/0120/Internet/Global/S003713.nsf/Alldocs/Raise*boring*products*2ARaise*boring*brochure/$FILE/raiseboring12671a.pdf), accessed June, 2011.
- Sanio, H.P., "Prediction of the Performance of Disc Cutters in Anisotropic Rock," *International Journal of Rock Mechanics and Mining Sciences and Geomechanics Abstracts*, Vol.22, No. 3, pp.153-161, 1985.
- Saperstein, L.W., Grayson, R.L., Summers, D.A., Garcia, J.J., Sutton, G., Woodward, M. and McNulty, T.P., "Breakthrough Energy Savings with Waterjet Technology", final report to *U.S. Department of Energy*, contract FG26-05NT42500, 2007.
- SAS, [www.support.sas.com/documentation](http://www.support.sas.com/documentation), accessed August 5, 2011.
- Sato, K., Gong, F. and Itakura, K., "Prediction of Disc Cutter Performance using Circular Rock Cutting Rig," *Proceedings of 1<sup>st</sup> International Mine Mechanization and Automation Symposium*, Colorado School of Mines, Golden, CO, 1991.
- Sato, K., Gong, F. and Itakura, K., "Measurement of Tool Force and Twist Exerted on TBM Disc Cutters," *Proceedings of 2nd International Mine Mechanization and Automation Symposium*, University of Lulea, Sweden, 1993.
- Schmitt, L., Forsans, T. and Santarelli, F.J., "Shale Testing and Capillary Phenomena," *Int. Journal of Rock Mechanics and Mining Sciences & Geomechanics Abstracts*, 31(5), pp. 411-427, 1994.
- Selimoglu, O., "A Fuzzy Logic Based Predictor Model for Disc Cutter Chip Production Rate," *Ph.D. Dissertation*, Missouri University of Science and Technology, Rolla, MO, USA, 2009.
- Sikarskie, D.L. and Cheatham, J.B., "Penetration Problems in Rock Mechanics," *Proceedings of the 11<sup>th</sup> Symposium on Rock Mechanics*, New York (AIME), pp. 41-71, 1973.



- Smith, M., "A Coupled Expert System Approach to Blast Optimization and Fragmentation Modeling," *SME Annual Meeting*, Denver, CO, February, Preprint number 91-50, 1991.
- Speight, H.E., "Observations on Drag Tool Excavation and the Consequent Performance of Roadheaders in Strong Rock," *The AusIMM Proceedings*, (1), pp.17-32, 1997.
- Steeghs, H.J.M.G., Koning, J.D. and Lubking, P., "25 Years of Dredging Research in the Netherlands: Physics as a Basis for Innovations," *Proceedings of the WODCON XII*, Orlando, Florida, pp. 15-32, 1989.
- Summers, D.A., "Waterjetting Technology," *Taylor and Francis*, p.882, 1995.
- Summers, D.A., "Personal Communication", 2009.
- Summers, D.A., "Personal Communication", 2012.
- Suárez-Rivera, F.R., Cook, P.J. and Cook, N.G.W., "The Role of Wetting Fluids during the Indentation of Porous Rocks," *Proceedings of the 32<sup>nd</sup> US Symposium on Rock Mechanics (USRMS)*, Norman, Oklahoma, pp.683-692, 1991.
- Sun, G.X., Whittaker, B.N., Singh, R.N., and Waller, M.D., "Prediction of Rock Cutting Performance using Fracture Mechanics Principles- A Review," *11<sup>th</sup> International Conference on Ground Control in Mining*, University of Wollongong, New South Wales, Australia, pp. 644-651, 1992.
- Swain, M.V. and Lawn, B.R., "Indentation Fracture in Brittle Rocks and Glasses," *International Journal of Rock Mechanics and Mining Sciences & Geomechanics Abstracts*, Vol. 13, pp. 311-319, 1976.
- Taggart, A.F., "Handbook of Mineral Dressing," John Willey & Sons, Inc., New York, 1945.
- Tandanand, S. and Hartman, H.L., "Stress Distribution beneath a Wedge-Shaped Drill-Bit Loaded Staticly," *Proceedings of the International Symposium on Mining Research*, Ed. G.B. Clark, University of Missouri, pp. 799-831, 1961.
- Tarkoy, P.J., "Rock Index Properties to Predict Tunnel Boring Machine Penetration Rates," *Proceedings of the Rapid Excavation and Tunneling Conference*, Chapter. 32, 1974.
- Tarkoy, P.J., "Predicting Raise and Tunnel Boring Machine Performance: State of the Art," *Proceedings of the 4<sup>th</sup> RETC*, Atlanta, Georgia, pp. 333-352, 1979.
- Thiercelin, M. and Cook, J., "Failure Mechanism Induced by Indentation of Porous Rocks," *Proceedings of the 29th U.S. Symposium on Rock Mechanics (USRMS)*, Minneapolis, MN, pp. 135-142, 1988.

- Thon, J.G., "Tunnel Boring Machines," In: *Tunnel Engineering Handbook*, Ch.10, pp. 235-278, Eds. J.O. Bickel and T.R. Kuesel, Van Nostrand, p. 670, 1983.
- Thuro, K and Plinninger, R.J., "Roadheader Excavation Performance-Geological and Geotechnical Influences," *The 9<sup>th</sup> ISRM Congress*, Theme 3: Rock Dynamic and Tectonophysics / Rock Cutting and Drilling, Paris, pp. 1241-1244, 1999.
- Tiryaki, B. and Dikmen, A.C., "Effects of Rock Properties on Specific Cutting Energy in Linear Cutting of Sandstones by Picks," *Rock Mechanics and Rock Engineering*, Vol. 39 (2), pp. 89-120, 2006.
- Tomlin, M.G., "Field Trials with a 10,000 psi Prototype System," *In Proceedings of Seminar on Water Jet Assisted Roadheaders for Rock Excavation*, Pittsburgh, PA, pp. C1-C11, May 1982.
- Tuncdemir, H., Bilgin, N., Copur, H. and Balci, C., "Control of Rock Cutting Efficiency by Muck Size," *International Journal of Rock Mechanics and Mining Sciences*, Vol. 45: pp. 278-288, 2008.
- Tutluoglu, L., Hood, M. and Barton, C., "An Investigation of the Mechanisms of Waterjet Assistance on Rock Cutting Process," *24<sup>th</sup> U.S. Symposium on Rock Mechanics (USRMS)*, College Station, TX, 1983.
- Uchibayashi, T., "Dredging Hard Soil and Rock with Cutter Suction Dredger," *Proceedings of World Dredging Marine Construction*, Vol.6, No. 11, pp. 35-37, 1970.
- US Army Corps of Engineers,  
<http://gsl.erdcl.usace.army.mil/SL/MTC/handbook/RT/RTH/116-95.pdf>, accessed July 9, 2012.
- Van Eeckhout, E.M., "The Mechanisms of Strength Reduction due to Moisture in Coal Mine Shales," *International Journal of Rock Mechanics and Mining Sciences & Geomechanics Abstracts*, Vol. 13, pp. 61-67, 1976.
- Van Kesteren, W.G.M., Steeghs, H.J.M.G. and Mastbergen, D.R., "Pore Water Behaviour in Dredging Processes," *Dredging for Development: Proceedings of the 13th World Dredging Congress*, Bombay, India, pp. 598-615, 1992.
- Van Kesteren, W.G.M., "Numerical Simulations of Crack Bifurcation in the Chip Forming Cutting Process in Rock. *Fracture of Brittle Disordered Materials: Concrete, Rock and Ceramics*," Ed. G. Barker and B.L. Karihaloo, E & FN Spon, London, UK, 1995.
- Vutukuri, V.S., "The Effect of Liquids on the Tensile Strength of Limestone," *International Journal of Rock Mechanics and Mining Sciences & Geomechanics Abstracts*, Vol. 11, pp. 27-29, 1974.

- Wanner, H., "On the Influence of Geologic Conditions at the Application of Tunnel Boring Machines," *Bull. Int. Assoc. Eng. Geol.*, Vol. 12, pp. 21-28, 1975.
- Whittaker, B.N. and Frith, R.C., "Tunnelling: Design, Stability and Construction," *The Institution of Mining and Metallurgy*, England, p. 460, 1990.
- Whittaker, B.N., Singh, R.N. and Sun, G., "Rock Fracture Mechanics: Principles, Design and Applications," *Elsevier Science Publishers*, Netherlands, p. 570, 1992.
- Yagiz, S., "Development of Rock Fracture and Brittleness Indices to Quantifying the Effects of Rock Mass Fractures and Toughness in the CSM Model Basic Penetration for Hard Rock Tunneling Machines," *PhD Thesis*, Colorado School of Mines, Golden, CO, USA, 2002.
- Yilmaz, N.G., Yurdakul, M. and Goktan R.M., "Prediction of Radial Bit Cutting Force in High-Strength Rocks using Multiple Linear Regression Analysis," *International Journal of Rock Mechanics & Mining Sciences*, Vol. 44, pp. 962-970, 2007.
- Yilmaz, I., "Influence of Water Content on the Strength and Deformability of Gypsum," *International Journal of Rock Mechanics and Mining Science*, Vol. 47, pp.342-347, 2010.

## VITA

After growing up in the city of Lahore, Pakistan, Muhammad Zubair Abu Bakar attended the University of Engineering and Technology (UET), Lahore. He earned his B.Sc. in Mining Engineering with distinction and M.Sc. in Computer Science in 2000 and 2003 respectively. After graduating from the UET, he joined Central Inspectorate of Mines, Ministry of Labor, Manpower, and Overseas Pakistanis, Islamabad as Training-cum-Safety Officer in 2003. He remained involved in the safety audits of exploration and production operations of oil and gas industry in Pakistan. After leaving the Central Inspectorate of Mines, he joined the faculty of the Mining and Geological Engineering Department at the UET as Lecturer in 2004. Along with the teaching responsibilities, he obtained his M.Sc. in Mining Engineering in 2005 from the UET. He was then awarded a scholarship from the UET to attend the University of Leeds, England, UK in 2005. He obtained his M.Sc. in Engineering Geology from the University of Leeds in 2006. He then joined back the UET in 2006 and served as Assistant Professor in the Department of Geological Engineering. He was later in 2006 was awarded a scholarship under Faculty Development Program to pursue his PhD. He started his PhD in Geological Engineering at Missouri University of Science and Technology, Rolla in 2008. He also worked as Teaching and Research Assistant during his PhD studies. He received his PhD in December 2012.